In-depth profiling of drug resistance to PI3K-mTOR inhibition and intra-tumour heterogeneity in NSCLC

A Thesis Submitted to the University of Dublin, Trinity College, for the Degree of Doctor of Philosophy

Samira Elbai BSc., MSc.

January 2021

Supervisor

Dr. Kathy Gately
Department of Clinical Medicine
Trinity Translational Medicine Institute
St. James's Hospital
Trinity College Dublin
Dublin D08 W9RT

Co-Supervisor

Dr. Paul Dowling
Department of Biology
Maynooth University
Callan Building
Maynooth
Co. Kildare

Table of contents

List of figures

List of tables

Publications and Conference Abstracts

Conference Abstracts

S. Elbai, S. Cuffe, S. P. Fnn, K. Gately **(2018).** Tracking the molecular evolution of drug resistance to PI3K/mTOR inhibition in NSCLC. Lung Cancer, vol. 115, supplement 1. *https://doi.org/10.1016/S0169-5002(18)30035-7*.

Gillian Moore, **Samira Elbai**, Susan Heavey, Stephen Finn, Michael O'Neill and Kathy Gately **(2020)**. Activation of the MACC1/PIM/cMyc axis confers resistance to PI3K/mTOR inhibition in PIK3CA mutant NSCLC. Molecular Cancer Research. DOI: 10.1158/1557-3125. PI3K-mTOR18-B14 Published October 2020.

S. Elbai, P. Dowling, K. Gately **(2020).** Detecting intra-tumour heterogeneity of lung squamous carcinoma using Label- Free Mass Spectrometry. Irish Association for Cancer Research (IACR)

Publications

Gillian Moore[1, 2], Clara Lightner[1], **Samira Elbai**[1], Lauren Brady[3], Siobhan Nicholson[3], Ronan Ryan[4], Katie E O'Sullivan[4], Kenneth J O'Byrne[5], Carmen Blanco[6], Sinead Cuffe[1], Michael O'Neill[7], Susan Heavey[8], Stephen P Finn[3], Kathy Gately[1*]. Co-targeting PI3K/mTOR and PIM kinase in NSCLC (Under review in Cancers).

Samira Elbai, Paul Dowling, Kathy Gately. Multi-region, multiomic profiling identifies spatial heterogeneity in lung adenocarcinoma (In preparation).

Samira Elbai, Paul Dowling, Kathy Gately. Detecting intra-tumour heterogeneity of lung squamous carcinoma using Label- Free Mass Spectrometry (In preparation).

List of ECTs

Biomedical imaging module (RCSI) 2ECTs credits.

Personal development & employability module (Maynooth university) 5ECTs.

Poster presentation at Irish Association for Cancer Research-IACR, Galway-Ireland, 2019.

Declaration

I, Samira Elbai, student No. 15340318, declare that this thesis has not been submitted in whole or part to Trinity College Dublin or any other university in/out Ireland for any degree, and is the authors' original work. I, Samira Elbai, agree to deposit this thesis in the University's open access institutional repository or allow the library to do so on my behalf, subject to Irish Copyright Legislation and Trinity College Library conditions of use and acknowledgement.

Author: Samira Elbai

Date signed: 21/09/2021

Acknowledgement

I would like to express my acknowledgement to the biotechnology research center in Libya for sponsoring my PhD project through the Ministry of higher education and scientific research of Libya. I also would like to thank my family; dad, mom, sisters, brothers, kids and husband for their patience and encouragement to continue working on my PhD project despite the social and psychological circumstances. I also would like to thank the North Kildare Disability Team, on top of them Mrs Caroline Green, for their daily basis support to cope with my life circumstances difficulties. I would like to thank my lab mates; Dr. Steven Gray and Dr. Martin Barr, who were helpful in all aspects of my work. Special thanks goes to Dr. Steven Gray for his training on qRT-PCR, consultation, and support during my laboratory work on my thesis. I also would like to thank all post-graduate students at St. James's Hospital campus, on top of them Leah Quinn, for their unlimited help and support. I would like to thank Dr. Paul Dowling for his co-supervision of my PhD project. I also would like to thank Dr. Abduladim Hmmier, my tutor, who guided me through all the entire thesis, especially the proteomic, functional validation and bioinformatics parts, as well as helping in linking all the thesis themes. A special thanks is addressed to my supervisor, Dr. Kathy Gately, for her training, guidance, support, and good management of my scholarship grant throughout this project.

Dedication

'This humble research work is dedicated to my family; parents, sisters, brothers, husband and kids, also to my friends and colleagues from whom I had the stamina to continue working on this project despite the difficult times.'

Thanks to all

List of abbreviations

Abbreviation	Full name
5HT	5-hydroxytryptamine
ABCB1	ATP-binding cassette B1
ACs	Atypical carcinoids
AD	Adenocarcinoma
AIS	Adenocarcinoma in-situ
ALK	Anaplastic lymphoma kinase
AMPK	AMP-activated protein kinase
ANCR	Anti-differentiation non-protein coding RNA
ANRIL	Antisense non-coding RNA in the INK4 locus
AREG	Amphiregulin
ARK1	Activated Cdc42 kinases
AS	Antisense
ASO	Antisense oligonucleotides
AUC	Area under curve
AXL	Greek word called anexelekto = uncontrolled
B-Raf	Proto-oncogene serine/threonine-protein kinase
BAL	Bronchoalveolar lavage
BANCR	BRAF-activated non-protein coding RNA
BCRP	Breast cancer resistance protein
BLK	B-lymphocyte development kinase
BMX	Bone marrow kinase on X-chromosome
BSA	Bovine serum albumin

BTK	Bruton’s tyrosine kinase
CCCR	The collective china cancer registry
CdKs	Cyclin-dependent kinases
CEA	Carcinoembryonic antigen
CISH	Chromogenic in situ hybridization
CK	Creatine kinase
CMTM6	CKLF Like MARVEL Transmembrane Domain 6
COL16A1	Collagen 16 alpha chain 1
COMP	Cartilage oligomeric matrix protein
COPD	Chronic obstructive pulmonary diseases
CPA7	Cytochrome P450 subfamily A member 7
CREB	cAMP-response element binding protein
CREBBP	CREB-binding protein
CSF1R	Colony stimulating factor 1 receptor
CSK	c-terminal Src kinase
CT-scan	Computed tomography scan
CTF1	Cardiotrophin 1
cTNM	Clinical staging “Tumour-node-metastasis”
CYFRA 21-1	Fragment of cytokeratin 19
DANCR	Differentiation Antagonizing Non-Protein Coding RNA
ddNTPs	Dideoxy nucleotides triphosphates
DDR1	Discoidin domain receptor tyrosine kinase 1
DM3	Disease resistance gene
DMSO	Dimethyl sulfoxide
DNA	Deoxyribonucleic Acid

dNTPs	Deoxyribonucleotide triphosphate
dTT	Dithiothreitol
EB	Elution buffer
ECM	Extracellular matrix
EDTA	Ethylenediaminetetraacetic acid
EIF4E	Eukaryotic translation initiation factor
ELAVL3	ELAV Like RNA Binding Protein 3
EMT	Epithelial-mesenchymal transition
EPH	Erythropoietin-Producing Hepatoma
EPHRA1	Erythropoietin-Producing Hepatoma A Receptor
ErbB	Epidermal growth factor receptor
ERK	Mitogen-activated protein kinase
ERO1-La	Endoplasmic reticulum oxidoreductase 1 alpha
ESI	Electrospray ionization
FAK	Focal adhesion kinase
FER	Family include fes-related kinases
FES	Feline sarcoma kinase
FGF18	Fibroblast growth factor 18
FGFR	Fibroblast growth factor receptor
FHL1	Four-and-a-half LIM domains
FNA	Fine-needle aspiration
FOXO3	Fork-head Box O3
FRK	Fyn Related Src Family Tyrosine Kinase
GP	General practitioner
GPCR	G-protein -coupled receptors

GYS	Glycogen synthase
hASH1	Highly express achaete-scute homolog 1
HCK	Hematopoietic cell kinase
HDI	Human development index
HER2	Human epidermal growth factor receptor 2
HER3	Human epidermal growth factor receptor 3
HER4	Human epidermal growth factor receptor 4
HGF	Hepatocyte growth factor
HIF-1	Hypoxia-induced factor 1
HKG	Housekeeping gene
IC50	Inhibitory concentration of 50% cell viability
IFR	Isoflavone reductase
IGF-1	Insulin-like growth factor 1
IGF1R	Insulin-like growth factor I receptor
IKK	IκB Kinase
IL13RA2	Interleukin-13- receptor subunit alpha 2
IL20RA	Interleukin-20- receptor subunit alpha
IL6ST	Interleukin 6 Signal Transducer
InsR	insulin receptor
IT	Intronic
ITH	Intra-tumour heterogeneity
ITK	Interleukin-2- inducible T-cell kinase
JAK	Janus kinase
KRAS	Kirsten rat sarcoma 2 viral oncogene homolog
LC-MS/MS	Liquid chromatography with tandem mass spectrometry

LCK	Lymphocyte-specific kinase
LCLC	Large cell lung cancer
LINC	Long intergenic non-coding RNA
LKB1	Liver kinase B1
Lmr2	Lemur tyrosine kinase 2
Lmr3	Lemur tyrosine kinase 3
lncRNAs	Long non-coding RNAs
LP9	Normal human mesothelial cell strain
LSqCC	Lung squamous cell carcinoma
LTK	Leukocyte receptor tyrosine kinase
LYN	Lyn tyrosine kinase
MACC1	Metastasis-associated in colon cancer 1
MAG1	Membrane-associated guanylate kinase 1
MALAT1	Metastasis Associated Lung Adenocarcinoma Transcript 1
MAPK	Mitogen-activated protein kinase
MATK	Megakaryocyte- associated tyrosine kinase
MDR1	Multiple drug resistance
MET	MET proto-oncogene-hepatocyte growth factor receptor
MMR	Mismatch repair
MRP1	Multidrug resistance associated protein 1
mTOR	Mechanistic Target Of Rapamycin Kinase
MTS	Medical thoracoscopy
MUSK	Muscle associated receptor tyrosine kinase
NEM	Neuroendocrine markers
NER	nucleotide excision repair

NGS	Next generation sequencing
NRTK	Non-receptor tyrosine kinase
NSCLC	Non-small cell lung cancer
NSCLC-NOS	Non-small cell lung cancer not otherwise specified
OG	Oncogenes
Cyt-P450	Cytochrome P450
pan-HDACi	Inhibit all histone-deacetylases
PCA	Principal component analysis
PCR	Polymerase chain reaction
PD-L1	Programmed death ligand-1
PDGFA	Platelet derived growth factor alpha
PDGFR	platelet derived growth factor receptor
PGP	P-glycoprotein
PI3K	Phosphatidylinositol-3-kinase
PIM1	Proviral Integration site-Moloney murine leukemia virus 1
PIM2	Proviral Integration site-Moloney murine leukemia virus 2
PIM3	Proviral Integration site- Moloney murine leukemia virus 3
PIP2	Phosphatidylinositol di-phosphate
PIP3	Phosphatidylinositol triphosphate
PKC	Phosphokinase C
POTEC	POTE Ankyrin Domain Family Member C
PPP2R5B	Protein Phosphatase 2 Regulatory Subunit Beta
PTEN	Phosphatase and tensin homolog
PTENP1	Phosphatase and tensin homology pseudogene 1
pTNM	Pathological-Tumour-lymph node-metastasis

PTPRZ1	Protein Tyrosine Phosphatase Receptor Type Z1
PYK2	Proline-rich tyrosine kinase 2
qRT-PCR	Quantitative reverse transcriptase polymerase chain reaction
RELN	Reelin
RLTPR	RGD motif, leucine rich repeats, tropomodulin proline-rich
RNA	Ribonucleic acid
ROR	receptor tyrosine kinase like orphan receptor
RPMI	Roswell Park Memorial Institute
RTKs	Receptor tyrosine kinases
SCLC	Small cell lung cancer
SGK	Serum/glucocorticoid regulated kinase
shRNA	Short hairpin RNA
siRNA	Small interfering RNA
SNP	Single nucleotide polymorphism
SOCS1	Suppressor of cytokine signalling 1
SPP1	Secreted Phosphoprotein 1
STAT	Signal transducer and activator of transcription
STTYK1	Serine/threonine/tyrosine kinase 1
SULT6B1	Sulfotransferase Family 6B Member 1
SYK	Soluble cytoplasmic tyrosine kinase
TCGA	The Cancer Genome Atlas
TCL1	T-cell leukaemia 1
THBS4	Thrombospondin 4
TIE1	Tyrosine kinase with immunoglobulin like domain 1
TIE2	Tyrosine kinase with immunoglobulin like domain 2

TINCR	Tissue differentiation-inducing non-protein coding RNA
TP53	Tumour protein 53
TSC1	The tuberous sclerosis-1
TSC2	The tuberous sclerosis-2
TSG	Tumour suppressor gene
TSLP	Thymic stromal lymphopoietin
TTF-1	Thyroid transcription factor-1
VATS	Video-assisted thoracic surgery
VEGFR	Vascular endothelial growth factor receptor
VEP	Variant Effect Predictor
ZAP70	Zeta chain of T-cell receptor associated protein kinase 70

Abstract

Lung cancer has an overall 5-year survival rate of less than 15% and is the leading cause of cancer-related death worldwide. As such, it is crucial we develop new treatment strategies to overcome this formidable disease. In 2004, the discovery of *EGFR* mutations that confer sensitivity to *EGFR* tyrosine kinase inhibitors in lung adenocarcinomas heralded the beginning of the era of precision medicine for lung cancer. The concerted effort to define molecular subgroups of lung cancer and identify novel therapeutic targets has significantly impacted the advancement of lung cancer treatment and patient survival. However, the clinical application of molecularly guided personalized treatment is challenging. The biggest hurdle is the inevitable emergence of drug resistance that ultimately renders therapy ineffective. Tumour cells have the innate ability to employ different mechanisms to resist the targeting agent, often driven by the heterogeneous nature of tumours, which is especially prevalent in lung cancer.

The *PI3K-mTOR* signalling pathway together with *AKT* phosphorylation is active in 50-70% of non-small cell lung cancer (NSCLC) and plays an overarching role in all the hallmarks of cancer, including evading immune destruction. Pathway dysregulation confers a poor prognosis making it an ideal target for treatment. Results from early-phase *PI3K* targeted therapy clinical trials have been mixed, with innate and acquired resistance to *PI3K* inhibition anticipated to be a major hurdle to overcome in the development of these drugs. Initial efforts to therapeutically target the *PI3K-mTOR* pathway in NSCLC have resulted in only a few partial responses; however, most of the Phase I studies did not select for patients with an activated *PI3K-mTOR* pathway. Several clinical trials combining a

PI3K inhibitor with another targeted therapy or immunotherapy are currently recruiting.

This project set out to further identify and validate biomarkers of drug resistance to *PI3K-mTOR* targeted therapies to guide clinicians in the design of improved treatment strategies for patients. Our group previously developed NSCLC cell line models of acquired resistance to *PI3K-mTOR* inhibitor apitolisib which were used in this study to validate specific bypass mechanisms of resistance. In-depth analysis of differentially expressed mRNAs and lncRNAs identified changes in genes involved in the regulation of metabolism and cellular response to stimuli. We are the first to show that inhibition of *PI3K-mTOR* in NSCLC leads to transcriptional activation of *PIM1*, *PIM2* and *PIM3* kinases as well as *c-Myc*. Activated *MACC1* expression was confirmed as an early event in the emergence of drug resistance, suggesting it may be involved in initiating the events leading to the upregulation of other genes such as *MYC*, *PIM1/2/3* and the acquired resistance to *PI3K*/*mTOR* inhibitors. Dual *PIM* kinase and *PI3K-mTOR* inhibition decreases cell proliferation, and this data provides a rationale for co-targeting treatment strategies for patients with tumours that have a dysregulated *PI3K-mTOR* pathway. This personalized medicine approach will improve response rates and survival benefits for patients with NSCLC. The second part of this thesis examined proteomic, phospho-proteomic, genomic and transcriptomic intra-tumour heterogeneity (ITH) to determine differences in the molecular profile of cancer cells within the tumour and in particular how this may affect the diagnosis and stratification of patients for personalized treatment. Proteomic and phospho-proteomic expression was quantified across three different regions of the same tumour and matched normal tissue from four patients with lung squamous cell carcinoma. Label-free L-C/MS-

MS comparative proteomics and principal component analysis was performed and demonstrated heterogeneous expression of proteins between different areas of the same tumour mass. Interestingly, for the most part, protein expression was identified in all tumour regions, albeit differentially expressed. A panel of four differentially expressed proteins (Enolase-1, desmoplakin, tenascin C and *EROI-La*) were selected for further validation by western blot analysis in the same protein samples. Phosphorylated proteins demonstrated a more divergent expression pattern between different areas of the same tumour with some undetectable in one area while present in another part of the tumour. It was unclear whether this lack of expression was a true reflection of tumour biology or may have been due to the instability of phosphorylated proteins.

Finally, whole-exome sequencing (WES) and a microarray for RNA and lncRNA profile analysis were used to quantify genomic and transcriptomic ITH respectively, across two different tumour regions and matched normal tissue from three patients with lung adenocarcinomas. The number of uniquely mutated genes per tumour region in all tumours infers a high level of heterogeneity. The microarray dataset identified novel lncRNA expression profiles in lung cancer that warrant further investigation for the identification of biomarkers and new therapeutic targets that can be used for NSCLC treatment.

In summary, ITH and clonal evolution enable the survival of residual disease cells that eventually cause tumour relapse and the failure of single-agent-targeted inhibitors to induce long-lasting durable responses to treatment. Our data further highlights the limitations of tumour tissue biopsies to predict molecular or proteomic profiles. Therefore, a panel of biomarkers allows for better patient stratification for personalized targeted treatment.

1. **Chapter I**: Introduction

1.1. Introduction

1.1.1. Lung anatomy and histology

The lungs are sponge-like organs that differ slightly in their anatomy. The right lung has three lobes while the left lung has two lobes to make space for the heart in the thoracic cavity. Conduction and respiration (gas exchange) are the two main functions of the lungs. Conduction is the movement and conditioning of the inhaled air, while respiration allows gas exchange. The air conduction starts from the trachea and ends in the terminal bronchioles. The air enters the trachea coming from the nasal cavity down through the nasopharynx, larynx. The trachea connects the lungs with the oral cavity, it divides into two main bronchi, the branching fork called carina, each of which enters the lung at the hilum level (Cersosimo, 2002). The bi-fork carina, when invaded by cancer, makes surgical resection a difficult treatment option (Figure 1.1). The two bronchi branch into two lobar bronchi, each of which branches to give two segmental bronchi, the segmental bronchi continue branching and lead to very small structures called terminal bronchioles or respiratory bronchioles (the site of gas exchange and blood oxygenation) (Brown, 2018). The air conduction and conditioning (warming, moisturizing and clearing dust particles) are modulated by five types of cells: **A.** The ciliated cells, the most abundant, act as a muco-ciliary escalator to repel debris and particles within air (Ganesan et al., 2013). **B.** The goblet cells (Goblet-shaped), secrete the mucus (mucins) that lubricates the mucosal linings. The number of goblet cells dramatically decreases as the bronchial branching becomes smaller (needed for gas exchange) and replaced by club cells at the level of respiratory bronchioles. **C.** The basal cells are connected to the basement membrane and provide an attachment layer for the ciliated and goblet cells (Evans et al., 2001). **D**. The brush cells,

distributed in all respiratory mucosa have chemoreceptors monitoring air quality as they associate with unmyelinated nerve endings (Brody, 2005). **E**. The neuroendocrine cells (Kulchitsky cells), present as small clusters (3% of the mucosal epithelium), and have neurosecretory granules eg. catecholamine, polypeptide hormones such as serotonin (5HT), calcitonin, and gastrin-releasing factors (La Rosa et al., 2010). Trapped within the bronchial submucosa, a mixture of serous and mucinous cells resembling the salivary glands, their secretions empty on to the bronchial mucosa via ducts. Smooth muscle fibres present at the level of main bronchi to help control the airway passages and also in the respiratory alveoli to maintain their plasticity (Janssen, 2012).

The respiration function of the lungs takes place in the respiratory alveoli, the terminal alveolar branches; this histological structure is characterized by an increased abundance of club cells, very low number of goblet cells, and the absence of cartilage. The respiratory bronchioles consist of acinar structures, each of which are composed of three parts; respiratory bronchioles, alveolar ducts, and alveolar sacs. The alveolar epithelium is composed of three types of cells: **A**. type I pneumocytes (90-95%), are squamous epithelia, their thin membrane allows for gas trapping and permeability. **B**. type II pneumocytes make up nearly the residual percentage of the cells (up to 5% of the cells). The type II pneumocytes secretes surfactants necessary to maintain open airways passages and also serve as stem cells to replace damaged type I and II pneumocytes. **C.** Macrophages are present in the respiratory alveoli either free or trapped in the alveolar walls and they offer a late line of defence (Mukaida et al., 2018, Vasudevan et al., 2018).

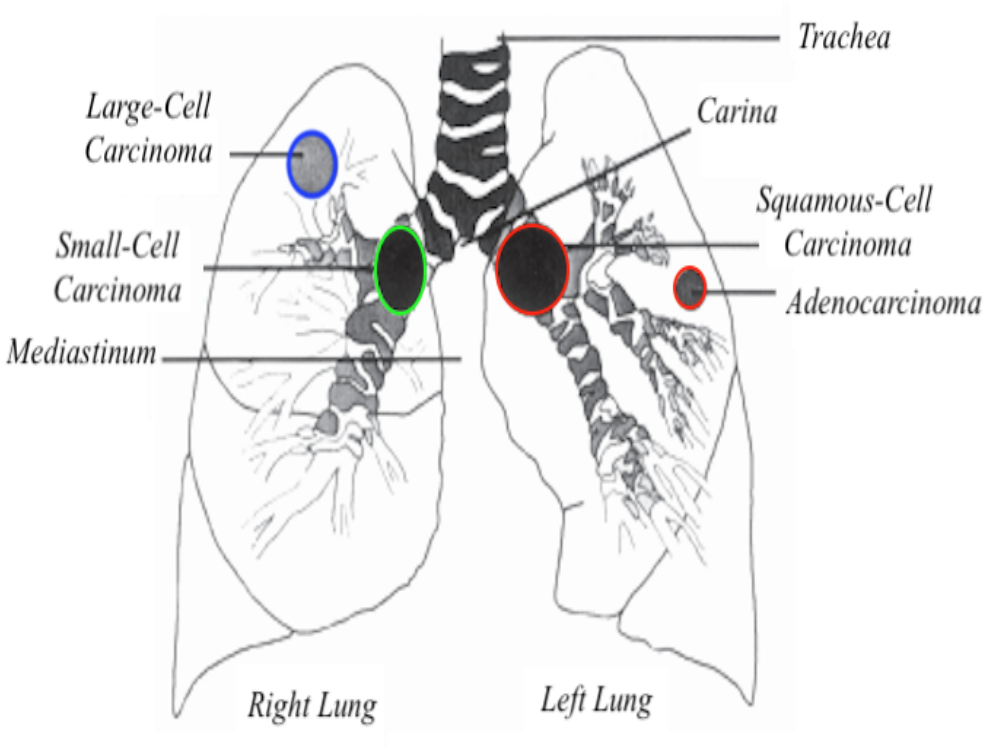

Figure 1.1. Basic anatomy of the lungs highlighting the common location of different types of lung tumours. Modified from Life art Medclip, Lippincott Williams & Wilkins, © 2001. Small cell lung cancer and squamous cell carcinoma are mostly located in the large airway passages as they are linked to smoking and environmental predisposing factors. Large cell cancer is limited to the bronchial alveoli and adenocarcinoma are located far from the airway passages.

1.2. Lung cancer epidemiology and its risk factor:

Epidemiology is the study of distribution, aetiology and incidence rates of health-related issues in specified populations and utilizes the collected information in the prevention and control of health problems (Hajat, 2011, Gulis and Fujino, 2015).

1.2.1. Human development index

The human development index (HDI) is a statistical tool used to measure a country's overall achievement in its social and economic dimensions. HDI has an impact on the incidence as well as the mortality rates of lung cancer. People in countries with high HDI live longer than those living in low HDI countries (Cheng et al., 2016, Rahi, 2011). In 2017, a study was conducted on the incidence and mortality rates of lung cancer, the study included 74 countries: 38 countries with

HDI including all region in Europe, North America, Australia, New Zealand and Japan, and 35 less developed countries with less HDI which include: all regions of Africa, Asia except Japan, Latin America, Caribbean, Melanesia, Micronesia and Polynesia countries. Per country HDI was found strongly correlated with the age-standardized incidence and mortality rates (r=0.7 and 0.67, respectively). The trend of incidence and mortality rates of lung cancer in men was found to decline in (22 out of 38 of high HDI) and in (30 out of 36 of low HDI) countries, the average annual percent changes (AAPCs) went from 2.8 to 0.6 (incidence) and from 3.6 to 1.1. In contrast, the trend of incidence and mortality in women was increasing from 0.4 to 8.9 (incidence) and from 1 to 4.4 (mortality) among these countries. Based on this study, lung cancer among women in all Western, Southern and Eastern Europe reported an increased mortality rates. The highest increase in the incidence rates of lung cancer among women was observes in Brazil, Spain and Cyprus (Wong et al., 2017).

The number of lung cancer cases in any selected country is directly proportional to the number of population. In China the population in 2012 was 1.351 billion, the lung cancer incidence accounted for 36% of the world total cases. The collective china cancer registry (CCCR) revealed that the number of lung cancer cases had increased between 1988 and 2011, the incidence rates in male and females were 48 and 22 per 100,000 population, respectively (Chen et al., 2015b, Chen et al., 2015a). The incidence and mortality of lung cancer was higher in urban areas compared to rural areas as concluded from data obtained from 177 cancer registries in China (Chen et al., 2016).

1.2.2. Cigarette smoking

Cigarette smoking is the leading cause of lung cancer, it accounts for 90% of lung cancers in men and up to 80% in women (Youlden et al., 2008). Cigarette smoking has been estimated to increase the chance of developing lung cancer by 30 fold in both sexes (Proctor, 2001). At age 40, women who smoke have a greater chance of dying from lung cancer than from breast cancer. Men are 10 times more likely to die from lung cancer than prostate cancer (Woloshin et al., 2008). Passive smoking can increase the susceptibility of lung cancer by 25% compared to non-smokers, this increases to 50% in people who are chronically exposed to heavy passive smoking (Wang et al., 2015). In addition to the active and passive tobacco smoking, occupational exposure to smoky coal as well as coal fine particulate matters was found to account for the main risk factors for lung cancer in China (Liu et al., 2017). Gene mutations such as KRAS mutations are strongly associated with cigarette smoking and occur in approximately 40% of adenocarcinomas (34% of smokers and 6% of non-smokers) and approximately 5% of squamous cell carcinomas.

On the other hand, EGFR mutations are more common in never smokers. In addition to air pollutants, poor nutrition and genetic susceptibility also have a role in shaping the geographical distribution of lung cancer worldwide (Malhotra et al., 2016). High radon areas have a direct impact on the prevalence of lung cancer according to a study conducted in Ireland including more than 5500 people aged above 50 (Dempsey et al., 2018). Another research study (83% smokers) to assess risk factors showed 6% of cases developed lung cancer after exposure to asbestos, 3% were passive smokers, while those exposed to radon were only 0.5% (Cuadras et al., 2016). Exposure to irradiation also has a great impact on the mutagenesis and transition of pre cancer tissue malignancy (Li et al., 2017a).

1.2.3. Genetic susceptibility

Susceptibility to lung cancer differs from one individual to another. Oncogenes are involved in the activation of cell growth and division, whereas tumour suppressor genes suppress these processes (Bello and Rey, 1995). The correct balance between oncogenes and tumour suppressor genes as well as the existence of a healthy DNA repair system is the best defence against the development of cancer. The ability of the gene repair machinery eg. nucleotide excision repair (NER), mismatch repair (MMR) to repair acquired mutations also plays an important role in susceptibility (Spitz et al., 2003) and/or protection against the disease (Valdiglesias et al., 2011, Chatterjee and Walker, 2017). Genetic polymorphisms, *e.g*. in epidermal growth factor receptor (EGFR) can contribute to increased susceptibility to lung cancer and failure of treatment with tyrosine kinase inhibitors (TKIs), such genetic polymorphisms can be utilized in the prediction of tumour resistance to TKI (Wang et al., 2017b). Since the somatic mutations in *EGFR* in the tyrosine kinase domain play an important function in both development and treatment of lung cancer, the frequent overexpression of EGFR poses it as a new and promising therapeutic target. DNA-repair gene polymorphisms (Yu et al., 2017b) can enhance and facilitate the production of bulky DNA adducts (conjugates between large reactive electrophiles and DNA) by environmental agents and is associated with an increased risk of lung cancer (Munnia et al., 2017). Inheritance of the susceptibility to cancer differs between people. The incidence of lung cancer in one family member represents a risk factor contributing to increased susceptibility of other family members to developing lung cancer; the risk is increased by daily exposure to different predisposing agents (Mattson et al., 1987).

1.3. Classification of lung cancer

Lung cancer is classified into two main types; small cell lung cancer (SCLC) and non-small lung cancer (NSCLC) accounting for 15% and 85% respectively. NSCLC is further classified into squamous cell carcinoma, adenocarcinoma, and large cell carcinoma in addition to other forms of non-small cell carcinomas (Figure 1.2). Neuroendocrine tumours (NET) of the lung account for approximately 20% of all lung cancers with the majority being represented by SCLC.. This thesis focusses on adenocarcinoma and squamous cell carcinoma and both are described in more detail below.

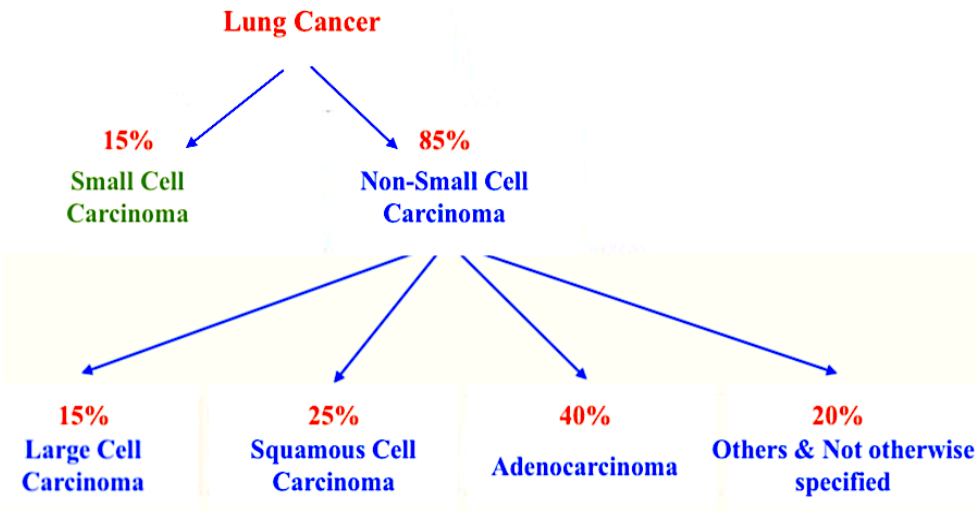

Figure 1.2. Classification of lung cancer by histopathologic subtype. Modified from (Gridelli et al., 2015).

1.3.1. Small cell lung cancer

Small cell lung cancer (SCLC), also called oat-like carcinoma, accounts for approximately 15-20% of lung malignancies and 95% of lung neuroendocrine tumours (Jackman and Johnson, 2005, Bertino et al., 2009). SCLC is a poorly-differentiated, high grade aggressive carcinoma with a tendency to metastasize and

is strongly associated with cigarette smoking (Kato et al., 1969, Rekhtman, 2010, Hendifar et al., 2017). SCLC is weakly reactive to the neuroendocrine markers chromogranin A and synaptophysin (Kwon and Chapman, 2011, D'amico et al., 2014). SCLC highly expresses the achuete-scute homolog 1 (hASH1) neuro-endocrine marker (Ye et al., 2016) and membrane-based NCAM/CD56, the latter is a very sensitive marker for the diagnosis of SCLC (Lantuejoul et al., 1998) but lacks specificity as it also stains NSCLC (Feng et al., 2017). SCLC and other neuroendocrine pulmonary tumours give negative staining to the high molecular weight keratins; CK1, 5, 10 and 14, also known as 34ßE12 clone (Sturm et al., 2001). Thyroid transcription factor-1 (TTF-1) is also used as a diagnostic marker when combined with other endocrine markers such as CD56 and P16 (Švajdler et al., 2019). SCLC is staged as a limited stage disease (local) or extensive stage (distant) (Micke et al., 2002). Two thirds of SCLC are diagnosed late as extensive carcinoma and the common metastasis sites are the liver, brain and bones (Kalemkerian et al., 2013, Travis, 2014). The five year survival rate is 2-5% and the treatment usually involves: etoposide plus cisplatin and surgery is highly recommended in early stage patients (Johnson et al., 2011, Fisseler-Eckhoff and Demes, 2012).

1.3.2. Non-small cell lung cancer

This group of lung carcinomas account for up to 85% of lung cancer cases and include; large cell lung carcinoma, adenocarcinoma, and squamous cell carcinoma.

1.3.2.1. Large cell lung cancer

Large cell lung cancer (LCLC), also called non-small cell lung cancer not otherwise specified (NSCLC-NOS), is one of the pulmonary neuroendocrine tumours associated with cigarette smoking. It accounts for 10%-15% of all NSCLC, and is

a poorly-differentiated, high grade, aggressive lung tumours, and tends to start at large airways and metastasizes early to the mediastinum (Lemjabbar-Alaoui et al., 2015, Hendifar et al., 2017). The five year survival rate is 16-57%, and the treatment involves cisplatin based chemotherapy plus surgery(Skuladottir et al., 2002, Johnson et al., 2011, Fisseler-Eckhoff and Demes, 2012).

1.3.2.2. Lung adenocarcinoma

Adenocarcinoma accounts for 40% of all lung cancer cases and is now the most common histological subtype of lung cancer in both men and women in Europe and the US (B'chir et al., 2007, Nakamura and Saji, 2014). The elevated rate of lung carcinoma in women who are non-smokers indicates that there are other risk factors involved in addition to smoking (Dubin and Griffin, 2020). Lung adenocarcinoma tumours are classified into 4 categories: 1) pre-invasive adenocarcinoma which include (atypical adenomatous hyperplasia, adenocarcinoma in-situ, non-mucinous, mucinous, mixed mucinous/non-mucinous), 2) minimally invasive adenocarcinoma which could be mucinous, non-mucinous or mix of both, 3) invasive which include (lepidic predominant, acinar predominant, papillary predominant, micropapillary predominant or solid predominant with mucin production), 4) variants of invasive adenocarcinoma are (invasive mucinous adenocarcinoma, colloid, fetal, enteric). For the purpose of clinical diagnosis lung adenocarcinomas biopsies are classified as: 1) Morphologic adenocarcinoma pattern clearly present (Adenocarcinoma + X, where X: lepidic, acinar, papillary, micropapillary or solid), 2) Morphologic adenocarcinoma is not clearly present (eg. Ancillary stained non-small cells suggest adenocarcinoma) (Lambe et al., 2020).

1.3.2.3. Lung squamous carcinoma

Lung squamous cell carcinoma (LSqCC) accounts for 20-25% of NSCLC subtypes with an incidence rate of 400,000 new cases per year worldwide (Gandara et al., 2015). LSqCC patients are usually both current and former heavy smokers (Thun et al., 1997). The Cancer Genome Atlas (TCGA) project revealed an overall high mutational load in tobacco users including LSqCC patients compared to lung carcinomas in never-smoker patients (Rock et al., 2009). Unlike lung adeno-carcinoma, somatic driver mutations are less common in lung squamous cell carcinoma. The most commonly dysregulated causative genes in LSqCC are the loss of *TP53* and *CDKN2A* (Zhou et al., 2016a). LSqCC is characterized by activation in the genes that modulate the response to oxidative stress, and also amplification of chromosome 7 at the p-arm band region clustering *TP63*, *PIK3CA*, *EGFR* and *FGFR1* genes. Mutations in some genes involved in PI3K/AKT pathway have also been reported (Fang et al., 2016). The pathological differential diagnosis between LSqCC and adenocarcinoma is that the former is characterized by keratinization and intercellular bridges, and the latter has acinar or tubular structure with mucin production. Immunohistochemical markers for LSqCC include positivity to p40, CK5/6 and TP63, while adenocarcinoma is positive for TTF-1 and Napsin-A (Inamura, 2018).

1.3.*3.* Pulmonary carcinoids

Pulmonary carcinoids are very rare lung tumours with an incidence rate that does not exceed 1:50,000 population per year in European countries and America (Alsina et al., 2011, Hallgrímsson et al., 1989, Hauso et al., 2008). Smoking, either light or heavy, is not associated with pulmonary carcinoids (Hassan et al., 2008, Travis, 2014). Pulmonary carcinoids are well-differentiated neuroendocrine tumours,

including low grade malignancy (typical carcinoids “TCs”) and intermediate grade carcinoids (atypical carcinoids “Acs”) (Hendifar et al., 2017). The five years survival rate in typical carcinoids is more than 80-100%, while atypical carcinoids demonstrate 50-80% survival rate and lobectomy is the best treatment option (Gustafsson et al., 2008, Johnson et al., 2011, Fisseler-Eckhoff and Demes, 2012). Pulmonary carcinoids can be diagnosed either by CT-scan, which is the recommended diagnostic tool, or by histopathological examination of tissue biopsy. Carcinoids are characterized by their high expression of somatostatin receptors therefore, imaging of these receptors by PET-scan is a very sensitive detection method for both primary and metastatic carcinoids (Caplin et al., 2015, Leboulleux et al., 2008).

1.4. Staging of non-small lung cancer

The staging system most often used for NSCLC is the American Joint Committee on Cancer (AJCC) TNM system. The eighth edition is effective since January 1, 2018 and is based on 3 key pieces of information tumour size (T), location and presence in lymph nodes (N) and whether it has metastasised (M). It is used to evaluate the overall treatment options for the patient (Lemjabbar-Alaoui et al., 2015). Lung cancer staging can be clinical (cTNM) or pathological (pTNM) staging upon resection (Travis et al., 2008). Clinical staging depends on the information obtained from the patient history, physical examination, blood tests, bronchoscopy, imaging or surgical exploration (Travis et al., 2008). Pathological TNM staging is performed when surgical resection is completed and provides more detailed information by pathological examination of the resected tumour (Tsim et al., 2010). Both depend on the number of tumour nodules (T), the location and number of the

lymph nodes (N) invaded, and also on the presence of distant metastasis (M) (Lemjabbar-Alaoui et al., 2015, Rusch et al., 2009, Choi and Lee, 2017).

Lung cancer is staged from I to IV (Tsim et al., 2010). Figure 1.2 illustrates the criteria needed to fulfil each stage. In stage I, the lymph nodes are not involved and the primary nodules can be 1 or 2 with sizes not exceeding 5cm. If the patient has two primary tumours sized > 5cm and not exceeding 7cm and there is no lymph node invasion, the cancer will be staged as stage II. Stage II also includes patients with one lymph node and up to 3 primary tumours. If four primary malignant nodules are present with one or no lymph nodes involved, this is stage III. Stage III includes patients with two or three lymph nodes invaded plus any number of malignant nodules (>1cm) invading the nearby tissue structures e.g. heart, oesophagus, carina, chest wall or trachea (Figure 1.2). Tumours are classified as stage IV when there is distal metastasis present e.g. to the liver, bone or brain regardless of how many N and T are present (Figure 1.2) (Lemjabbar-Alaoui et al., 2015, Travis et al., 2008).

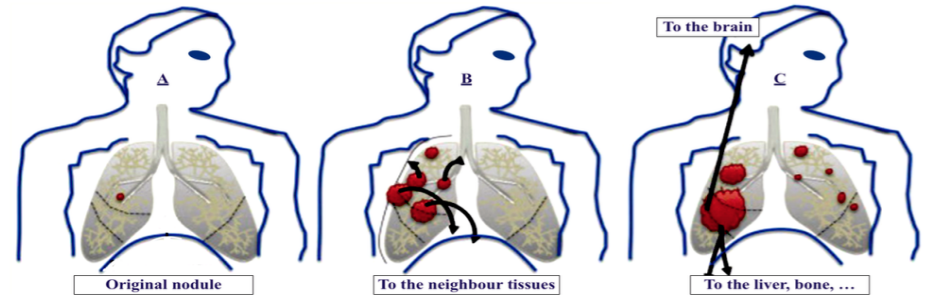

Stage I/II	Stage III	Stage IV
Stage I N0 + T1a < 2cm, T1b > 2-3cm, T2a > 3-5cm Stage II (N0 + T2b) or N1 + T1a < 2cm, T1b > 2-3cm, T2a > 3-5cm, T2b > 5-7cm, T3	(N0 + T4) or (N1 + T4) (N2 or N3) + any T Neighbour tissues invaded Trachea Main bronchus Carina Parietal pleura Chest wall Diaphragm Mediastinum Parietal pericardium Oesophagus Heart Recurrent laryngeal nerve Vertebral body	any T, any N + Distant to 1 or > organs Liver (23% & 47%) Bone (21% & 41%) Brain (17% & 39%) Adrenal gland (2% & 30%) Kidney (15% & 20%)

Figure 1.3. ***TNM staging of NSCLC.*** The 8th edition of the TNM staging for lung cancer was enacted on the 1st of January, 2018. T, tumour; N, node; M, metastasis.

1.5. Lung tumour grading

After the tumour is resected or the biopsy is harvested, fixed in formalin and with the aid of the light microscope, the pathologist examines a tissue section to determine the type of cancer cells present and whether they have spread beyond the tumour margins (Carriaga and Henson, 1995). There are standard guidelines for the collection of the biopsy as well as the description of resected tumour margin (Ehrhart, 1998). Arrangement of cells within the tissue biopsy would determine the tumour grade and accordingly tumours can be either: undetermined grade (Gx: cells look like normal cells), low grade (G1: well-differentiated) such as typical and atypical carcinoids (Hendifar et al., 2017), intermediate grade (G2: moderately differentiated), high grade (G3: cells are poorly differentiated and look different from the normal cells) such as SCLC and LCLC (Hendifar et al., 2017), or very high grade (G4: cancer cells appear totally different from the normal cells and so

called undifferentiated). However, Grade x and grade 1: denote tumours that are very slow growing, grade 2/3: denote very heterogeneous and aggressive cells that rapidly metastasize (Powers et al., 1995).

1.6. Clinical diagnosis of non-small cell lung cancer

Patients with lung cancer are usually referred to a respiratory physician by their general practitioner (GP) or from a variety of casualty and trauma departments. The signs and symptoms differ from one patient to another. Dyspnoea, haemoptysis (coughing with blood), digital clubbing, weight loss and tiredness are all common symptoms (Latimer, 2018). If symptoms have not improved by an appropriate course of antibiotics, or if the patient has other risk factors including being a smoker the following set of interventions may be requested (Quekel et al., 2003, Freedman, 2004).

1.6.1. Chest x-ray

For accurate diagnosis, two factors should be considered; the sensitivity (low threshold) and specificity (no false positive) of the diagnostic test or tool. A study presented by Quekel et al, based on their daily hospital-routine work, concluded that, the sensitivity of x-ray to detect lung cancer nodules was very low (28% and improved to 37% if the x-ray was read by two radiologists), but there isn't any effect on the specificity (up to 93%) which somehow compensates for the low sensitivity (Quekel et al., 2003). The disadvantage of using x-ray for the diagnosis of lung cancer is that often it cannot detect small nodules (early stage-curable nodules) and also the malignant nodules cannot be discriminated from benign ones (Loverdos et al., 2019). If a x-ray fails to detect lung cancer lesions, due to superimposed layers of tissues, the next step is to perform chest Computerized Tomography Scan (CT-

Scan) which has a much better sensitivity (Hossain et al., 2018, Quekel et al., 2003, Latimer, 2018).

1.6.2. Chest computed tomography

A chest computed tomography (CT) scan is an x-ray based technique. It allows the slicing of the superimposed structures of thoracic tissue layers which interfere with the cancer lesions. It improves the clinical diagnosis of lung cancer in suspicious x-ray results (Hossain et al., 2018, Sone et al., 1998). For the sake of diagnosis, a CT-Scan is only indicated if the x-ray failed to detect cancer nodules, and is usually indicated for cancer staging purposes when confirmed by histopathology (Hossain et al., 2018, Freedman, 2004). The advantage of using CT-Scan over the x-ray is connected with its high sensitivity for detecting lung cancer in suspicious x-ray, however, the specificity remains low, therefore CT-scan is not recommended as the first line in the diagnosis (Quekel et al., 2003, Freedman, 2004).

1.6.3. Tumour biopsy

Once a decision is made by the thoracic team, a biopsy from the suspicious nodule should be obtained to confirm/exclude malignancy. The following are the methods by which tissue biopsies are harvested:

1.6.3.1. Bronchoscopy

Bronchoscopy is the visualization of trachea and bronchi by a device called bronchoscope. The bronchoscope is an open tube which can be a rigid or flexible fibreoptic tube (Soyer, 2016). A bronchoscopy is indicated for obtaining samples for diagnosis such as bronchoalveolar lavage (D'amico et al., 2014) and bronchial tissue biopsy (Soyer, 2016). The bronchoscope is passed down to the trachea and the bronchi via the mouth or the nose (Van't Westeinde and van Klaveren, 2011). A video chip at the tip enables the respiratory physician to correctly and safely

harvest the required tissue biopsies (Cabrera César et al., 2018, Sakurada et al., 2005).

1.6.3.2. Medical thoracoscopy

Medical thoracoscopy (MT) is a procedure that involves access to the pleural space with an endoscope which aids in obtaining tissue under direct visual guidance. It can be done under conscious sedation without the need to put the patient under general anaesthesia, therefore considered less invasive and safe (Loddenkemper, 1998). A MT is indicated when a needle aspiration fails to obtain a diagnosable biopsy (Loddenkemper and Schönfeld, 1998).

1.6.3.3. Fine needle aspiration

A fine-needle aspiration (FNA) biopsy is harvested by a transthoracic needle introduced into a mass or cellular exudate aggregate under CT-scan guidance (Amedee and Dhurandhar, 2001). FNAs are used to minimize the un-necessary surgical resection of non-malignant nodules which accounts for up to 40% of suspicious lung neoplasm nodules (Smith et al., 2006, Aberle et al., 2011, Barta et al., 2017). According to a study conducted by Schreiber, G et al., in 2001, the sensitivity of CT-guided fine needle aspiration was 92% and the specificity was 97% in the diagnosis of lung cancer nodules (Schreiber and McCrory, 2003, Barta et al., 2017).

1.6.3.4. Sputum Cytology

Sputum can be collected spontaneously by asking the patient to cough up the mucus or induced by inhalation of saline mist to moisturize and ease sputum release (Field et al., 2002). Sputum is collected and immediately fixed in 50% ethanol and 2% carbowax and tested for the presence of cancer cells (Field et al., 2002, Ng and Horak, 1983). The sensitivity of sputum can reach 65% if the tumour is located

centrally (Squamous > adenocarcinoma) and at late stages of the disease, therefore sputum is now limited and not used for early detection of lung cancer (Sing et al., 1997, Thunnissen, 2003).

1.7. Laboratory diagnosis of non-small cell lung cancer

The histopathological classification of lung cancer relies on microscopic examination of small biopsies or cytological specimens, rendering clear histological distinctions difficult. Tumour cell shape and size (nucleus to cytoplasm ratio) and reactivity to neuroendocrine markers are assessed (Hiroshima et al., 2006). Thyroid transcription factor-1 or napsin-A are used as markers for adenocarcinoma, and p40 or p63 are used to identify a squamous cell carcinoma (Kawai et al., 2015). More recently the preservation of sufficient specimen material for appropriate molecular testing e.g. *EGFR* or *ALK* and PD-L1 expression is critical to guide therapeutic decision making (Gregg et al., 2019).

1.8. Treatment of non-small cell lung cancer

When diagnosed early, surgery is the main therapeutic intervention for lung cancer. Surgical resection via lobectomy is the standard of care in early stage NSCLC, with the goal being complete anatomic resection of the tumour and mediastinal lymph node evaluation (Padda et al., 2014). In stage IIIA, IIIB and IV NSCLC patients, surgical resection may be carried out in addition to adjuvant or neoadjuvant chemotherapy or radiotherapy (Varela and Thomas, 2014).

Screening for somatic mutations using oncogene panels such as the Oncomine Focus Hotspot panel is highly recommended for patients with advanced disease (Kerr et al., 2014). Currently, there are FDA and EMA approved targeted therapies for lung cancer tumours that harbour specific sensitising mutations (Table 1.1, 1.2 and 1.3) as in the epidermal growth factor receptor (*EGFR*) gene. *EGFR* is screened

for point mutations and deletions in the tyrosine kinase domain including L858R, Del19, G719X, S768I and L861Q (Solassol et al., 2019). Treatment includes first and second-generation tyrosine kinase inhibitors (TKIs). The T790M *EGFR* mutation confers resistance to first and second generation TKIs, so a third-generation TKI Osimertinib is now approved for treatment. Patients are also tested for mutations in the Anaplastic lymphoma kinase (*ALK*) gene and the *EML4-ALK* translocation (Wu et al., 2012). In 2011, the first generation *ALK* inhibitor Crizotinib was approved for the treatment of advanced *ALK*-positive NSCLC. Since then a further three next-generation *ALK* inhibitors have been approved including alectinib, ceritinib, and brigatinib (Uemura and Hida, 2017).

Over the past several years, immunotherapy has shown significant promise in the treatment of NSCLC. Immune checkpoint inhibitors (ICIs), composed of monoclonal antibodies that target the PD-1/PD-L1 axis have been developed which improve the antitumour immune response. Checkpoint inhibitors Nivolumab (OPDIVO) and Pembrolizumab (Keytruda) were the first to be FDA approved for NSCLC in 2015 (Vaddepally et al., 2020). Nivolumab was approved as a second-line drug to treat previously treated patients with advanced NSCLC. Initially Pembrolizumab was also approved as a second-line treatment in 2015, where the PD-L1 immunohistochemistry (IHC) > 1% tumour proportion score (TPS). However, in 2016, it was also approved as a first- line drug to treat NSCLC in patients that do not have *EGFR* mutations or ALK rearrangements where PD-L1 IHC > 50% TPS. They target PD-1 and prevent it binding to its ligand PD-L1, thus preventing the inactivation of T-cells. Atezolizumab (Tecentriq) was approved in 2016 to treat late stage NSCLC where the disease progressed after or during platinum-based chemotherapy. The combination of drugs like nivolumab and

ipilimumab have shown enhanced overall survival rate compared with chemotherapy as the first-line therapy for advanced NSCLC patients with programmed cell death ligand 1 (PD-L1) expression of at least 1% (Vaddepally et al., 2020, Alsaab et al., 2017). PD-L1 expression emerged as the first potential predictive biomarker on tumour or immune cells (Davis and Patel, 2019). Tumour mutational burden (TMB) is defined as the total number of somatic coding mutations found in cancer cells. It too has potential as a biomarker to predict response to immunotherapy (Klempner et al., 2020). Adverse-effects associated with immunotherapy such as skin rash, pneumonitis, colitis etc. are wide ranging and can involve almost every organ system. As the field advances at such a fast rate, it is crucial that these side effects are closely monitored to ensure the safety of patients (Cappelli et al., 2017).

1.8.1. Tyrosine kinases

Protein kinases are of two types: the serine/threonine kinases, transduce deep in the cytoplasm and not directly phosphorylated by the receptor tyrosine kinases and phosphorylated by lipid-based kinases such as protein kinases C (PKC) and PI3K. eg. of these kinases are cell cycle kinases, AKT/PBK and MAP kinases. The second type of protein kinases is the tyrosine kinases which plays a major role in regulation of various cellular processes that catalyse the transfer of a phosphate group from ATP to a hydroxyl group of a serine or a threonine. Among the 90 identified genes encoding proteins with tyrosine kinase activity, 58 encode receptors divided into 20 subfamilies and 32 are non-receptor tyrosine kinases, clustered in 10 sub-families (Robinson et al., 2000). Of these subfamilies, EGFR/ErbB (class I), the receptor for insulin (class II), for PDGF (Class III), for FGF (class IV), for VEGF (class V) and HGF (MET, Class VI) are mainly linked with oncological diseases. The main

characteristics of RTKs are having single trans-membrane domain and a glycosylated N-terminal extracellular domain with large number of disulfide bonds (Ségaliny et al., 2015).

The basic function of these tyrosine kinases is to regulate cell signalling that modulate cell growth and differentiation as well as cells adhesion, mobility and cells viability. Receptor tyrosine kinases (RTKs) consist of three regions: the extracellular binding domain, the transmembrane helix domain, and a cytoplasmic catalytic domain of the tyrosine kinase. Binding of the binding domain to its agonist would lead to oligomerization/ dimerization, or multimerization of the receptor which ends with auto-phosphorylation of the catalytic subunit, which then passes the phosphate group to downstream signalling molecules e.g. PI3K and MAPK (Du and Lovly, 2018, Lahiry et al., 2010).

Table 1.1. Targeted receptor tyrosine kinase family in cancer.

Class	Sub-Class	Inhibitor	Reference
Class I	EGFR	Afatinib	(Davis et al., 2011)
	HER2, 4	Poziotinib	(Romero, 2018)
	HER3	Pyrazolopyrimidine	(Lim et al., 2015)
Class II	InsR	Linsitinib (OSI-906)	(Davis et al., 2018)
	IGF1R	GSK-1838705A	(Sabbatini et al., 2009)
Class III	PDGFRa, b	CP-673451	(Roberts et al., 2005)
	KIT	Sunitinib	(Davis et al., 2011)
	CSFR	Ki-20227	(Ohno et al., 2006)
	FLT3	G749	(Lee et al., 2014)
Class IV	VEGFR1	Pazopanib	(Zhu et al., 2020)
Class V	VEGFR2,3	Pazopanib	(Harris et al., 2008)
	FGFR1	LY2874455	(Roskoski, 2020)
	FGFR2, 3	LY2874455	(Zhao et al., 2011)
	FGFR4	BLU-9931	(Jiang et al., 2017a)
Class VII	trkA	AZ-23	(Thress et al., 2009)
	trkB	GNF-5837	(Albaugh et al., 2012)
	trkC	AZD1332	(Thress et al., 2009)
Class X	MET	SGX-523	(Buchanan et al., 2009)
	Ron	BMS-777607	(Schroeder et al., 2009)
Class XIV	RET	tamatinib	(Clemens et al., 2009)
Class XIX	ALK	ceritinib	(Hoang et al., 2020)

(Davis et al., 2011, Romero, 2018, Lim et al., 2015, Davis et al., 2018, Sabbatini et al., 2009, Roberts et al., 2005, Ohno et al., 2006, Lee et al., 2014, Zhu et al., 2020, Harris et al., 2008, Roskoski, 2020, Zhao et al., 2011, Jiang et al., 2017a, Thress et al., 2009, Albaugh et al., 2012, Buchanan et al., 2009, Schroeder et al., 2009, Clemens et al., 2009, Hoang et al., 2020).

Table 1.1. Targeted non-receptor tyrosine kinase family in cancer.

Class	Sub-Class	Inhibitor	Reference
Class I	ABL1	K0706	(Antelope et al., 2019)
	ABL2	Imatinib, dasatinib, nilotinib	(Haguet et al., 2018)
Class II	ACK1	I-9b	(Lawrence et al., 2015)
Class III	CSK	dasatinib	(Tiwari et al., 2017)
Class IV	FAK	GSK2256098	(Brown et al., 2018)
	PYK2	PF-4594755, PF-4520440	(Guidetti et al., 2016)
Class V	FER	E260	(Elkis et al., 2017)
Class VI	BRK	XMU-MP-2	(Jiang et al., 2017b)
Class VII	JAK1, 3	delgocitinib	(Ma et al., 2020, Dhillon, 2020)
	JAK2	Delgocitinib, 16mI	(Ma et al., 2020, Dhillon, 2020)
Class VIII	BLK	ibrutinib	(Burger and Buggy, 2013)
	HCK	Pyrazolo-3,4-pyrimidine	(Tintori et al., 2013)
	LCK	A-770041	(Stachlewitz et al., 2005)
	LYN	Bafetinib	(Santos et al., 2010)
Class IX	BMX	MK2206	(Liu et al., 2013a)
	BTK, ITK	PCI-32765	(Vargas et al., 2013)
Class X	SYK	R788	(Weinblatt et al., 2010)

(Antelope et al., 2019, Haguet et al., 2018, Lawrence et al., 2015, Tiwari et al., 2017, Brown et al., 2018, Guidetti et al., 2016, Elkis et al., 2017, Jiang et al., 2017b, Ma et al., 2020, Dhillon, 2020, Burger and Buggy, 2013, Tintori et al., 2013, Stachlewitz et al., 2005, Santos et al., 2010, Liu et al., 2013a, Vargas et al., 2013, Weinblatt et al., 2010).

1.8.2. *PIM* kinases

The PIM family of serine/threonine kinases regulate cell survival pathways, are implicated in the progression of lung cancer (Jiang et al., 2020, Jinesh et al., 2016) and play a role in drug resistance and immune evasion in cancer (Malone et al., 2020). PIM1 enhances the transforming potential of oncogenes such as c-Myc (Wang et al., 2012) and has been shown to promote EMT and stemness in IL-6-induced breast cancer cells via c-Myc activation (Gao et al., 2019a).

MACC1 (metastasis-associated in colon cancer 1) is upregulated in several cancer types and is a marker of cancer invasion and metastasis (Wang et al., 2013, Stein et al., 2009). MACC1 and PIM3 expression are correlated in ovarian cancer (Stein et al., 2009). MACC1 activation has been shown to induce trastuzumab resistance, enhance altered metabolism known as the Warburg effect and activate the PI3K pathway in gastric cancer (Liu et al., 2016). Therefore co-targeting PI3K and PIM kinase pathways may provide a more durable response in patients (Heavey et al., 2016). Studies suggested that elevated expression of MACC-1 is positively associated with disease progression and prognosis in NSCLC patients in turn leading to short-term survival period. Recent research identified MACC1 to be over expressed in NSCLC patients and is responsible for tumourigenesis and expression of metastasis-associated genes, which enhance NSCLC cell proliferation, migration and invasion by inducing the EMT signalling pathway (Shi et al., 2017).

The majority of research focused on PIM1 has showed that PIM inhibitors are responsible for significantly increasing in ROS which in turn has a crucial cytotoxic effect towards cancer cells. However the process by which PIM produces ROS is poorly understood. Recent research has shown that lung cancer patients staging I to III have high level of PIM1, stage III had the highest level of PIM1. Patient with

high PIM 1 had significantly worse survival and poor response to chemotherapy compared with low PIM1. Since the PIM kinases expression increases are persuade in response to cellular and mechanical stress, hypoxia and nutrient deprivation, they are more likely to alter the tumour environment which accounts for the observed increase in PIM1 in later stage NSCLC. Shailender et al., 2019 with the help of mitoSOX live cell imaging demonstrated that blocking PIM directly affects mitochondrial function, independent of its ability to inhibit the Nrf2 antioxidant pathway (Chauhan et al., 2020).

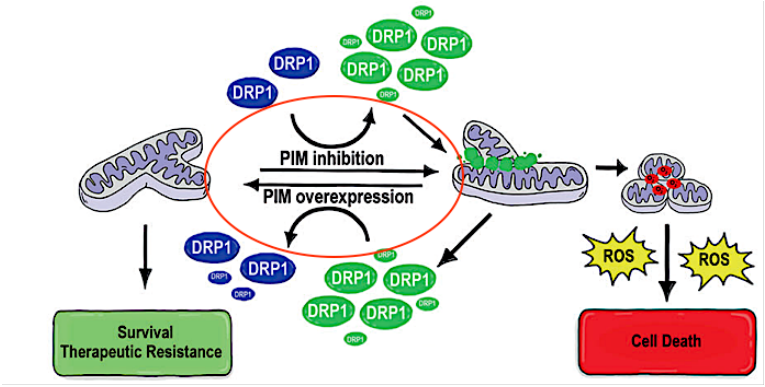

Figure 1.4. Model describing the role of PIM in regulating the mitochondrial phenotype, ROS production, and survival/therapeutic resistance. Modified from (Chauhan et al., 2020).

1.8.3. The PI3K pathway

The PI3K pathway regulates cell growth and proliferation and is often dysregulated in cancer due to mutation, amplification, deletion, methylation and post-translational modifications. PI3K pathway activation in NSCLC has been shown to lead to more aggressive disease relating to poor prognosis for patients. There are three classes of PI3K enzymes I, II and III. Class I PI3Ks are most implicated in human cancers and function as a heterodimeric lipid kinase consisting of a regulatory subunit and a catalytic subunit. There are five regulatory subunits

including p85α, p85β, p55γ, p101 and p84. p85α is encoded by the *PIK3R1* gene, which is often found to be somatically mutated in cancers including NSCLC as well as ovarian and colon tumours, with decreased expression indicating a tumour suppressing role for the gene (Philp et al., 2001, Taniguchi et al., 2010).

There are four catalytic p110 subunits including p110α, p110β, p110δ (Class 1A) and p110γ (Class 1B). The p110α isoform is encoded by *PIK3CA*, which is frequently somatically mutated in human cancers (Samuels et al., 2004). *PIK3CA* is frequently amplified (12%-20%) or mutated (2%-5%) in NSCLC, and is associated with increased AKT activity (Yamamoto et al., 2008, Kim et al., 2017, Sanders and Albitar, 2010, Courtney et al., 2010, Okudela et al., 2007, Karakas et al., 2006, Kawano et al., 2006, Zhong et al., 2006). *PIK3CA* amplification is more frequently observed in squamous cell carcinoma (SCC) than adenocarcinoma. *PIK3CA* mutations frequently coexist with *EGFR*/*KRAS* mutations (Wang et al., 2014a). p110β has been shown to be amplified in 5% of serous epithelial ovarian cancers (Brugge et al., 2007), and roles for this isoform have also been described in breast cancer (Crowder et al., 2009) and PTEN-deficient cancer cell lines (Wee et al., 2008). While p110α and p110β both commonly occur in all tissues, p110δ expression is restricted largely to the immune system (Utermark et al., 2012).

1.8.4. Targeting the PI3K pathway in NSCLC

Pan- and isoform-specific inhibitors targeting major nodes of the PI3K pathway have been evaluated in clinical trials. Initial efforts to therapeutically target the PI3K-mTOR pathway in NSCLC resulted in only a few partial responses in patients however most of the Phase I studies did not select for patients with an activated PI3K-mTOR pathway (Yang et al., 2019a). Recent *in silico* evidence demonstrated that dual targeting of mTOR and PI3K may be a promising therapeutic strategy in

patients with lung cancer with LKB1 loss (Cheng et al., 2014, Shukuya et al., 2019). Combined inhibition of PI3K and CDK4/6 in lung squamous cell carcinoma patient derived xenograft (PDX) models with *PIK3CA* mutations resulted in greater antitumour effects compared with either monotherapy alone.

Dual targeting resulted in inhibition of the PI3K and cell-cycle pathways (Shukuya et al., 2019). The BATTLE-2 study and other trials that evaluated combinations of PI3K/Akt and MEK inhibitors demonstrated modest activity and poor tolerance related to on-target inhibition of the MAP kinase and PI3K pathways in normal tissues (Papadimitrakopoulou et al., 2016, Tolcher et al., 2015, Tan, 2020, Haas et al., 2018, Jokinen and Koivunen, 2015). Several clinical trials combining a PI3K inhibitor with another targeted therapy or immunotherapy are currently at the recruitment stage including PI3K/mTOR inhibitor (gedatolisib) in combination with CDK 4/6 inhibitor (Palbociclib) for solid cancers including lung squamous cell carcinoma, PI3K-delta inhibitor (idelalisib) plus PD-1 receptor antagonist (pembrolizumab) for NSCLC, and PI3K-gamma inhibitor (IPI-549) and PD-1 receptor antagonist nivolumab in advance solid tumours including NSCLC (Knudsen et al., 2020). The FDA has recently granted fast track designation for a combination of (IPI-549) plus nivolumab for the treatment of patients with advanced urothelial cancer. As with all targeted therapies PI3K targeted inhibition has been hampered by a high rate of innate and acquired resistance. Mutations in KRAS and B-RAF, ERK hyper activation as well as extensive PI3K-MEK pathway cross-talk may provide bypass mechanisms of resistance (Heavey et al., 2018). Cen *et al.* showed that inhibition of PI3K/Akt leads to transcriptional induction of PIM1 kinase which in turn regulates the expression of RTKs in prostate cancer (Cen et al., 2013).

1.8.5. Non-coding RNAs role in non-small cell lung cancer

There are more than 8500 human non-protein coding genes and pseudogenes identified and named by the HUGO Gene Nomenclature Committee compared to 38,000 protein coding genes. Non-coding RNA are either short microRNA, which share a common function and have a conserved sequence homology, or long non-coding RNAs (ncRNAs), share no conserved sequence and thus their function is variable and only related to each other by their approximately 200 nucleotides length (Wright, 2014, Wright and Bruford, 2011, Kung et al., 2013). Both are found to play a role in many cellular processes such as cell cycle progression, cell differentiation, chromatin modification as well as controlling gene expression of protein coding genes (Spizzo et al., 2012).

1.8.5.1. MicroRNAs

MicroRNAs, are small non-coding RNAs, have a role in controlling gene expression and consequently involved in tumourigenesis and drug resistance (Mansoori et al., 2017).

1.8.5.2. LncRNA expression and nomenclature

Only 2% of human genome is translated into proteins. Cancer mutations are often found in non-coding regions when compared with coding regions. Recently, long non-coding RNAs (lncRNAs), predominantly occupy the non-coding RNAs (ncRNAs), which are considered to be the hotspots in cancer research. Due to the large number of lncRNAs, with an estimate of 102,000, lncRNA-based research holds great promise in cancer treatment.

Long non- coding RNAs, like mRNAs are transcribed by RNA polymerase II, subjected to capping and poly-adenylation and the only difference is that they are neither translated to peptide chains nor assembled as proteins (Li et al., 2016, Quinn

and Chang, 2016). LncRNAs are >200 nucleotides length, very unique, have no conserved homology sequences, and their function is variable (Wu et al., 2016, Cabili et al., 2011). LncRNAs are expressed at levels difficult to detect (very low) but found to play a role in tissue development and differentiation of specific tissues (Clark and Mattick, 2011, Wu et al., 2016, Salviano-Silva et al., 2018). LncRNA gene names are either derived from their function or from their location if they are of unknown function.

A) LncRNAs of known function: there are general guidelines for the nomenclature of lncRNAs with known function which include: 1) given a unique abbreviation describing the full gene name eg: (i) BANCR (function: BRAF-activated non-protein coding RNA) which triggers apoptosis and suppresses cancer cell invasion and migration in NSCLC (Yang and Liu, 2019), (ii) DANCR (function: Differentiation antagonizing non-protein coding RNA) which promotes cancer progression via upregulating IGF2 gene (Gao et al., 2019b), (iii) ANCR (function: Anti-differentiation non-protein coding RNA that suppress progenitor differentiation) (Kretz et al., 2012), (iv) TINCR (function: tissue differentiation-inducing non-protein coding RNA) (Kretz et al., 2013). 2) consisted of capital Latin letters and numbers (distinguishes them from rodents) eg. HOTAIR *homosapiens* vs Hotair*mus-musculus*, no punctuation but hyphens are used in certain situations eg. -AS in BACEI-AS to denote the lncRNA gene located on the negative DNA strand (anti-sense) (Wright and Bruford, 2011, Wright, 2014).

B) Pseudogene lncRNAs: Pseudogene lncRNAs even if they are linked to a function should be given the gene name plus P which stands for pseudogene eg. PTENP1 (phosphatase and tensin PTEN homology pseudogene 1) which has a tumour suppressant activity via negatively regulating AKT/PKB signalling

pathway, also binds and interferes with miRNAs that target the expression of PTEN gene (Yu et al., 2014).

C) LncRNAs of unknown function: Names of lncRNAs of unknown function, located within a protein coding gene, are derived from that gene suffixed at the end to indicate its location which can be antisense (-AS), intronic (IT), overlapping (OT). If they are located between genes, they take the root symbol LINC plus numbers (long intergenic non-coding RNA) (Harrow et al., 2012).

1.8.5.3. LncRNA as a biomarker for lung cancer diagnosis.

LncRNAs regulate splicing of mRNA, giving rise to the existence of mRNA variants, also found to play role in gene transcription and modulate protein activity and are involved in the assembly of multi protein complexes and their subcellular localisation (Wilusz et al., 2009). MALAT1 was found strongly associated with NSCLC and counted as a promising blood-based biomarker with sensitivity and specificity of 56% and 96%, respectively, with an area under ROC curve of 0.79 (Weber et al., 2013). The potential diagnostic value increased when measured in serum-isolated exosomes (sensitivity 60%, specificity 81%, AU-ROC curve 0.70), which was found positively correlated with cancer spread to lymph nodes (Zhang et al., 2017b). GAS5 lncRNA has tumour suppressant activity and is found associated with increased tumour progression and metastasis when its level is downregulated. In blood samples, GAS5 was found highly expressed in patients with NSCLC compared to healthy individuals with specificity, sensitivity and AUC of 72%, 82% and 0.83, respectively (Liang et al., 2016). HIF1A-AS1 lncRNA levels were also found in lower levels in post- surgical resection of malignant lung tumours compared to normal lung tissues (Tantai et al., 2015). The clinical utility of lncRNAs increases when used in combination as a panel of lncRNAs or in

combination with protein markers in order to increase the AUC as well as to increase the sensitivity and specificity eg. XIST (AUC=0.83) and HIF1A-AS (AUC=0.87) when combined yields an AUC of 0.93 (Tantai et al., 2015). Combinations of lncRNAs with tumour biomarkers can yield an improved diagnostic approach e.g. ANRIL and SOX2OT when combined with SCCA, CEA and CYFRA 21-1 NSCLC protein markers panel increase the sensitivity, specificity and the AUC of this protein panel in diagnosis of LSqCC (Lu et al., 2018). Table 1.1 summarizes the most common validated lncRNAs that have a potential clinical value in the diagnosis and prognosis of patients with non-small cell lung cancer. LncRNAs can be subtype-specific, and therefore might serve as important biomarkers to form a molecular signature in stratifying squamous cell carcinoma from adenocarcinoma (White et al., 2014, Zhao et al., 2014).

Table 1.2. LncRNA associated with poor prognosis in NSCLC.

lncRNA	Role in NSCLC	Reference
MALAT1	Promotes cell proliferation, migration, and invasion	(Schmidt et al., 2011)
PVT1		(Cui et al., 2016)
CARLo-5		(Luo et al., 2014)
HOTAIR		(Yao et al., 2014)
CCAT2		(Qiu et al., 2014)
MEG3	Promotes cell invasion and metastasis	(Zhang et al., 2017a)
ZXF1		(Zhang et al., 2014)
H19	Promotes cell growth	(Zhang et al., 2016a)
TUG1	Suppresses cell proliferation	(Zhang et al., 2017b)
PANDAR		(Lu et al., 2018)
BANCR		(Sun et al., 2014)
MetaLnc9	Promotes cell invasion and metastasis via Activation of AKT/mTOR signalling pathway	(Yu et al., 2017a)
MALAT1	Circulating lncRNA	(Weber et al., 2013)
	Exosomal	(Zhang et al., 2017a)
GAS5	Circulating GAS5	(Liang et al., 2016)
XIST and HIF1A-AS1 SPRY4-IT1, ANRIL, and NEAT1 SOX2OT and ANRIL	Circulating lncRNA	(Tantai et al., 2015) (Hu et al., 2016) (Xie et al., 2018)
CAR10	Upregulated /Up-regulation of EGFR	(Wei et al., 2016)

(Schmidt et al., 2011, Cui et al., 2016, Luo et al., 2014, Yao et al., 2014, Qiu et al., 2014, Zhang et al., 2017d, Zhang et al., 2014, Zhang et al., 2016a, Zhang et al., 2017a, Lu et al., 2018, Sun et al., 2014, Yu et al., 2017a, Weber et al., 2013, Liang et al., 2016, Tantai et al., 2015, Hu et al., 2016, Xie et al., 2018, Wei et al., 2016).

1.8.5.4. Targeting lncRNAs in the treatment of NSCLC

In addition to their potential role as diagnostic biomarkers, lncRNAs can also be used as biomarkers to predict responsiveness of the patient to both targeted therapy and chemotherapy (Ricciuti et al., 2016). LncRNAs can also be targeted to re-sensitise NSCLC cells to chemotherapeutic drugs (Lu et al., 2018).

Interfering RNAs (siRNAs, shRNA and antisense oligonucleotides) targeting lncRNAs were extensively tested in cell lines and showed promising results in reducing tumour invasion in many solid tumours such as prostate, breast and NSCLC e.g. HOTAIR silencing by RNAi (Yao et al., 2014), MALAT1 knockdown by shRNA (Qi and Du, 2013). Interfering with the expression of HOTAIR also restored sensitivity of lung adenocarcinoma tumour cells to cisplatin (Liu et al., 2013b).

Despite the advancement in the delivery of targeted therapy such as interfering RNA and other chemotherapeutic drugs, the use of lncRNA silencing and knockdown is still under investigation for potential clinical utility. The advantage of using antisense oligonucleotides (ASO) in the treatment of NSCLC is that they have less off-target side effects and improved specificity (Li and Chen, 2013). Knockdown of MALAT1 by ASO reduced the number of nodules and inhibited tumour progression and metastasis in a mouse xenograft model (Gutschner et al., 2013). Small molecules interfere with lncRNAs by occupying their target protein(s) interacting site and can bind lncRNAs changing its secondary structure to mimic its ability to bind and interact strongly with its partner protein, nucleic acids (Turoverov et al., 2010). Small molecules are not yet tested in lung cancer but were successful in interfering with cancer progression and metastasis in breast cancer (Lu et al., 2018).

Currently, the well-recognized lncRNA is PCA3, which has been approved for use in the diagnosis of prostate cancer. Recent research shows that lncRNAs are indeed closely related to chemoresistance, shedding new light on valuable therapeutic strategies against cancer but there is less information on the Lncrna involved clinical trials.

1.9. Mechanisms of drug resistance

To avoid the effect of chemotherapy, receptor-targeted therapy or small inhibitory molecules cancer cells can; (**A)** alter their pharmacokinetics (absorption, metabolism, elimination), or (**B)** interfere with their target receptors, thus preventing their effect (pharmacodynamics).

1.9.1. Pharmacokinetic-alteration- mediated drug resistance

Pharmacokinetic-alteration- mediated drug resistance is accomplished by either reducing drug absorption or increased drug metabolism; reducing drug absorption involves pre- and post-absorption mechanisms. Interfering with the drug entry is common with some forms of drug resistance. Anticancer agents enter cells by passive transport (eg. Doxorubicin), others by facilitative diffusion and some others via active transport such as nucleoside analogues agents e.g. fluorine-containing nucleoside analogues (Cavaliere et al., 2017). On the other hand, other drugs use specific transporters e.g. the anti-folate drug, methotrexate, competes folic acid absorption, (required for cancer cell proliferation), by binding folate carriers. So, resistance to methotrexate only occurs when folate carrier genes are mutated e.g. substitution of lysine by glutamic acid in folate transporter gene as in acute leukaemia leads to decreased methotrexate binding to folate carriers (Gifford et al., 2002, Croop et al., 1989). Hyper-methylation of ATP-binding cassette B1 (ABCB1) multiple drug resistant-1 (MDR1) was found to induce multiple drug resistance e.g.

cisplatin via decreasing the amount of drug inside the cell cytoplasm (Li et al., 2016).

Cancer cells also have the ability to repel chemotherapeutic agents outside their cytoplasm after being absorbed this reduces the availability of the drug in tumour cells (Sampath et al., 2006, Zahreddine and Borden, 2013). A family of ATP-dependent transporters mediates this process, also called ATP-binding cassette (ABC). This transporter cassette is composed of two cytoplasmic domains and two transmembrane domains (Townsend and Tew, 2003). Here are three examples of ABC-transporter cassette family members which have been found involved in the resistance of chemotherapy: 1) P-glycoprotein (PGP), which is known to pump chloride ions back outside cell membrane, binds a range of chemotherapeutic agents e.g. doxorubicin and Taxol (Townsend and Tew, 2003, Wang et al., 2019, Abe et al., 1996, Berger et al., 2005). 2) multiple drug resistance-associated protein-1 (MRP1): 12 proteins encoded by ABCC1, 9 of them are involved in transmembrane efflux of several anticancer drugs and their active metabolites in lung cancer as well as other types of malignancies (Slot et al., 2011, Young et al., 2001, Hu et al., 2018), 3) breast cancer resistance protein (BCRP/ABCG2) (Wiese, 2015).

Increased drug metabolism minimizes the availability of the drug at its target site allowing the cancer cells to tolerate and resist chemotherapy. When drugs enter the body, they are subjected to two phases of metabolism; firstly, a set of enzymes to inactivate and prepare them for further detoxification steps, these enzymes could be oxidases, reductases, and hydrolases. The second phase involves conjugation with glucuronic acid, making them more soluble for excretion through the kidneys in the urine. Cytochrome P450 is the major enzyme involved in the detoxification of drugs, activation of this enzyme results in drug inactivation and drug resistance, e.g.

docetaxel in breast and lung malignancies (Inaba et al., 2013). Inactivation of cytochrome P450 was also observed to enhance treatment response (Longo-Sorbello and Bertino, 2001). In phase II metabolism, drug conjugates to glucuronic acid, sulfate, or glutathione. Glutathione conjugation mediated by glutathione transferase enzyme, the enzyme was found responsible for resistance to alkylating agents and platinum-based chemotherapeutic agents such as cisplatin and doxorubicin (Miyake et al., 2012, Ozgencli et al., 2018).

1.9.2. Pharmacodynamics-alteration- mediated drug resistance

Two possibilities can happen to the drug-receptor interaction and consequently affects the overall expected anti-malignancy response; the level of gene expression, or the presence of certain mutations that lead to receptor conformational changes, thus masking the drug target. Epigenetic alteration also can lead to drug resistance in cancer both via decreasing drug absorption or indirectly via affecting the level of the drug target receptor expression level. DNA methylation and histone acetylation/methylation are the main post-translation modification involved in epigenetic-induced drug resistance. DNA methylation at genes coding for tumour suppression genes could silence their expression, while hyper-methylation of oncogenes genes enhance their expression (Baguley, 2016). Addition of negatively charged acetyl groups to the lysine residues of the histone terminus or non-histone proteins by the enzyme histone-acetyl transferase would open the chromatin compaction making transcription factors more accessible to their promoters, thus controlling gene expression. Overexpression of HDACS was found correlated with drug resistance to TKIs and the use of pan-HDAC inhibitor found to re-sensitize non-small cell lung cancer cell lines resistant to carboplatin chemotherapy (Holohan et al., 2013, Wang et al., 2018), and TKI (Yu et al., 2017b).

1.9.3. Non-coding RNAs role in drug resistance

Here are three examples to demonstrate how miRNAs play a role in the emergence of drug resistance in cancer: 1) miR-7 has both tumour suppressor activity (Yu et al., 2017a) and also oncogenic activity. miR-7 has been shown to mediate small cell lung cancer resistance to anthracyclines by repressing MRP1/ABCC1 expression (Liu et al., 2015). 2) miR-181a was shown to be involved in tumour resistance to cisplatin and paclitaxel in A549-NSCLC by suppression of PTEN (Yu et al., 2014) gene expression (Li et al., 2015b). 3) miR-196a was found overexpressed in A549 lung adenocarcinoma cells resistance to cisplatin. The role of miR-196a in cisplatin resistance was found mediated via suppression of MDR1/MRP1 mRNA translation. The use of anti-miR-196a small molecules reverse the resistance by interference with drug efflux mechanisms (Li et al., 2016).

In addition to their potential role as diagnostic biomarkers, lncRNAs, can also be used as biomarkers to predict responsiveness of the patient to both; targeted therapy and chemotherapy (Ricciuti et al., 2016), also to re-sensitise NSCLC to chemotherapeutic drugs (Lu et al., 2018). Interfering RNAs (SiRNAs, shRNA and antisense oligonucleotides) targeting lncRNA were extensively tested at cell lines level and showed a promising results in reducing tumour invasion in many solid tumours such as prostate, breast and NSCLC (eg. HOTAIR silencing by RNAi(Yao et al., 2014), MALAT1 knockdown by shRNA (Qi and Du, 2013)). Interfering with the expression of HOTAIR also restored sensitivity of lung adenocarcinoma tumour cells to cisplatin (Liu et al., 2013b).

1.9.4. Resistance to PI3K targeted therapy

Intrinsic resistance or the development of acquired resistance to targeted therapies may be due to the multilevel complex cross-talk signalling that occurs between the

targets of the biological agent and several signal transduction pathways. Blocking only one of these pathways may not always be an effective treatment strategy as this approach may open the door for others to act as bypass mechanisms within tumour cells. The most promising approaches to the treatment of NSCLC will be drugs with multiple targets or the use of a combination of targeted therapies.

1.9.4.1. De novo resistance to PI3K inhibition

Growing evidence has demonstrated that cross-talk, compensatory signalling and feedback mechanisms can be critical to the clinical activity of PI3K inhibitors, with PI3K inhibition being overcome within a matter of hours in some cases. Feedback induction of AKT resulting in the promotion of cell survival has been observed in response to treatment with mTOR inhibitors such as rapamycin and RAD001 (Zhou et al., 2010, O'Reilly et al., 2006). Inhibition of mTOR has also been shown to activate the ERK and IGF1 pathways, again rescuing cell survival signalling (Castro et al., 2010, Soares et al., 2013, Aksamitiene et al., 2012, Manning and Toker, 2017). Direct inhibition of PI3K and AKT has been shown to induce FOXO-mediated transcription of RTKs including IGF1R and HER3, which can then transduce survival signals to the PI3K and MEK pathways (Santo et al., 2013, Chandarlapaty et al., 2011, Faes and Dormond, 2015, Carracedo et al., 2008). These feedback and cross talk mechanisms highlight the rationale for co-targeting signalling pathways.

1.9.4.2. Acquired resistance to PI3K inhibition

Acquired resistance to targeted therapy usually occurs within 6-12 months of treatment. The mechanisms of acquired resistance typically fall into two categories: firstly; secondary mutations/amplification of the target gene, and secondly; independent reactivation of downstream signalling. Independent reactivation of

downstream signalling can also be achieved by mutation in a downstream effector gene. For example, PIK3CA mutations have been associated with acquired resistance to EGFR targeted therapy, allowing survival signalling to be sustained in the presence of RTK inhibition (Eng et al., 2015, Sequist et al., 2011). Amplification of MET has also been associated with acquired resistance to EGFR targeted therapy in NSCLC, where MET has been observed to reactivate PI3K and MEK signalling. In this case, inhibition of MET in combination with EGFR was sufficient to block downstream signalling and induce tumour regression *in vitro* and *in vivo* (Engelman et al., 2008, Bean et al., 2007). This type of acquired resistance is also referred to 'bypass track' signalling, and is similar in nature to the *de novo* resistance though it develops over a period of months rather than hours.

1.10. Intra-tumour heterogeneity

Tumour heterogeneity including: intra-tumour heterogeneity (ITH) and inter-tumour heterogeneity, is responsible for tumour aggressiveness, lack of upfront sensitivity to treatment, the emergence of acquired resistance to treatment, and tumour progression (Figure 1.3). The origin of ITH can be clonal, due to genomic instability, or non-clonal acquired from interaction with the micro-environment adjacent to the tumour mass. Knowledge of the patient tumour mass mosaic structure helps determine more appropriate treatment strategies and give more accurate information about disease prognosis (Stanta and Bonin, 2018a, Stanta and Bonin, 2018b, Fedele et al., 2014, De Sousa E Melo et al., 2013). Genomic instability includes: 1) DNA instability resulting from increased DNA replication in certain mutated RNA polymerases which have been shown to correlate with ITH, increased tumour immunogenicity and the accumulation and infiltration of immune cells in the tumour microenvironment (Briggs and Tomlinson, 2013, van Gool et

al., 2015). 2) An impaired DNA repair system during/after DNA replication, at cell cycle checkpoints resulting in chromosomal instability and leading to gene copy number alteration which in turn affects gene expression, protein function, and the acquisition of gene mutations such as point mutations, insertions, and deletions. Such alterations generate new clones of cancer cells that might be more aggressive and possibly not respond to certain targeted treatment (Rausch et al., 2017).

Epigenetics also controls gene expression and protein function. There is always a balance between oncogenes (OG) and tumour suppressor genes (TSG) to maintain controlled cell proliferation. One of the mechanisms leading to tumourigenesis is the interference with TSG expression by e.g.: methylation of their promoters which is seen in lung adenocarcinoma tumours with high degree of ITH (Quek et al., 2017). TSG activity can be compromised by altering post-translational modifications such as phosphorylation (Son et al., 2019), de-acetylation (Hu et al., 2019), or by accelerating protein turnover rate through ubiquitinated degradation (Kitagawa et al., 2009, Cole et al., 2015). The interaction between the tumour cells and their surrounding microenvironment leads to the emergence of new clones or cell populations different from those clones located in the centre of the tumour mass (Tissot et al., 2017). As the tumour grows angiogenesis occurs within the tumour mass. The random pattern of cancer angiogenesis makes the blood supply within the tumour heterogeneous, leading to the existence of clones different in their metabolic behaviour (Feron, 2009)

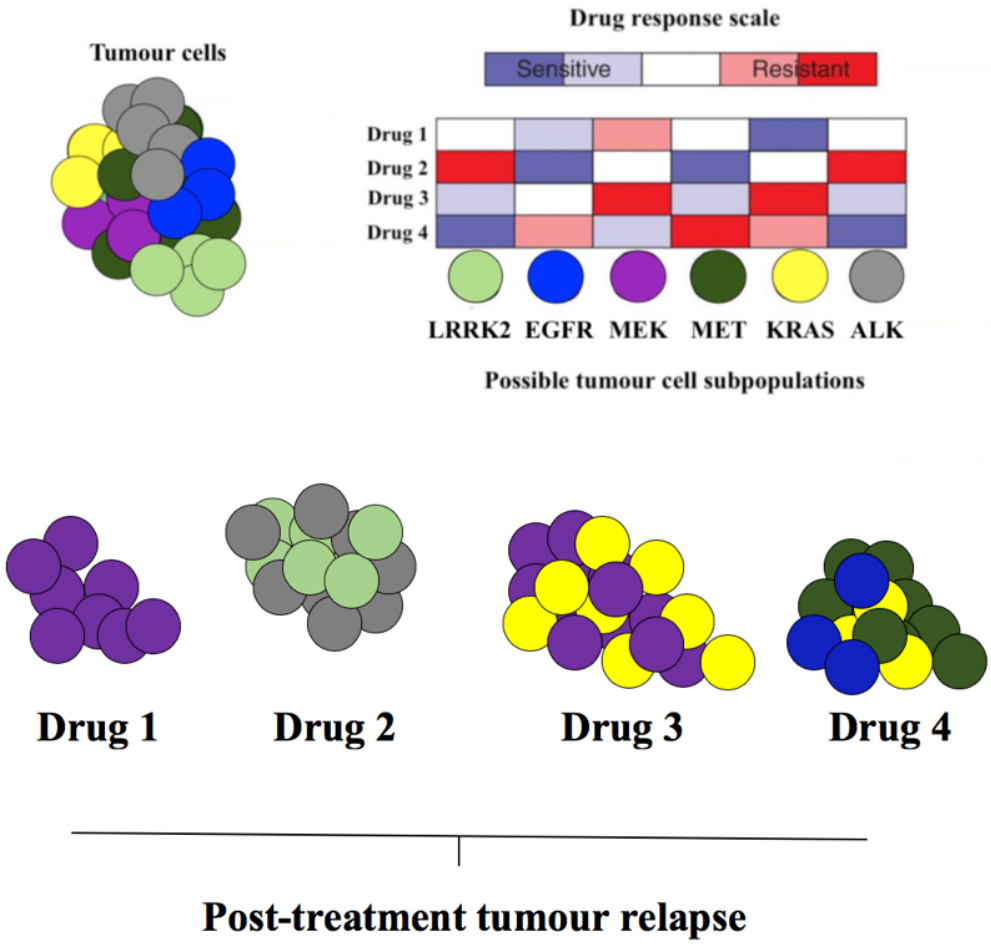

Figure 1.5. Heterogeneity theorem of treatment failure, drug resistance and disease relapse. Treatment response varies across patients and this is referred to as the heterogeneity of treatment effect. Recent studies have demonstrated that several features of tumours, such as tumour heterogeneity, altered tumour dynamics, persistence of clones, and response to therapy can be obtained not necessarily just by mutations but also from gnomically similar clones. Modified from (De Sousa E Melo et al., 2013, Fedele et al., 2014).

Cells at the centre of the tumour become hypoxic (less oxygen and nutrients as old vasculature become occluded as the tumour grows) and their metabolic behaviour is different from the cells at the marginal or sub-marginal layers which have more blood and oxygen (Okegawa et al., 2017, Eddy and Casarett, 1973). The net result of the interaction between the tumour cells and their microenvironment is variable for two reasons; cancer cells that meet the microenvironment are of multiple clones, or the stroma or the microenvironment itself is heterogeneous so, in accordance the

clonal evolution would be different (Dunne et al., 2017). The overall interaction results in changing of tumour plasticity that might alter the treatment outcome and drive the emergence of drug resistance (Stanta et al., 2016, Stanta and Bonin, 2018a, Stanta and Bonin, 2018b, Chien et al., 2013).

1.11. Epithelial to mesenchymal transition (EMT)

Epithelial to mesenchymal transition is a highly dynamic process where the epithelial cells lose its polarity and cell-cell adhesion remodelling of the cytoskeleton, and changes in cell–matrix adhesion. On the other side it is associated with cells gaining migratory and invasive properties this quality helps them to become mesenchymal stem cells often exchanging the epithelial marker E-cadherin with expression of the mesenchymal marker vimentin. EMT occurs during wound healing, tissue regeneration, embryonic development (Roche, 2018). However, EMT also plays a role in tumour progression with metastatic expansion, and the generation of tumour cells with stem cell properties. EMT is incomplete in cancer cells, and tumour cells are in various transitional states and express diverse epithelial and mesenchymal genes. Therefore cells in partial EMT move as a clusters, and can be more aggressive than cells with a complete EMT phenotype hence EMT is becoming a target of interest for anticancer therapy (Pastushenko and Blanpain, 2019).

Tumour cells derived from EMT acquire stem cell property, cell mobility, invasiveness and a reinforced resistance to apoptosis. Several signalling mechanisms are involved in the EMT process such as Epidermal Growth Factor and Transforming Growth Factor while the other pathways are known to drive EMT. Recent evidences proved that transcription factors associated to EMT may directly be involved in Carcinogenesis. *TWIST*, *SNAIL* and *ZEB* are the main transcriptional

factors which are involved in causing cancer through EMT process. In case of lung cancer *TWIST* protein plays a major role, approximately 38% of NSCLC. *TWIST* results in degradation of E-cadherin-mediated cell-cell adhesion and an EMT in epithelial cells whereas in case of *EGFR* mutant cell lines *TWIST* 1 causes low E-cadherin expression and low disease-free survival. EMT is common in NSCLC and this is due to tobacco exposure. Indeed, smoking was proved to persuade EMT. In lung adenocarcinoma cell lines (H358), cigarette smoke concentrate was able to induce EMT with activation of *SRC* kinase and the *SRC* kinase inhibitor. Up regulation or activation of EMT in NSCLC leads to resistance towards treatment particularly for cisplatin, docetaxel in A549 and for the pemetrexed-cisplatin combination. Additionally resistance to adjuvant treatment was also reported. In NSCLC having *EGFR* mutations or *ALK* fusions, EMT was also linked to resistance towards tyrosine-kinase inhibitors (TKI). NSCLC cell lines showing E-cadherin expression had greater sensitivity to *EGFR* inhibition. In contrast, NSCLC lines expressing vimentin and/or fibronectin were insensitive to *EGFR* inhibition (Legras et al., 2017).

1.12. Hypothesis and aims of this project

Intrinsic or acquired drug resistance and intra-tumour heterogeneity (ITH) result in tumour relapse and the failure of single agent targeted inhibitors. We hypothesise that elucidation of the mechanisms of resistance to PI3K-mTOR inhibition will provide a rationale for co-targeting treatment strategies for patients with dysregulated PI3K-mTOR tumours.

In-depth DNA, RNA, protein and phosphorylated protein expression profiling, within different regions of the same tumour, will provide a greater insight into the precise levels of ITH in NSCLC. Taken together these data will identify more

robust biomarkers for drug development and patient stratification for personalised targeted treatment.

Aims:

Chapter 1 - To validate markers of resistance to dual PI3K-mTOR inhibitor GDC-0980 (Apitolisib) in the H1975P/GR NSCLC cell line model of resistance, previously developed in our laboratory, to pinpoint specific bypass mechanisms of resistance.

Chapter 2 - To quantify protein and phosphorylated protein expression within different areas of the same tumour and in comparison, with matched normal tissue in a cohort of patients with lung squamous cell carcinoma.

Chapter 3 - To identify DNA mutations and quantify mRNA expression within different areas of the same tumour and in comparison, with matched normal tissue in a cohort of patients with lung adenocarcinoma.

2. **Chapter II**: Validation of markers of resistance to PI3K-mTOR inhibition in NSCLC

2.1. Introduction

Phosphatidylinositol-3-kinase *PI3K*/*AKT*/mammalian target of rapamycin (*mTOR*) signalling is one of the most important intracellular pathways, regulating diverse cellular functions including cell growth, proliferation and metabolism (Sarris et al., 2012, Memmott and Dennis, 2010). The *PI3K-mTOR* signalling pathway together with *AKT* phosphorylation is active in 50-70% of non-small cell lung cancer (NSCLC) and plays an overarching role in all the hallmarks of cancer including evading immune destruction (Yip, 2015). Pathway dysregulation confers a poor prognosis making it an ideal target for treatment (Akinleye et al., 2013). Pathway activation occurs through mutations or alterations within this pathway or parallel pathways (e.g. *EGFR* and *KRAS*) resulting in an increase in cell survival, proliferation and differentiation. Diverse genomic alterations involved in pathway activation include *PIK3CA*, *PIK3R1*, *PTEN*, *AKT*, *TSC1*, *TSC2*, *LKB1*, *MTOR* as well as upstream RTKs that drive tumour growth in a ligand-independent manner (Zhang et al., 2017c). *PIK3CA* mutations occur in 3.7% of NSCLC with higher rates in squamous cell carcinoma than adenocarcinoma (8.9% versus 2.9% respectively) and are a possible mechanism of resistance to *EGFR* tyrosine kinase inhibitor (TKI) therapy in *EGFR* mutated NSCLC (Scheffler et al., 2015). Inactivating mutations of *PTEN* (a negative regulator of *PI3K*/*Akt* signalling) (Chalhoub and Baker, 2009) as well as high frequency of *PTEN* loss (~45%) or reduced protein expression (~29%) all play a role in NSCLC tumourigenesis (Gkountakos et al., 2019).

Targeting the *PI3K* pathway has not been straightforward due to the effect of hyperglycaemia which is a mechanism-based toxicity of these agents (Khan et al., 2016). Certain high frequency mutations in the *PIK3CA* gene, which encodes the p110α protein the catalytic subunit of *PI3K*, were found to increase the catalytic

activity of the enzyme in human tumours (Samuels et al., 2004). Inhibitors targeting mutant *PI3K* and *PI3K*- isoform selective inhibitors have improved overall treatment efficacy and circumvent on-site toxicity (Hanker et al., 2019). Although there have been significant responses to targeted therapies the inevitable endpoint is drug resistance. Cancer cells become resistant to targeted agents through several mechanisms such as drug inactivation either by altering its uptake, metabolism, or excretion, or by altering the drug target or the drug itself. Other mechanisms include: bypass signalling through a parallel proliferative pathway, epigenetic modulation, gene amplification and mutations including deletions, insertions, translocations of DNA and alteration of microRNA expression (Mansoori et al., 2017, Nathanson et al., 2014).

GDC-0980 (apitolisib) is a small molecule orally bioavailable, potent, dual catalytic site inhibitor of PI3K and mTOR. In respective order, the IC50s for PI3K are 5, 27, 14 and 7 nmol/L for class I PI3Kα, PI3Kβ, PI3Kγ and PI3Kδ kinases, with an inhibition constant of 17.3 nmol/L for mTOR kinase (Sutherlin et al., 2011). The efficacy of GDC-0980 was tested in a panel of cell lines and many cell line-derived xenograft cancer models of breast, NSCLC, pancreatic, colon, prostate and melanoma with mutant KRAS and PI3K genes (Wallin et al., 2011). GDC-0980 effectively induced apoptosis and inhibited cell cycle in prostate (100%), NSCLC (88%) and breast cancer cell lines (78%) at IC50 <500 nmol/L and was less effective in melanoma (33%) and pancreatic cancer cell lines (67%) at IC50 concentration of <500 nmol/L (Wallin et al., 2011). Cell lines and cell line-derived xenograft models have long been used to undertake pre-clinical studies on the effect of drug treatment on tumour cells (Hanahan and Weinberg, 2011, Shafer and Williams, 2003) and to monitor the emergence of resistance to chemotherapy and

targeted therapies (Xavier et al., 2016, Zhang et al., 2010, McDermott et al., 2014). A panel of lung cancer cell line models of resistance to GDC-0980 was previously developed by Dr. Gately's group. The H1975 cell line was exposed to its IC50 dose of 0.58μM GDC-0980 for a period of 4 months until a log fold difference in IC50 between the resistant cells (H1975GR) and the sensitive parental cells (H1975GP) was observed (Heavey et al., 2018). H1975 cells harbour mutations in *EGFR, PIK3CA* and *PIK3R1*, and our group has previously shown they express *PI3K* pathway signalling phosphoproteins more highly than the other cell lines used in the study (Heavey et al., 2018). The H1975 cells were the most sensitive cell line to GDC-0980 (apitolisib) treatment and were the first to develop resistance. In fact, this cell line began to exhibit decreased sensitivity to the drug after just one month. As such, the drug mediated significant effects in the short term, but the increased selective pressure activated bypass signalling escape mechanisms that allowed the cells to become rapidly resistant to the drug. The aim of this chapter was to validate previously elucidated drug resistance mechanisms in the GDC-0980 resistant cell line H1975GR.

2.2. Experimental design

GDC-0980 (apitolisib®) sensitive (H1975GP) and resistant (H1975GR) lung adenocarcinoma cells were cultured as described in section 2.3.2. Total RNA was isolated and analysed on the Arraystar Human LncRNA Microarray V4.0 and the expression of 20,730 mRNAs & 40,173 lncRNAs were quantified.

The set of lncRNAs covered by the Arraystar Human LncRNA Microarray V4.0 is carefully constructed using public transcriptome databases (Refseq, UCSC known genes, Gencode, etc), as well as landmark publications.

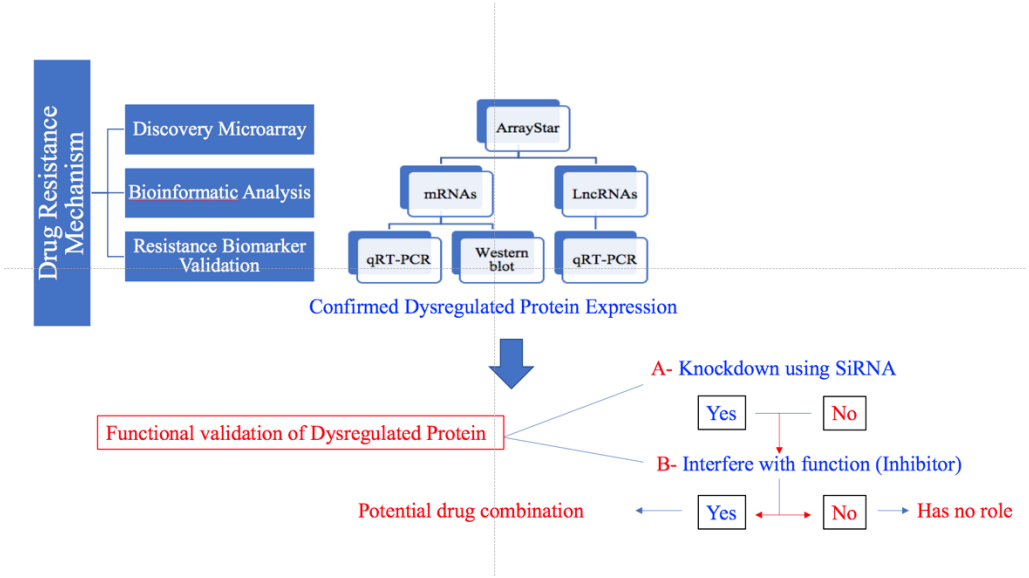

Figure 2.1. Detailed experimental design flowchart of GDC-0980 resistance study in H1975 adenocarcinoma cells.

A list of upregulated and down-regulated mRNAs and long non-coding RNAs were identified and are tabulated in appendices 2.1 to 2.56. The *PIM* kinase pathway and its regulators; LncRNA (*AC008*, *LINC01510*, *LINC01969*, *CASC11*) and mRNA (*MACC1*, *PIM1/2/3, CMTM6, c-Myc*) and protein levels were validated by qRT-PCR and western blot, respectively (Figure 2.1). To evaluate the role of *MACC1* and PIM kinases in the development of GDC-0980 resistance in H1975 cells, small interfering RNAs (siRNAs) targeting both genes were used to inhibit their expression. DharmaFECT 1™ (Horizon™ Inspired Cell Solutions) was used as the transfection reagent (Jensen et al., 2014). The effect of siRNA or GDC-0980 treatment alone or in combination was then assessed using Cell Titer-Blue® Cell Viability Assay utilizing the reduction of Resazurin to Resorufin in the viable cells. A pan-PIM kinase inhibitor AZD-1208 was used to evaluate the role of PIM kinases in GDC-0980 resistance in H1975 cells. Finally four genes *DSP* (desmoplakin), *TNC-c* (tenascin c), *ERO1A* (*ERO1-La*), *ENO1* (enolase-1) were also assessed in the H1975GR compared to H1975GP on the basis they were linked to drug resistance in the literature and were found heterogeneously expressed on different

tumour regions (n=3) in four patients with lung squamous cell carcinoma (chapter 3).

2.3. Materials and methods

2.3.1. PI3K-mTOR inhibitor (GDC-0980) resistant cell line model

H1975 cells resistant to GDC-0980 (apitolisib) were previously developed in the lab as follows: H1975 lung adenocarcinoma cells were treated with different concentrations of PI3K-mTOR dual inhibitor GDC-0980 and the IC50 concentration was then calculated using the BrdU proliferation assay (Roche diagnostics Ltd, Ca #6813S). The IC50 for the H1975 parent cells was 0.58μM GDC-0980 (seeding density 10000 cells). A BrdU assay was carried out each month to assess the development of resistance to GDC-0980 by comparing the IC50 of H1975 resistant cells (H1975GR) to the IC50 of the age-matched parental cells H1975GP. When matched parent-resistant cell line pairs reached a log fold difference of IC50, acquired resistance was deemed to have developed (Heavey et al., 2018).

2.3.2. Cell culture of resistant cell line models

H1975 Lung adenocarcinoma cells (NCI-H1975, ATCC® CRL-5908™) were cultured in RPMI-1640 medium (Sigma R5886), supplemented with 10% foetal bovine serum (Sigma, Lot: BCBR 1178V) and 1% penicillin-streptomycin-glutamine (Gibco™ Cat No: 10378-016).

H1975GR cells were cultured in the same medium with the addition of 0.58μM GDC-0980 at all times. Cells were harvested at 80% confluence, washed three times with 3 mL of sterile 1X PBS, detached by using 3 mL of trypsin (1X trypsin/EDTA, Sigma-Aldrich®) incubated for 2 min at 37°C and then gently tapped. When the cells detached from the flask, 5 mL of complete RPMI media was then added to

deactivate trypsin. Cells were harvested in 15 mL falcon tubes, labelled accordingly, and centrifuged at 1300 rpm for 1 min at room temperature, the cells pellets were then resuspended in complete media and passed to new flasks.

2.3.3. Total RNA extraction

H1975GP and H1975GR cells, grown in T75 flasks in RPMI medium, were harvested at 80% confluency. The All Prep-DNA/RNA/miRNA universal kit (Qiagen Cat. #80224) was used to extract total RNA from both cell lines. The cells pellets were lysed in 350 µL RTL Plus (provided) and sonication for 3 cycles each of 30 seconds with 1 minute intervals of ice incubation. The disrupted cells suspension was then transferred to an All-prep DNA mini spin column placed on 2 mL collection tube (supplied) centrifuged for 1 min (the membrane now contains the DNA). The flow-through containing RNA was then treated with 50 µL proteinase K and 350 µL 96% ethanol, mixed well and then incubated at room temperature for 10 minutes, then more 750 µL 96% ethanol was added and 700 µL of the ethanol-containing RNA was then transferred to RNeasy Mini spin/2 mL collection tube (provided), centrifuged for 15 s, the flow-through was then discarded. 80 µL of DNase I cocktail (10 µL of DNase I in 70 µL buffer RDD) was then applied onto the RNeasy Mini spin column membrane (to degrade DNA contaminant), then incubated for 15 minutes at room temperature. 500 µL buffer FRN was then added to the spin column membrane, centrifuged for 15s (flow-through was then returned onto the RNeasy spin column/new 2 mL collection tube, centrifuged again to bind as much RNA as possible), the flow-through was then discarded. The RNeasy column membrane was then treated with 500 µL buffer RPE, centrifuged and the flow-through was then discarded. The membrane was then washed by adding 500 µL ethanol/ centrifugation for 2 min (flow-through returned

back, centrifuged again at same speed/time). The RNeasy column was then placed onto 1.5 µL RNase-free collection tube and the RNA was eluted in 50 µL RNase-free water/ centrifugation at 10,000 x g for 1 min. All centrifugation steps were at 20,000 x g unless otherwise specified.

2.3.4. Arraystar® Human LncRNA Microarray V4.0

5 µg of RNA, from GDC-0980 naïve cells (H1975GP), one month GDC-0980 treated H1975 (H1975GR1) and six months GDC-0980 treated H1975 cells (H1975GR6) (cells are now resistant to GDC-0980), was analyzed on the Arraystar® Human LncRNA Microarray V4.0 and the expression of 20,730 mRNAs & 40,173 LncRNAs were quantified. The set of LncRNAs covered by the Arraystar® Human LncRNA Microarray V4.0 is carefully constructed using public transcriptome databases (Ref. sequence, UCSC known genes, Gene code, etc.) as well as landmark publications.

2.3.5. Validation of ArrayStar® data using RT-PCR

A set of mRNAs including *MACC1*, *PIM1*, *PIM2*, *PIM3, c-Myc*, *CMTM6* and *MACC1* and their expression regulatory lncRNAs: *CASC11*, *LINC01510*, *LINC01969*, and *AC008163.4* were identified from the arraystar dataset and then validated by RT-PCR as follows:

2.3.5.1. Primer design.

NCBI sequences of the above mentioned mRNAs and lncRNAs were retrieved from PubMed nucleotides, their reference numbers are: *PIM1: NM_001243 186.1, PIM2: NM_006875.4, PIM3: NM_001001852.4, CMTM6: NM_0178 01.3, MACC1: NM_182762.4, c-Myc: NM_002467.6, CASC11: NR_117101.1, LINC01510: NR_120506.1, LINC01969: NR_110806.1, AC008163.4 NR_12602 5.1.* and Beta actin (*ACTB*) PubMed reference number NM_001101.5 was used as

a loading control. The online Primer3Plusat http://www.bioinformatics.nl/cgi-bin/primer3plus/primer3plus.cgi. was used to design PCR primers for qRT-PCR (Table 2.1).

2.3.5.2. Total RNA extraction for PCR

RNeasy mini kit (Qiagen®, Cat No./ID: 74104) was used to extract the total RNA from H1975GP and H1975GR cells, the amount of total RNA was measured by NanoDrop and stored at -80°C.

2.3.5.3. Synthesis of first strand cDNA

Volumes equivalent to 500ng total RNA was used from both H1975GP and H1975GR cells and the mRNA was converted to cDNA using SuperScript™ III Reverse Transcriptase (Cat. 18080093). The reaction involved incubation of the following contents; 1 µL oligo dT (50 µM) + 500ng total RNA + 1µM dNTPs (10 mM) + 13 µL sterile H_2O, at 65°C for 5 min followed by 1 min ice incubation and spun down the contents. The following reagents were then added to the reaction; 4 µL 5x PCR buffer + 1 µL dTT (0.1M)+ 1 µL RNase inhibitor + 1 µL SuperScript™ III reverse transcriptase (200 unit/µl), mixed well by pipetting and the reaction was then incubated at 50°C for 1h. The reaction was deactivated by heating to 70°C for 15 min.

Table 2.1. List of primers used for qRT-PCR validation of selected arrayStar-altered mRNAs and lncRNAs.

Gene	Primer sequence	Start/End	Flanked junctions	PCR product
ACTB	FWD 5'TGTTTGAGACCTTCAACACCC'3	452	[4/5]	529bp
	REV 5'AGCACTGTGTTGGCGTACAG'3	980		
PIM1	FWD 5'CAGAGTGGATCCGCTACCAT'3	1059	[5/6]	226bp
	REV 5'TGGATTTCTTCGAAGGTTGG'3	1284		
PIM2	FWD 5'TCGAGGCCGAGTATCGACT'3	273	[2/3] [3/4]	161bp
	REV 5'TGGGCATGTGA CTGAGTCTG'3	433		
PIM3	FWD 5'TCTCCAAGTTCGGCTCCCT'3	184	[1/3]	222bp
	REV 5'TCACCCGC TCCTTCACCAC'3	405		
CMTM6	FWD 5'CCACACATGACAGGACTTCAGC'3	484	[3/4]	189bp
	REV 5'CTCCCCAGA GTCTTTAGGCATT'3	672		
MACC1	FWD 5'TGGTGAACCAGTTGCACAGT'3	1509	5	204bp
	REV 5'AGCACTGCCTTCAGGGTTAC '3	1712		
c-Myc	FWD 5'GGAGAATGTCAAGAGGCGAA'3	1461	3	183bp
	REV 5'TTTTGCTCCT CTGCTTGGAC'3	1643		
CASC11	FWD 5'CCACTGCTAATGAACATCACCC'3	110	[1/2]	174bp
	REV 5'GCTC TTTTCACTAGAGGACCAACTC'3	283		
LINC01510	FWD 5'GATGAAGTCAACAGCTGCTGGA'3	710	[4/5]	162bp
	REV 5'CTGCTCTGTGCGGTTTCTGA'3	871		
LINC01969	FWD 5'TGTGTCCCATCTCCCCTTC G'3	11	[1/2] [2/3]	247bp
	REV 5'AGGCACTGGTGATTGGGCAA'3	257		
AC008163.4	FWD 5'CTACTCTTTGGAAACTGAGGCAAC'3	1181	[10/11]	215bp
	REV 5'CTGGTTCAGCCAAGCTTGTAGT'3	1395		

2.3.5.4. PCR amplification

To demonstrate the importance of *DSP* (desmoplakin), *TNC* (tenascin c), *ERO1A* (ERO1-La), *ENO1* (enolase-1) as a resistance gene panel, chosen based on the literature review, beside the PIM kinases, their levels were tested in a lung adenocarcinoma cell line panel: A549, H1975, H3255, H3122, H2228, HCC827, H1819 (derived from metastatic site-lymph-node), adeno-squamous lung carcinoma: H596, large-cell lung carcinoma (derived from metastatic site-pleural effusion: H460). 1 µL of H1975GP or H1975GR cDNA was used per reaction. The primers used to amplify *AC008163*, *LINCO1969*, *LNICO510*, *CASC11*, *PIM1/2/3*, *CMTM6*, *c-Myc* and *MACC1* are listed in table 2.1. The PCR reaction involved 12.5 µL 2XGOTaq + FW primer 1 µL + Rev primer 1 µL + 9.5µl dH_20. The PCR cycling program consisted of an initial denaturation at 95°C for 1 min followed by 40 cycles as follows (denaturation for 1 min at 95°C, annealing for 1 min at X°C temperature (Table: 2.2), extension at 72°C for 1 min) and incubation at 72°C for 10 min to allow the synthesis of incomplete synthesized amplicons. The PCR reactions were held at 10°C until their removal for analysis on 2% agarose gel electrophoresis.

Table 2.2. mRNA PCR validation (primers annealing temperature)

Amplicon type	Gene mRNA						lncRNA			
Amplicon name	CMTM6	MACC1	PIM1	PIM2	PIM3	c-Myc	CASC11	Linc01510	Linc01969	AC008
Annealing temperature	58°C	58°C	58°C	58°C	58°C	58°C	64°C	58°C	65°C	61°C
Left primer Tm	61.45°C	60.0°C	60.1°C	59.4°C	62.2°C	58.5°C	59.3°C	60.9°C	61.3°C	59.8°C
Right primer Tm	59.49°C	60.0°C	60.0°C	60.9°C	64.7°C	58.4°C	61.1°C	60.6°C	62.8°C	60.8°C

2.3.5.5. Agarose gel electrophoresis

8 µL of PCR product from both H1975GP and H1975GR were loaded into a 2% agarose gel, prepared in 1 x Tris-Acetate-EDTA (TAE), containing 5 µL ethidium bromide, a 100 bp ladder was used to identify the amplicon size. Images were taken on the Vilber Fusion Smart Imaging System and saved as tiff images.

2.3.5.6. PCR bands quantification by ImageJ

The tiff image of the PCR results was imported into ImageJ software and a rectangle was drawn around the first band and given number 1 (cmd+1), then moved to the next right band and given number 2 (cmd+2), then the rest of bands were given number 2 until the last one which given number 3 (cmd+3). The values were then copied and inserted into the prism 7 software for column graphical presentation.

2.3.5.7. Quantitative real time PCR (qRT-PCR)

1 µL of H1975GP or H1975GR cDNA was added (in triplicate) to the PCR reaction as follows: 12.5 µL 2XGOTaq, 1 µL FW primer, 1 µL Rev primer, 9.5µl dH_20. The PCR cycling program consisted of initial denaturation at 95°C for 1 min followed by 40 cycles of (denaturation for 1 min at 95°C, 1 min annealing temperature and an extension step at 72°C for 1 min (Table 2.2)). The average of each set of triplicates was presented as a column graph and the significance was calculated using unpaired two-tailed parametric t test by prism 7 software.

2.3.5.8. Fold change calculation

The average Ct (threshold cycle) was taken and the Ct value of each tested RNA was then normalized (ΔCt) as in equation 1 by subtracting the value of its average housekeeping gene (HKG) Ct value. The change in the copy number (ΔΔCt) of the tested RNA (coding/non-coding) in the H1975GR compared to the H1975GP was

then calculated as in equation 2 by subtracting ΔCt of the H1975GP from the ΔCt of the H1975GR. At the end, the fold change was calculated as in equation 3.

$$Normalized\ Ct\ values\ (Ct) = Mean\ Ct\ (Test) - Mean\ Ct\ (HKG) \qquad Equation\ 1$$

$$Ct = Ct\ (H1975GR) - Ct\ (H1975GP) \qquad Equation\ 2$$

$$Fold\ change\ (FC) = 2^{-Ct} \qquad Equation\ 3$$

HKG: housekeeping gene.

2.3.5.9. Western blot

30µg of total protein was used to compare the expression of proteins in H1975GP compared to the matched age H1975GR. Primary and secondary antibodies used in this study are listed in table 2.4.

2.3.5.9.1. SDS-proteins resolving

30 µg of each protein sample was diluted in a 2X Laemmli buffer in a fume hood (recipe see table 2.3) and heated to 95°C for 10 min on a heating block. Samples were immediately cooled down by incubation on ice for at least 2 min and then loaded onto a 12 % SDS polyacrylamide gel. The electrophoresis conditions were: 400V and 50mA for 80 min in 1X electrophoresis running buffer (recipe see table 2.3). Pre-stained coloured protein marker (Cell-Signalling Technology: cat. #14208) was used to assess the molecular sizes.

2.3.5.9.2. Electro-transfer of the resolved proteins onto PVDF membrane

The resolved proteins were transferred from the gel onto PVDF membrane (0.4 µm pore diameter) in 1X transfer buffer (recipe see table 2.3) using Bio-Rad® transfer unit at 100 V and 400mA for 90 minutes, or at 25 V overnight depending on the molecular size of the protein (large proteins needs longer time). The transfer

cassette order from positive to negative as follow: Sponge, three absorbent papers, followed by a PVDF membrane, then by the SDS gel containing the resolved proteins (with coloured protein marker to the left) and on top three more layers of absorbent paper followed by another sponge at the end.

Table 2.3. Required reagents for protein electrophoresis

Sample loading Laemmli buffer (2X) recipe: 4 ml β-mercaptoethanol, 10 µL of 10% bromophenol blue, 4 mL glycerol, SDS 1g and 2 mL of 1M Tris-HCL pH 6.8.
Electrophoresis running buffer (5X) recipe: 15g Tris base, 72g glycine and 5g SDS in 1000 mL ddH2O. Mix 200mL of 5X running buffer and add up to 1000 mL ddH2O to make 1X working running buffer.
SDS polyacrylamide gel 12% recipe: **a-** 12% resolving gel (8 mL per gel): 3.2 mL 30% acrylamide, 2 mL 1.5M Tris pH 8.8, 80 µL APS, 80 µL 10%SDS, 8 µL TEMED* and 2.6 mL ddH2O. **b-** 6% stacking gel (5 mL per gel): 1 mL 30% acrylamide, 1.25 mL 0.5M Tris pH 6.8, 50 µL 10% APS, 50 µl 10% SDS, 5 µL TEMED* and 2.6 mL ddH2O.
Electro-Transfer buffer 10X recipe (1L): 15.2g Tris base, 72.1g glycine and 5g SDS in up to 1000mL H2O. To make 1X transfer buffer Mix 80 mL of 10X transfer buffer, 200 mL methanol and 720 mL H2O.
Blocking buffer recipe: 5% w/v non-fat skimmed milk (Marvel skimmed milk powder, Premier Food Group Ltd., UK) in 1X PBS containing 0.01% Tween-20® (PBST).

* added at the end when the cast is ready.

2.3.5.9.3. Membrane blocking and antibody incubation

At the end of the transfer step, the membrane was immediately immersed into the blocking buffer (recipe see table 2.3) for 1h at medium shaking. The membrane was then washed x3 with 1X PBS/0.1% Tween-20®, then incubated with the primary antibody (Table 2.4) overnight at 4°C slow/medium speed rotation. The PVDF membrane was washed 3X-times with 1X PBS/0.1 Tween-20® and then incubated

with the secondary antibody (anti-mouse IgG HRP-linked antibody (Cell Signalling cat. No. 7076) or anti-rabbit IgG HRP-linked antibody (Cell Signalling cat. No. 7074) for the duration of 1 h. The membrane was then washed x3 TBST and stored in 1X TBS/0.1 Tween-20® washing buffer at 4°C until the signal developed.

2.3.5.9.4. Signal retrieval (chemiluminescence) and ImageJ quantification

5 mL (at 1:1 volume ratio of reagents A and B) of ECL western blotting substrate (Pierce Thermo-Scientific, prod. #32106) was directly applied onto the membrane for 2-3 min. The chemiluminescent signal corresponding to the amount of the protein in the sample was captured using Vilber-Fusion Smart Imaging System (was set to auto-detection of signal). Captured images were then saved as tiff files and Image-J software (version K 1.45) was used for densitometry analysis to quantify protein expression. The chemiluminescent signal values equivalent to the amount of tested protein were recorded, then normalized to beta-actin/or alpha tubulin content measured on the same membrane, and then compared between the H1975GP and H1975GR cells using GraphPad Prism8.

Table 2.4. mAbs used to quantify protein expression in H1975GP and H1975GR cells.

Product. No	1ry antibody	Iso- type	Size (kDa)
9402S	c-Myc (D84C12)	mAb	57/70
34557S	CMTM6	mAb	22
4560S	C-Met	mAb	145
86290S	MACC1 (D2K2V)	mAb	97
54523S	Pim-1 (D8D7Y)	mAb	S34/L44
4730S	Pim-2 (D1D2)	mAb	34/38/40
4165T	Pim-3 (D17C9)	mAb	35
2148S	a/b tubulin	mAb	52/55
8457S	Beta actin (D6A8)	mAb	45

All antibodies were ordered from Cell Signalling Technology®.

2.3.6. Functional validation

2.3.6.1. Cell viability assay

H1975GP and H1975GR were cultured and seeded at a density of 5000 cells/well in separate 96-well plates as described under section 2.3.2. The cells were then treated accordingly with siRNAs or GDC-0980 or AZD-1208 or combination of both, incubated at 37C/5%CO2 for 72h. The medium was then replaced with 100 µL freshly prepared RPMI, and 20 µL CellTiter-Blue® (Cat# G8080) was added to each well, mixed for 10 seconds, protected from light and incubated for 3h at room temperature (1-4h recommended). The plate was then read at 604 nm emission and 578 nm excitation.

2.3.6.2. siRNA

siRNAs targeting *PIM1*, *PIM3*, *MACC1* and *CMTM6* were transfected separately into H1975GP and H1975GR cells as follows: The recommended volume of siRNA is 0.5µl (5µM) and the recommended volume of DharmaFECT1™ stock solution was between 0.05-0.5µl per 100µl per well (0.2µl per 100µl per well was used). siRNA stock concentration (5nmol) diluted to 20µM with serum-free RPMI medium and further diluted to 2µM (1:20 dilution): 75µl (20µM SiRNA) plus 1425µl serum-free RPMI to make 1.5 ml of 2µM siRNA. H1975GP or H1975GR cells were seeded in triplicates at a density of 5,000 per well of 96 well-plate in antibiotic-free complete RPMI medium and incubated at 5% CO2 and 37°C overnight. The plate map was illustrated below (Figure 2.2B). Untreated cells and non-targeting siRNA (CTL) were used as a control. H1975GP or H1975GR, were seeded in triplicates in eight series; un-treated, *MACC1* treated, GDC-0980 treated, *MACC1*+GDC-0980 treated, CTL treated, CTL+GDC-0980 treated, *PIM3* treated and *PIM3*+GDC-0980 treated cells. The following day the siRNA and the

DharmaFECT1™ transfection solution were diluted to the recommended volume and concentration with serum-free medium and the transfection mixture was prepared as shown in Figure 2.2A. Serum-free medium was supplemented with 0.58μM GDC-0980 for siRNA+GDC-0980 treatments. 100 μl of the prepared transfection medium was then added to each well and the plate was incubated for 72 hours. Cell viability assay was carried out as mentioned above under section 2.3.6.1. The treatment fluorescence values were normalized to the average of the untreated fluorescence values and were then plotted against treatment combinations and the significance p-values were calculated by prism 8.0 software.

A

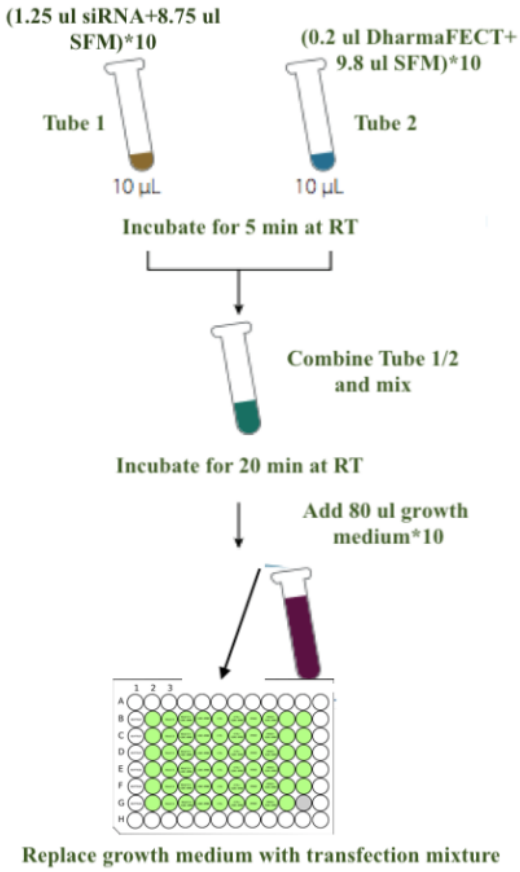

B

H1975GP	UT	MACC1	MACC1+GDC	GDC	CTL	CTL+GDC	PIM3	PIM3+GDC
H1975GP	UT	MACC1	MACC1+GDC	GDC	CTL	CTL+GDC	PIM3	PIM3+GDC
H1975GP	UT	MACC1	MACC1+GDC	GDC	CTL	CTL+GDC	PIM3	PIM3+GDC
H1975GR	UT	MACC1	MACC1+GDC	GDC	CTL	CTL+GDC	PIM3	PIM3+GDC
H1975GR	UT	MACC1	MACC1+GDC	GDC	CTL	CTL+GDC	PIM3	PIM3+GDC
H1975GR	UT	MACC1	MACC1+GDC	GDC	CTL	CTL+GDC	PIM3	PIM3+GDC

Figure 2.2. Overview of siRNA functional validation. A: experiment schematic diagram **B**: plate map and proteins being validated. The H1975GP were seeded in the upper three rows wells, while H1975GR were seeded in the lower three rows wells. In both experimental sections; the first triplicate the cells were not treated, in the second column triplicates cells were treated with MACC1 siRNA, the next column triplicates cells were treated with MACC1 plus GDC-0980, in the next right column cells were treated with GDC-0980, the next column cells treated with non-specific targeting siRNA (CTL) as a control, next column cells were treated with CTL and GDC-0980, and in the last two columns, cells were treated with PIM3 siRNA and PIM3 plus GDC-0980, respectively.

2.3.6.3. Targeting PIM kinase in GDC-0980 resistant cells (H1975GR)

2.3.6.3.1. Dose response curve to evaluate the IC50 of AZD1208 in H1975GP and H1975GR cell lines

Serial dilutions (n=8) from 60µM till 20µM of AZD1208 were prepared as follows: 520 µL of 2.5µM AZD1208 was prepared in RPMI (130 µL 10 mM AZD1208 + 390 µL RPMI). Then 8 tubes were labelled and received volumes mentioned in table 2.5 to make final concentrations ranging from 120 to 40 µM. All replicates of cultured cells (H1975GP and H1975GR) in 100 µL RPMI received 100 µL of the prepared AZD1208 concentrations (Table 2.5) to make final concentrations of 60µM, 50µM, 45µM, 40µM, 35µM, 30µM, 25µM and 20µM AZD1208. Cell viability assay was carried out as mentioned above. IC50 was calculated using IC50 calculator available at https://www.aatbio.com/tools /ic50-calculator (Dratkiewicz et al., 2019).

Table 2.5. Optimized AZD1208 serial dilutions to calculate the IC50.

	Tube 1	Tube 2	Tube 3	Tube 4	Tube 5	Tube 6	Tube 7	Tube 8
AZD1208 (2.5mM)	48	40	36	32	28	24	20	16
RPMI	952	960	964	968	972	976	980	984
Conc. (µM)	120	100	90	80	70	60	50	40

2.3.6.3.2. Dose response curve to evaluate the IC50 of GDC-980 in H1975GP and H1975GR cell lines

GDC-0980 10 mg (RG7422) Cat.S2696 (Selleckchem.com) was dissolved in 2 ml DMSO to make 10 mM final concentration stock solution. 60 µL of the stock solution were then added to 5940µl RPMI to make 6 mL of 100µM GDC0980 in RPMI. This 6ml of (100µM GDC-0980) was then used to prepare 2 ml serial dilutions of: 2, 4, 5, 10, 30, 35, 50, 80µM as in table 2.6. All cell replicates received 100µl of prepared concentrations to make final concentrations of 40, 25, 17.5, 15, 5, 2.5, 2 and 1µM GDC-0980 (from left to right). Cell viability assay was made as mentioned above. The dose-response curve was then constructed by plotting the cell viability fluorescence values against the log GDC-0980 concentration (nM). The IC50 was then calculated using the online AAT Bioquest® IC50% calculator at https://www.aatbio.com/tools/ic50-calculator (Dratkiewicz et al., 2019).

Table 2.6. GDC-0980 preparation for dose-response curve.

	Tube 1	Tube 2	Tube 3	Tube 4	Tube 5	Tube 6	Tube 7	Tube 8
GDC-0980 (100 µM)	40	80	100	200	600	700	1000	1600
RPMI (µL)	1960	1920	1900	1800	1400	1300	1000	400
Conc. (µM)	2	4	5	10	30	35	50	80

2.3.6.3.3. Drug combination of GDC0980 and AZD1208

Calculated GDC-0980 IC40 13.8µM and 4 AZD1208 doses; (A) IC90: 60.255µM, (B) IC60: 47.863µM, (C) IC50: 39.810µM and (D) IC30: 30µM were selected for drug combination study. H1975GR cells were seeded at a density of 5000 cells/well, left to adhere overnight at 37°C/5%CO2. Cells were treated in replicates as detailed in Figure 2.3 and then incubated at 37°C/5%CO2 for 72h. Cell viability assay was carried out as described in section 2.3.6.1. The dose-response curve was then constructed by plotting the cells viability versus treatment concentrations/combinations and the IC50 was calculated using the online AAT Bioquest® IC50% calculator at https://www.aatbio.com/tools/ic50 -calculator (Dratkiewicz et al., 2019).

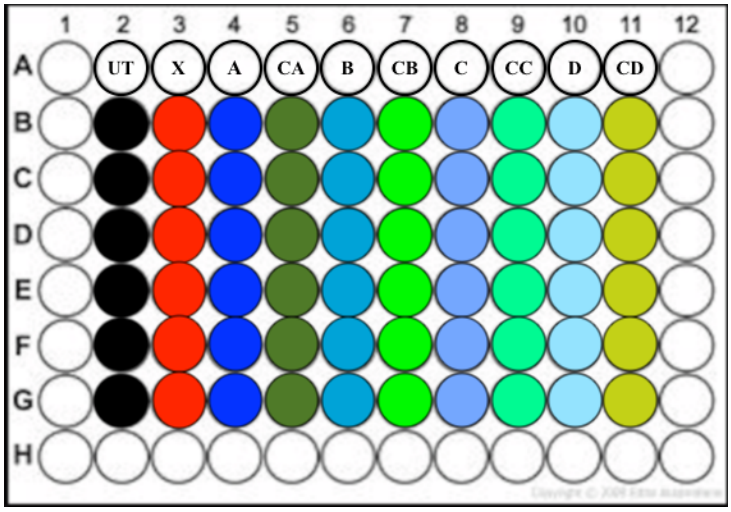

Figure 2.3. Drug combination plan of GDC098 and AZD1208. Black (UT): Un-treated cells, **Red** (X): Cells treated with (IC40) 13.8µM GDC-0980, **Blue** (A): cells treated with (IC90) 60µM AZD1208, **Green** (CA) cells treated with combination of X&A, (B): cells treated with (IC60) 47.8µM AZD1208, (CB): Cells treated with combination of X&B, (C): cells treated with (IC50) 39.8µM AZD1208, (CC): cells treated with combination of X&C, (D): cells treated with (IC30) 30µM AZD1208, (CD): cells treated with combination of X&D. Seeding density: 5000 cells per well and six replicates per drug dilution were used.

2.4. Results

2.4.1. ArrayStar® analysis of differentially expressed genes

Scatter plot analysis of the array data compares differentially expressed mRNAs between the H1975GR1 (H1975GP treated for 1 month with GDC-0980) or H1975GR6 (H1975 cells treated for 6 month with GDC-0980, become resistant to the drug) and H1975GP (drug naïve cells) with > 2 fold upregulated (Red) and down-regulated (Green) mRNAs illustrated in Figure 2.4A. The number of genes detected up-regulated: down-regulated: unchanged was 4169 (red): 2702 (green): 12579 (black) genes, when H1975GR1 was compared to H1975GP respectively. When H1975GR6 was compared to H1975GP, the number of upregulated, down-regulated and unchanged genes mRNAs expression was 6006 (red): 4018 (green): 9426 (black) genes, respectively.

When the fold change difference between the compared groups was set to >2-fold, 1673 mRNAs were upregulated (*appendix* 2.1) and 907 mRNAs were down-regulated in H1975GR1 compared to H1975GP cells (*appendix* 2.2). These numbers were duplicated in H1975GR6 cells with 3557 mRNAs up-regulated (*appendix* 2.3) and 2177 down-regulated (*appendix* 2.4). 2085 and 1430 mRNAs were detected up-regulated (*appendix* 2.5) and down-regulated (appendix 2.6) in both H1975GR1 and H1975GR6, respectively (Figure 2.4B). 420 mRNAs were upregulated in H1975GR1 cells that were down-regulated in H1975GR6 cells (*appendix* 2.7) and 360 had an opposite profile, i.e. down-regulated in H1975GR1 and upregulated in H1975GR6 (*appendix* 2.8). The appendices contain the following information: mRNA gene symbol, genome location (chromosome number, nucleotide start and end location) and RNA length.

Changes in mRNA expression in H1975GR1 cells may highlight those mRNAs that are involved in the early development of resistance to GDC-0980 in H1975 cells.

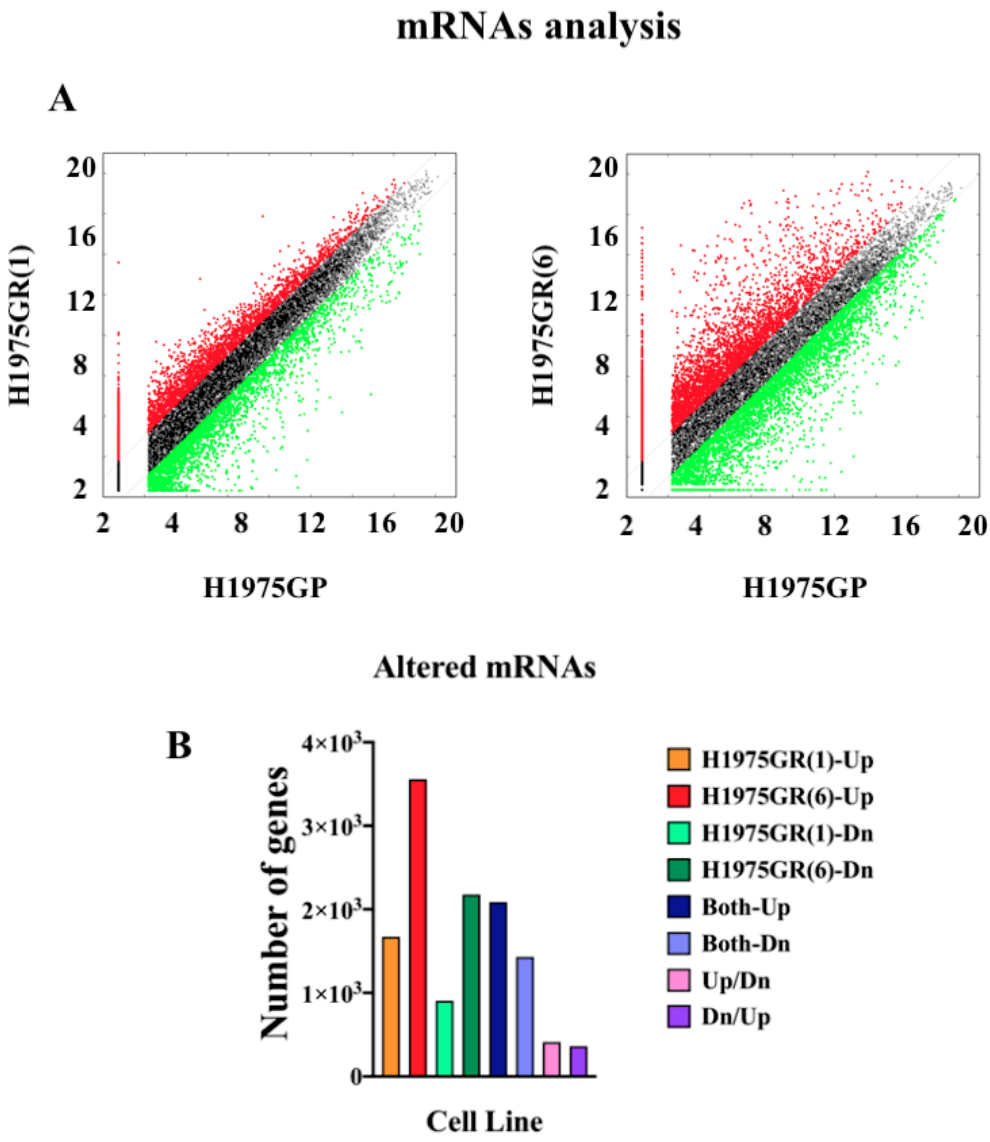

Figure 2.4. Altered expression of protein coding genes in H1975GR1 and H1975GR6 compared to H1975GP. A: Scatter-plot analysis of mRNA expression data; (red) upregulated, (green) down-regulated and (black) unaltered. H1975P was compared to H1975R1 (left) and to H1975GR6 (right). B. Summary of unique and shared up/down-regulated genes in H1975GR1 or H1975GR6 compared to H1975GP (GDC-0980 sensitive cells).

Panther-Slim biological process analysis of all unique upregulated and down-regulated genes mRNAs in H1975GR1 (Figure 2.4A/B, *appendix*: 1 and 2) and in H1975GR6 (Figure 2.4C/D, *appendix*: 3 and 5) compared to GDC-0980 sensitive H1975GP cells showed that the function of 298 upregulated genes and 162 down-regulated genes in H1975GR1 was regulation of cell metabolism. This number of metabolism-controlling genes was 683 up-regulated genes and 458 down-regulated genes in H1975GR6. Panther-Slim biological process analysis also showed that 76 upregulated genes in H1975GR1 were genes involved in cellular response to external stimuli, these genes were doubled to 185 genes in H1975GR6. While 55 down-regulated genes mRNAs in H1975GR1 were involved in the cell response to the external stimuli as well. These genes were increased to 78 genes in H1975GR6 (Figure 2.5).

Panther-Slim biological process classification of the genes detected upregulated and down-regulated in both H1975GR1 and H1975GR6 (Figure 2.6 C/D, *appendix:* 2.5 and 2.6) and the genes that exhibit an opposite expression trend over the time from H1975GR1 to H1975GR6 (Figure 2.6 A/B, *appendices*: 2.7 and 2.8) clustered the most searched genes into four major biological functions: metabolism, biological regulators, cellular process and response to stimuli genes. Details about the number of genes clustered per expression profile and function is summarized in figure 2.5.

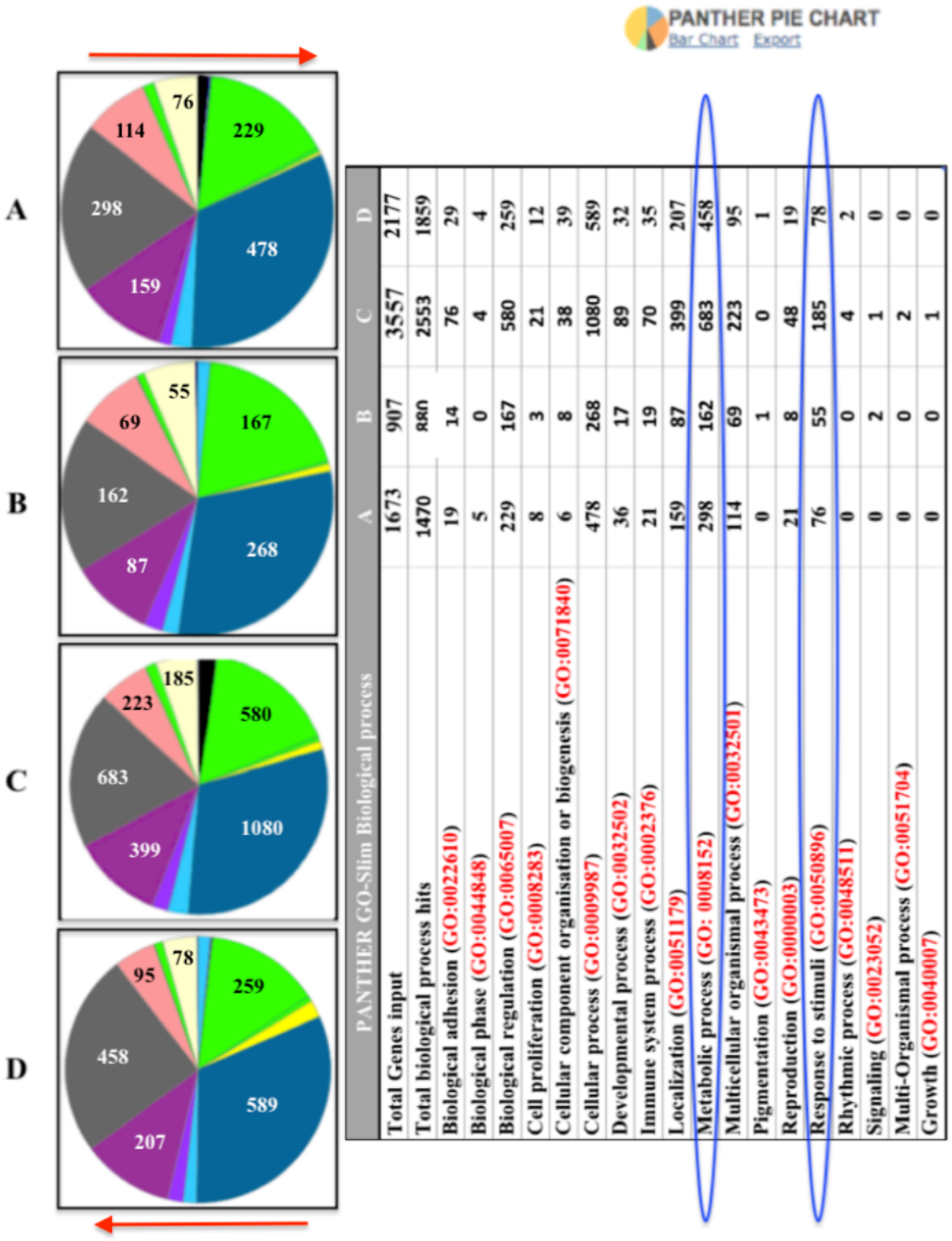

PANTHER GO-Slim Biological process	A	B	C	D
Total Genes input	1673	907	3557	2177
Total biological process hits	1470	880	2553	1859
Biological adhesion (GO:0022610)	19	14	76	29
Biological phase (GO:0044848)	5	0	4	4
Biological regulation (GO:0065007)	229	167	580	259
Cell proliferation (GO:0008283)	8	3	21	12
Cellular component organisation or biogenesis (GO:0071840)	6	8	38	39
Cellular process (GO:0009987)	478	268	1080	589
Developmental process (GO:0032502)	36	17	89	32
Immune system process (GO:0002376)	21	19	70	35
Localization (GO:0051179)	159	87	399	207
Metabolic process (GO: 0008152)	298	162	683	458
Multicellular organismal process (GO:0032501)	114	69	223	95
Pigmentation (GO:0043473)	0	1	0	1
Reproduction (GO:0000003)	21	8	48	19
Response to stimuli (GO:0050896)	76	55	185	78
Rhythmic process (GO:0048511)	0	0	4	2
Signaling (GO:0023052)	0	2	1	0
Multi-Organismal process (GO:0051704)	0	0	2	0
Growth (GO:0040007)	0	0	1	0

Figure 2.5. PANTHER Pie Chart and Slim Biological process classification of mRNA differentially expressed in H1975GR1 or H1975GR6 compared to H1975GP cells. A: mRNAs up-regulated in H1975GR1, B: mRNAs down-regulated in H1975GR1, C: mRNAs up-regulated in H1975GR6, D: mRNAs down-regulated in H1975GR6.

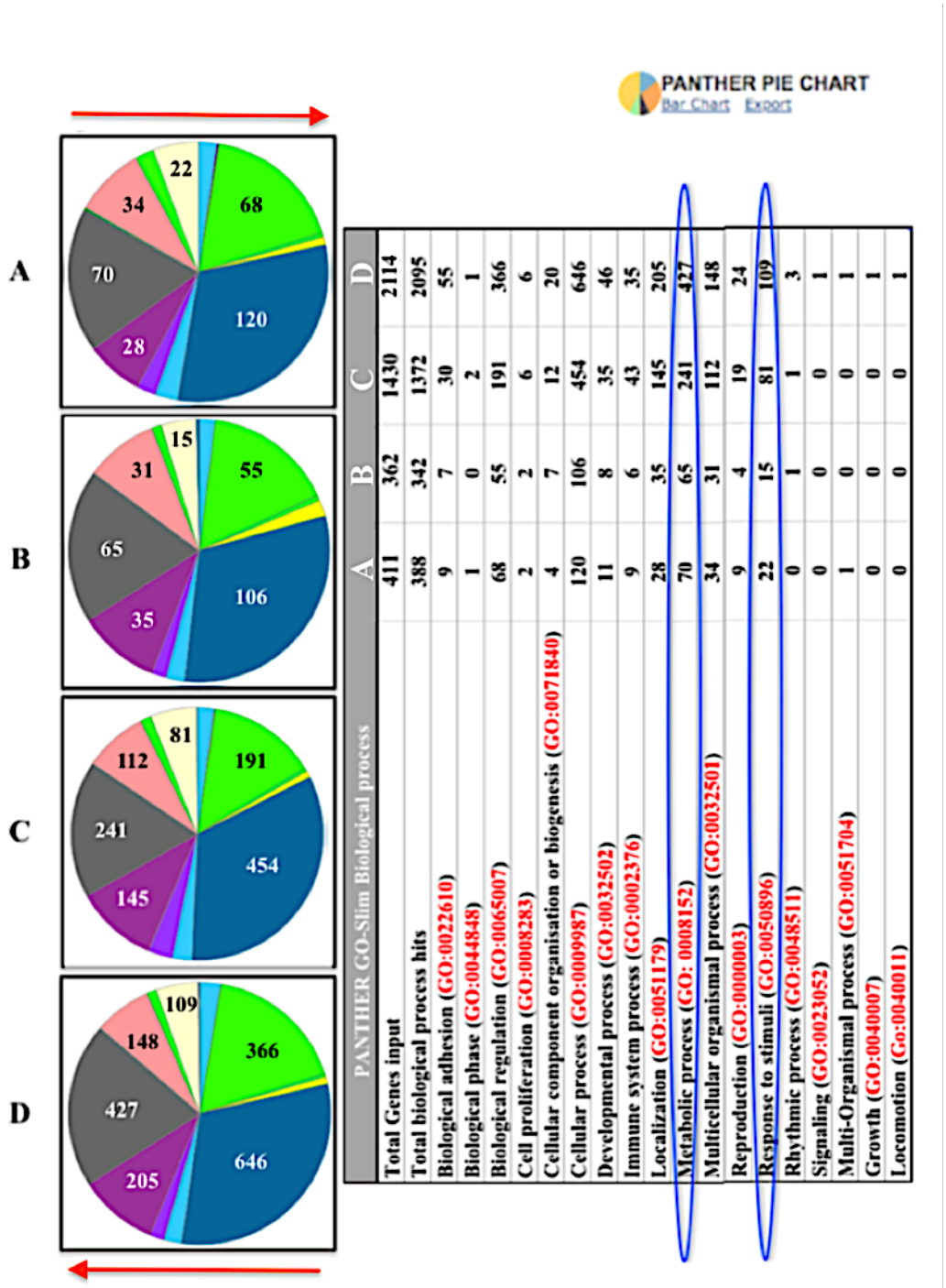

PANTHER GO-Slim Biological process	A	B	C	D
Total Genes input	411	362	1430	2114
Total biological process hits	388	342	1372	2095
Biological adhesion (GO:0022610)	9	7	30	55
Biological phase (GO:0044848)	1	0	2	1
Biological regulation (GO:0065007)	68	55	191	366
Cell proliferation (GO:0008283)	2	2	6	6
Cellular component organisation or biogenesis (GO:0071840)	4	7	12	20
Cellular process (GO:0009987)	120	106	454	646
Developmental process (GO:0032502)	11	8	35	46
Immune system process (GO:0002376)	9	6	43	35
Localization (GO:0051179)	28	35	145	205
Metabolic process (GO: 0008152)	70	65	241	427
Multicellular organismal process (GO:0032501)	34	31	112	148
Reproduction (GO:0000003)	9	4	19	24
Response to stimuli (GO:0050896)	22	15	81	109
Rhythmic process (GO:0048511)	0	1	1	3
Signaling (GO:0023052)	0	0	0	1
Multi-Organismal process (GO:0051704)	1	0	0	1
Growth (GO:0040007)	0	0	0	1
Locomotion (Go:0040011)	0	0	0	1

Figure 2.6. PANTHER Pie Chart and Slim Biological process classification of mRNAs differentially expressed in H1975GR compared to H1975GP cells. A: mRNAs were up-regulated at 1 month-time of H1975 challenging with GDC-0980 (H1975GR1) and down-regulated at month 6 (H1975GR6), B: mRNAs were down-regulated at 1 month-time of H1975 challenging with GDC-0980 (H1975GR1) and up-regulated at month 6 (H1975GR6), C: mRNAs were down-regulated in both H1975GR1 and H1975GR6, D: mRNAs were up-regulated in both H1975GR1 and H1975GR6 exposure to GDC-0980.

Increased expression of genes involved in metabolism is associated with an aggressive phenotype, increased growth and metastatic capabilities and drug resistance. The *JAK*/*STAT* pathway was activated during the development of resistance to GDC-0980 in H1975 cells and it has been shown to play a role in cell metabolism, proliferation and response to several stimuli such as interleukins and growth hormones. Several members of the *IL6/STAT3* pathway were upregulated including *PIM1* kinase (19.8 fold) and its co-regulator *c-Myc* (25.6 fold), and Metastasis-associated in colon cancer 1 (*MACC1*) (44.8 fold) in H1975GR6 cells. *MACC1* (77 fold) and its regulated proteins; *HGF* (10-fold) and *MET* (1.6) were also upregulated in H1975GR1 cells. *MET* mRNA expression is 6-fold increased at 6 months of treatment. These markers of resistance were validated by qRT-PCR and Western blot analysis. In-depth analysis of the lists of differentially expressed mRNAs also identified an increase in mRNA expression of two checkpoint proteins *CTLA4* (4.01 fold) and *CD274* (*PD-L1*) (1.6 fold) in H1975GR6 compared to H1975GP cells. *CMTM6* was also selected for further validation given its role as a regulator of checkpoint protein *PD-L1*.

2.4.2. Validation of differentially expressed mRNAs.

2.4.2.1. Validation of PIM1, PIM2 and PIM3 kinase mRNA expression by qRT-PCR.

Microarray expression analysis revealed *PIM* kinases mRNAs were differentially expressed in H1975GR1 and H1975GR6 cells compared to drug sensitive H1975GP cells (Figure 2.7A). *PIM1* was detected almost the same in H1975GR1 and H1975GR6 compared to H1975GP. *PIM3* was 2.1-fold elevated in H1975GR1 compared to the H1975GP and starts to drop at H1975GR6. *PIM2* mRNA expression was detected elevated by 19.8-fold in H1975GR1 and 29.2-fold in H1975GR6 compared to GDC-0980 naïve cells (H1975GP). However validation of *PIM1/2/3* kinase mRNA expression was undertaken by qRT-PCR (n=3) in H1975GP and H1975GR6 cells. All three *PIM* kinases were significantly elevated in H1975GR6 compared to H1975GP cells ($p=<0.05$) (Figure 2.7B).

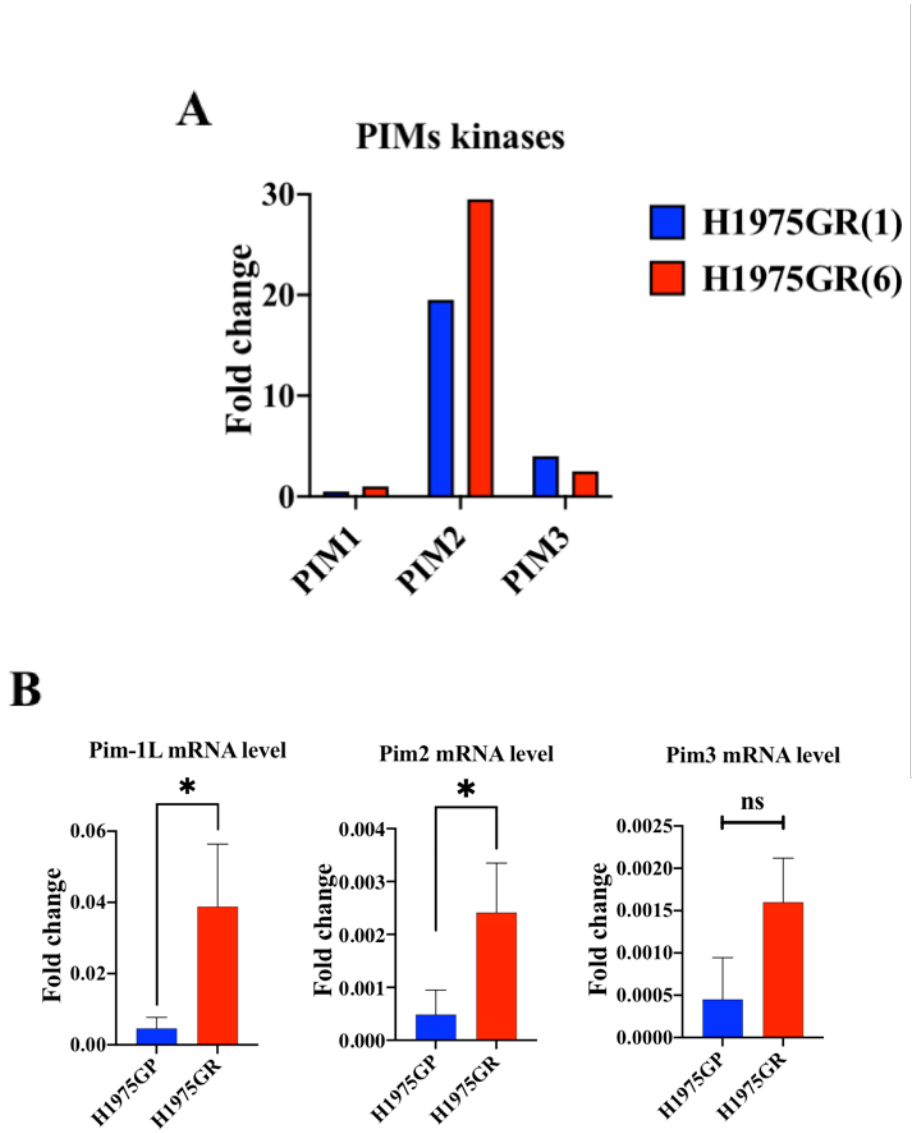

Figure 2.7. Validation of PIM1, PIM2 and PIM3 mRNA expression. A: ArrayStar® analysis of PIM kinases mRNA expression. H1975GR1 and H1975GR6 were treated with GDC-0980 for one month and six months respectively. X-axis represent the control group (H1975GP) and the blue columns represent fold change detected by arrayStar in H1975GR6, red columns represent the fold change detected by arrayStar in H1975GR1. **B**: RT-qPCR assessment of PIM kinases in H1975GR and H1975GP. Fold change calculated using β-actin as a loading control. (*: p=0.02-0.03, ns: p=0.05).

2.4.2.1.1. Western blot validation of *PIM* kinase expression in H1975GP and H1975GR cells.

PIM1, 2 and 3 protein expression was quantified in H1975GP and H1975GR6 cells by western blot analysis. There was no change in the level of *PIM1*-small variant (*PIM1S*) between the cell lines, while the large variant (*PIM1L*) was (9-fold) elevated in H1975GR6 ($p=0.0002$). *PIM2* kinase was also significantly elevated (double) in H1975GR6 cells compared to H1975GP cells ($p=0.03$). PIM3 kinase was significantly ($p=0.01$) elevated (double) in the resistant cells compared to the drug sensitive cells (Figure 2.8).

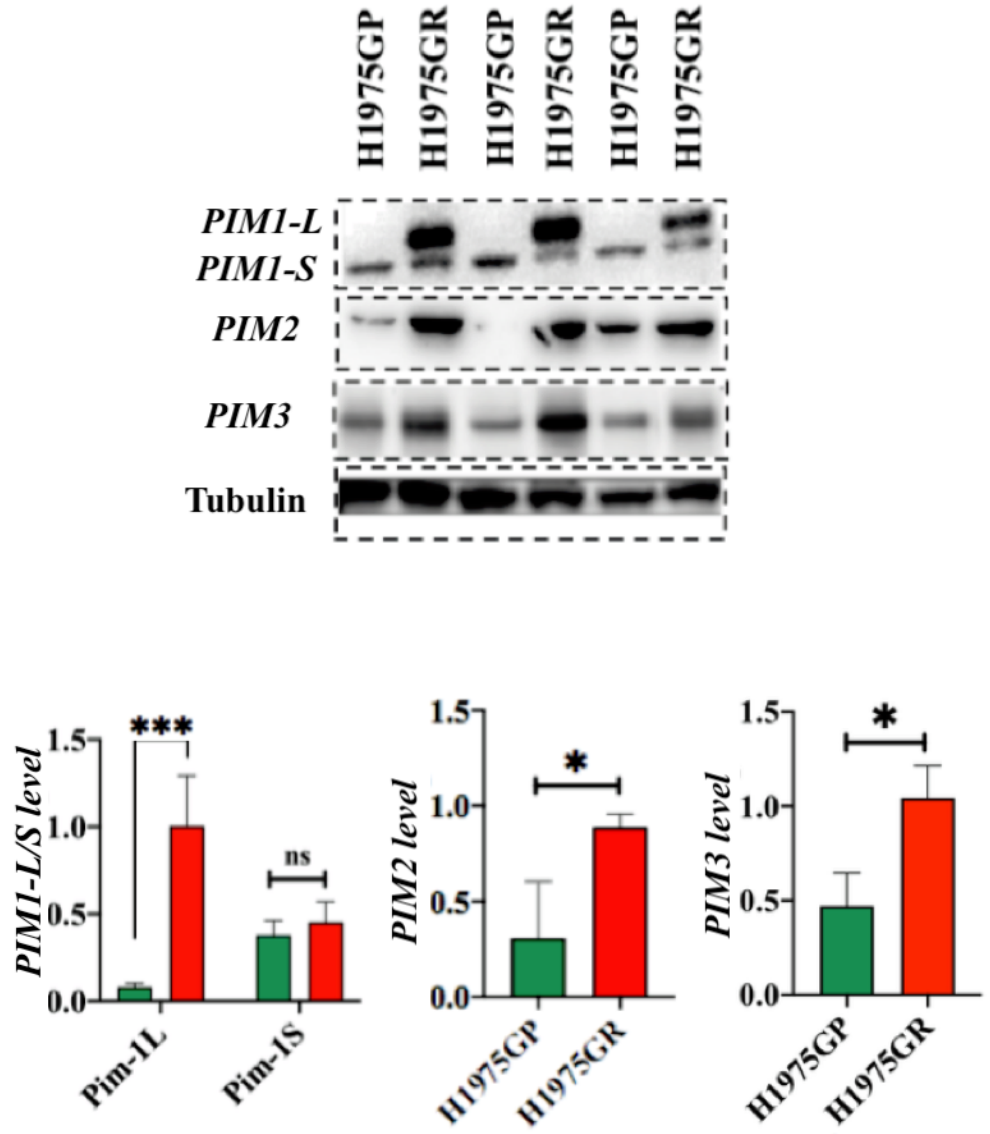

Figure 2.8. Western blot analysis of PIM1, PIM2 and PIM3 kinase protein abundance. H1975GP: GDC-0980 sensitive cells, H1975GR: GDC-0980 resistant cells, PIM1L: large variant, PIM1S: Small variant. PIM2 and PIM3 protein abundance was significantly upregulated in the resistant cells (H1975GR) compared to the parent cells (H1975GP) (n=3) with p value of 0.03 and 0.01, respectively. PIM1 kinase large variant was also significantly upregulated (n=3) with p value of 0.0002, while the small variant was unchanged. Tubulin was used as a loading control.

2.4.2.1.2. The effect of GDC-0980 and siRNA knockdown of PIM1 or PIM3 on H1975GP and H1975GR cells viability.

Knock down of *PIM1* and *PIM3* kinase by siRNA was done to elucidate the role of *PIM* kinases in the development of GDC-0980 resistance in H1975 cells. Both H1975GP (green) and H1975GR (red) were treated with the *PIM1* or 3 siRNA either as single treatment or in combination with their correspondent GDC-0980 IC50. The IC50 of GDC-0980 for both H1975GP and H1975GR was used (Table 2.7). The siRNA knock down of *PIM1* kinase expression reduced the cell viability by 15% in both H1975GP and H1975GR compared to the untreated cells (P=0.01 and 0.001, respectively). *PIM3* siRNA also significantly reduced the cell viability of both H1975GP and H1975GR by 60% (p= 0.006 and 0.001, respectively) (Figure 2.8). No difference in the effect of *PIM1* and *PIM3* siRNA between H1975GP and H1975GR was observed. *PIM3* kinase knockdown had more effect on the suppression of cell viability of H1975GP and H1975GR than *PIM1* kinase knock down (Figure 2.9).

PIM1 siRNA had no additive effect in combination with GDC-0980 (GDC-0980-treated versus non-treated), while *PIM3* siRNA had a significant little additive effect on GDC-0980-treated cells in both H1975GP and H1975GR cells compared to GDC-0980 treated cells alone. Cells viability ratio between H1975GP and H1975GR remains the same as in single GDC-0980 treatment (Figure 2.9).

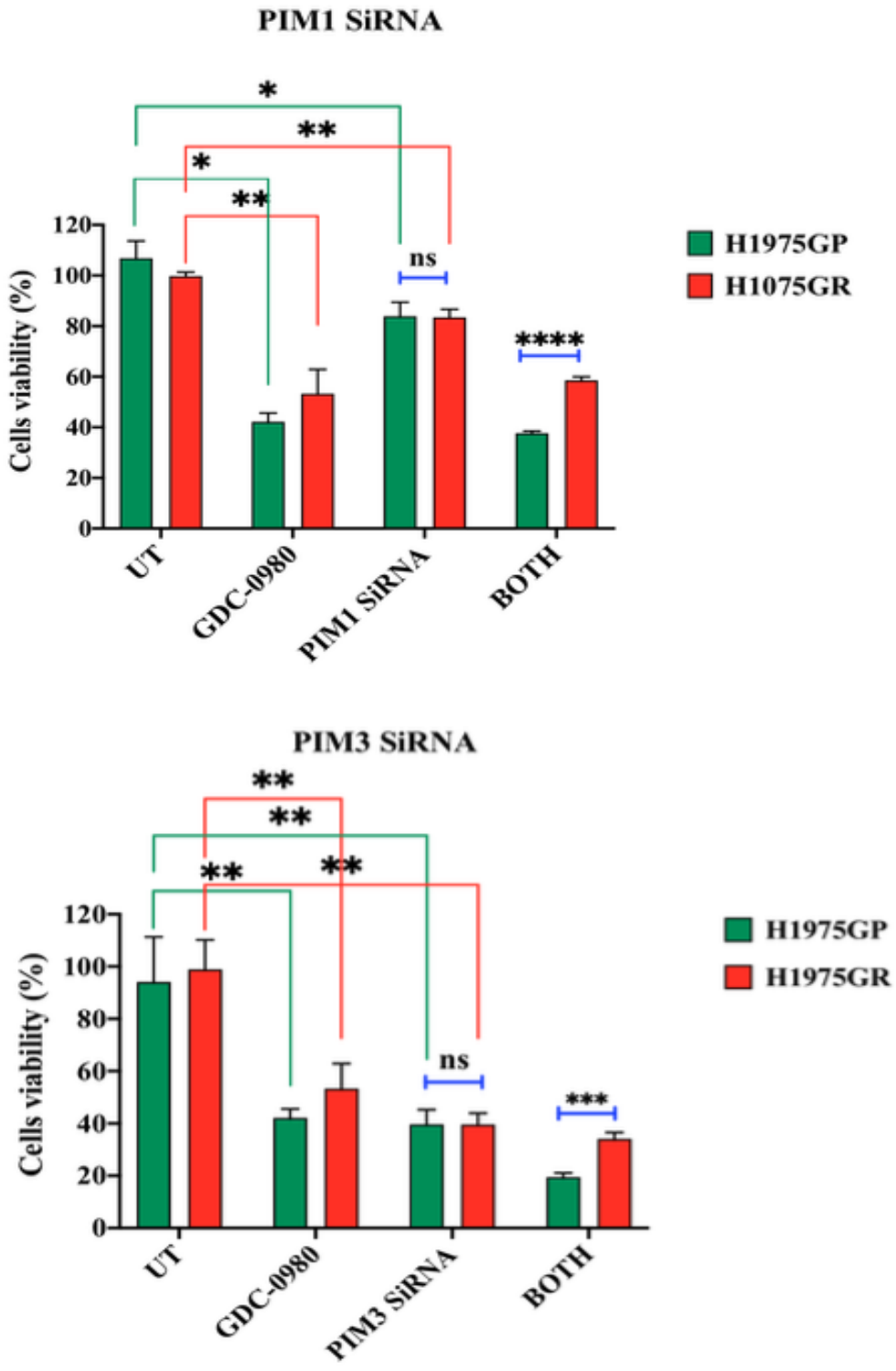

Figure 2.9. siRNA knockdown of PIM kinases gene expression in H1975GP and H1975GR cells. H1975GP: GDC-0980 sensitive H1975 cells, H1975GR: GDC-0980 resistant H1975 cells, siRNA: small interfering RNA. Cell viability: the percentage of live cells after treatment. CTL: non-targeting siRNA. (**: p=0.003-6, ***: p=0.0003).

2.4.2.1.3. Cell viability assay of GDC-0980 and AZD-1208 in H1975GR and H1975GP cells.

A dose-response curve for H1975GP (red) and H1975GR (blue) treated with GDC-0980 (dose range: 2μM, 4μM, 5μM, 10μM, 30μM, 35μM, 50μM, 80μM) or AZD-1208 (dose range: 20μM, 25μM, 30μM, 35μM, 40μM, 50μM, 55μM and 60μM) are shown in figure 2.10A & 2.10B, respectively. The calculated IC50 for GDC-0980 was 1.86μM for H1975GP and 15.85μM for H1975GR cells. The IC50 for AZD-1208 was 30μM for H1975GP and 46.5μM for H1975GR cells. Per drug, ICs from 10 to IC98 were calculated by the online AAT Bioquest® IC50% calculator and tabulated in table 2.7 https://www.aatbio.com/tools/ic50 -calculator (Dratkiewicz et al., 2019).

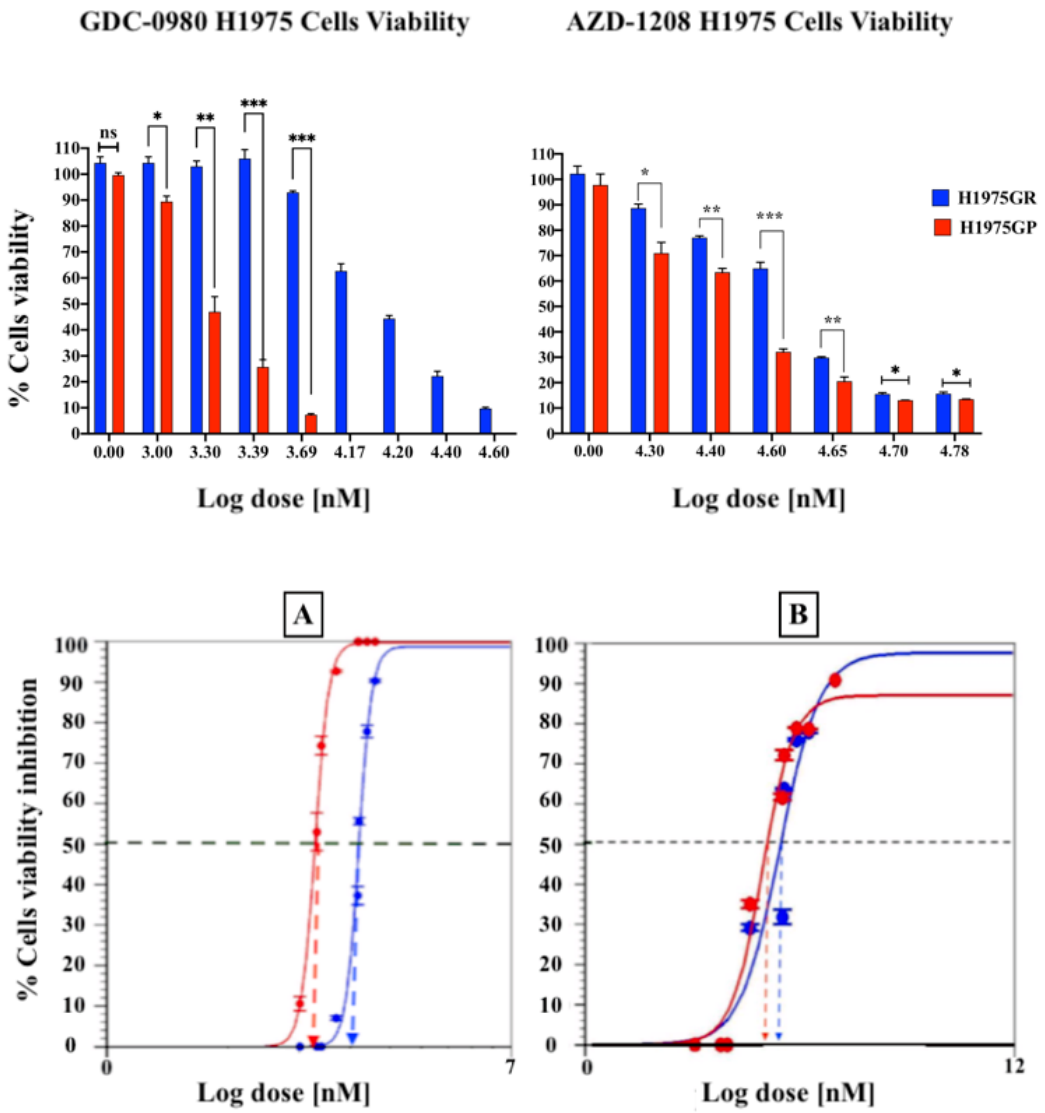

Figure 2.10. Cell viability study of GDC-0980 and AZD-1208 in H1975GP and H1975GR cells. Cell viability inhibition = Treated (X-dose) cells CTB fluorescent signal/UT cells CTB fluorescent signal X100). CTB: Cell-Titre blue, X-doses (8-point assay). *: p=0.0(1-4), **p=0.00(1-9), ***p=0.000(1-9).

Table 2.7. Calculated inhibitory concentrations (ICs) for GDC-0980 and AZD-1208.

	GDC0980 DOSE [M]		*AZD-1208 DOSE [M]*	
IC	**H1975GR**	**H1975GP**	**H1975GR**	**H1975GP**
10	7.586	1.000	19.952	13.182
20	9.772	1.259	25.703	17.782
30	11.749	1.445	30.902	21.379
40	13.804	1.660	34.673	25.118
50	**15.849**	**1.862**	**39.810**	**30.549**
60	18.621	2.089	43.651	33.884
70	21.878	2.399	47.863	39.810
80	26.915	2.884	53.703	47.863
90	38.019	3.715	60.255	60.255
98	107.152	9.333	69.183	93.325

IC values in green (IC40 GDC-0980, IC30/50/70/90 AZD-1208) were selected for combination study.

2.4.2.1.4. The effect of GDC-0980 or AZD-1208 alone or in combination on H1975GR6 and H1975GP cells viability.

In this experiment, only GDC-0980 resistant cells (H1975GR) were used. The principle of drug combination was to treat H1975GR with their GDC-0980 IC40 (13.8μM), then to combine this dose with different IC doses of AZD-1208: **A**: IC90 (60μM), **B**: IC70 (47.8μM), **C**: IC50 (39.8μM), **D**: IC30 (30.9μM). All AZD-1208 ICs doses (A, B, C and D) (green arrows) had a significant effect on the H1975GR cells viability compared to the un-treated cells (black) (P=<0.0001). GDC-0980 IC40, when combined with IC70, IC50 and IC30 of AZD-1208, the growth suppression was additive. Combination with IC90 had no difference between AZD-1208 single treatment or combined with GDC-0980 IC40 (Figure 2.11).

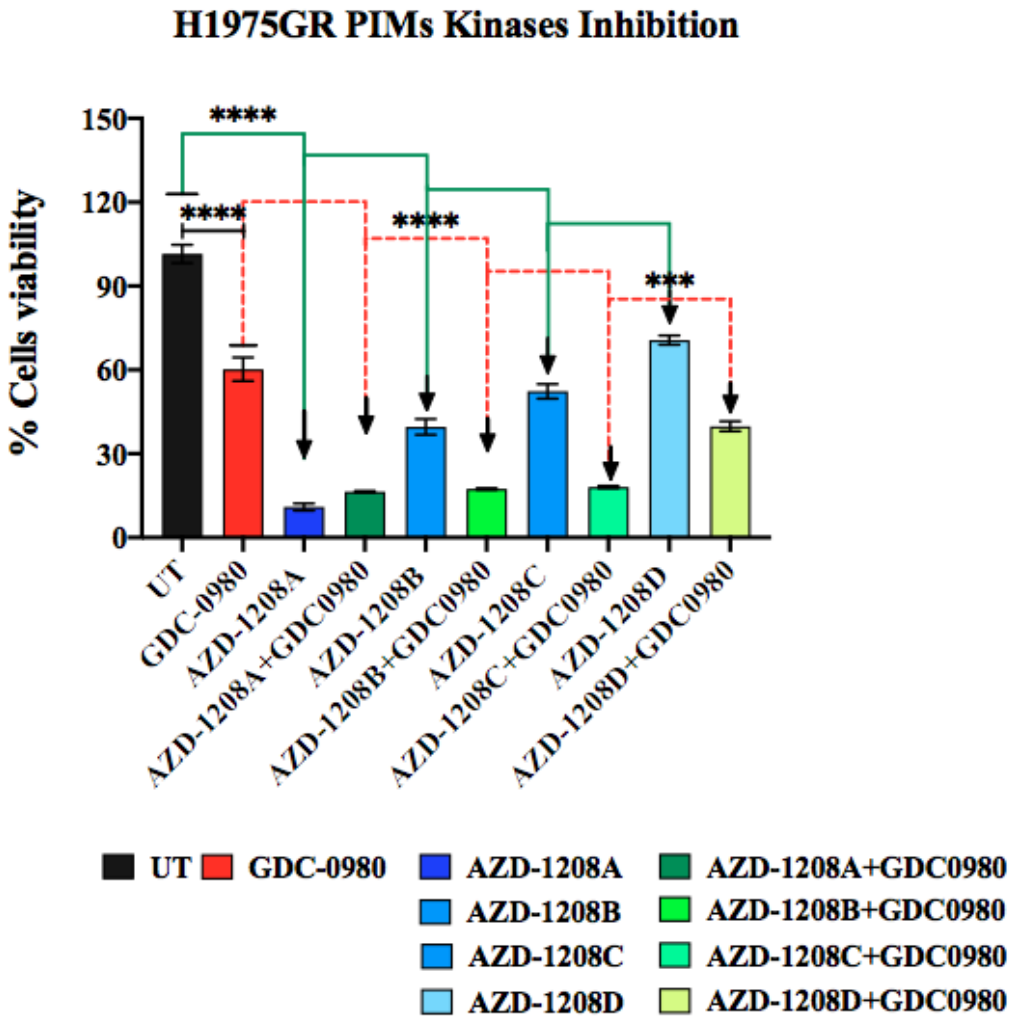

Figure 2.11. Cell viability assay for GDC-0980 and AZD-1208 alone or in combination in H1975GR cells. GDC-0980 dose: IC40 (13.8µM), AZD1208 doses: A: IC90: 60.255µM, B: IC70: 47.863µM, C: IC50: 39.810µM, D: IC30: 30.000µM. Significance p-value: (***: p=0.0002, ****:<0.0001).

2.4.3. Validation of c-Myc expression by western blot analysis

ArrayStar expression data for c-*Myc* mRNA in H1975GR1 cells (green) and H1975GR6 cells (red) compared to the drug sensitive (H1975GP) cells, showed an increase of 2-fold in H1975GR1 and 25-fold in H1975GR6 cells compared to H1975GP by array analysis (Figure 2.12A). Assessment of c-*Myc* mRNA levels in the resistant H1975GR cells by qRT-PCR (n=3) showed increased mRNA in the resistant cells compared to the sensitive cells (H1975GP) (7.7±6.7, Mean±STD), despite statistical insignificance (p=0.3) (Figure 2.12B). Western blot analysis of c-*Myc* protein expression in H1975GR compared to H1975GP showed c-Myc protein was significantly increased in the resistant H1975GR cells (p=0.03) (Figure 2.12C).

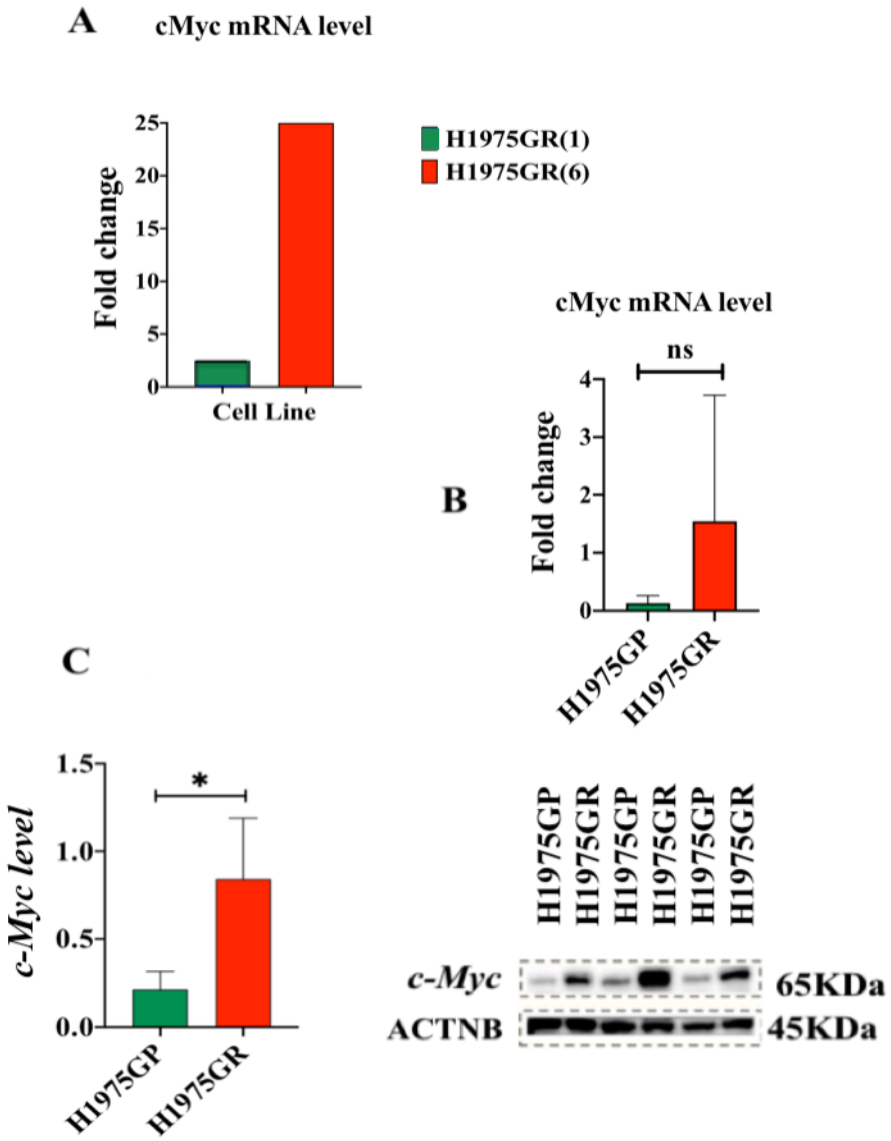

Figure 2.12. Validation of c-Myc mRNA and protein levels by qRT-PCR and western blot analysis. A: ArrayStar® analysis of c-Myc gene expression. H1975GR1 (green): H1975GP were treated with GDC-0980 for one month, H1975GR6 (red): cells tested after six months of GDC-0980 treatment. B: qRT-PCR assessment of c-Myc mRNA levels in H1975GR cells (red) compared to the sensitive H1975GP cells (green) (p=0.3). C: western blot assessment of c-Myc in H1975GP (green) and H1975GR (red) (*: p = 0.03).

2.4.4. Validation of *MACC1* protein expression by Western blot analysis

ArrayStar analysis showed that *MACC1* mRNA expression was increased by 79-fold in H1975GR1 and 42-fold in H1975GR6 cells compared with H1975GP cells by array analysis (Figure 2.13A). Western blot analysis showed elevation of *MACC1* protein expression in H1975GR compared to H1975GP cells (Figure 2.13B).

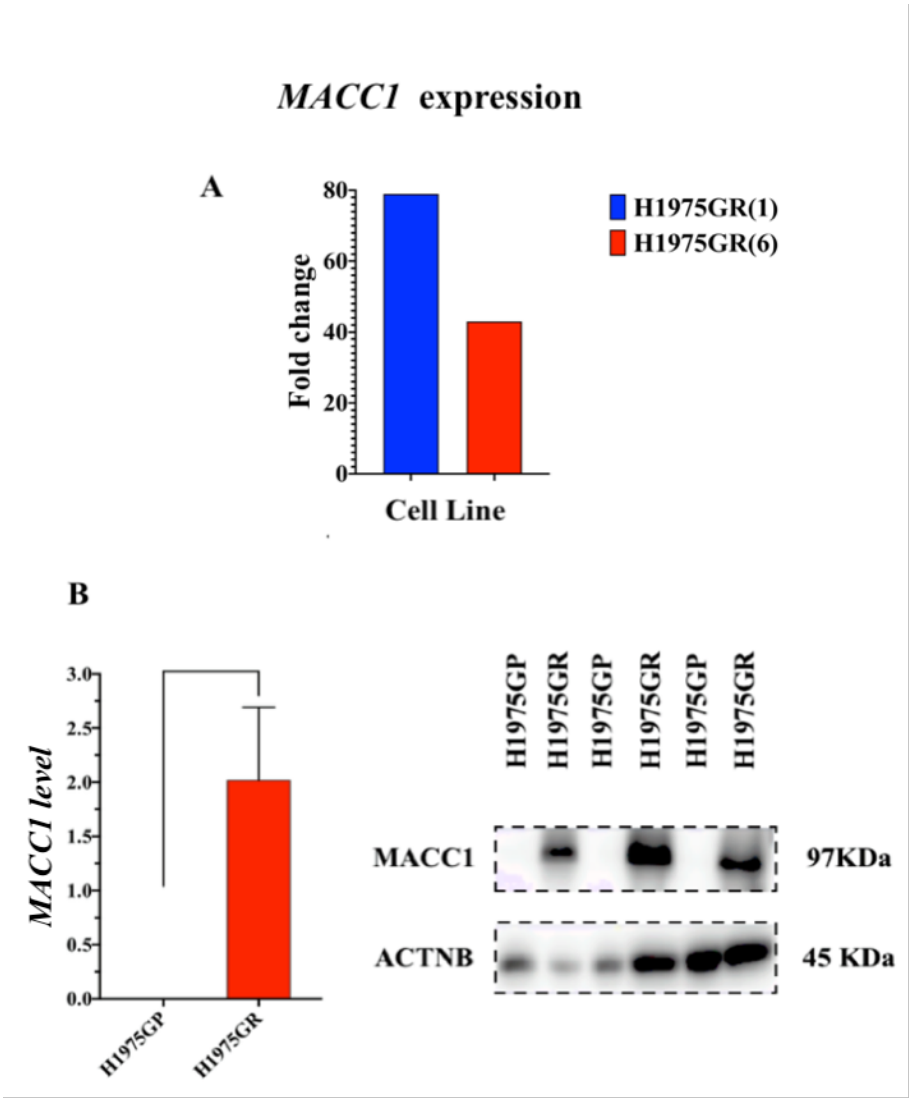

Figure 2.13. Validation of MACC1 expression in H1975GP and H1975GR. A: ArrayStar® analysis of MACC1 mRNA expression in one month GDC-0980 treated cells H1975GR1 and six months GDC-0980 treated cells H1975GR6 compared to GDC-0980 sensitive (H1975GP). **B**: Western blot analysis of MACC1 protein abundance in H1975GR cells compared to H1975GP cells, β-actin was used as a loading control.

2.4.4.1. The effect MACC1 siRNA alone or in combination with GDC-0980 on H1975GR cell viability.

Knocking down *MACC1* gene expression by *MACC1* targeting siRNA was done to elucidate the possible role of *MACC1* in the development of GDC-0980 resistance. The IC50 of GDC-0980 for both H1975GP and H1975GR cells were used (Table 2.7). The difference of *MACC1* siRNA effect on H1975GP and H1975GR cells was significant (p=0.002), H1975GP was more affected than the H1975GR (H1975GP had 50% viability of H1975GR). No differences in the cell's viability was observed between H1975GP and H1975GR when treated with GDC-0980 and siRNA combination, H1975GR cells were significantly affected (p value: 0.0003), while H1975GP no additive combination was observed (Figure 2.14).

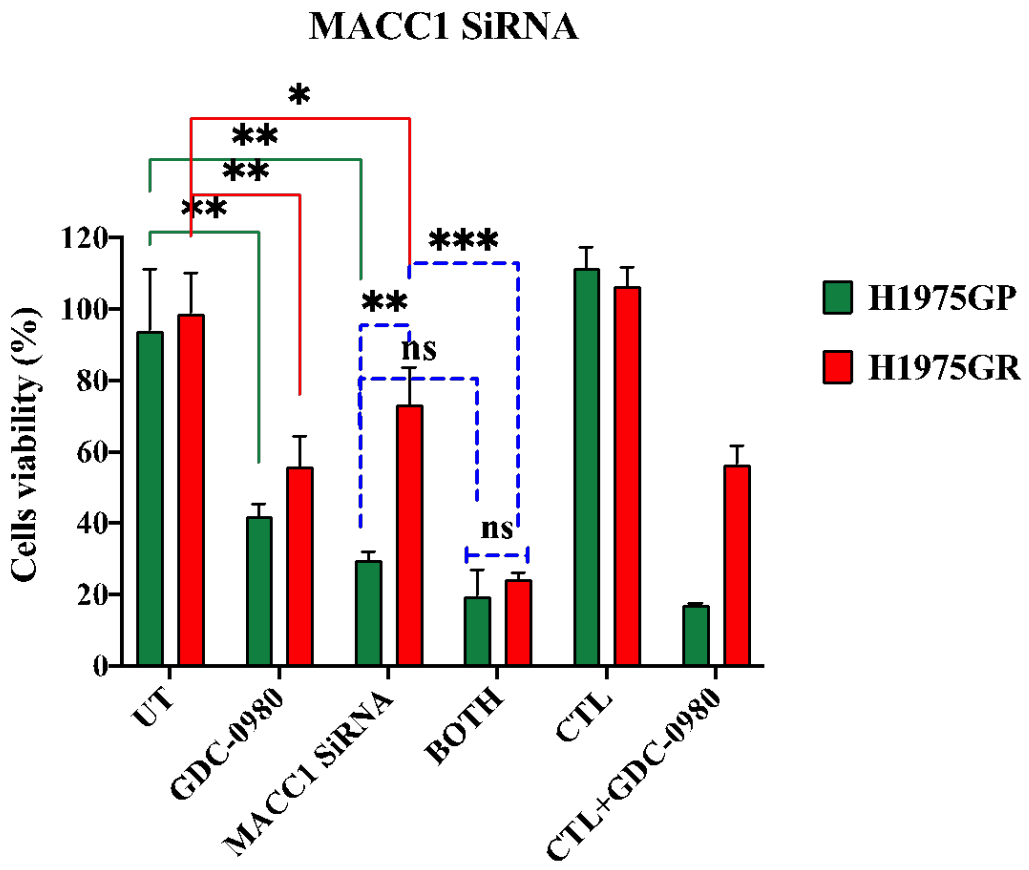

Figure 2.14. Effect of MACC1 knockdown alone or in combination with GDC-0980 on cell viability in H1975GR cells. H1975GP: GDC-0980 sensitive cells, H1975GR: GDC-0980 resistant cells, siRNA: small interfering RNA. Cell viability: the percentage of life cells in treated compared to the non-treated cells, CTL: non-targeting siRNA. (*: p=0.03), **: p=0.002-6, ***:p=0.0003).

2.4.5. Validation of *c-Met* expression by western blot analysis

ArrayStar data detected *c-Met* mRNA expression was increased 6-fold in H1975GR6 and by 0.5-fold in H1975GR1 compared to the drug sensitive H1975GP cells (Figure 2.15A). Western blot analysis showed no change in *c-Met* protein expression between the H1975GP and H1975GR cells (Figure 2.15B).

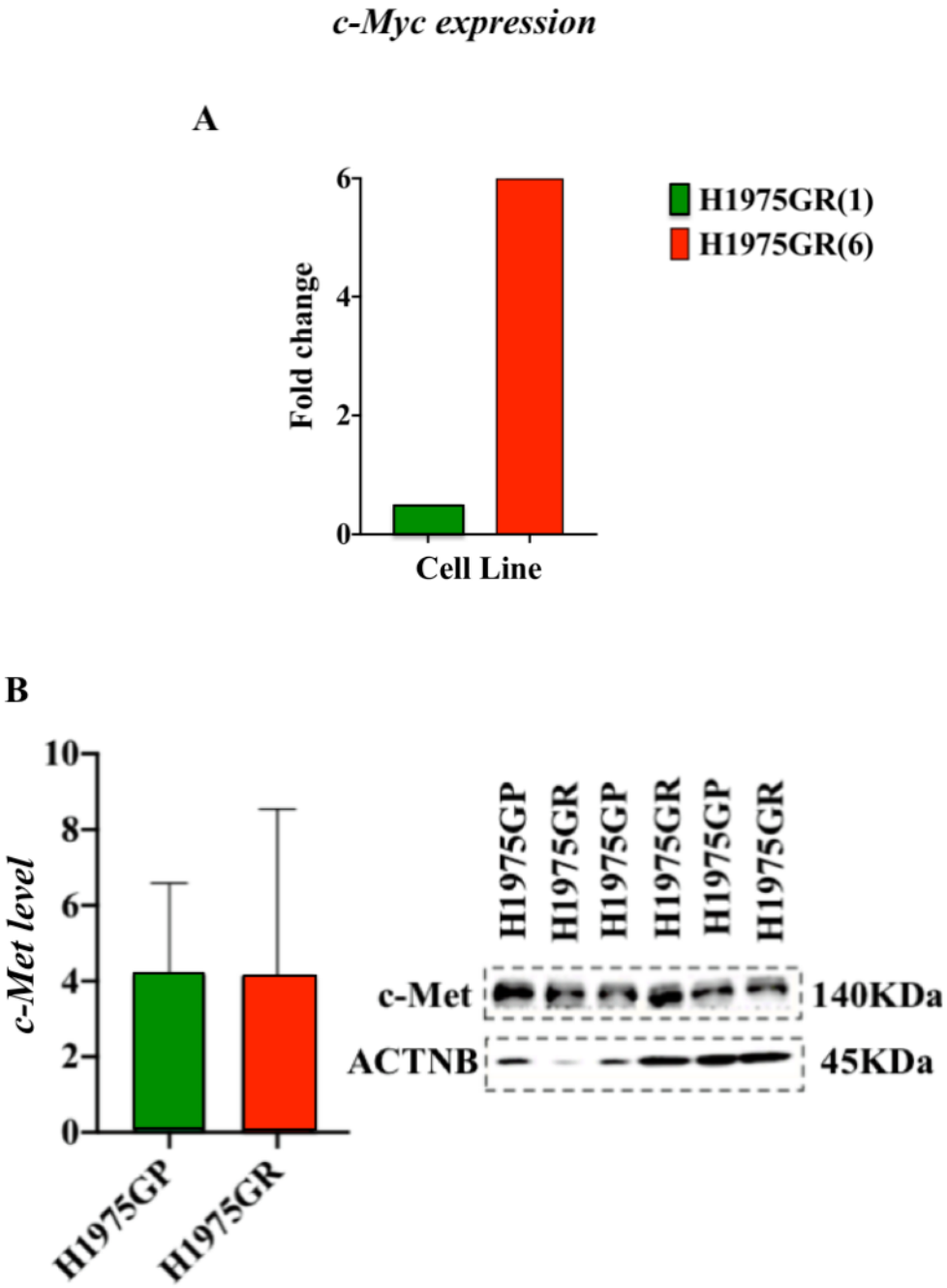

Figure 2.15. Validation of c-Met mRNA and protein expression in H1975GR1 and H1975GR6 compared to H1975GP cells. A: ArrayStar® analysis of c-Met mRNA expression in GDC-0980 resistant H1975GR1 and H1975GR6 cells compared to GDC-0980 sensitive H1975GP cells. B: Western blot assessment of c-Met protein expression in GDC-0980 parent and resistant H1975GR cells, β-actin was used as a loading control.

2.4.6. Validation of *CMTM6* expression by western blot analysis

The ArrayStar® expression analysis of *CMTM* gene isoforms mRNA in H1975GR1 and H1975GR6 cells compared to H1975GP showed that the expression of *CMTM2* and 8 were detected 2.1 and 4.9-fold downregulated in H1975GR1 and H1975GR6 compared to the H1975GP, respectively. *CMTM3*, 6 and 7 were all upregulated in H1975GR6 compared to the parent cells. *CMTM6* was chosen for further qRT-PCR and western blot validation (Figure 2.16A). qRT-PCR analysis of *CMTM6* showed a significant ($p=0.03$) increase (36.2 ± 18.8) in *CMTM6* mRNA levels in H1975GR cells (red) compared to H1975GP cells (green) (Figure 2.16B). CMTM6 protein expression was detected up-regulated by western blot in H1975GR cells (red) compared to H1975GP cells (green), but this did not reach statistical significance (Figure 2.16C).

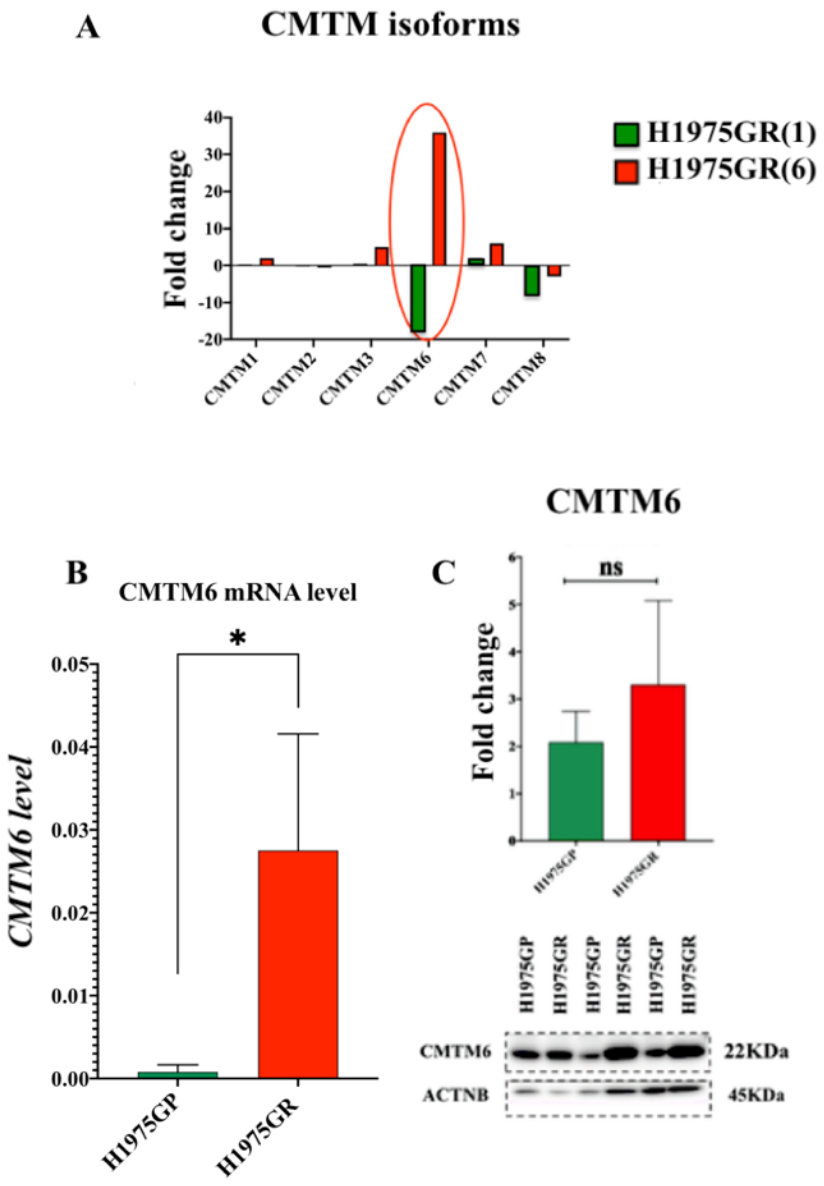

Figure 2.16. Assessment of CMTM6 mRNA and protein expression in H1975GP and H1975GR. A: ArrayStar® analysis of CMTM gene mRNA expression in H1975GR1 (Green): H1975 cells were treated with GDC-0980 for one month, H1975GR6 (Red): cells tested at month six of GDC-0980 treatment compared to H1975GP. B: qRT-PCR assessment of CMTM6 mRNA expression in H1975 GDC-0980 resistant H1975GR cells compared to the sensitive (H1975GP) cells, 18S was used as a loading control, *: P=0.03. C: Western blot analysis of CMTM6 protein levels in H1975GR and H1975GP cells, beta actin used as a loading control.

2.4.7. Assessment of desmoplakin, tenascin c, enolase 1 and ERO1-La in NSCLC cell lines and in H1975GR versus H1975G P cells.

The expression of desmoplakin (*DSP*), tenascin c (*TNC*), enolase-1 (*ENO1*) and ERO1-La (*ERO1A*) in a panel of lung carcinoma (mainly adenocarcinoma) cell lines showed the expression of *TNC* (pink) and *DSP* (blue) were very low in A549, H1819 and H460 lung adenocarcinoma cells. *DSP* was also low in HCC827 lung adenocarcinoma cells. The other cell lines examined had higher mRNA expression of this panel of markers as measured by q-PCR using S18 as an internal control. *ERO1A* (red) expression was high in all cell lines except H3255 which was half the abundance of 18S mRNA. *ENO1* (green) mRNA was at least equal or more than 18S in all assessed cell lines (Figure 2.17A). *DSP*, *TNC*, *ERO1A* and *ENO1* mRNA expression was assessed in H1975GR and H1975GP by qRT-PCR and detected *ERO1A* and *TNC* mRNA abundance to be significantly elevated ($p=<0.0001$) in the H1975GR6 (red) compared to H1975GP (green), *ENO1* mRNA was also found elevated in the GDC-0980 resistant cells despite the insignificant, while *DSP* mRNA showed no difference between H1975GP and H1975GR cells (Figure 2.17B).

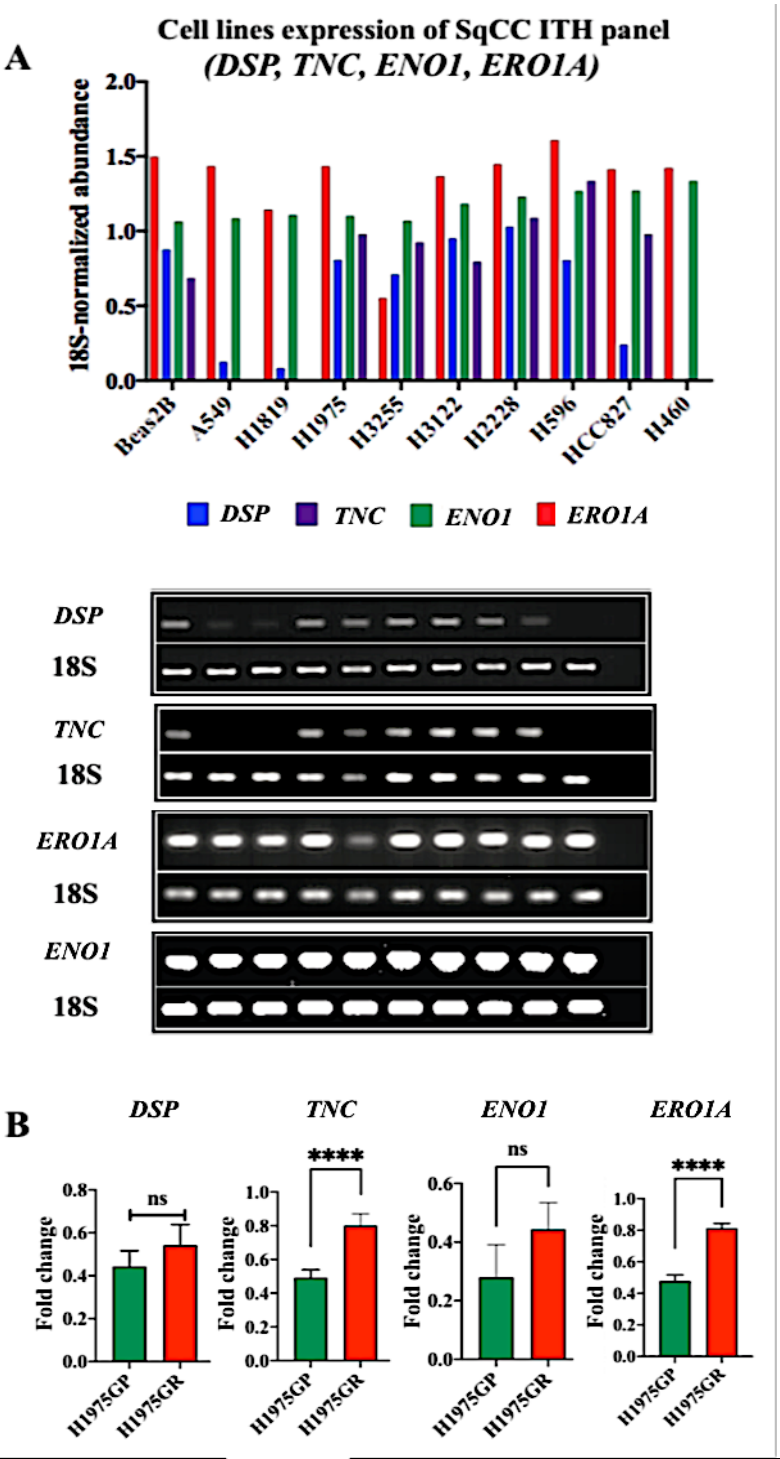

Figure 2.17. Expression of SqCC ITH panel. A: In selected cell lines expression panel Beas-2B: normal bronchial epithelial cells, A549: human alveolar epithelial adenocarcinoma cells, H1319, H1975: human lung adenocarcinoma, H3255: EGFRL85R NSCLC, H3122: lung adenocarcinoma (non-smoker), H2228: lung adenocarcinoma (non-smoker), H596: lung adeno-squamous carcinoma, HCC827: lung adenocarcinoma, H460: lung adenocarcinoma, 18S was used as a loading control. **B**: qRT-PCR assessment of mRNA abundance of desmoplakin (DSP), Tenascin (TNC-c), enolase (ENO1) and EROI-La. ns: p=0.06-7, ****:p=<0.0001, H1975GP: GDC-0980 sensitive H1975, H1975GR: GDC-0980 resistant H1975, 18S was used as a loading control.

2.4.8. Long non-coding RNA (lncRNA)

LncRNA expression in H1975GR1 or H1975GR6 compared to drug sensitive H1975GP cells was quantified by the ArrayStar Human lncRNA Microarray V4.0. Scatter-plot analysis of the lncRNA expression variation between the two compared groups of samples is illustrated in figure 2.18A. The total of (upregulated genes were 6736 "red"), (down-regulated genes were 4971 "green") and (no differential expressed genes were 18521 "black") when H1975P compared to H1975GR1, while (the upregulated, down-regulated and un-changed genes were 7528, 7033 and 15667 genes, respectively when H1975P was compared to H1975GR6). The numbers of altered genes based on their genomic location are detailed in figure 2.18B and summarized in table 6 and the full detailed list on the altered lnRNAs is included in the appendices: (exon sense-overlapping "E-S" lncRNAs in appendices 2.9-2.16, intron sense-overlapping "I-S" lncRNA in appendices 2.17-2.24, intron antisense-overlapping "I-AS" lncRNAs in appendices 2.25-2.32, bi-directional overlapping "BD" lncRNAs in appendices 2.33-2.40, naturally antisense overlapping "N-AS" lncRNAs in appendices 2.41-2.48, and intergenic lncRNA in appendices 2.49-2.56) (Table 2.8). The appendices contain the following information: lncRNA gene symbol, genome location (chromosome number, nucleotide start and end location), RNA length and the associated gene symbol (except the intergenic). The fold change values were sorted from the highest to the lowest values. Changes in lncRNA expression in H1975GR1 cells may highlight those lncRNAs that are involved in the early development of resistance to GDC-0980 in H1975 lung adenocarcinoma cells. The p-value and fold change were set to <0.05 and 2.0, respectively.

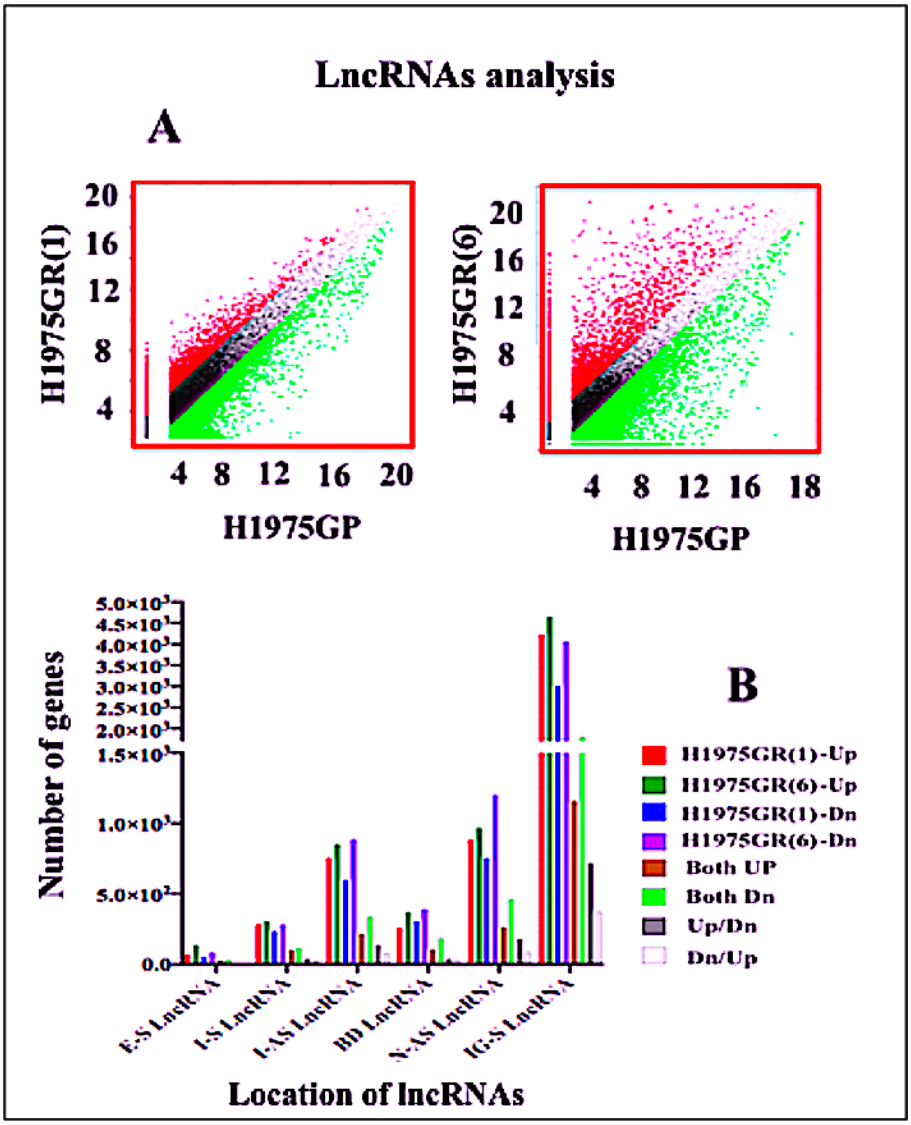

Figure 2.18. Altered expression of lncRNAs in H1975GR1 and H1975GR6 compared to H1975GP. A. Scatter plot analysis of lncRNA expression data; (red) upregulated, (green) down-regulated and (black) unaltered. B. classification of the altered lncRNAs based on their location (E-S: exon sense-overlapping, I-S: intron sense-overlapping, I-AS: intron antisense-overlapping, BD: bi-direction-overlapping, N-AS: natural antisense overlapping, IG: intergenic overlapping, lncRNA: long non-coding RNA).

Table 2.8. Differentially expressed lncRNAs in H1975GR1 and H1975GR6.

	H1975GR(1)	H1975GR(6)	H1975GR(1)	H1975GR(6)
	Up/ exon-sense-overlapping lncRNAs		**Dn/ exon-sense-overlapping lncRNAs**	
Unique	64 (appx: 2.9)	135 (appx: 2.11)	51 (appx: 2.10)	82 (appx: 2.12)
Both	21 (appx: 2.13)		28 (appx: 2.14)	
Up/Dn	8 (appx: 2.15)	6 (appx: 2.16)		8 (appx: 2.15)
	Up/ intronic sense-overlapping lncRNAs		**Dn/ intronic sense-overlapping lncRNAs**	
Unique	283 (appx:2.17)	303 (appx: 2.19)	233(appx: 2.18)	282 (appx: 2.20)
Both	101 (appx: 2.21)		112 (appx: 2.22)	
Up/Dn	38 (appx: 2.23)	19(appx: 2.24)		38(appx: 2.23)
	Up/ intronic anti-sense-overlapping lncRNAs		**Dn/ intronic anti-sense-overlapping lncRNAs**	
Unique	754 (appx: 2.25)	852 (appx: 2.27)	597 (appx: 2.26)	885 (appx: 2.28)
Both	214 (appx: 2.31)		334 (appx: 2.32)	
Up/Dn	136 (appx: 2.29)	79 (appx: 2.30)		136 (appx: 2.29)
	Up/ bi-directional lncRNAs		**Dn/ bi-directional lncRNAs**	
Unique	254 (appx: 2.33)	370 (appx: 2.35)	305 (appx: 2.34)	389 (appx: 2.36)
Both	104 (appx: 2.37)		183 (appx: 2.38)	
Up/Dn	37 (appx: 2.39)	33 (appx: 2.40)		37 (appx: 2.39)
	Up/ natural anti-sense-overlapping lncRNAs		**Dn/ natural anti-sense-overlapping lncRNAs**	
Unique	883 (appx: 2.41)	965 (appx: 2.43)	753 (appx: 2.42)	1200 (appx: 2.44)
Both	262 (appx: 2.45)		459 (appx: 2.46)	
Up/Dn	180 (appx: 2.47)	88 (appx: 2.48)		180 (appx: 2.47)
	Up/ intergenic lncRNAs		**Dn/ intergenic lncRNAs**	
Unique	4228 (appx: 2.49)	4640 (appx: 2.51)	2988 (appx: 2.50)	4072 (appx: 2-52)
Both	1157 (appx: 2.53)		1793 (appx: 2.54)	
Up/Dn	714 (appx: 2.55)	374 (appx: 2.56)		714 (appx: 2.55)

Specific lncRNAs were selected for further assessment by qRT-PCR in H1975GR6 compared to H1975GP cells. The selection was based on their location within the genes that modulate/or are modulated by *JAK/STAT* pathway, and including *PIM1*, and *PIM2* kinases upregulated in the resistant cells compared to the sensitive cells (19.8 and 3.3 fold) (Table 2.9). Other *STAT3* regulators were also upregulated in the resistant cells such as *SOCS1*, and *SOCS3* (fold change 3.2 and 7.7, respectively) and *Mcl-1* (fold change 3.7).

Table 2.9. lncRNAs selected for further qRT-PCR assessment.

GENE	FC-LncRNA	Reg.	NG	FC-mRNA	Reg.
AC008163.4	7.7	Down	*HGF*	2.2	Up
LINC01969	8.4	Up	*PDK2*	7.9	Up
CASC11	4.6	Up	*c-MYC*	25.7	Up
LINC01510	6.3	Down	*MET*	6.1	Up

FC: fold change, Reg.: regulation at 6-months GDC-0980 treatment (H1975GR6) compared to the drug sensitive H1975 cells. NG: nearby gene, HGF: hepatocyte growth factor, *PDK2*: pyruvate dehydrogenase kinase-2, *MYC*: v-myc: myelocytomatosis viral oncogene homology, *MET*: *MET* proto-oncogene, receptor tyrosine kinase.

2.4.8.1. Validation of AC008163.4 lncRNA expression by qPCR

The arrayStar data showed AC008 (AC008163.4) lncRNA expression was significantly decreased in both H1975GR1 and H1975GR6 cells compared to H1975GP cells (cut-off value= 2.0-folds, $P<0.05$) (Figure 2.19A). Assessment of AC008 expression in (tested in three independent experiments) H1975GP versus H1975GR6 by comparative qRT-PCR showed a decreased AC008 mRNA level in the resistance cells compared to the parent cells despite the statistical insignificance (Figure 2.19B).

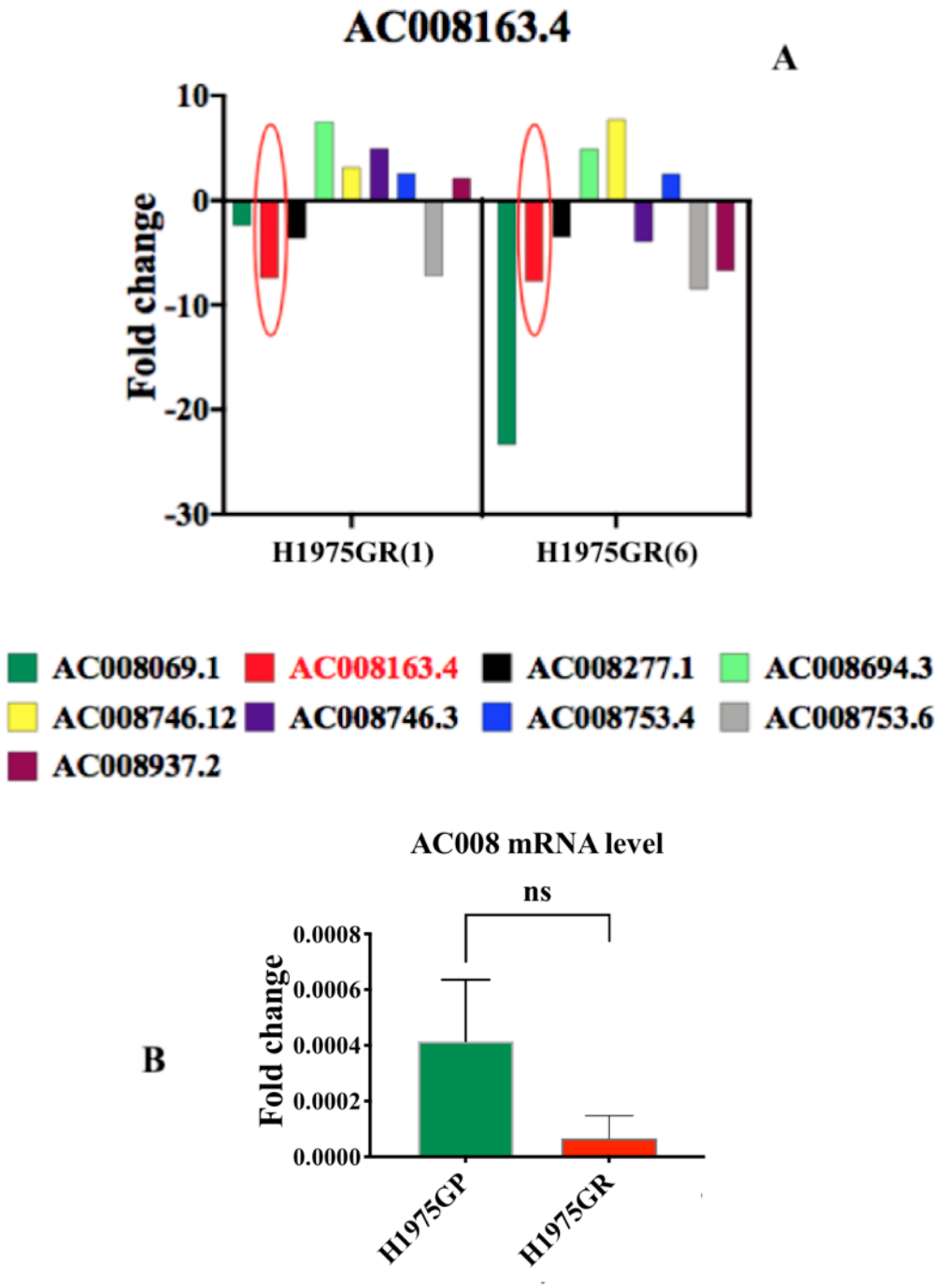

Figure 2.19. ArrayStar assessment of AC008 lncRNA expression followed by qRT-PCR validation. A: ArrayStar® analysis of AC008 lncRNA gene in H1975GR1: H1975 cells were treated with GDC-0980 for one month, and H1975GR6: H1975 cells were treated with GDC-0980 for six months compared to GDC-0980 sensitiveH1975 cells. B: qRT-PCR assessment of AC008163.4 in H1975 GDC-0980 resistant H1975GR cells compared to the drug sensitive H1975GP cells.

2.4.8.2. Validation of CASC11 lncRNA expression by qRT-PCR

ArrayStar showed *CASC11* lncRNA expression was increased in both H1975GR1 and H1975GR6 compared to H1975GP cells (cut-off value= 2.0-folds, $P<0.05$) (Figure 2.20A). Assessment of CASC11 expression (tested in three independent experiments) in H1975GP versus H1975GR by comparative qRT-PCR showed insignificant increase in the CASC11 levels in the resistant cells compared to the parent cells (Figure 2.20B).

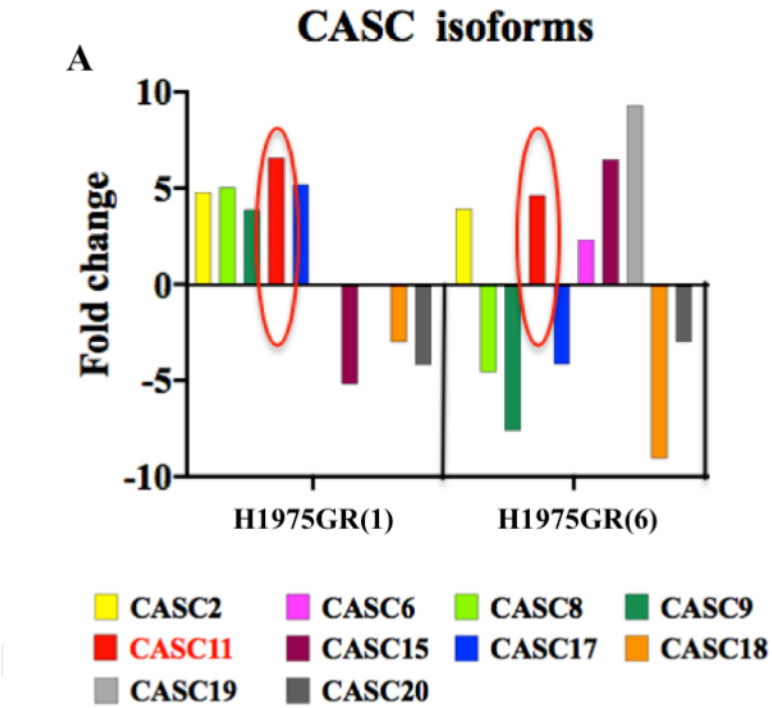

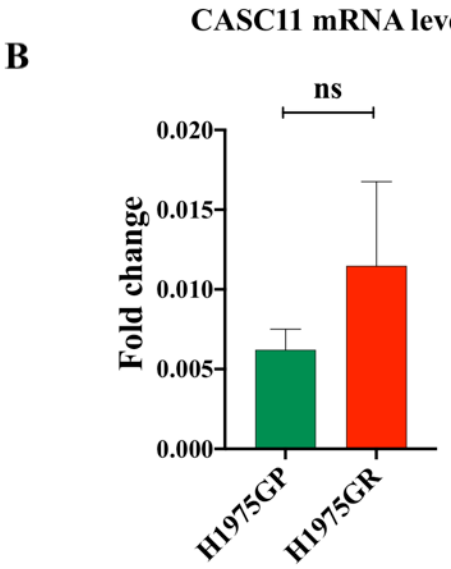

Figure 2.20. **ArrayStar® assessment of CASC11 lncRNA expression followed by qRT-PCR validation.** A: ArrayStar® analysis of CASC lncRNA genes in H1975GR1: H1975 cells were treated with GDC-0980 for one month, and H1975GR6: H1975 cells treated with GDC-0980 for six months, compared to GDC-0980 sensitive H1975 cells. B: qRT-PCR assessment of CASC11 in H1975 GDC-0980 resistant H1975GR cells compared to the drug sensitive H1975GP cells.

2.4.8.3. Validation of Linc1510 lncRNA expression by qPCR

ArrayStar® comparison analysis of linc-lncRNAs between linc01500 and linc01600 showed Linc1519, linc1544 and linc1591 were elevated in H1975GR6 cells compared to H1975GR1 cells. There was no significant change in the expression of linc1534, linc1535, linc1586, linc1556, linc1558 and linc1518. Linc1521 was decreased in both H1975GP1 and 6, compared to the sensitive cells H1975GP. Linc1510 was down-regulated in H1975GR1 and in H1975GR6 cells (Figure 2.21A). Assessment of linc1510 expression in (three independent experiments) H1975GP versus H1975GR by comparative qRT-PCR revealed insignificant decrease in the H1975GR compared to H1975GP (Figure 2.21B).

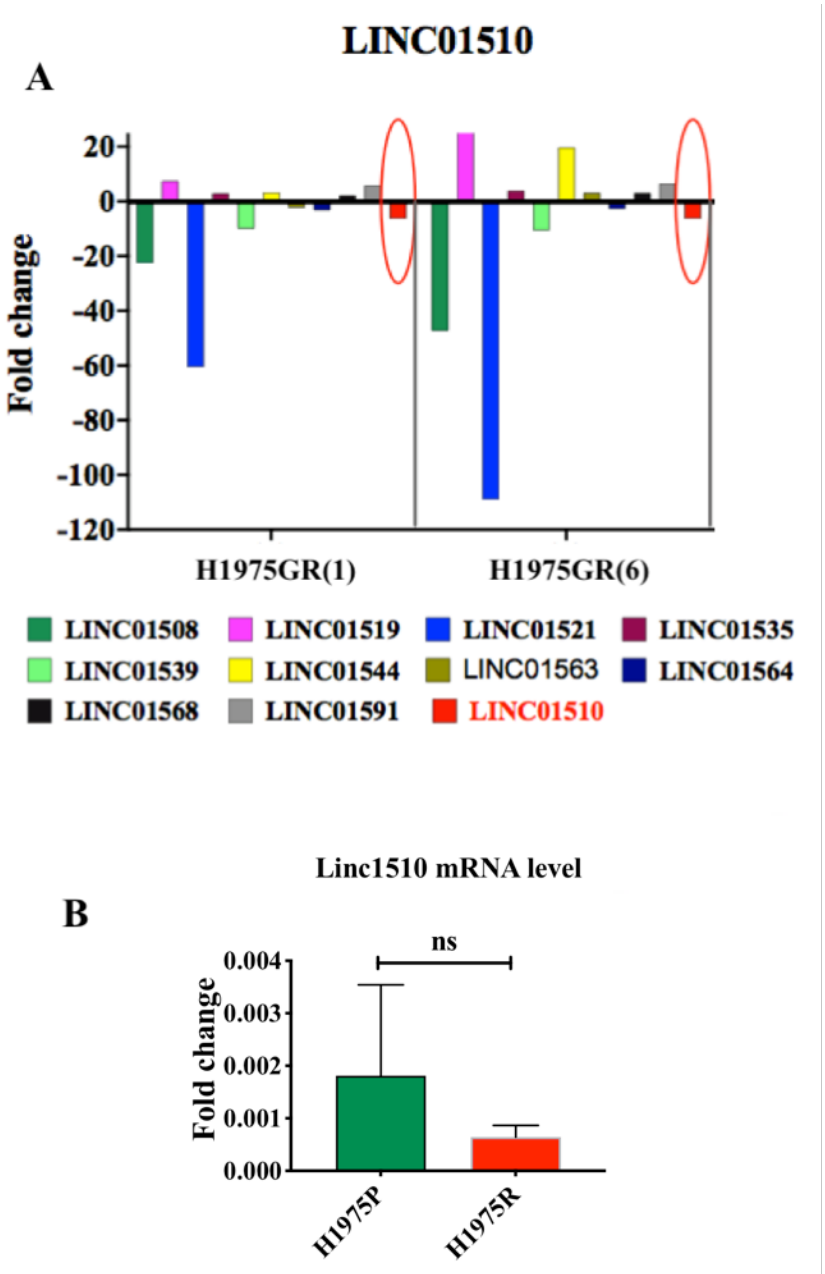

Figure 2.21. **ArrayStar assessment of linc1510 lncRNA expression followed by qRT-PCR Validation.** A: ArrayStar® analysis of linc1500 to linc15100 lncRNA genes in H1975GR1: H1975GP were treated by GDC-0980 for one month, H1975GR6: cells were treated with GDC-0980 for six months compared to H1975 sensitive cells. B: qRT-PCR assessment of linc1510 in H1975 GDC-0980 resistant H1975GR cells compared to the drug sensitive H1975GP cells.

2.4.8.4. Validation of Linc 1969 lncRNA expression by qPCR

ArrayStar® expression analysis of linc01969 lncRNA (at cut-off value= 2.0-folds, P<0.05) showed that linc01969 lncRNA was down-regulated in H1975GR1 then significantly increased in H1975GR6 in comparison to H1975GP cells (Figure 2.22A). Assessment of linc1969 expression in (three independent experiments) H1975GP versus H1975GR by comparative qRT-PCR revealed insignificant change among the compared groups (Figure 2.22B).

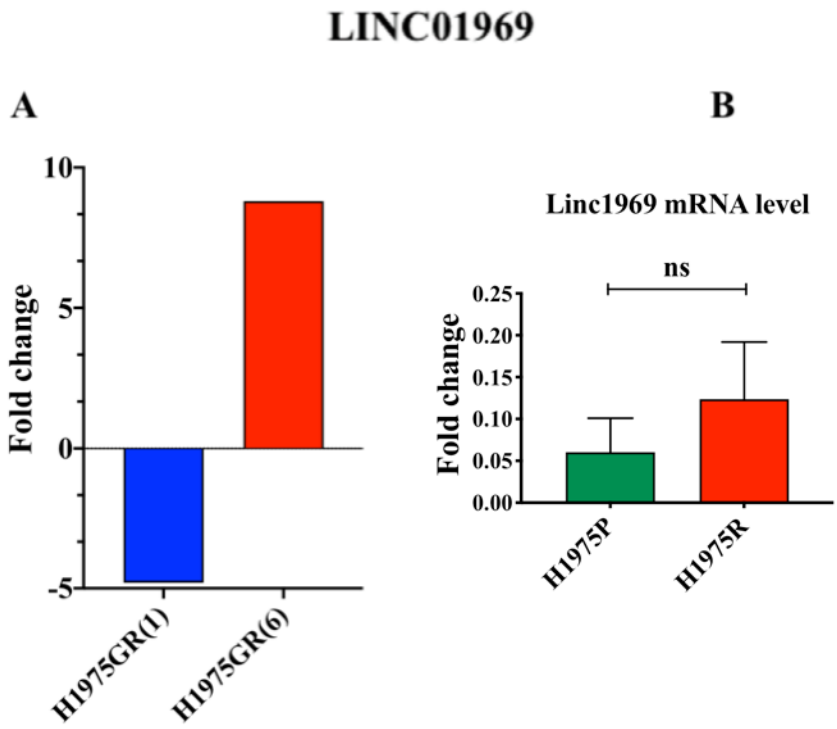

Figure 2.22. ArrayStar assessment of Linc01969 expression followed by qPCR validation. A: arrayStar® analysis of Linc01969 lncRNA mRNA in H1975GR1/6 compared to H1975GP. B: The average level of Linc1969 mRNA lncRNA in the GDC-0980 resistant H1975GR cells compared to the drug sensitive H1975GP compared to β-actin.

Figure 2.23 is a schematic which hypothesises the signalling cascade involved in the emergence of acquired resistance to GDC0980 in H1975 cells. Activation of the *PI3K* pathway is shown by the numbering system with red numbers in black boxes: (1): The binding of integrins, ligands to RTKs or cytokines such as *IL6* result in *PI3K* phosphorylation/activation. (2) Once phosphorylated *PI3K* converts *PIP2* to *PIP3*. (3) *PIP3* phosphorylates *PDK1* or (4) recruits and phosphorylates *AKT* directly. (5) *PDK1* phosphorylates *AKT*. (6) *AKT*/*pkB* leads to activation of transcription of genes needed for cell cycle (growth and proliferation), metabolism, protein synthesis and others. The resistance bypass signalling mechanism is shown by the numbering system with red numbers in green boxes: *MAPK* phosphorylates and activates *AKT* directly (1) adding survival bonus to the H1975GR cells, Or/and phosphorylates *PIM1* (2) or cross talk with other genes such as *MACC1* (3) leading to enhanced transcription of *c-Met* (4). *c-Met* leaves the nucleus (5) and then becomes phosphorylated by *HGF* (6). *c-Met* could phosphorylate and activate *STAT3* leading to their dimerization (7). *STAT3* homo-dimer will enter the nucleus and promote *PIM1*, *c-Myc*, *Mcl-1*, cytokines and *SOCs* genes transcription (8). Cytokines will be translated and the cytokines would lead to an additive stimulation of *JAK*/*STAT* pathway (10). *PIM1* in the cytoplasm (11) will be phosphorylated and activated by *MAPK* (2), then the phosphorylated *PIM1* either phosphorylates *AKT* (12) to enhance cells proliferation (13) or cooperate with *c-Myc* (14) to phosphorylate *BAD* (15) and interfere with the apoptosis (16). *Mcl-1* can also inhibit apoptosis by attaching the mitochondrial membrane (17) and interfering with cytochrome-c release from the mitochondria (18), the enzyme needed to initiate apoptosis.

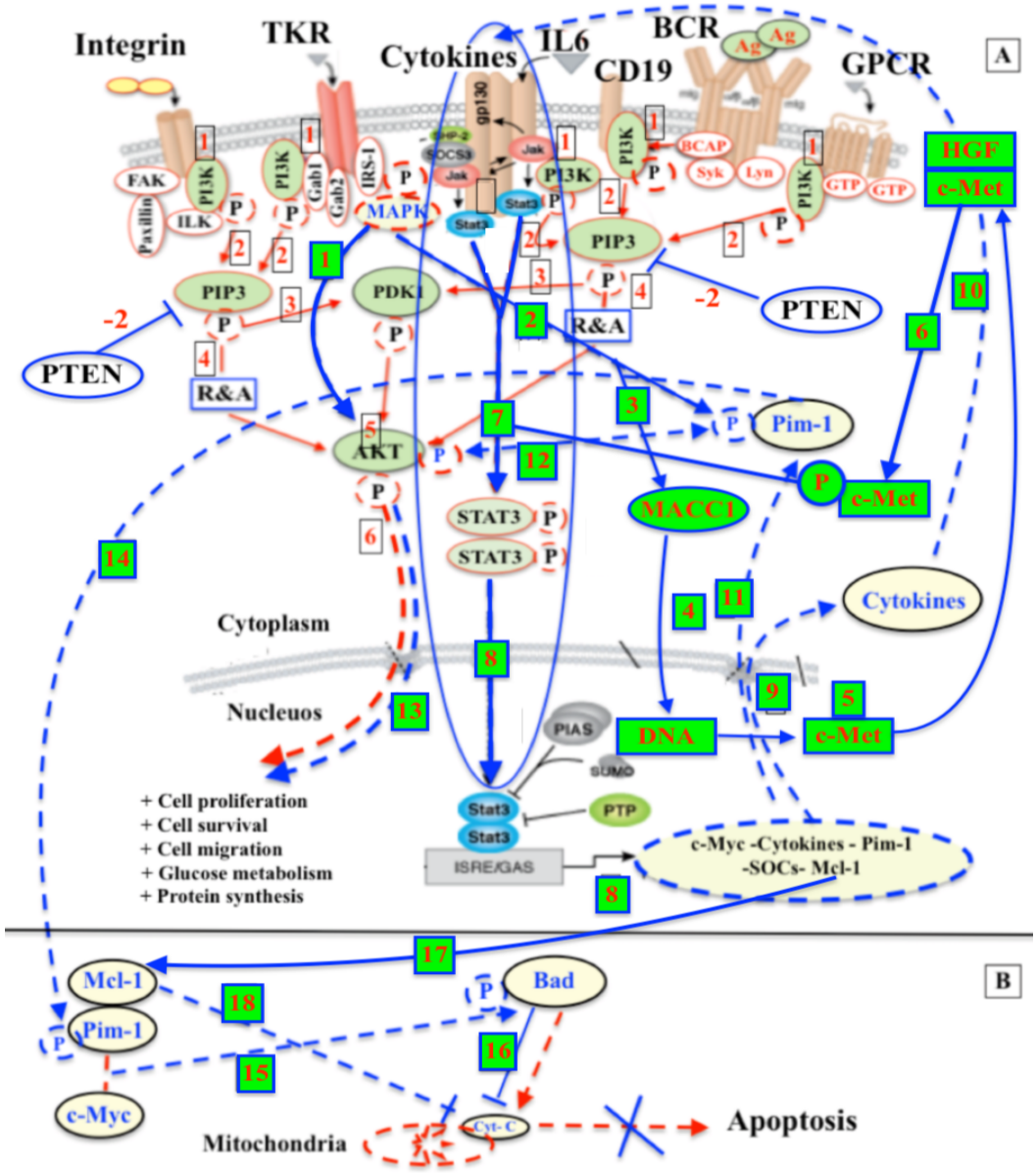

Figure 2.23. Schematic depicting the role of PIM kinase signalling in development of resistance to GDC0980 in H1975GR cells.

2.5. Discussion

We hypothesized that the initial sensitivity to PI3K inhibition in the H1975 cells could imply a reliance on PI3K pathway signalling, with the cells being addicted to the pathway. As such, the drug mediated significant effects in the short term, but the increased selective pressure led to the cells becoming rapidly resistant to the drug and effectively mimicking what happens in patients treated with targeted therapies in the clinic. This study set out to validate markers of resistance to dual PI3K-mTOR inhibitor GDC-0980 (apitolisib) in the H1975GR NSCLC cell line model of resistance, previously developed in our laboratory to pinpoint specific bypass mechanisms of resistance (Heavey et al., 2018).

A RNA microarray was employed to profile changes in mRNA and lncRNA in the GDC-0980 resistant NSCLC cell line models that were previously generated.

Both long non-coding RNA (lncRNA) and coding RNA (mRNA) were quantified after one month of treatment with GDC-0980 (H1975GR1) and after six months of treatment (H1975GR6). Panther-Slim biological process analysis of all differentially regulated mRNAs in H1975GR1 (Figure 2.5A/B) and in H1975GR6 (Figure 2.5C/D) compared to H1975GP showed that 298 upregulated genes and 162 down-regulated genes in H1975GR1 and 683 upregulated genes and 458 down-regulated genes in H1975GR6 were involved in the regulation of metabolism. Given that the PI3K-mTOR signalling network has diverse downstream effects on cellular metabolism, through either direct regulation of nutrient transporters and metabolic enzymes or the control of transcription factors that regulate the expression of key components of metabolic pathways it is therefore not surprising that so many of the deregulated genes are involved in metabolism. Panther-Slim biological process analysis also showed that 76 upregulated and 55 down-regulated

genes in H1975GR1 and 185 upregulated genes and 78 down-regulated genes in H1975GR6 were involved in cellular response to stimuli (Figure 2.5). These are genes involved in the physiological response of a cell to a stimulus such as exposure to GDC-0980 and include genes involved in drug efflux and epigenetic regulation.

Activation of MACC1, a regulator of PIM kinase, is an early event in resistance to GDC-0980:

Differentially expressed mRNAs and lncRNAs in H1975GR1 cells may elucidate genes and gene regulators that are involved in the early development of resistance to GDC-0980 in H1975 cells. To this end, activation of metastasis-associated in colon cancer 1 (*MACC1*) gene emerged as a possible early driver of the resistance to GDC-0980 in H1975GR1 cells with a 77.89 fold increase and 44.89 fold increase in H1975GR1 and H1975GR6, respectively (Figure 2.13A). Further validation of *MACC1* protein expression by western blot analysis revealed a significant increase (p: <0.05) in the abundance of *MACC1* in the resistant cells (H1975GR) compared to the drug-sensitive cells (H1975GP), with the latter undetectable by western blot (Figure 2.13B).

It has been previously shown in lung cancer that cisplatin resistance was mediated by *MACC1* via activation of *PI3K/AKT* pathway (Zhang et al., 2018). *MACC1* was also found to facilitate chemoresistance in colorectal cancer (Wang et al., 2017a) and gastric cancer via activation of PI3K/AKT pathway (Duan et al., 2017). Down-regulation of *MACC1* was found to inhibit proliferation, invasion and migration in salivary adenocarcinoma, and this was associated with enhanced apoptosis (Li et al., 2015a). Knock down of *MACC1* was found associated with increased cisplatin sensitivity in cisplatin resistant ovarian epithelial cells (Zhang et al., 2016b). Elevated *MACC1* mRNA levels correlated to a poor prognostic marker for post-

surgery tumour recurrence in colorectal cancer (Isella et al., 2013) and lung adenocarcinoma (Shimokawa et al., 2011). In NSCLC, *MACC1* overexpression correlates with a poor prognosis (Wang et al., 2014b) and is considered a good biomarker for metastasis (Zhou et al., 2016b). *MACC1*- targeted antibodies were found to suppress tumour growth and metastasis in NSCLC (Shi et al., 2017). Taken together these data highlight a role for *MACC1* in both chemoresistance and disease progression. *MACC1* has also been shown to play a role in resistance to targeted therapy trastuzumab in gastric cancer through activation of the Warburg effect and PI3K/Akt signalling (Liu et al., 2016). To our knowledge our data is the first to demonstrate the role of *MACC1* in resistance to PI3K-mTOR inhibition.

Activation of HGF and c-Met and lncRNA regulators in H1975GR cells:

In a study by Stein et al., *MACC1* triggered hepatocyte growth factor (HGF) induced colon cancer metastasis in a mouse model (Stein et al., 2009). Interestingly, we also observed *HGF* mRNA and its receptor the hepatocyte growth factor receptor (*HGFR*) or *MET* mRNA, which is a transcriptional target of *MACC1* (Boardman, 2009), were activated 10.06 and 1.66 fold respectively in H1975GR1 cells as well as 2.22 and 6.06 fold in H1975GR6 cells (Figure 2.15A). c-Met protein expression analysis by western blot showed no significant change in c-Met protein expression between the parent and resistant cells (Figure 2.15B). The lncRNA (AC008163.4) is a regulator of the *HGF* gene and was decreased by 7.7 fold in H1975GR6 cells compared to H1975GP cells (Figure 2.19A). However, qRT-PCR validated in GDC-0980 resistant H1975 revealed a significant increase in the levels of lncRNA (AC008163.4) in the resistant cells (H1975GR6) in compare to the sensitive cells (H1975GP) (Figure 2.19B).

The lncRNA linc01510, which regulates the *MET* gene, was decreased by 6.1 fold in the H1975GR6 resistant cells compared to drug sensitive H1975GP cells H1975GP by RNA sequencing (Figure 2.21A). However, validation of this lncRNA by qRT-PCR detected no significant difference in expression between H1975GR and H1975GP cells (Figure 2.21B).

HGF gene expression is regulated by STAT3, NFKB and IL6 (Tomida and Saito, 2004). Once HGF binds to its receptor HGFR or c-Met it results in dimerization and activation as the intracellular domain of c-Met becomes phosphorylated. c-Met in turn phosphorylates STAT3 via JAKs (Runge et al., 1999). Genes whose transcription is modulated by STAT3 transcription factor include PIM kinases, HGF and transcription of JAKs-negative feedback genes including SOCS3 (Hung and Elliott, 2001, Tomida and Saito, 2004, Tokumaru et al., 2005).

IL6/STAT3 pathway activation in GDC-0980 resistant H1975GR cells:

Activation of the *IL6/STAT3* pathway leads to the activation of the PIM kinase family of proteins and c-Myc which co-regulate each other (van Lohuizen et al., 1989). In depth characterisation of the resistant cell line models identified activation of the *IL-6/STAT3* pathway including all 3 *PIM* genes and their co-regulator the proto-oncogene *c-Myc*. RNA sequencing arrays revealed *PIM* mRNA expression as follows: a decrease in *PIM1* by -1.29 fold (< 2 fold cut-off), an increase in *PIM2* by 1.69 fold (< 2 fold cut-off) and an increase in *PIM3* by 2.08 fold in H1975GR1 cells and an increase in *PIM1* by 19.8 fold, *PIM2* by 3.3 fold and *PIM3* by 32 fold in H1975GR6 cells compared to H1975GP cells (Figure 2.7A). Validation of *PIM1, 2* and *3* by qRT-PCR in H1975GR6 compared to H1975GP cells revealed a significant elevation of all PIM kinases (however *PIM3* was not significant) as indicated by low Ct (Figure 2.7B). Validation of protein expression of PIM1, 2 &

3 kinases by western blot analysis in H1975GR6 and H1975GP cells revealed a significant increase in expression of all three *PIM* kinase proteins (Figure 2.8). *PIM* kinases are a class of serine/threonine kinases that play a role in several of the hallmarks of cancer including cell cycle progression, metabolism, inflammation and immune evasion. Their constitutively active nature and unique catalytic structure has led them to be an attractive anticancer target through the use of small molecule inhibitors. One previous study showed *PIM1* highly expressed, at both mRNA and protein levels, in the normal lung mesothelial cells but expressed at very low levels in NSCLC (Warnecke-Eberz et al., 2008). *PIM* gene expression is modulated by the activation of various transcription factors; including *STAT3* homodimer and *STAT3/5* heterodimer via the *JAK/STAT* pathway, *NF-κB* and HOXA9 (Brault et al., 2010). PIM kinase has a potential role in the tumourigenesis and progression of several types of cancers with *PIM1* and *PIM3* found more specifically in haematological malignancies, whereas increased abundance of *PIM2* was found more common in solid tumours (Brault et al., 2010). *PIM1* kinase has been shown to play a role in cell death protection and to enhance tumour growth and metastasis. Increased levels of *PIM1* expression was also found associated with increased expression signature of *c-Myc* transcription factor-modulated genes. Activation of *PIM* kinases was shown to trigger *Met*-small molecule inhibitors resistance (Horiuchi et al., 2016). All PIM tyrosine kinases enhance tumour cells proliferation through their downstream signalling through cMyc-inhibition of apoptosis (Chen et al., 2005).

Activation of transcription factor and co-regulator of PIM kinase c-Myc:

RNA sequencing array data showed *c-Myc* mRNA was increased by 2 fold in H1975GR1 cells compared to the untreated H1975GP cells. mRNA expression continued to increase until it reached 25.7 fold in H1975GR6 cells (Figure 2.12A). Validation of these results by qRT-PCR, did not show significant increase in *c-Myc* mRNA abundance as indicated by low Ct values in the H1975GR6 cells compared to H1975GP cells (Figure 2.12B). However, validation of *c-Myc* protein expression by western blot analysis showed a significant increase in the abundance of *c-Myc* protein in H1975GR6 cells compared to H1975GP cells (Figure 2.12C). *c-Myc* gene regulator lncRNA *CASC11* was activated by 25.7 fold in H1975GR6 cells compared to H1975GP cells (Figure 2.20A) however validation by qRT-PCR revealed no difference between the compared cells (Figure 2.20B). *c-Myc* is a multi-function phospho-protein transcription factor required for rapid cell division, cell adhesion, increased metabolic and biosynthesis rates, mitochondrial biogenesis and to inhibit anti-proliferation genes' expression (Miller et al., 2012, Dang et al., 1999). c-Myc inhibition was found to sensitize cancer cells resistant to vincristine better than other small molecule inhibitors such as *PI3K*, *MAPK* and *NF-kB* inhibitors (Sheikh-Zeineddini et al., 2020). *PIM* kinases alone are only weakly oncogenic, however when co-expressed with *c-Myc* they can phosphorylate /stabilise it, enhancing *c-Myc*-driven tumourigenicity (Wang et al., 2010). *PIM1* facilitates the transcriptional activation of approximately one fifth of *c-Myc* targets through a *Myc*-driven recruitment of *PIM1* to chromatin where it can phosphorylate Histone H3, and allow the subsequent initiation of transcription (Zippo et al., 2007). The synergism of *PIM* kinases and c-Myc is also evidenced through their common targets, such as the cell cycle phosphatase, *cdc25A*, which is transcription-ally

regulated by *c-Myc* and also substrate of *PIM1* phosphorylation /activation (Mochizuki et al., 1999).

Inhibition of MACC1 and PIM kinases by targeted siRNAs to determine effect on H1975GR6 cells:

Inhibition, by siRNA knockdown, of *MACC1* (Figure 2.14), *PIM1* and *PIM3* (Figure 2.9) was examined to evaluate if their activation in GDC-0980 resistance in H1975GR6 cells played a role in cell survival . Figure 2.14 demonstrates that there was a significant difference between the effect of *MACC1* siRNA on the viability of H1975GR and H1975GP cells, the latter had 50% of cell viability of H1975GR, and this indicates H1975GR had much more *MACC1* than H1975GP. Upon combination, *MACC1* siRNA re-sensitized H1975GR cells for GDC-0980 (when the cells were pre-treated with GDC-0980), and both GDC-0980 sensitive and resistant cells were killed equally. This data supports our hypothesis that *MACC1* is involved in acquired resistance to GDC-0980.

PIM1 siRNA had a little and equal effect on the viability of both H1975GR and H1975GP cells. Combination of both GDC-0980 had no additive effect compared to the effect of GDC-0980 alone (Figure 2.9A). *PIM3* siRNA had a more significant effect on the cells viability of both H1975GR and H1975GP cells, and again the effect was equal in both cells phenotype. Upon the combination of GDC-0980 and siRNA, the effect was only additive in the GDC-0980 sensitive H1975 and no noticeable effect was observed on the resistant cells (siRNA as reference) (Figure 2.9B). This result could be attributed to the increased expression of *PIM* isoforms expression in the resistant cells and the siRNA concentration was not sufficient to cope with mRNA levels in the resistant cells (H1975GR).

Determining the efficacy of pan-PIM inhibitor AZD1208 in the H1975GR cells:

Pan-*PIM* inhibitor (AZD-1208) was shown to re-sensitize triple negative breast cancer (TNBC) cells and patient-derived xenograft to radiotherapy, modulated by activation of *c-Myc* and *PIM1* which had a synergic effect to *Mcl-1* (Brasó-Maristany et al., 2016). *PIM1* kinase inhibition was also successful to re-sensitize NSCLC cells that displayed resistance to radiotherapy (Kim et al., 2013). In this research work, the efficacy of AZD-1208 was examined in *PIM* kinase activated resistant H1975GR cells (Figure 2.11). Different inhibitory concentration (IC) values were calculated as described in figure 2.9 and tables 2.5 to 2.7. AZD-1208 IC90 had no additive effect on GDC-0980 IC40, while AZD-1208 IC70 and 50 had an additive effect on GDC-0980 growth inhibition effect, while IC30 had a little additive effect to the GDC-0980 effect. The best dose combination was the IC 50 of AZD-1208 with GDC-0980 IC40. The use of small molecule inhibitors was better than the use of siRNA, this could be attributed to the incomplete success of abolishing the whole mRNA translation by siRNA. In contrast the small molecule inhibitor would interfere with the *PIM* site of action leading to diminished cell proliferation and less protection against apoptosis mediated by all three *PIM* kinases.

In summary, *c-MET*, *c-Myc* and *PIM* kinases were upregulated across all the models of resistance to GDC-0980 suggesting their importance in generating drug resistance. Figure 2.23 is a schematic that summarizes the role of *PIM* kinase and its coregulators as an escape signalling mechanism in GDC-0980 resistant H1975GR cells. Co-targeting strategies involving both *PIM* kinase and *PI3K-mTOR* pathways may provide a more durable response to treatment in patient cohorts known to have an activated *PI3K-mTOR* pathway.

Activation of CMTM6 a regulator of PD-L1 in GDC-0980 resistant H1975GR cells:

RNA sequencing data identified another activated gene of interest *CMTM6*. *CMTM6* is an abbreviation of chemokine-like factor (*CKLF*) like *MARVEL* transmembrane domain containing-6. *CMTM6* binds PD-L1 at the cell membrane leading to an increased chance of its interaction with *PD-1* on the CD8+ T lymphocytes leading to protection against immune-destruction (Boussiotis, 2016, Imamovic and Vranic, 2017). *CMTM6* mRNA expression was decreased by 20 fold in H1975GR1 cells but increased by30 fold in H1975GR6 cells compared to H1975GP cells (Figure 2.16A). Validation by qRT-PCR revealed a significant increase in *CMTM6* mRNA levels as indicated by low delta CT (early take-off) (Figure 2.16B). Western blot revealed increased *CMTM6* levels in the resistant cells but this did not reach significance (Figure 2.16C).

Evaluation of desmoplakin, tenascin c, enolase-1 and ERO1-La expression in H1975GR cell lines:

The last part of this chapter evaluates a panel of proteins (desmoplakin, tenascin c, enolase-1 and ERO1-La) identified in chapter 3 that examined intra-tumour heterogeneity (ITH) in squamous cell carcinoma (SqCC). Here the expression of these four proteins were examined in the H1975GR6 cells compared to H1975GP cells to determine whether they may also play a role in resistance to *PI3K-mTOR* inhibitor GDC-0980. Desmoplakin is a tumour suppressor gene, known to suppress tumour metastasis by inhibiting Wnt/ß-catenin signalling pathway (Yang et al., 2012). Tenascin c is an extracellular matrix glycoprotein, involved in tumour angiogenesis (Tanaka et al., 2004) and known to induce tumour cells-resistance to apoptosis (Shi et al., 2015). Enolase-1 was found to promote chemoresistance via

stimulation of glycolysis (Qian et al., 2017). *ERO1-La* upregulation in tumour cells was found to increase *PD-L1* levels and to promote immune-escape in breast cancer. These four proteins were differentially expressed across different parts of the same tumour in patient tumours with a diagnosis of SqCC (n=3) (chapter 3). Initially mRNA expression was examined by qRT-PCR in the GDC-0980 resistance cells (H1975GR6) compared to the sensitive cells (H1975GP) (Figure 2.17B). *TNC*, *ERO1A* and *ENO1* mRNAs were all significantly upregulated in the H1975GR cells compared to the drug sensitive cells (H1975GP) as demonstrated by low delta Ct-values, while *DSP*, was down-regulated (but not significant). The panel was also evaluated in normal bronchial epithelial cells and nine lung adenocarcinoma cell lines as a control expression in cancer cells (Figure 2.17A), to evaluate the expression profile change. Our findings support the previous literature finding linking the elevated/lowered expression of these genes to drug resistance.

In conclusion, the present study demonstrates that the *IL6/STAT3* signalling pathway plays a significant role as an escape mechanism in H1975 cells treated with GDC-0980. *PIM* kinases and their co-regulator *c-Myc* are activated in response to *PI3K-mTOR* inhibition in NSCLC. *MACC1* activation was an early event in *PI3K-mTOR* drug resistance and may have regulated the induction of *c-Myc*, *PIM* kinases and *CMTM6* genes. These results, together with previous data in other cancer types highlight the potential for dual targeting of both the *PI3K-mTOR* and *PIM* kinase pathways as a promising strategy for the future treatment of patients with *PI3K-mTOR* activated NSCLC. Interestingly three of four biomarkers identified in chapter 3 namely, *TNC*, *ERO1A* and *ENO1,* are also activated in the resistant H1975GR6 cell lines compared to the H1975 drug sensitive cells and further evaluation at the protein level is warranted.

3. **Chapter III**: Quantification of phosphor-proteomic & proteomic expression within squamous cell carcinoma lung tumours

3.1. Introduction

Lung squamous cell carcinoma (LSqCC) is strongly associated with cigarette smoking and affects the central bronchi with only about 15-30% of lung SqCC commonly diagnosed in the lung periphery (Tomashefski et al., 1990).

The treatment for LSqCC includes; cytotoxic chemotherapy such as paclitaxel and cisplatin (Schiller et al., 2002). *EGFR* targeted therapy can be used for mixed adenosquamous lung carcinoma with mutations in *EGFR* associated with gain of function (Rekhtman et al., 2012), eg. Erlotinib, Afatinib, Cetuximab, Necitumumab (Paz-Ares et al., 2015). Also immunotherapies such as *CTLA-4* inhibitors e.g. ipilimumab and tremelimumab (Lynch et al., 2012), *PD-1* inhibitors such as nivolumab and pembrolizumab (Rizvi et al., 2015), and *PD-L1* inhibitors such as BMS-*936559*, *MPDL3280A* and *MEDI4736* (Lynch et al., 2012) can also be used. Inhibition of the *VEGF* receptor by Bevacizumab has also shown good efficacy in both adenocarcinoma and squamous cell carcinomas, but increased haemoptysis limited its use for LSqCC (Socinski et al., 2013). The insulin-like growth factor 1 (*IGF-1*) receptor and fibroblast growth factor receptor (*FGFR*) both tyrosine kinase receptors have recently been demonstrated to activate *PI3K*/*AKT-mTOR* and *K-RAS* signalling pathway in squamous cell carcinoma. Several small molecule inhibitors targeting *FGFR1* amplification in LSqCC have been tested eg. *Aea4* and *Aea25* and showed promising results, inhibiting cell proliferation, initiating cell cycle arrest and induction of cell death (Wu et al., 2014).

A study carried out by the Cancer Genome Atlas research Network (TCGA) and published in the journal Nature (September 2012) demonstrated that LSqCC is characterised by complex genomic alterations and is superior to breast and

colorectal cancers in the frequency of mutations (8 mutations per 10^6 bases) (Network, 2012).

In this TCGA research work on SqCC, 122 out of 178 lung SqCC cases analysed had at least the *K-RAS* or *PI3K*/*AKT* signalling pathways altered. Based on these findings, multiple potential therapeutic targets were identified that could be used in the treatment and assessment of patients with SqCC (Chen et al., 2014). The *PI3K-AKT* pathway has been previously shown as a potential target for therapy in solid tumours. About 6.5% of lung SqCC were found to harbour the *PIK3CA* mutation and are associated with increased activity of PI3K (Papadimitrakopoulou, 2012). *PIK3CA* amplification (copy number) was also found in 20% of both adeno and squamous cell carcinoma (Heist et al., 2012, Okudela et al., 2007, Kawano et al., 2007). Both selective, pan-*PI3K* inhibitors as well as *PI3K-mTOR* dual inhibitors has been synthesized (Papadimitrakopoulou, 2012), and have been tested in several clinical trials (Vansteenkiste et al., 2015).

The tumour tissue biopsy removed from the patient for diagnostic purposes is key to the success of targeted therapy. Failure of the biopsy to represent the entire tumour mass might lead to treatment failure and tumour relapse. In this chapter, a comparative proteomic study was undertaken on multiple biopsies (n=3) from fresh frozen tumour tissues along with matched normal lung tissues using LC-MS/MS. The aim was to identify and quantify intra-tumour heterogeneity across different geographical regions of the same tumour as well as differences in protein expression between adjacent normal tissue and tumour tissue. A panel of four proteins; desmoplakin (*DSP*), tenascin c (*TNC-c*), enolase-1 (*ENO1*) and *EROI-La*, which were heterogeneously expressed across the three tumour regions, and play a role in drug resistance, were chosen for further validation. Desmoplakin (*DSP*) is a

member of the plakin family of proteins that localise to desmosomes. Desmosomes are intercellular junctions that confer strong cell–cell adhesion. Desmosomes have an impact on tumourigenesis through their ability to modify signalling by armadillo proteins plakoglobin (*γ*-catenin) and plakophilins. Plakoglobin is closely related to *β*-catenin, an important player in the Wnt/*β*-catenin pathway, and both interact with DSP which is the most abundant component of desmosomes (Zhou et al., 2017). Epithelial-mesenchymal transition (EMT), during which cancer cells lose the epithelial phenotype and gain the mesenchymal phenotype, results in tumour migration and invasion. Dysregulation of the *Wnt/β-catenin* signalling pathway gives rise to EMT, which is characterized by nuclear translocation of β-catenin and E-cadherin and DSP suppression as a result of genetic and/or epigenetic mechanisms. During EMT disruption of both adherents junctions and desmosomes must occur for dissociation of epithelial cells. Several studies have shown that decreased or altered expression of DSP correlates with increased tumour invasion, advanced tumour grade, and poor patient prognosis (Papagerakis et al., 2009). It has also been shown to play a role in cell proliferation, differentiation, migration, and apoptosis (Huber and Petersen, 2015). A study by Yang L et. al, showed that *DSP* acts as a tumour suppressor in lung cancer. When *DSP* is inactivated in lung cancer, by an epigenetic mechanism, it increases the sensitivity to anticancer drug-induced apoptosis and has tumour-suppressive function, possibly due to upregulation of plakoglobin and thereby inhibition of the *Wnt/β-catenin* signalling pathway. The epigenetic regulation of *DSP* and its ability to increase the sensitivity to anticancer drug-induced apoptosis has potential implications for clinical application (Yang et al., 2012).

Tenascin-C (*TNC*) is an extracellular matrix (ECM) glycoprotein, that plays a major role in cell proliferation, migration, and tumour invasion in various cancers. In healthy mammals, *TNC* is highly expressed during embryonic development, particularly in the developing central nervous system, in migrating neural crest cells and at epithelial – mesenchymal interaction sites. In adult tissues, *TNC* expression is tightly regulated and generally repressed (Jones and Jones, 2000). The *TNC* protein has various structural domains that play distinct roles in *TNC* function (Jones and Jones, 2000). In humans *TNC* out of 17, 9 of *FNIII* repeats are alternatively spliced leading to different *TNC* isoforms. Various spliced FNIII repeats have been identified in cancer. *FNIII* domains A1 and C are expressed in lung cancer and A1 domain in renal cell carcinoma (Lowy and Oskarsson, 2015). *TNC* overexpression is often observed in cancer, generally at the invasive tumour front and is associated with poor clinical outcome (Cai et al., 2017). *TNC* is upregulated by *TGF* beta signalling (Islam et al., 2014) and plays a major role in EMT evidenced by its expression in the invasion borders of cancer tissues and in microinvasive foci around intraductal carcinomas, where cells may undergo EMT (Nagaharu et al., 2011). *TNC* expression was observed in NSCLC tumours by a mechanism involving downregulation of Dickkopf-1 (DKK1) and activation of *Wnt* signalling (González-Sancho et al., 2005).

The human enolase (*ENO*) family consist of three members; *ENO1* is present in almost all tissues, *ENO2* is neuron and neuroendocrine tissue-specific and *ENO3* is present in muscle tissues (Díaz-Ramos et al., 2012). *ENO1* plays a major role in different types of human cancer, such as retinoblastoma, hepatocellular carcinoma, pancreatic cancer, renal cell carcinoma, cholangiocarcinoma and gastric cancer. Abnormally upregulated *ENO1* is associated with poor survival and prognosis in

patients with mammary carcinoma (Chen et al., 2020). Furthermore, *ENO1* enhances cell transformation in numerous cancer cell lines. Studies have shown *ENO1* can be either up or downregulated in lung cancer (Chen et al., 2020). Overexpression of *ENO1* significantly elevated cell glycolysis, proliferation, clone formation, migration, and invasion *in vitro*, as well as tumourigenesis and metastasis *in vivo* by regulating the expression of glycolysis, cell cycle, and EMT-associated genes in NSCLC. Conversely, *ENO1* knockdown reversed these effects. Another study revealed that stably upregulated *ENO1* activated *FAK*/*PI3K*/*AKT* and its downstream signals to regulate the glycolysis, cell cycle, and EMT-associated genes. On the contrary, *ENO1* protein levels were significantly reduced in NSCLC and overexpression of *ENO1* inhibited EMT in the A549 cell line (Fu et al., 2015). Therefore, neither expression nor the functional mechanisms of *ENO1* in NSCLC have been clearly established.

Endoplasmic reticulum oxidoreductin-1 alpha (*ERO1α*) is an oxidizing enzyme that exists in the *endoplasmic reticulum* (ER) in concert with protein disulfide isomerase. It facilitates proper protein folding and maintains homeostasis within the ER. Generally during cancer ER stress increases and this is more evident in secretory tumours such as multiple myeloma, breast, lung and pancreatic. However hypoxia and chemotherapy induces ER stress. Given the significance of ER homeostasis, *ERO1α-PDI* interaction, and the formation of ***de novo*** disulfide bridges, *ERO1α* has emerged as a major player in the regulation and tolerance of cancer cells to ER stress (Yadav et al., 2016). Elevation in ER-stress results in two possible outcomes: A. unfolded protein response (UPR) once activated ultimately brings ER stress back to homeostasis via inhibition of translation and inducing cell cycle arrest, or B. if ER stress continues then apoptosis occurs through release of

cytochrome C and caspase activation, ultimately protecting the organism from rogue cells that display misfolded proteins (Haeri and Knox, 2012). Interestingly, overexpression of *ERO1α* tends to have a worse prognosis in multiple cancer indications; multiple myeloma, breast and hepatocellular carcinoma, as well as lung, oesophageal, diffuse B-cell lymphoma, and others according to The Cancer Genome Atlas (TCGA) and The Protein Atlas (Johnson et al., 2020). *ERO1α* plays a major role in the processing and folding of *PD-L1* and *PD-1* (Johnson et al., 2020). *PD-L1* is a transmembrane protein present on the cell surface of placental, vascular endothelium, pancreatic islet, muscle, and mesenchymal stem cells. A study by Tanaka et al, demonstrated that *ERO1α* up-regulates *PD-L1* surface expression not only via oxidative folding, but also through augmentation of hypoxia inducible factor-1alpha (*HIF-1α*) in human triple negative breast cancer cell lines (Tanaka et al., 2017). Knockout of *ERO1A* reduces the growth, migration and tumourigenesis of cervical cancer cells, through downregulation of the H_2O_2-correlated epithelial-mesenchymal transition (Zhang et al., 2019).

PathScan® intracellular signalling arrays were used to elucidate the extent of heterogeneity between phosphorylated protein across tumour regions and also to examine activation of *PI3K-AKT-mTOR* and *JAK/STAT* signalling pathways within these tumours that could drive intrinsic resistance mechanisms for specific targeted therapies such as *PI3K-mTOR* dual inhibitor (GDC-0980).

3.2. Experimental design

Four patients with a diagnosis of lung squamous cell carcinoma (LSqCC) were identified in the Thoracic Oncology Research biobank at St. James's Hospital. For each patient three tumour tissue biopsies from different geographical regions of the same tumour along with adjacent normal tissue were investigated (Table 3.1 under

section 3.3.1.1). After the tumour was surgically dissected along with adjacent normal lung tissue, it was divided into three pieces by the consultant pathologist (Figure 3.1 under section 3.3.1.1) and immediately stabilized in All protect® Qiagen (Cat. #: 76405) overnight at 4°C. The buffer was then removed, and the samples were stored at -80°C until use.

Total protein was extracted, 20μg of protein per tumour trisect and matched normal lung tissue taken from the same patient was quantitatively tested by LC-MS/MS in triplicate (comparative quantitation of the whole proteome). Principal component analysis was first performed to demonstrate the heterogeneous expression of proteins between the different areas of each single tumour mass (intra tumour heterogeneity). Four proteins; desmoplakin (*DSP*), tenascin c (*TNC-c*), enolase-1 (*ENO1*) and *EROI-La*, with the following criteria ($p<0.05$, fold change >2, heterogeneous expression pattern among the three tumour regions), and based on their link to drug resistance (in the literature), were selected to validate the consistency of the mass-spectrometry analysis by western blot analysis. These genes were also quantified by qRT-PCR in the apitolisib resistant cell line models (chapter II) and in the lung adenocarcinoma tumour tissue (chapter IV). Activation of *PI3K-mTOR*, *JAK*/*STAT* pathways were examined by PathScan® array phosphorylated protein analysis to determine whether these tumours may benefit from GDC-0980, a small molecule inhibitor used to target the PI3K-mTOR pathway.

3.3. Materials and methods

3.3.1. Lung squamous cell carcinoma tissue

3.3.1.1. Tumour tissue collection

Patients diagnosed with early stage (IB-IIA), squamous cell lung carcinoma, at St. James's Hospital (SJH) were consented to this study as part of biobanking procedures at SJH. The thoracic biobank received ethical approval from the St. James's Hospital and Tallaght University Hospital Research Ethics Committee-REC (Ref# 2005/3/6). Tissue samples were collected from theatre following resection and immediately reviewed by the lung pathologist. Tumour tissue from three distinct areas of the tumour along with surrounding normal tissue was isolated by the consultant pathologist and immediately stabilized in Allprotect® Tissue Reagent from Qiagen (Cat. #: 76405) overnight at 4°C. The buffer was removed, and the samples were frozen at -80°C until use. Haematoxylin and eosin staining were performed by the consultant pathologist to ensure that the percentage of malignant cells within the resected tumour mass is >50%. Patient clinicopathological data are shown in Table 3.1.

Table 3.1. Patients Clinicopathological Data.

Biobank No.	Age	Gender	Histology	Stage (AJCC)	Stage
260	72	Male	LSqCC	pT2a, N0	IB
261	68	Male	LSqCC	pT1b, N1	IIA
266	73	Male	LSqCC	pT2a, N1	IIA
298	66	Male	LSqCC	pT2b, N0	IIA

AJCC: American Joint Committee on Cancer 7th Ed.

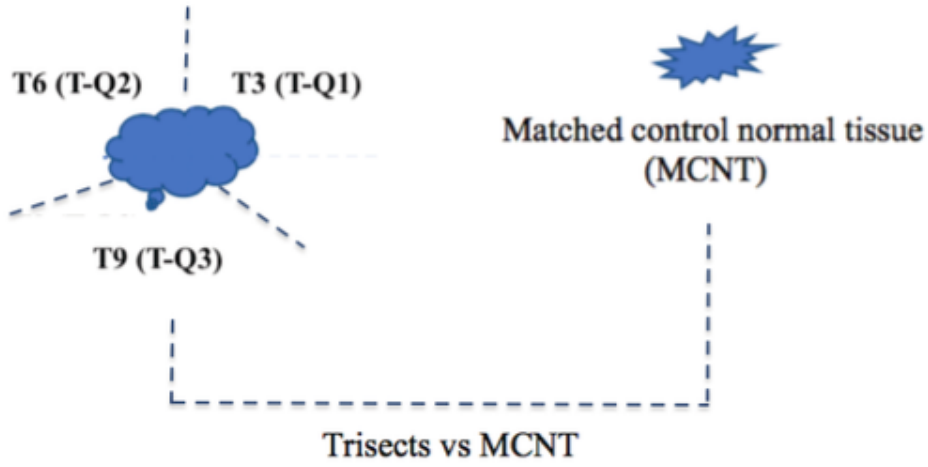

Figure 3.1. Processing of dissected tumour. The dissected tumour mass was cut into four randomly; three of them were included in this study along with their matched control normal tissue (MCNT) that was taken from the tumour surrounding normal tissues.

3.3.1.2. Nucleic acid extraction

All Prep-DNA/RNA/miRNA universal kit, Qiagen (Cat. #80224) was used to extract RNA and DNA from the resistant cell line models and the tissue samples.

3.3.1.2.1. Total RNA extraction

Matched normal and tumour tissues trisects, previously stabilized in All protect® buffer and stored at -80°C, were homogenized in RLT Plus cell lysis buffer (Product # 7018) on the Tissue Lyzer (Qiagen) for 2 minutes at 25HZ twice with 5 minutes interval on ice and then centrifuged at 14,000 rpm for 15 minutes at 4°C. The supernatant were then transferred into the spin column (provided) and centrifuged at 14,000 rpm for 30 seconds. The flow-through containing RNA was transferred into a new 2 mL tube (provided), mixed with 50 µL proteinase K by pipetting up and down, then 200 µL absolute ethanol was added and the mixture incubated at room temperature for 10 minutes. Rneasy Mini spin columns were then activated by absolute ethanol (400 µL), the mixtures were then transferred (in two steps) onto

the Mini spin column and centrifuged at 14,000 rpm/30 seconds, the flow-through discarded. The filter was then washed with 500 µL of buffer RPE/ETOH at centrifugation speed of 14,000 rpm/15 seconds. The filter was then incubated with 80 µL of DNase I (prepared in buffer RDD in ratio of 1:8) for 15 minutes at room temperature to degrade DNA contaminants. Membranes were then washed with 500 µL of buffer FRN/Isopropanol, centrifuged at 14,000 rpm/15 seconds. The spin column was placed onto a new collection tube (provided), and centrifuged again at 14,000 rpm/15 seconds and the flow-through was then discarded. The spin column filters were then washed with 500 µL of buffer RPE, centrifuged at 14,000 rpm/15 min, then the flow-through discarded and filters were put onto a new collection tube (provided). Filters then washed with 70% ethanol, centrifuged and then placed onto a new 1.5 mL collection tube. The filters-bound RNA was then eluted by adding 50 µL of RNase-free water and centrifugation at 14,000 rpm and stored at -80°C. The eluted RNA samples were measured by Nanodrop ND-1000. RNA qualitative and quantitative results are tabulated in *appendix* 3.1.

3.3.1.2.2. Genomic DNA extraction

The All Prep DNA Mini spin columns from step 2 were washed with 350 µL Buffer AW1/ethanol centrifuged at 14,000 rpm/1min, the flow-through discard. The spin filters were then treated with 80 µL Proteinase K prepared in AW1 buffer (1:3 ratio) and incubated at room temperature for 5 minutes. Filters were washed twice with 350 µL AW1, then with 350 µL AW2/ethanol buffer, followed by centrifugation at speed of 14,000 rpm/15 seconds and the flow-through was then discarded. The bound DNA was then eluted in a new 1.5 mL collection tube (supplied) by centrifugation at 14,000 rpm/1 min then incubated with 100 µL elution buffer (EB)

for 2 minutes. The DNA was quantified on the Nanodrop-1000 and stored at – 80°C. DNA qualitative and quantitative results are tabulated in appendix 3.25.

3.3.1.2. Tissue protein extraction

Tissue samples (sized approximately 4mm^3) were homogenized in 350 µL of cell lysis buffer (product no. 7018), using the Tissue Lyser-Qiagen, at frequency of 25HZ and for 2 minutes duration. Homogenized samples were then sonicated four times for 5 seconds with 1min interval ice incubation between bursts. To remove cellular debris, samples were centrifuged 15 minutes at speed 14,000 rpm at 4°C and the supernatants containing the extracted protein were then transferred into a new Eppendorf tube and stored at -80°C.

3.3.1.3. Protein quantification

Tissue protein concentrations were estimated using the BCA protein assay kit (abcam Cat. ab102536) (Chen et al., 2012). 1 part of copper was added to 50 parts of BCA reagent as indicated by the protocol. Samples were diluted 10 times in sample buffer then 50 µL samples were mixed with 100 µL Bradford reagent in a 96-well microplate, incubated for 30 minutes at 37°C protected from light and then measured in the Synergy HT Bio-TEK reader at 595nm. Sample concentrations were calculated using standard curve method and bovine serum albumin (BSA) was used as standard.

3.3.1.4. Protein sample preparation for mass spectroscopy

Protein samples were prepared using the FFPE-FASP protein digestion kit (part #: 44255). Samples were suspended in 200 µL 8M urea (Sigma, U5128) prepared in 0.1M Tris-HCL pH 8.5. The protein mixture was loaded onto a filter unit, centrifuged at 14,000 rpm for 15 minutes and the flow-through was then discarded. The filters were then washed with 200 µL urea, centrifuged at 14,000 rpm for 15

minutes and the flow-through was then discarded. The filter-bound proteins were then reduced using 100 µL Iodoacetamide (IAA), mixing at 600 rpm for 1 minute in a thermos-mixer and then incubated in dark for 20 minutes, then centrifuged at 14,000 rpm for 10 minutes and then washed twice using 100 µL urea buffer and centrifugation at 14,000 rpm for 15 minutes. Filters were then washed twice by 100 µL 50mM ammonium bicarbonate (NH4HCO3), centrifuged for 10 minutes at 14,000 rpm. The reduced protein samples were then digested with 40 µL trypsin in NH_4HCO_3 (1:50 enzyme to protein ratio), mixed in thermos-mixer for 1 minute at 600 rpm, wrapped with paraffin film, put inside humid box and incubated overnight at 37°C. On the next day, filters were transferred onto a new collection tubes and centrifuged at 14,000 rpm for 10 minutes, washed twice with 40 µL ammonium bicarbonate at 14,000 rpm centrifugation for 10 minutes. Trypsin digestion was then stopped by adding 50mM ammonium bicarbonate (ratio of 3:1 v/v sample to buffer), samples were then centrifuged at 14,000 rpm for 15 minutes and the top 30 µL of each sample was then transferred to MS vials (Hmmier, 2018).

3.3.1.5. Protocol for Label-free MS/MS

Q Exactive™ mass spectrometer coupled to a Dionex Rapid Separation LC (RSLC) instrument (Thermo Scientific, Waltham, MA, USA) was used. A single 100 mm length C18 PicoFrit® column (Thermo-Fisher Scientific, Hemel Hempstead, UK) was used to separate the digested peptides. Electrophoresis solvents consisted of: solvent-A: (2%v/v acetonitrile plus 0.1%v/v formic acid in LC–MS grade water) and 2–40% gradient of solvent-B: (80%v/v acetonitrile plus 0.08%v/v formic acid in LC–MS grade water) and the running time was set to 65 min at 250nL/min flow rate. 140,000 resolutions at a range of 300–1700 m/z were scanned. The most intense 15 peptides were selected (Manzanares-Miralles et al., 2016), then a second

MS/MS was performed at 17,500 resolution between 200–2000 m/z (Hmmier, 2018).

3.3.1.6. Retrieval of Label-free MS/MS quantitative data

Raw data files obtained from the LC-MS/MS analysis were uploaded into the MaxQuant software. The text file obtained for protein groups was then uploaded into Perseus software to obtain the accession number of each protein and the log X2 correspondent to their quantity compared to the control normal tissue. Principal component analysis (PCA) and heat maps were generated using the Perseus software. The log X2 values were then converted back into numeric data at *http://www.endmemo.com/algebra/log2.php.* Protein abundance (fold change) was then calculated by dividing the average number per quadrant by the average number of the normal tissue. Numbers above 1.0 represent the up regulated proteins per quadrant, while below 1.0 indicate the protein is down regulated (Hmmier, 2018). Up and down regulated proteins per quadrant per patient were listed in tables, and analysed online using Venn diagram at *http://bioinformatics.psb.ugent.be/webtools/Venn/.* Shared and unique proteins in the up and down protein lists were put in tables for further bioinformatics analysis (Hmmier, 2018).

3.3.1.7. PathScan® Intracellular pathway signalling

The PathScan® Intracellular signalling array kit (chemiluminescent readouts) Cat. #7323, (Figure 3.2) was used to quantify the phosphorylation of 18 proteins (Akt was tested for two phosphorylation sites) involved in the PI3K/m-TOR/AKT and JAK/STAT pathways. The array slide was affixed to the 16 multi-well gaskets as described in the user manual. The array slide was first blocked by adding 100 µL freshly prepared 1X blocking buffer per well, sealed and incubated for 15 minutes at room temperature in the orbital shaker. The blocking buffer was then decanted

and 75 µL (1µg/µL) of each protein sample was added to each well, sealed and incubated for 2 hours at room temperature in the orbital shaker. 4-wells per patient were used; one for control normal tissue and three wells for the tumour trisections. The excess fluid was decanted, and the wells washed 3 times for 5 minutes duration on the orbital shaker using freshly prepared 1X wash buffer. The wash buffer was then decanted, and the wells were incubated with 75 µL of 1X detection antibodies cocktail for 1 hour at room temperature on an orbital shaker. The wells were then washed 4 times with 1X wash buffer and then 75 µL of 1X HRP-linked Streptavidin was added to each well, then covered and incubated for 30 minutes at room temperature on an orbital shaker. The wells were then washed 4 times using 1X wash buffer, shaking on an orbital shaker. At the end, the multi-well gasket is removed, and the array slide was placed facing-up in a plastic dish and washed with a 10 mL 1X wash buffer. LumiGLO® peroxide (at working concentrations in ratio of 1:1) was added to cover the array slide and the signal was read in Vilber Fusion Smart Imaging System. Quantification of activated protein expression was calculated using ImageJ 3D-viewer software. Circular ROIs of same diameters were drawn around the protein correspondent signals and the count per well was represented in column graphs.

A

	Target	Phosphorylation site	Modification
1	Pos. control	NA	NA
2	Neg. control	NA	NA
3	ERK1/2	Thr202/Tyr204	phosphorylation
4	STAT1	Tyr701	phosphorylation
5	STAT3	Tyr705	phosphorylation
6	Akt	Thr308	phosphorylation
7	Akt	Ser473	phosphorylation
8	AMPKα	Thr172	phosphorylation
9	S6 RP	Ser235/236	phosphorylation
10	mTOR	Ser2448	phosphorylation
11	HSP27	Ser78	phosphorylation
12	Bad	Ser112	phosphorylation
13	p70 S6 kinase	Thr389	phosphorylation
14	PRAS40	Thr245	phosphorylation
15	p53	Ser15	phosphorylation
16	p38	Thr180/Tyr182	phosphorylation
17	SAPK/JNK	Thr183/Tyr185	phosphorylation
18	PARP	Asp214	Cleavage
19	Caspase	Asp175	Cleavage
20	GSK-3β	Ser9	phosphorylation

B

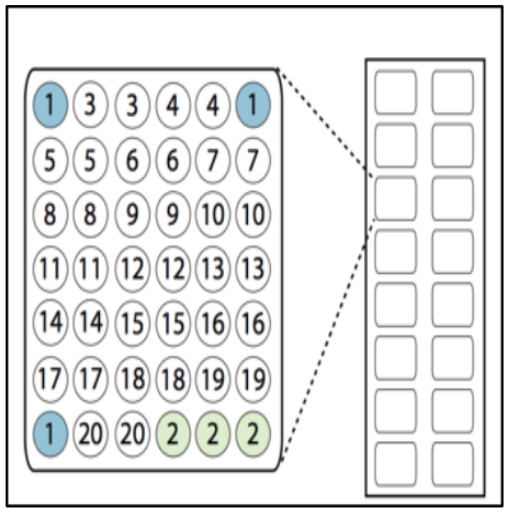

Figure 3.2. PathScan® Intracellular signalling array. The array slide contains 16 wells and each 4 wells were used per patient (patient tumour Trisects and their control normal tissue). Each well contains 3 positive controls (#1-B), 3 negative controls (#2-B) and monoclonal antibodies to 18 different phosphorylated proteins spotted in duplicates (A). Akt was tested for two different phosphorylation sites.

3.3.1.8. Western blot for validation of selected LC-MS/MS data

The list of primary and secondary antibodies purchased from Cell Signalling Technology®, used in this chapter, are listed in table 3.3. The anti-rabbit IgG, HRP-linked secondary antibody purchased from Cell Signalling Technology® was used. 30 µg of total protein was used to compare the expression of proteins in tumour trisects compared to the matched control normal tissues.

3.3.1.8.1. SDS-proteins resolving

30 µg of each protein sample was diluted in a 2X Laemmli buffer in a fume hood (recipe see table 3.2) and heated to 95°C for 10 min on a heating block. Samples were immediately cooled down by incubation on ice for at least 2 min and then loaded onto a 12 % SDS polyacrylamide gel. The electrophoresis conditions were: 400V and 50mA for 80 min in 1X electrophoresis running buffer (recipe see table 3.2). Pre-stained coloured protein marker (Cell-Signalling Technology-cat. #14208) was used to assess the molecular sizes.

3.3.1.8.2. Electro-transfer of the resolved proteins onto PVDF membrane

The resolved proteins were transferred from the gel onto PVDF membrane (0.4 µm pore diameter) in 1X transfer buffer (recipe see table 3.2) using Bio-Rad® transfer unit at 100 V and 400mA for 90 minutes, or at 25 V overnight depending on the molecular size of the protein (large proteins needs longer time). The transfer cassette order from positive to negative as follow: Sponge, three absorbent papers, followed by a PVDF membrane, then by the SDS gel containing the resolved proteins (with coloured protein marker to the left) and on top three more layers of absorbent paper followed by another sponge at the end.

Table 3.2. Required reagent for protein electrophoresis

Sample loading Laemmli buffer (2X) recipe: 4 ml β-mercaptoethanol, 10 µL of 10% bromophenol blue, 4 mL glycerol, SDS 1g and 2 mL of 1M Tris-HCL pH 6.8.
Electrophoresis running buffer (5X) recipe: 15g Tris base, 72g glycine and 5g SDS in 1000 mL ddH2O. Mix 200mL of 5X running buffer and add up to 1000 mL ddH2O to make 1X working running buffer.
SDS polyacrylamide gel 12% recipe: **a-** 12% resolving gel (8 mL per gel): 3.2 mL 30% acrylamide, 2 mL 1.5M Tris pH 8.8, 80 µL APS, 80 µL 10%SDS, 8 µL TEMED* and 2.6 mL ddH2O. **b-** 6% stacking gel (5 mL per gel): 1 mL 30% acrylamide, 1.25 mL 0.5M Tris pH 6.8, 50 µL 10% APS, 50 µl 10% SDS, 5 µL TEMED* and 2.6 mL ddH2O.
Electro-Transfer buffer 10X recipe (1L): 15.2g Tris base, 72.1g glycine and 5g SDS in up to 1000mL H2O. To make 1X transfer buffer Mix 80 mL of 10X transfer buffer, 200 mL methanol and 720 mL H2O.
Blocking buffer recipe: 5% w/v non-fat skimmed milk (Marvel skimmed milk powder, Premier Food Group Ltd., UK) in 1x PBS containing 0.01% Tween-20® (PBST).

* added at the end when the cast is ready.

3.3.1.8.3. Membrane blocking and antibodies incubation

At the end of the transfer step, the membrane was immediately immersed into the blocking buffer (recipe see table 3.2) for 1h at medium shaking. The membrane was then washed 3X-times with 1X PBS/0.1% Tween-20®, then incubated with the primary antibody (Table 3.3) overnight at 4°C slow/medium speed rotation. Then, again the PVDF membrane was washed 3X-times with 1x PBS/0.1 Tween-20® and then incubated with the secondary antibody (anti-mouse IgG HRP-linked antibody-Cell Signalling cat. No. 7076) or (anti-rabbit IgG HRP-linked antibody-Cell Signalling cat. No. 7074) for the duration of 1h. The membrane was then washed 3X-times TBST and kept in 1X TBS/0.1 Tween-20® washing buffer at 4°C until the signal developed.

3.3.1.8.4. Signal retrieval (chemiluminescence) and ImageJ quantification

5 mL (at 1:1 volume ratio of reagents A and B) of ECL western blotting substrate (Pierce Thermo-Scientific, prod. #32106) was directly applied onto the membrane for 2-3 min. The chemiluminescent signal corresponding to the amount of the protein in the sample was captured using Vilber-Fusion Smart Imaging System (was set to auto-detection of signal). Captured images were then saved as tiff files for further Image-J software quantitative analysis. Image-J software (version K 1.45) was used for densitometry analysis to quantify protein expression. Briefly a rectangle was drawn around the most left band (then press Ctr+1), the rectangle was then moved to the next right band …. (press Ctr+2 then continue Ctr+2) until the last band (press Ctr+3). The chemiluminescent signal values equivalent to the amount of tested protein were recorded, then normalized to beta-actin/or beta tubulin content measured on the same membrane, and then compared between the

tumour trisects and their correspondent control normal tissue in GraphPad Prism8 as column graphs.

3.3.1.9. qPCR

3.3.1.9.1. Desmoplakin primer design

Homosapiens desmoplakin (*DSP*), transcript variant 1, mRNA NCBI reference sequence (>NM_004415.4) was retrieved from PubMed nucleotides and Primer3Plus was used to design the primer set (Table 3.4).

3.3.1.9.2. Tenascin c primer design

Homosapiens Tenascin C (*TNC*), mRNA NCBI reference sequence (>NM_002160.4) was retrieved from PubMed nucleotides and Primer3Plus was used to design the primer set (Table 3.4).

Table 3.3. Primary antibodies used in this chapter.

Product. No	1ry antibody	Iso- type	Size (kDa)
12221	Tenascin c (D16C4)	Rabbit IgG.	240
3264	ERO1-La	Rabbit IgG.	60
13410	Enolase-1 (D2S1A)	Rabbit IgG.	47
8457S	Beta actin (D6A8)	Rabbit IgG.	45
54523S	*PIM*-1 (D8D7Y)	Rabbit IgG.	S34/L44
4730S	*PIM*-2 (D1D2)	Rabbit IgG.	40/38/34
4165T	*PIM*-3 (D17C9)	Rabbit IgG.	35
2148S	a/b tubulin	Mouse IgG	52/55
9080	Desmoplakin*	Mouse IgG	250

Antibodies were purchased from Cell Signalling Technology® except Desmoplakin* was purchased from R&D systems®.

3.3.1.9.3. ERO1-La Primer design

Homo sapiens endoplasmic reticulum oxidoreductase-1 alpha (*ERO1A*), transcript variant X1 mRNA, NCBI reference sequence (>NM_014584.3) was retrieved from PubMed nucleotides and Primer3Plus was used to design the primer set (Table 3.4).

3.3.1.9.4. Enolase-1 Primer design

Homo sapiens enolase-1 (*ENO1*), transcript variant 1 mRNA, NCBI reference sequence (>NM_001428.5) was retrieved from PubMed nucleotides and Primer3Plus was used to design the primer set (Table 3.4).

3.3.1.9.5. qRT-PCR assessment of *PIM* kinases as an activated JAK/STAT pathway marker in the heterogeneous parts of the tumour tissue.

PIM 1, 2 and 3 kinases were assessed in two regions per tumour compared to their matched normal tissue. The assessed parts were selected based on the extent of their total proteome heterogeneity detected by PCA (the far quadrants were selected).

Table 3.4. List of primers used for validation of ITH

Gene	Primer sequence	Start/End	Flanked junction	PCR product
ACTB	FWD 5'TGTTTGAGACCTTCAACACCC'3	452	[4/5]	529bp
	REV 5'AGCACTGTGTTGGCGTACAG'3	980		
Desmoplakin	FWD 5'CAGGGATCTTCTCACCACATCA'3	2331	[15/16]	123bp
	REV 5'AGAACCTCTGAAGTTGGCAAGC'3	2431		
Tenascin c	FWD 5'AAAGGGGCTTTCT GGTACAGG'3	6733	[27/28]	172bp
	REV 5'GCCTGCCTTCAAGATTTCTG'3	6877		
ERO1-La	FWD 5'CTGGGGATAAAAAAGAAGCACAC'3	1171	[27/28]	148bp
	REV 5'ATCTTCA G AGCAGTGCCCAA'3	1318		
Enolase-1	FWD 5'CGTTCGGGGGAGACTGAAGA'3	1230	[10/11/] [11/12]	155bp
	REV 5'AACTTAGCCTTGCTGCCCAG C'3	1384		

3.3.1.9.6. First strand cDNA synthesis

RNA was prepared for qRT-PCR using amplification grade-DNase I (Catalog no. AMPD1) purchased from SIGMA-ALDRICH®. Where samples (in duplicates) equivalent to 500ng RNA (Table 3.5) were mixed with 1µl DNase I (1 unit/µl in 50% glycerol Cat. No. D5307) containing (10 mM Tris-HCL pH 7.5, 10 mM CaCl2 and MgCl2), and 1µl 10X reaction buffer containing 200 mM Tris-HCL pH 8.3, 20mM MgCl2 (Cat.no. R6273). The cocktail per sample was mixed gently and incubated at room temperature for 15 minutes then the reaction was stopped by adding 1µl stop solution (50 mM EDTA Cat. no. S4809) to chelate the Ca++ and Mg++ needed for the enzyme activity. The cocktail was then heated at 70°C for 10 minutes to denature both DNase I and RNA and then chilled on ice immediately.

Table 3.5. Samples RNA quantification and their correspondent 500ng volumes.

Sample ID	RNA (ng/µl)	Volume (500ng)	10X reaction buffer	Dnase I (1unit/µl) (µl)	Rnase-free water
T260N	228.5	2.2	1	1	5.8
T260T3	300.8	1.7	1	1	6.3
T260T6	617.5	0.8	1	1	7.2
T260T9	871.3	0.6	1	1	7.4
T261N	659.6	0.8	1	1	7.2
T261T3	666.8	0.7	1	1	7.3
T261T6	417.0	1.2	1	1	6.8
T261T9	966.8	0.5	1	1	7.5
T266N	230.3	2.2	1	1	5.8
T266T3	545.8	0.9	1	1	7.1
T266T6	450.17	1.1	1	1	6.9
T266T9	582.9	0.9	1	1	7.1
T298N	377.8	1.3	1	1	6.7
T298T3	481.52	1.0	1	1	7.0
T298T6	441.0	1.1	1	1	6.9
T298T9	633.0	0.8	1	1	7.2

RevertAid Reverse Transcriptase (Cat. no. EP0441) purchased from Thermo Fisher Scientific™ was used to synthesize the first strand cDNA. 1µL (100 pmol) of random hexamer (Cat. no. SO142) was added to the chilled cocktail and the volume then completed to 12.5 µL with DEPC-treated water (Cat. no. R0601). Then the total volume per reaction was made to 20 µL by adding {(4 µL 5X reaction buffer (Cat. no. EP0442), 2µL dNTP Mix (10mM each) 1mM final concentration, 0.5 µL Thermo Fisher Scientific™ Ribolock Rnase inhibitor (Cat. no. R0191) and 1 µL RevertAid Reverse Transcriptase (Cat. no. EP0441)} (N.B: Controls do not contain transcriptase). The cocktail was again briefly mixed and incubated at 42°C for 1h. The reaction was then terminated by heating at 70°C for 10 min. The cDNA was then used freshly the same day, the rest amount was stored at -20° and used within 1 month (J.F. Sambrook and D.W. Russell, 2001).

3.3.1.9.7. qRT-PCR reaction

2X SYBR Green qPCR Master Mix, containing hot-start DNA polymerase, dNTPs, Mg++, SYBR Green I dye, purchased from Bimake (Cat. no. B21202) was used. 1 µL cDNA (2 µg) per sample was used, the following reagents (10 µL 2X Bimake™SYBR Green master mix (Cat. no. B21202) containing hot-start DNA polymerase, dNTPs, Mg++ and SYBR Green I dye, 2 µL Primer_FWD (2.5µM), 2 µL Primer_REV (2.5µM), 0.5 µL ROX reference dye) were added, then the volume was made to 20 µL by ddH2O.

3.3.1.9.8. qRT-PCR program setting

Eco™ Real-Time PCR system was used in comparing the expression of desmoplakin, Tenascin c, Enolase-1 and ERO1-La in two selected regions in the tumour and their matched control normal tissue. The two-step procedure mentioned in the bimake 2X SYBR Green qRT-PCR Master Mix protocol was followed: the

thermal cycling involved Hot-Start DNA polymer (reaction hold at 95°C for 5 min), followed by 35 cycles of (denaturation at 95°C/15 sec then anneal/extend at 60°C for 45 sec), then followed by the melt-curve cycle that consisted of (denature at 95°C/15 sec then 60°C/1 min then 95°C for 15 sec). Eco™Software v4.0.7.0 was used for comparative qRT-PCR analysis (see below screenshot).

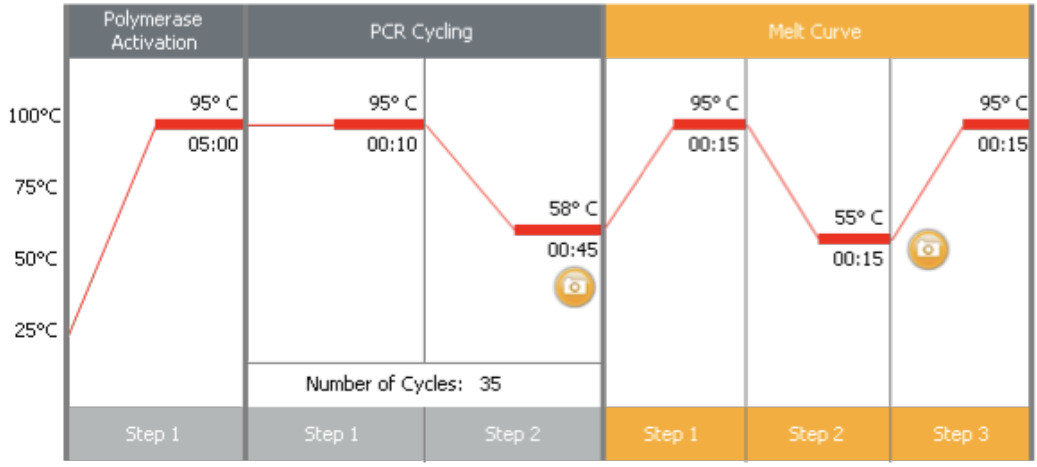

3.4. Results

3.4.1. Characterisation of intra-tumour heterogeneity of lung SqCC using LC-MS/MS comparative abundance analysis compared to matched normal lung tissues.

The label-free mass spectrometry analysis results of comparative proteins abundance of tumour versus normal tissue from four patients are listed in the appendices section at the end of the thesis. The upregulated and downregulated proteins in (all tumour regions, two regions and one region) sequence are listed under (*appendix* 3.2-3.3) and (*appendix* 3.4- 3.5) for patient 260, and under (*appendix* 3.6-3.7), (*appendix* 3.8-3.9) for patient 261, (*appendix* 3.10- 3.11) and (*appendix* 3.12- 3.13) for patient 266, and (*appendix* 3.14- 3.15) and (*appendix* 3.16- 3.17), respectively.

The number of up and down regulated proteins per tumour region per patient compared to the matched normal tissues at fold change (FC) 1.2-fold and 2-fold and p value of <0.05 are listed in table 3.6.

Table 3.6. Differentially proteins in tumour regions compared to the normal tissue.

	FC		Q1	Q2	Q3		Q1	Q2	Q3
260	2	Up	88	90	76	Down	63	60	37
	1.2		182	192	212		127	115	99
261	2		66	77	72		76	59	65
	1.2		149	177	177		153	131	133
266	2		112	112	107		63	43	64
	1.2		202	217	199		118	91	123
298	2		36	44	44		40	34	62
	1.2		161	193	193		103	88	113

3.4.1.1. Venn-diagram intersection of up and down-regulated proteins

The Venn diagram analysis stratified the over expressed proteins (fold change cut off =1.2, p=<0.05) per each SqCC tumour region compared to matched normal lung tissue for the four patients (Figure 3.3-I), and the downregulated proteins per tumour region compared to the normal matched tissues (Figure 3.3-II). In respective order (up/down); (A) **In patient 260**, the number of detected proteins was 232 and 144 proteins; 68.5% and 54.9% of the proteins were shared in all tumour regions, 5.6% and 20.1% proteins were shared between T3 (T-Q1) and T6 (T-Q2), 6.5% and 0.7% were shared between T6 (T-Q2) and T9 (T-Q3), 2.2% and 4.2% were shared between T3 (T-Q1) and T9 (T-Q3). 1.7%, 1.7% and 13.8% proteins were found unique upregulated and 8.3%, 3.5%, 8.3% were uniquely downregulated in T3 (T-Q1), T6 (T-Q2) and T9 (T-Q3), respectively. (B) **In patient 261**, the number of detected proteins was 184 and 169 proteins; 68% and 60.4% proteins were shared in all tumour regions, 0% and 6.5% proteins were shared between T3 and T6 and between T3 and T9, 23.3% and 1.8% were shared between T6 and T9. 8.7% and 14.8% were unique in T3. No unique upregulated proteins were detected in T6 and T9 while there were 4.7% and 5.3% proteins were unique down-regulated in T6 and T9, respectively. (C) **In patient 266**, the number of detected proteins was 234 and 132 proteins; 72.2% and 57.6% proteins were expressed in all regions, 4.7% and 1.5% were shared between T3 and T6, 2.6% and 3% were shared between T6 and T9, 4.7% and 17.4% were shared between T3 and T9. 2.1%, 10.3%, 3.4% and 8.3%, 3%, 9% were uniquely up and down-regulated in T3, T6 and T9, respectively. (D) **In patient 298**, the number of detected proteins was 201 and 124 proteins; 75.1% and 59.7% were shared in all tumour regions, 4.5% and 5.6% were uniquely expressed in T3 at cut-off value level, 1% and 9.7% were uniquely down regulated

in T6 and T9, respectively. T6 and T9 intersected in 20.4% upregulated proteins and both share no upregulated proteins with T3. 2.4%, 6.5% and 14.5% were shared downregulated between two regions.

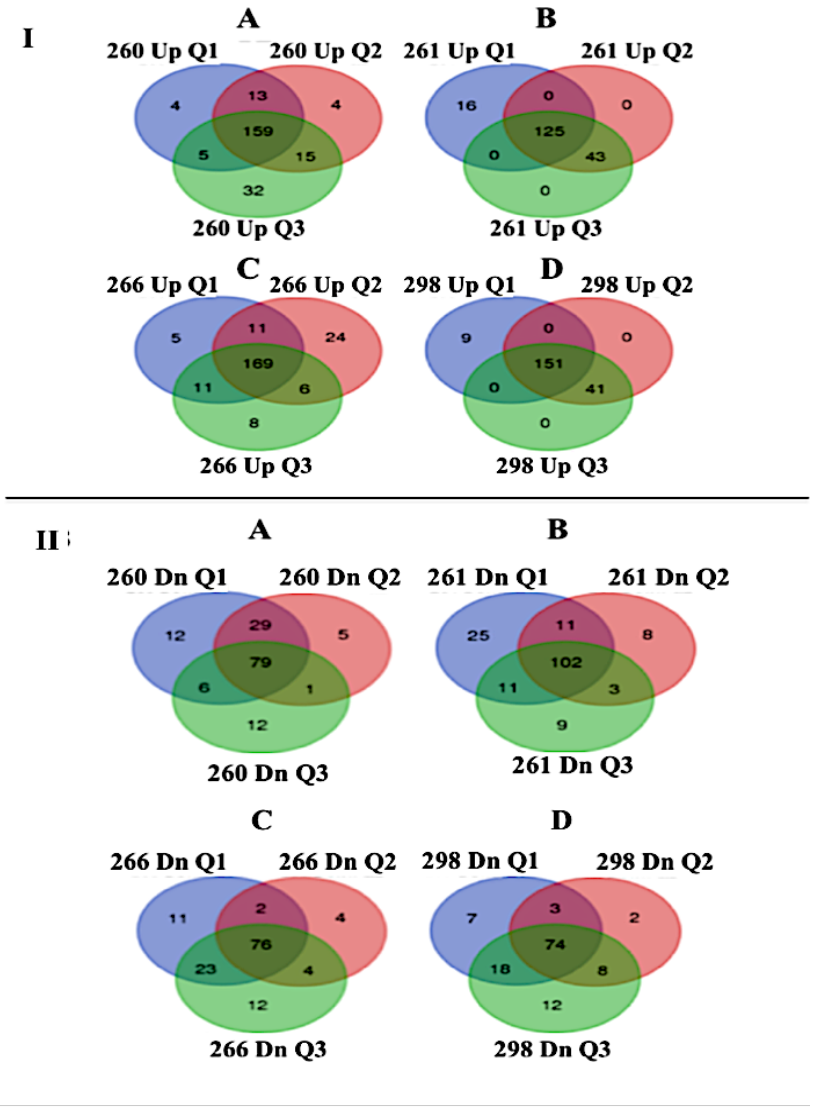

Figure 3.3. **Venn-diagrams demonstrating altered protein expression in each tumour trisect compared to matched normal tissue.** I: up-regulated and II: down-regulated proteins per tumour part regardless of their expression differences (at $p<0.05$, Fold change 1.2). A: patient coded 260, B: patient coded 261, C: patient coded 266 and D: patient coded 298. Q1(blue), Q2 (red), Q3 (green) are three different regions of tumour per patient.

3.4.1.2. Principal component analysis (PCA)

Data from the mass spectrometry analysis comparing the malignant tumour trisects and the normal surrounding tissues with fold change of >2 and p value of <0.05 were selected to build up the Principal component Analysis (Figure 3.4). The principal component analysis (PCA) of four SqCC tumour specimens from patients coded 260, 261, 266 and 298 is shown in figure 3.4. The component 1 (horizontal) quantifies protein expression between normal tissue (circles to the right) and the three tumour tissue regions (green squares, blue cubes and red triangles) to the left of the graph. The second component (vertical) quantifies protein expression heterogeneity between each trisect of a single tumour (overall proteome signature), the variance percentage represents the number of proteins and their expression profile differences among the total proteome between the tumour regions (up and down). PCA demonstrates 16.8% variance between T9 (T-Q3) and T3 (T-Q1), T6 (T-Q2) among the tumour trisects of patient 260, T-Q3 location might explain this part of the tumour might contain some normal tissue, T-Q1 and T-Q2 were close to each other. In patient 266, T6 (T-Q2) was clustered as heterogeneous, the % variance value was 16.7. In patient 261 and 298 had T3 (T-Q1) as the different part within their tumour specimen, the variance values were 11.6% and 12.3% for 261 and 298, respectively.

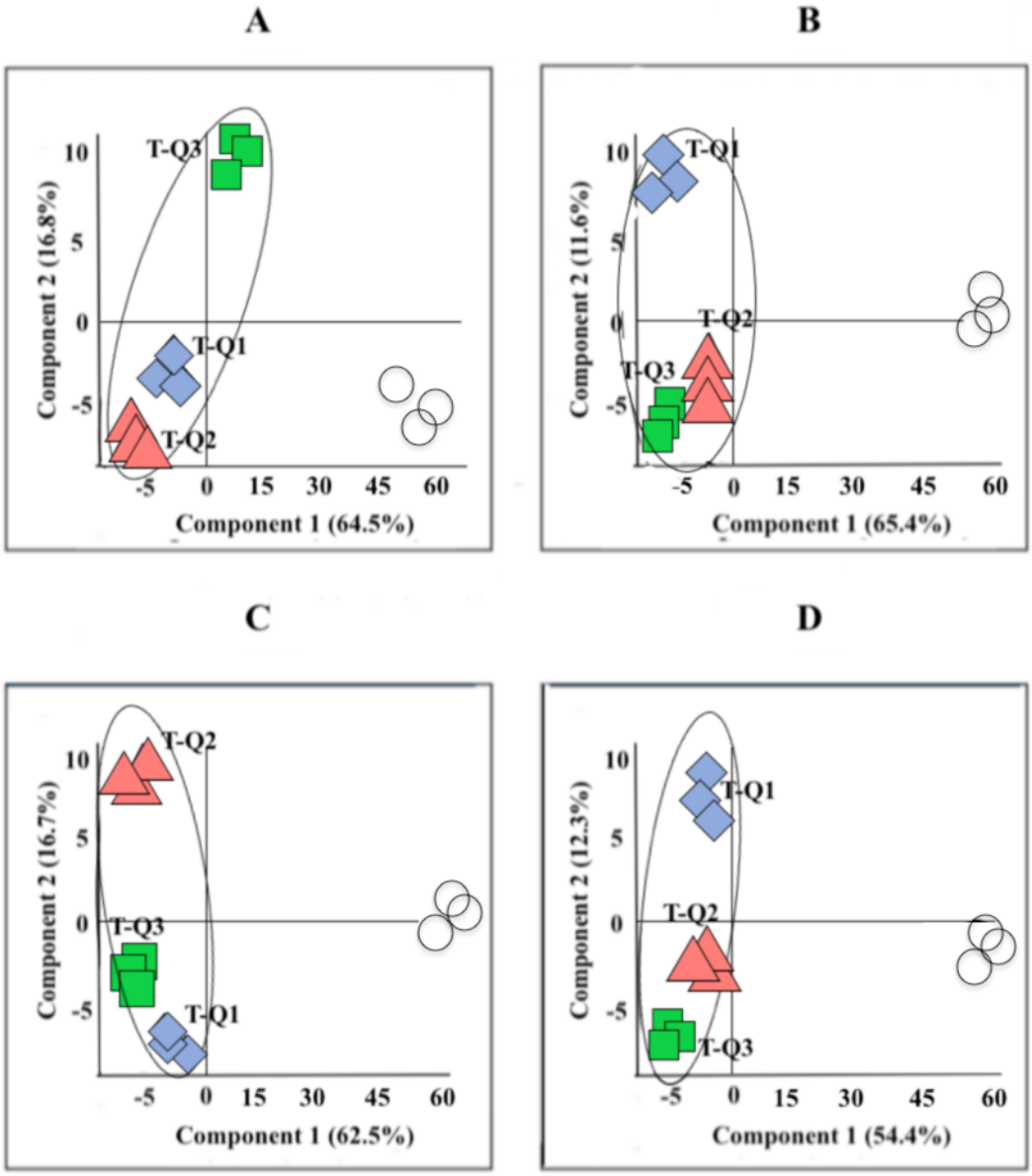

Figure 3.4. Principal component analysis (PCA) compares altered protein expression between each tumour trisect and between tumour and matched normal tissue. A: specimen coded 260, B: specimen coded 261, C: specimen coded 266, D: specimen coded 298. Component 1 represents the variance in the protein expression between normal control tissues (black balls) and malignant tissue trisects; T-Q1 (blue diamond), T-Q2 (red triangular), T-Q3 (green squares). Component 2 explains the protein expression differences within the same tumour.

3.4.1.2.1. T260-Q3 centred analysis of dysregulated proteins

To demonstrate why Q3 in sample 260 was clustered away from the other two regions with 16.8% variance (Figure 3.4), up and down regulated proteins that were close in their expression in Q1 and Q2 and were expressed differently in Q3 (minimum of 2-fold difference) were sorted from the highest to lowest in table 3.7. Proteins exhibit an opposite expression profile in Q3 also listed in table 3.8 (i.e. up in Q3 and down in Q1/Q2 or down in Q3 and up in Q1/Q2).

3.4.1.2.1.1. Differential protein expression within tumour T-260

The 232 upregulated and 144 down-regulated proteins in sample 260 were sorted from the lowest to the highest fold change in Q3 compared to the normal tissues (appendices 3.2 and 3.5). Dysregulated proteins that make Q3 region different from the other two regions (i.e. big expression difference between Q3 and the other two regions) were selected and presented in table 3.7. The upregulated proteins that fulfilled the criteria were 26 proteins, Q3 had the lowest expression levels of these proteins and a minimum of 2-fold difference is observed compared to the other two tumour regions. ERO1-La was selected for further validation as the fold change was 4.2-fold increase in Q3 and 13.9 and 10.6-fold in the other two regions of the tumour (2.5 and 3 times more). On the other hand, 18 down-regulated proteins fulfilled the same criteria, Q3 had the least decrease in the expression compared to the other two tumour regions except desmoplakin and keratin (at the bottom of the table). Desmoplakin was selected for further validation as it was 4-times more downregulated (-21.6 fold) compared to the other two regions (-5.2 and 5.3 in the other two tumour regions) (Table 3.7).

Table 3.7. List of heterogeneously expressed proteins between the different tumour regions for patient 260.

Patient 260				
Tumour regions			Gene ID	protein name
T-Q1	T-Q2	T-Q3		
14.3	10.8	7.9	P78527	DNA-dependent protein kinase catalytic subunit
8.3	8.4	6.3	P06744	Glucose-6-phosphate isomerase
9.6	10.0	5.9	P27695	DNA-(apurinic or apyrimidinic site) lyase
7.7	9.0	4.6	Q16851	UTP--glucose-1-phosphate uridylyltransferase
10.6	13.9	4.2	Q96HE7	ERO1-like protein alpha
8.2	7.5	3.6	P50454	Serpin H1
5.5	3.9	3.2	O43175	D-3-phosphoglycerate dehydrogenase
4.5	4.1	3.1	P17858	ATP-dependent 6-phosphofructokinase, liver type
6.9	5.3	2.8	P80723	Brain acid soluble protein 1
5.4	4.0	2.8	P06733	Alpha-enolase
7.8	5.9	2.5	P31949	Protein S100-A11 (Calgizzarin)
4.0	4.0	2.5	P14618	Pyruvate kinase PKM
4.8	6.4	2.2	B1ALD8	Periostin
3.4	3.5	2.2	O43390	Heterogeneous nuclear ribonucleoprotein R
3.4	3.4	2.0	P07237	Protein disulfide-isomerase
5.8	3.9	1.9	Q5T8U5	Surfeit 4
3.4	2.7	1.9	E7EX73	Eukaryotic translation initiation factor 4 gamma 1
3.0	3.2	1.9	P18669	Phosphoglycerate mutase 1
4.4	3.5	1.8	Q00610	Clathrin heavy chain 1
3.2	2.9	1.8	P10253	Lysosomal alpha-glucosidase
2.9	2.8	1.8	P00338	L-lactate dehydrogenase A chain
3.0	2.4	1.5	P30085	UMP-CMP kinase
2.7	2.7	1.5	P12814	Alpha-actinin-1
2.7	1.9	1.3	P23142	Fibulin-1
2.4	2.2	1.3	Q14195	Dihydropyrimidinase-related protein 3
2.3	2.2	1.2	F8W6I7	Heterogeneous nuclear ribonucleoprotein A1
-9.1	-4.0	-1.9	P00915	Carbonic anhydrase 1
-3.6	-3.1	-1.9	Q13813	Spectrin alpha chain, non-erythrocytic 1 (Alpha-II spectrin)
-4.7	-5.0	-2.0	Q01469	Fatty acid-binding protein,
-3.7	-4.1	-2.0	Q5TCU3	Tropomyosin beta chain
-4.0	-4.2	-2.3	P01009	Alpha-1-antitrypsin (Alpha-1 protease inhibitor)
-7.9	-4.2	-2.3	P69905	Hemoglobin subunit alpha (Alpha-globin) (Hemoglobin alpha chain)
-3.9	-4.0	-2.3	P35580	Myosin-10
-13.3	-5.9	-2.4	P12110	Collagen alpha-2(VI) chain
-5.7	-4.7	-2.7	P01023	Alpha-2-macroglobulin (Alpha-2-M)
-8.4	-3.8	-2.7	P68871	Hemoglobin subunit beta (Beta-globin)
-6.0	-5.8	-2.8	Q9BW30	Tubulin polymerization-promoting protein family member 3
-15.4	-9.4	-2.9	Q6NZI2	Caveolae-associated protein 1 (Cavin-1)
-7.4	-11.9	-3.0	P51888	Prolargin (Proline-arginine-rich end leucine-rich repeat protein)
-10.5	-6.8	-3.5	P21810	Biglycan (Bone/cartilage proteoglycan I)
-14.4	-7.6	-4.5	P02042	Hemoglobin subunit delta (Delta-globin)
-8.6	-15.3	-7.4	P04114	Apolipoprotein B-100 (Apo B-100)
-3.2	-3.5	-8.7	F5GWP8	Keratin, type I cytoskeletal 17
-5.3	-5.2	-21.6	P15924	Desmoplakin (DP) (250/210 kDa paraneoplastic pemphigus antigen)

T denotes tumour, Q1, Q2, Q3 are three regions in the tumour, (+) indicate fold change of upregulated proteins, (-) values of fold change of downregulated proteins, heat-map: (Green: lowest F.C values of down-regulated proteins, Red: highest FC values of upregulated proteins). Gene ID: uniport accession number. The order of the protein list was centred to their expression levels from the highest to the lowest in T9 (T-Q3).

3.4.1.2.1.2. Proteins exhibit opposite expression in T9 (T-Q3)

Among the 232 upregulated proteins in sample 260, 1.7% (appendix 3.4-uniquly upregulated in Q3) of the proteins showed an opposite expression profile in Q3 (upregulated) compared to that in Q1 and Q2 (unchanged). Also, among the 144 down-regulated proteins in sample 260, 8.3% of the proteins were uniquely down-regulated in Q3 and were unchanged in the other two tumour regions (Q1/Q2) (appendix 3.7). Proteins with this criteria were also involved in clustering Q3 away from the Q1 and Q2 in the principal component analysis (Figure 3.4) (Table 3.8).

Table 3.8. List of dysregulated proteins in 260T-Q3 with an opposite trend in other regions.

Patient 260				
Tumour regions			Gene ID	protein name
T-Q1	T-Q2	T-Q3		
-1.2	-1.2	3.3	P07099	Epoxide hydrolase 1
-1.2	-1.3	2.8	P51659	Peroxisomal multifunctional enzyme type 2
-4	-2.5	1.8	P05091	Aldehyde dehydrogenase, mitochondrial
-1.6	-1.2	1.7	P07108	Acyl-CoA-binding protein
-4.2	-2.8	1.7	O95994	Anterior gradient protein 2
-6.2	-2.8	1.7	P09467	Fructose-1,6-bisphosphatase 1
-1.2	-1.3	1.6	P08758	Annexin A5
-1.5	-1.2	1.6	P09960	Leukotriene A-4 hydrolase
-2.8	-6.8	1.6	P21980	Protein-glutamine gamma-glutamyltransferase 2
-1.3	-1.2	1.5	P08133	Annexin A6
-1.7	-1.2	1.5	P00488	Coagulation factor XIII A chain
-1.3	-1.2	1.5	P52566	Rho GDP-dissociation inhibitor 2
-1.2	-1.2	1.4	P07355	Annexin A2
-1.2	-1.2	1.4	P17655	Calpain-2
-1.2	-1.2	1.4	P00367	Glutamate dehydrogenase 1, mitochondrial
-1.2	-1.2	1.4	P29401	Transketolase
-3.2	-3.5	1.3	P05783	Keratin 18
-1.5	-1.5	1.3	P26038	Moesin
-2.1	-1.5	1.3	P35241	Radixin
-1.8	-1.6	1.2	P15311	Ezrin
1.7	1.9	-1.2	P01861	Immunoglobulin heavy constant gamma 4
1.6	1.4	-1.2	B9A064	Immunoglobulin lambda-like polypeptide 5
1.5	2.8	-1.2	P05164	Myeloperoxidase
1.4	1.2	-1.2	P35579	Myosin-9
1.2	1.2	-1.2	Q15149	Plectin
1.2	2.2	-1.2	P36952	Serpin B5
1.9	1.7	-1.3	Q86UP2	Kinectin
2.1	4	-1.3	E7EQB2	Lactotransferrin
1.8	1.7	-1.4	P05109	Calgranulin-A
2.3	2	-1.6	O00151	PDZ and LIM domain protein 1

T denotes tumour, Q1, Q2, Q3 are three regions in the tumour, (+) indicate fold change of upregulated proteins, (-) values of fold change of downregulated proteins, heat-map (Green: lowest F.C values of down-regulated proteins, Red: highest FC values of upregulated proteins). Gene ID: uniprot accession number. The order of the protein list was centred to their expression levels from the highest to the lowest in T9 (T-Q3).

3.4.1.2.2. T261-Q1 centred analysis of dysregulated proteins

To demonstrate why Q1 in sample 261 was clustered away from the other two regions (Q2 and Q3) with 11.6% variance (Figure 3.4), shared up and down regulated proteins that were close in their expression in Q2 and Q3 and were expressed differently in Q1 (minimum of 2-fold difference) were sorted from the highest to lowest in table 3.9. Proteins exhibit an opposite expression profile in Q1 (i.e. up in Q1 and down in Q2/Q3 or down in Q1 and up in Q2/Q3) also listed in table 3.10.

3.4.1.2.2.1. Differential protein expression within tumour T-261

The 184 upregulated and 169 down-regulated proteins in sample 261 were sorted from the lowest to the highest fold change compared to the normal tissues (Appendices 3.8 and 3.11). Dysregulated proteins that make Q1 region different from the other two regions (i.e. proteins fold change in Q2 and Q3 were close to each other) were selected and presented in table 3.9. The upregulated proteins that fulfilled this criteria were 16 proteins, proteins such as lactate dehydrogenase-A, GAPDH, periostin, nucleolin, collagen and others can cluster Q1 from Q2 and Q3 despite the low fold change difference between Q1 and the other tumour regions. Desmoplakin was selected for further validation as the fold change was 137.9-fold increase in Q1 and 90.6 and 50.6-folds in the other two regions of the tumour (highest in Q1). ERO1-La was also selected for further validation as it was heterogeneous among the tumour regions. On the other hand, 22 down-regulated proteins were more successful in clustering Q1 from the other two tumour regions. Among the down regulated proteins, Q1 had the maximum expression decrease as in Spectrin alpha and beta, Cathepsin D, Epoxide hydrolase and was the least expression decrease as in Annexin 3 and 4, Calpactin-1 light chain.

Table 3.9. List of heterogeneously expressed proteins in all patient 261 tumour regions.

Patient 261				
Tumour regions			Gene ID	protein name
T-Q1	T-Q2	T-Q3		
137.9	90.6	50.6	P15924	Desmoplakin
19.9	12.5	20.0	P10809	60 kDa heat shock protein, mitochondrial
19.3	11.2	13.8	D6RGG3	Collagen alpha-1(XII) chain
18.8	17.0	10.2	Q96HE7	ERO1-like protein alpha
4.1	5.8	6.3	E7EX73	Eukaryotic translation initiation factor 4 gamma 1
3.1	5.0	7.1	P19971	Thymidine phosphorylase
3.0	2.3	2.3	P04406	Glyceraldehyde-3-phosphate dehydrogenase
2.8	2.0	2.2	P00338	L-lactate dehydrogenase A chain
2.5	3.7	4.0	P40926	Malate dehydrogenase, mitochondrial
2.1	6.9	6.7	B1ALD8	Periostin
2.1	1.4	1.2	Q14254	Flotillin-2
1.7	1.4	1.4	Q9HDC9	Adipocyte plasma membrane-associated protein
1.4	2.0	2.3	P19338	Nucleolin (Protein C23)
1.3	1.8	2.0	P29692	Elongation factor 1-delta
1.2	1.6	2.3	Q13185	Chromobox protein homolog 3
1.2	1.8	2.0	P38646	Stress-70 protein, mitochondrial
-1.3	-2.6	-3.1	P60903	Protein S100-A10 (Calpactin I light chain)
-1.8	-1.3	-1.3	Q03252	Lamin-B2
-2.6	-3.7	-4.0	P09525	Annexin A4 (35-beta calcimedin)
-3.1	-2.2	-1.9	P21291	Cysteine and glycine-rich protein 1
-3.1	-10.6	-5.6	P12429	Annexin A3 (35-alpha calcimedin)
-3.4	-2.7	-2.8	Q99536	Synaptic vesicle membrane protein VAT-1
-3.6	-2.7	-1.9	P13489	Ribonuclease inhibitor
-3.8	-3.0	-2.9	P00387	NADH-cytochrome b5 reductase 3
-3.8	-2.2	-2.6	Q9Y3Z3	Deoxynucleoside triphosphate triphosphohydrolase SAMHD1
-3.9	-1.6	-1.6	P20774	Mimecan
-4.2	-2.8	-3.4	Q9Y490	Talin-1
-4.2	-2.6	-3.4	P12111	Collagen alpha-3(VI) chain
-4.6	-3.9	-3.6	P08670	Vimentin
-4.8	-8.1	-13.1	P05091	Aldehyde dehydrogenase, mitochondrial
-4.9	-2.8	-1.7	E7EVA0	Microtubule-associated protein
-5.4	-2.7	-2.5	P52566	Rho GDP-dissociation inhibitor 2
-6.3	-3.9	-3.5	P07099	Epoxide hydrolase 1
-6.6	-4.6	-3.9	P07339	Cathepsin D
-12.5	-6.9	-7.3	Q13813	Spectrin alpha chain, non-erythrocytic 1
-42.5	-39.3	-56.3	Q03135	Caveolin-1
-72.0	-14.3	-21.6	Q01082	Spectrin beta chain, non-erythrocytic 1

T denotes tumour, Q1, Q2, Q3 are three regions in the tumour, (+) indicate fold change of upregulated proteins, (-) values of fold change of downregulated proteins, heat-map (Green: lowest F.C values of down-regulated proteins, Red: highest FC values of upregulated proteins). Gene ID: uniport accession number. The order of the protein list was centred to their expression levels from the highest to the lowest in T9 (T-Q3).

3.4.1.2.2.2. Proteins exhibit opposite expression in 261 T3 (T-Q1)

Among the 184 upregulated proteins in sample 261, 8.7% (appendix 3.10-uniquly upregulated in Q1) of the proteins showed an opposite expression profile in Q1 compared to that in Q2 and Q3 (appendix 3.12-down in both Q2/Q3). Also, among the 169 down-regulated proteins in sample 261, 14.8% of the proteins were uniquely down-regulated in Q1 and were unchanged in the other two tumour regions (Q2/Q3) (appendix 3.13). Keratin, Apolipoprotein B-100 and Prolargin were highly upregulated in Q1 and were down-regulated in the two other regions. Proteins under this criteria were more successful in clustering Q1 away from the Q2 and Q3 in the principal component analysis (Figure 3.4) (Table 3.10).

Table 3.10. List of dysregulated proteins in 261T-Q1 exhibit opposite trend in other regions.

Patient 261				
Tumour regions			Gene ID	Protein name
T-Q1	T-Q2	T-Q3		
8.9	-1.4	-1.3	P35908	Keratin, type II cytoskeletal 2 epidermal
5.0	1.7	-4.0	P04114	Apolipoprotein B-100
4.5	-1.7	-1.2	P51888	Prolargin
1.7	-1.7	-3.3	P01023	Alpha-2-macroglobulin
1.6	-1.2	-1.2	P02774	Vitamin D-binding protein
1.6	1.9	-1.3	C9JEU5	Fibrinogen gamma chain
1.4	1.6	-1.6	P02675	Fibrinogen beta chain
1.3	-1.2	-1.7	P02647	Apolipoprotein A-I
1.3	2.0	-1.2	P02671	Fibrinogen alpha chain
-1.3	1.3	1.2	P46777	60S ribosomal protein L5 (Large ribosomal subunit protein uL18)
-1.3	1.3	1.2	P53621	Coatomer subunit alpha
-1.3	1.5	-1.3	P51884	Lumican
-1.3	1.2	1.5	F8W6I7	Thioredoxin
-1.6	2.1	1.9	P42704	Leucine-rich PPR motif-containing protein, mitochondrial
-1.8	1.3	-1.8	Q14195	Dihydropyrimidinase-related protein 3

T denotes tumour, Q1, Q2, Q3 are three regions in the tumour, (+) indicate fold change of upregulated proteins, (-) values of fold change of downregulated proteins, heat-map (Green: lowest F.C values of down-regulated proteins, Red: highest FC values of upregulated proteins). Gene ID: uniport accession number. The order of the protein list was centred to their expression levels from the highest to the lowest in T9 (T-Q3).

3.4.1.2.3. T266-Q2 centred analysis of dysregulated proteins

To demonstrate why Q2 in sample 266 was clustered away from the other two regions (Q1 and Q3) with 16.7% variance (Figure 2.4), shared (up and down regulated) proteins that were close in their expression in Q1 and Q3 and were expressed differently in Q2 were sorted from the highest to lowest in table 3.11. Proteins that exhibit an opposite expression profile in Q2 (i.e. up in Q2 and down in Q1/Q3 or down in Q2 and up in Q1/Q3) also listed in table 3.12.

3.4.1.2.3.1. Differential protein expression within tumour T266

The 234 upregulated and 132 down-regulated proteins in sample 266 were sorted from the lowest to the highest fold change compared to the normal tissues (appendices 3.14 and 3.17). Dysregulated proteins that make Q2 region different from the other two regions (i.e. proteins fold change in Q1 and Q3 were mostly close to each other) were selected and presented in table 3.11 (list A&B), respectively. T266-Q2 in this patient had the highest upregulation fold change of protein disulphide-isomerase A4, superoxide dismutase, Macrophage capping protein, TXNDC5, TRAP-alpha, PPIase-B, V-type ATPase catalytic subunit A, Plastin, Cathepsin D, Integrin beta. T266-Q2 also had some upregulated proteins with the lowest fold change compared to the other investigated two regions eg. peroxiredoxin-6, stress induced-phosphoprotein 1, electron transfer flavoprotein subunit alpha, 40S ribosomal protein S3a, DNA-dependent protein kinase, adenosyl homocysteinase. Among the downregulated proteins, the lowest level of desmoplakin and cytoskeletal keratin type I proteins were in T266-Q2 compared to the rest of the tumour regions. Some other proteins' expression were less down-regulated in Q2 than in the other analysed tumour regions eg. Filamin B, Emilin-1,

Calponin-3, Prelamin-A/C, Plectin, Filamin-A, Talin-1, Myosin-9, Lacto-transferrin, collagen alpha, Hemopexin, Vimentin and Mylo-peroxidase.

Table 3.11. List of heterogeneously expressed proteins in all T- 266 tumour regions.

Patient 266				List A
Tumour regions			Gene ID	protein name
T-Q1	T-Q2	T-Q3		
19.6	22.6	17.3	P19971	Thymidine phosphorylase
9.9	10.0	12.7	O75874	Isocitrate dehydrogenase [NADP] cytoplasmic (IDH)
7.2	9.0	6.6	P13667	Protein disulfide-isomerase A4
24.5	7.7	7.1	P24821	Tenascin (TN)
9.3	6.0	8.4	P26641	Elongation factor 1-gamma
8.5	5.9	9.1	P26599	Polypyrimidine tract-binding protein 1
13.4	5.6	9.3	B4DQJ8	6-phosphogluconate dehydrogenase, decarboxylating
1.8	5.4	1.3	P04179	Superoxide dismutase [Mn], mitochondrial
8.3	5.0	6.2	Q14974	Importin subunit beta-1 (Importin-90)
2.7	4.7	2.3	P40121	Macrophage-capping protein (Actin regulatory protein CAP-G)
3.8	4.7	2.9	Q86UY0	TXNDC5 protein
1.8	4.3	2.5	P43307	Translocon-associated protein subunit alpha (TRAP-alpha)
6.2	4.2	8.7	P61604	10 kDa heat shock protein, mitochondrial
3.5	4.0	4.9	P30086	Phosphatidylethanolamine-binding protein 1
2.7	3.8	2.6	P23284	Peptidyl-prolyl cis-trans isomerase B (PPIase B)
5.1	3.4	5.8	P13639	Elongation factor 2
2.1	3.4	1.8	P49755	Transmembrane emp24 domain-containing protein 10
2.5	3.4	2.3	P53999	Activated RNA polymerase II transcriptional coactivator p15
5.3	3.2	4.1	P37837	Transaldolase
6.6	3.1	7.3	P31947	14-3-3 protein sigma
1.9	3.0	1.8	B7Z1R5	V-type proton ATPase catalytic subunit A
6.4	3.0	6.0	E7EX73	Eukaryotic translation initiation factor 4 gamma 1
4.5	2.9	4.6	F8W6I7	Heterogeneous nuclear ribonucleoprotein A1
2.0	2.8	2.0	Q9UJ70	N-acetyl-D-glucosamine kinase (N-acetylglucosamine kinase)
2.0	2.8	2.0	P13796	Plastin-2 (L-plastin)
5.5	2.8	1.7	Q5T8U5	Surfeit 4
3.2	2.5	3.2	P19338	Nucleolin (Protein C23)
3.1	2.5	5.5	Q14103	Heterogeneous nuclear ribonucleoprotein D0
3.1	2.4	3.8	P23526	Adenosylhomocysteinase
1.3	2.4	1.3	P07339	Cathepsin D
1.3	2.2	1.3	A8MYE6	Integrin beta
1.4	2.2	1.2	P01623	Immunoglobulin kappa variable 3-20 (Ig kappa chain V-III region B6)
3.6	2.0	3.3	P48643	T-complex protein 1 subunit epsilon (TCP-1-epsilon)
2.7	2.0	2.8	P49368	T-complex protein 1 subunit gamma (TCP-1-gamma)
3.9	2.0	5.1	P19367	Hexokinase-1
1.5	1.8	1.4	P14314	Glucosidase 2 subunit beta
1.4	1.8	1.2	P30481	HLA class I histocompatibility antigen, B-44 alpha chain
2.3	1.7	2.0	I3L0N3	Vesicle-fusing ATPase
2.7	1.7	2.3	P30044	Peroxiredoxin-5, mitochondrial
2.6	1.6	2.2	Q00839	Heterogeneous nuclear ribonucleoprotein U
1.9	1.6	1.8	P50990	T-complex protein 1 subunit theta (TCP-1-theta)
1.8	1.6	1.9	P61088	Ubiquitin-conjugating enzyme E2 N
2.6	1.6	2.2	P14866	Heterogeneous nuclear ribonucleoprotein L
3.8	1.6	2.3	P78527	DNA-dependent protein kinase catalytic subunit
2.0	1.5	2.3	P49411	Elongation factor Tu, mitochondrial
3.2	1.5	3.1	Q86VP6	Cullin-associated NEDD8-dissociated protein 1
1.9	1.5	1.8	D6RG13	40S ribosomal protein S3a
1.8	1.4	2.2	G5E972	Lamina-associated polypeptide 2, isoforms beta/gamma
2.3	1.4	2.4	P13804	Electron transfer flavoprotein subunit alpha, mitochondrial (Alpha-ETF)
1.8	1.4	1.7	P63104	14-3-3 protein zeta/delta
2.1	1.3	1.8	B1AHC9	X-ray repair cross-complementing protein 6
1.9	1.2	2.4	P30041	Peroxiredoxin-6
3.0	1.2	2.7	P31948	Stress-induced-phosphoprotein 1

Patient 266				List B
Tumour regions			Gene ID	protein name
T-Q1	T-Q2	T-Q3		
-4.8	-1.2	-3.2	Q9Y6C2	EMILIN-1
-2.7	-1.2	-3.2	Q15417	Calponin-3
-2.8	-1.3	-2.3	P02545	Prelamin-A/C [Cleaved into: Lamin-A/C (70 kDa lamin)
-1.9	-1.3	-2.2	Q15149	Plectin (PCN) (PLTN)
-1.9	-1.4	-1.8	P21333	Filamin-A (FLN-A)
-1.8	-1.4	-1.8	Q9Y490	Talin-1
-1.9	-1.4	-2.8	Q99536	Synaptic vesicle membrane protein VAT-1 homolog
-1.9	-1.5	-2.0	P35579	Myosin-9
-2.2	-1.6	-2.4	E7EQB2	Lactotransferrin
-3.4	-1.6	-2.5	P12111	Collagen alpha-3(VI) chain
-2.1	-1.7	-2.9	Q9BUB1	cAMP-dependent protein kinase type II-alpha regulatory subunit
-19.9	-1.7	-25.2	O75369	Filamin-B
-3.6	-1.7	-2.9	P02751	Fibronectin (FN)
-2.0	-1.7	-2.3	P02790	Hemopexin (Beta-1B-glycoprotein)
-2.8	-1.7	-3.1	P08670	Vimentin
-3.5	-2.1	-2.9	P12110	Collagen alpha-2(VI) chain
-3.4	-2.1	-3.9	P05164	Myeloperoxidase (MPO)
-3.2	-2.2	-1.3	P62736	Actin, aortic smooth muscle (Alpha-actin-2)
-3.9	-2.2	-3.1	P12109	Collagen alpha-1(VI) chain
-2.0	-2.7	-3.8	C9JEU5	Fibrinogen gamma chain
-1.6	-2.7	-1.3	F5GWP8	Keratin, type I cytoskeletal 17
-3.6	-2.8	-3.7	P01009	Alpha-1-antitrypsin
-1.9	-2.9	-3.0	P68871	Hemoglobin subunit beta
-4.7	-3.1	-4.5	Q5TCU3	Tropomyosin beta chain
-4.8	-3.4	-6.5	Q09666	Neuroblast differentiation-associated protein AHNAK
-2.5	-3.5	-5.8	P02675	Fibrinogen beta chain
-3.3	-3.8	-3.5	F5GXS0	Complement C4-B
-4.7	-3.9	-5.4	Q13813	Spectrin alpha chain, non-erythrocytic 1
-2.4	-7.0	-1.3	P15924	Desmoplakin
-5.3	-9.8	-20.0	P02671	Fibrinogen alpha chain
-13.3	-11.5	-9.9	Q6NZI2	Caveolae-associated protein 1
-28.7	-12.7	-15.6	Q03135	Caveolin-1

T denotes tumour, Q1, Q2, Q3 are three regions in the tumour, (+) indicate fold change of upregulated proteins, (-) values of fold change of downregulated proteins, heat-map (Green: lowest F.C values of down-regulated proteins, Red: highest FC values of upregulated proteins). Gene ID: uniprot accession number. The order of the protein list was centred to their expression levels from the highest to the lowest in T9 (T-Q3).

3.4.1.2.3.2. Proteins exhibit opposite expression in one region of T266

Among the 234 upregulated proteins in sample 266, 10.3% (appendix 3.16-uniquly upregulated in Q2) of the proteins were detected with an opposite expression profile in Q2 compared to that in Q1 and Q3. Also, among the 132 down-regulated proteins in sample 266, 3% of the proteins were uniquely down-regulated in Q2 and were unchanged in the other two tumour regions (Q1/Q3) (appendix 3.19). Proteins such as Biglycan, fructose-1,6-bisphosphatase 1, Prolargin, Clusterin were up in Q2 and were down in Q1 and Q3 except for Clusterin in Q3 was 1.2 upregulated (Table 3.12). Beta tubulin, and transcription intermediary factor 1-beta were downregulated in Q2 while were upregulated in Q1 and Q3 (Table 3.12).

Table 3.12. List of dysregulated proteins in T-Q2 exhibit opposite trend in other regions.

Patient 266				
Tumour regions			Gene ID	protein name
T-Q1	T-Q2	T-Q3		
-187.0	-150.8	1.6	P35749	Myosin-11
1.9	-1.6	1.9	Q13263	Transcription intermediary factor 1-beta (TIF1-beta)
1.3	-1.3	1.2	P68371	Tubulin beta-4B chain (Tubulin beta-2 chain)
UC	-1.2	1.8	P21980	Protein-glutamine gamma-glutamyltransferase 2
1.3	1.2	-1.4	Q96QK1	Vacuolar protein sorting-associated protein 35 (hVPS35)
UC	1.2	-1.4	P42765	3-ketoacyl-CoA thiolase, mitochondrial
-1.5	1.3	-1.4	P07686	Beta-hexosaminidase subunit beta
-4.3	1.3	-1.8	P21810	Biglycan
1.2	1.5	-7.7	P36871	Phosphoglucomutase-1 (PGM 1)
-1.3	1.6	2.0	P13611	Versican core protein (Chondroitin sulfate proteoglycan core protein 2)
-1.2	1.7	-1.2	P09382	Galectin-1 (Gal-1)
UC	1.8	-1.7	P01903	HLA class II histocompatibility antigen, DR alpha chain
-1.5	2.0	-2.9	P09467	Fructose-1,6-bisphosphatase 1
-2.5	2.1	1.2	P35555	Fibrillin-1
-2.7	2.7	-1.8	P51888	Prolargin (Proline-arginine-rich end leucine-rich repeat protein)
-2.4	3.8	1.3	P02452	Collagen alpha-1(I) chain
-1.2	4.7	1.2	P10909	Clusterin (Aging-associated gene 4 protein)

T denotes tumour, Q1, Q2, Q3 are three regions in the tumour, (+) indicate fold change of upregulated proteins, (-) values of fold change of downregulated proteins, heat-map (Green: lowest F.C values of down-regulated proteins, Red: highest FC values of upregulated proteins). Gene ID: uniprot accession number. The order of the protein list was centred to their expression levels from the highest to the lowest in T9 (T-Q3).

3.4.1.2.4. T298-Q1 centred analysis of dysregulated proteins

To demonstrate why Q1 in sample 298 was clustered away from the other two regions with 12.3% variance (Figure 3.4), up and down regulated proteins that were close in their expression in Q2 and Q3 and were expressed differently in Q1 were sorted from the highest to lowest in table 3.13. Proteins exhibit an opposite expression profile in Q1 (i.e. up in Q1 and down in Q2/Q3 or down in Q1 and up in Q2/Q3) also listed in table 3.14.

3.4.1.2.4.1. Differential protein expression within tumour T298

The 201 upregulated and 124 down-regulated proteins in sample 266 were sorted from the lowest to the highest fold change compared to the normal tissues (appendices 3.20 and 3.23). Dysregulated proteins that make Q1 region different from the other two regions (i.e. proteins fold change in Q2 and Q3 were mostly close to each other) were selected and presented in table 3.13. All the upregulated proteins were more abundant in Q2 and Q3 than that in Q1 except for phosphate carrier protein which was more abundant in Q1. Decorin, lumican, Mimecan, collagen alpha 1, 2 and 3 (VI) chains, prolargin, collagen alpha CS 18, Biglycan, Caveolin-1 were all downregulated in all T298 tumour regions and were the least reduced in Q1 than in Q2 and Q3, while microsomal Cytochrome b5, Plectin, cytoskeletal 18 keratin type I, carbonic anhydrase 1, Annexin A3 were detected more decreased in Q1 than the other two tumour parts.

Table 3.13. List of heterogeneously expressed proteins in all T- 266 tumour regions.

Patient 298				
Tumour regions			Gene ID	protein name
T-Q1	T-Q2	T-Q3		
4.2	5.0	5.5	P80723	Brain acid soluble protein 1 (22 kDa neuronal tissue-enriched acidic protein)
3.8	4.9	6.1	P33241	Lymphocyte-specific protein 1 (47 kDa actin-binding protein)
2.6	3.9	3.8	P29350	Tyrosine-protein phosphatase non-receptor type 6 (EC 3.1.3.48)
2.0	2.9	3.1	P04233	HLA class II histocompatibility antigen gamma chain
2.0	3.3	2.5	P36871	Phosphoglucomutase-1 (PGM 1) (EC 5.4.2.2) (Glucose phosphomutase 1)
2.0	1.5	1.3	Q00325	Phosphate carrier protein, mitochondrial (Phosphate transport protein)
2.0	2.8	2.7	F8W6I7	Heterogeneous nuclear ribonucleoprotein A1
2.0	2.6	3.1	G3V5Q1	DNA-(apurinic or apyrimidinic site) lyase
1.7	2.1	2.6	P01861	Immunoglobulin heavy constant gamma 4
1.7	2.1	2.0	P13796	Plastin-2 (L-plastin) (LC64P) (Lymphocyte cytosolic protein 1)
1.7	2.9	2.5	Q14019	Coactosin-like protein
1.6	1.9	2.3	Q9UQ80	Proliferation-associated protein 2G4 (Cell cycle protein p38-2G4 homolog)
1.5	1.9	2.0	Q9UL46	Proteasome activator complex subunit 2 (11S regulator complex subunit beta)
1.5	2.1	2.0	Q96AE4	Far upstream element-binding protein 1 (FBP)
1.5	2.1	2.0	P19367	Hexokinase-1
1.5	1.9	1.8	P07108	Acyl-CoA-binding protein (ACBP) (Diazepam-binding inhibitor)
1.5	2.5	2.3	P14550	Alcohol dehydrogenase
1.5	1.8	2.1	Q00839	Heterogeneous nuclear ribonucleoprotein U
1.3	1.7	2.2	Q13185	Chromobox protein homolog 3
1.3	2.0	2.3	B1AHC9	X-ray repair cross-complementing protein 6
-1.2	-3.0	-2.7	P07585	Decorin (Bone proteoglycan II) (PG-S2) (PG40)
-1.2	-2.4	-3.1	P51884	Lumican (Keratan sulfate proteoglycan lumican)
-1.6	-4.5	-3.7	P20774	Mimecan (Osteoglycin) (Osteoinductive factor) (OIF)
-2.2	-4.4	-4.3	P12111	Collagen alpha-3(VI) chain
-2.2	-1.5	-1.4	P00167	Cytochrome b5 (Microsomal cytochrome b5 type A)
-2.3	-1.3	-1.5	Q15149	Plectin (PCN) (PLTN) (Hemidesmosomal protein 1)
-2.5	-6.4	-5.4	P12110	Collagen alpha-2(VI) chain
-2.5	-5.2	-3.8	P51888	Prolargin (Proline-arginine-rich end leucine-rich repeat protein)
-2.7	-6.3	-6.0	P12109	Collagen alpha-1(VI) chain
-2.7	-1.7	-1.5	P05783	Keratin, type I cytoskeletal 18
-3.1	-1.5	-2.6	P00915	Carbonic anhydrase 1
-3.7	-1.8	-2.5	P21291	Cysteine and glycine-rich protein 1 (Cysteine-rich protein 1)
-3.9	-12.4	-11.0	P21810	Biglycan (Bone/cartilage proteoglycan I) (PG-S1)
-4.2	-5.7	-5.7	Q03135	Caveolin-1
-5.2	-3.4	-3.7	P12429	Annexin A3 (35-alpha calcimedin) (Annexin III)

T denotes tumour, Q1, Q2, Q3 are three regions in the tumour, (+) indicate fold change of upregulated proteins, (-) values of fold change of downregulated proteins, heat-map (Green: lowest F.C values of down-regulated proteins, Red: highest FC values of upregulated proteins). Gene ID: uniprot accession number. The order of the protein list was centred to their expression levels from the highest to the lowest in T9 (T-Q3).

3.4.1.2.4.2. Proteins exhibit opposite expression in one region of T298

Among the 201 upregulated proteins in sample 298, 4.5% (appendix 3.22-uniquely upregulated proteins in Q1) of the proteins were detected with an opposite expression profile in Q1 compared to that in Q2 and Q3 (appendix 3.21). Also, among the 124 down-regulated proteins in this patient, 5.6% of the proteins were detected with an opposite expression profile in Q1 compared to that in Q2 and Q3 (appendix 3.25). Ten heterogeneous proteins were expressed among sample 298 tumour specimen, and exhibit an opposite expression pattern between Q1 and the other two tumour regions eg. Histone H2A and Collagen alpha-1 (I) chain were upregulated in Q1 but were downregulated in the other compared tumour regions, other proteins exhibited an opposite profile eg. Clathrin heavy chain 1, V-type proton ATPase catalytic subunit A, i.e. were down-regulated in Q1 and upregulated in Q2 and Q3 (Table 3.14).

Table 3.14. List of dysregulated proteins in T-Q1 exhibit opposite trend in other regions.

Patient 298				
Tumour regions			Gene ID	protein name
T-Q1	T-Q2	T-Q3		
1.9	-1.2	-4.0	Q93077	Histone H2A type 1-C (Histone H2A/l)
-1.3	1.2	1.2	Q14764	Major vault protein (MVP) (Lung resistance-related protein)
-1.3	1.3	1.3	Q15233	Non-POU domain-containing octamer-binding protein
-1.4	1.2	1.2	B7Z1R5	V-type proton ATPase catalytic subunit A
-1.2	1.2	1.2	Q5JP53	Tubulin beta chain
2.0	-1.3	-4.0	P02452	Collagen alpha-1(I) chain (Alpha-1 type I collagen)
-1.2	1.2	1.2	Q14240	Eukaryotic initiation factor 4A-II (eIF-4A-II)
-1.8	1.5	1.5	Q00610	Clathrin heavy chain 1 (Clathrin heavy chain on chromosome 17)
-1.2	1.4	1.4	B4DQJ8	6-phosphogluconate dehydrogenase, decarboxylating
-1.2	1.2	1.2	P05091	Aldehyde dehydrogenase, mitochondrial

T denotes tumour, Q1, Q2, Q3 are three regions in the tumour, (+) indicate fold change of upregulated proteins, (-) values of fold change of downregulated proteins, heat-map (Green: lowest F.C values of down-regulated proteins, Red: highest FC values of upregulated proteins). Gene ID: uniprot accession number. The order of the protein list was centred to their expression levels from the highest to the lowest in T9 (T-Q3).

3.4.1.3. Validation of 4 differentially expressed proteins (Desmoplakin, Tenascin C, Enolase-1 and *ERO1-La*) by western blot and qRT-PCR

3.4.1.3.1. Desmoplakin

The results of investigating desmoplakin expression (mRNA and protein) in three selected parts per tumour T3-Q1: blue, T6-Q2: red, T9-Q3: green) compared to matched control normal tissues in four lung squamous carcinoma patients (coded 260, 261, 266, 298) for detecting intra-tumour gene expression heterogeneity are detailed in figure 3.5-A. **In patient coded 260**, LC-MS/MS has detected 4-fold decrease in region T9-Q3 compared to the other two regions, the other two regions level of desmoplakin was 5.3 and 5.2-fold decreased compared to the matched control normal tissue. Western blot analysis showed an opposite profile, where they were all upregulated and T9-Q3 had the least abundance of desmoplakin (Figure 3.5-B). At the level of mRNA, both T9-Q3 and T6-Q2 had the same amounts of desmoplakin mRNA and both were 3-fold more than the matched control normal lung tissue (Figure 3.5-C). **In patient 261**, the abundance of desmoplakin was detected by LC-MS/MS increased by 138, 90 and 50-fold more than in control normal tissues. Western blot revealed increased expression of desmoplakin as well which was tremendous in T6-Q2 (approximately 6-fold more than in T9-Q3) (Figure 3.5-B). qRT-PCR showed more than 2-fold increase in the amount of desmoplakin in T3-Q1 more than in T6-Q2. T6-Q2 showed an opposite expression (down-regulated) profile which was half of the level of mRNA in the normal tissues (Figure 3.5-C). LC-MS/MS did not detect desmoplakin in the other two patients (266 and 298) within the cut-off value (1.2-fold). **In patient 266**, the level of mRNA was detected significantly increased by 3-fold in T9-Q3 more than in the control normal tissues. The difference between T9-Q3 and T3-Q1 was also

significant with a 2-fold difference (Figure 3.5-C). **In patient 298**, western blot and qRT-PCR detected opposite levels. At the protein level, desmoplakin was overexpressed in T3-Q1 and T9-Q3 regions and was 5-fold more in T9-Q3 than the control normal tissues (Figure 3.5-B), while the mRNA level was half the control normal tissue levels in T3-Q1 and 9-fold less than normal in T9-Q3 (Figure 3.5-C).

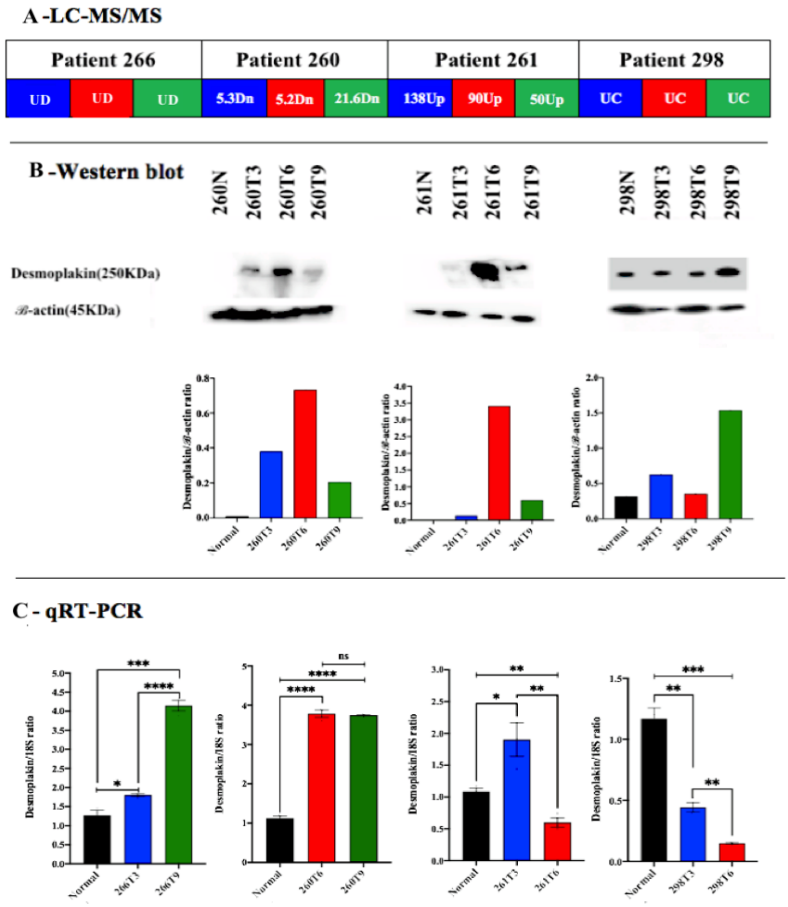

Figure 3.5. Desmoplakin heterogeneity validation. A: Desmoplakin protein abundance in three regions per tumour compared to the surrounding normal tissues per patient by LC-MS/MS (n=3 technical repeats), **B**: Desmoplakin protein abundance in the tested trisects by western blot (n=1 technical repeats, ß-actin used as a loading control), **C**: qRT-PCR assessment of desmoplakin mRNA level (n=3 technical repeats, 18s used as a loading control). Black colour: normal lung tissue, Blue colour: tumour part T3-Q1, Red colour: tumour part T6-Q2, Green colour: tumour part T9-Q3. T3, T6, T9 are three biopsies taken from the same patient tumour, the number of patients n=4 (260, 261, 266, 298).

3.4.1.3.2. Tenascin C

The results of investigating Tenascin-c expression (mRNA and protein) in three selected parts per tumour; T3-Q1: blue, T6-Q2: red, T9-Q3: green, in reference to matched normal control tissues in four lung squamous carcinoma patients (coded 260, 261, 266, 298) for detecting intra-tumour gene expression heterogeneity are detailed in figure 3.6. **In patient 260**, tenascin c was not detected by LC-MS/MS within the cut-off value (1.2-fold). Western blot showed increased abundance of tenascin c in all investigated regions. T6-Q2 was the most abundant part of the tested regions, where it was 2-fold more abundant than the other two parts (Figure 3.6-B). qRT-PCR, revealed no change in the level of mRNA between normal and T3-Q3 region while there was 6-fold more abundant in T6-Q2 compared to both normal and T9-Q3 tumour region (Figure 3.6-C). **In patient 261**, LC-MS/MS has detected double amounts of tenascin c in T6-Q2 than in the other two regions, and was 8-fold more than the control normal tissue. Western blot revealed T3-Q1 was the most abundant part of the tumour in tenascin c with 2X-times the abundance in the control normal tissue. T9-Q3 was the least part of patient 261 tumour regions in the abundance of tenascin c level and was opposite of the mass-spectrometry detection (downregulated) (Figure 3.6-B). qRT-PCR also showed a significant increase (6-fold) in tenascin c mRNA in T3-Q1 than control normal tissues. T6-Q2 had no significant change at the level of transcription (Figure 3.6-C). **In patient 266**, LC-MS/MS has detected 7-fold increase in both T6-Q2 and T9-Q3 compared to the normal tissue, and was detected 3X-times this level in T3-Q1. qRT-PCR revealed 2-fold less mRNA in T9-Q3 than in control normal tissue, T3-Q1 had no significant change although tends to rise (Figure 3.6-C). **In patient 298**, tenascin c was not detected by mass spectrometry (out of the cut-off value: 1.2 fold), while it

was detected by western blot 5-fold increase in T9-Q3 than in control normal tissue (Figure 3.6-B). qRT-PCR revealed no significant difference between T3-Q1 and T9-Q3 and both exhibited a significant 2-fold decrease compared to normal control tissue (Figure 3.6-C).

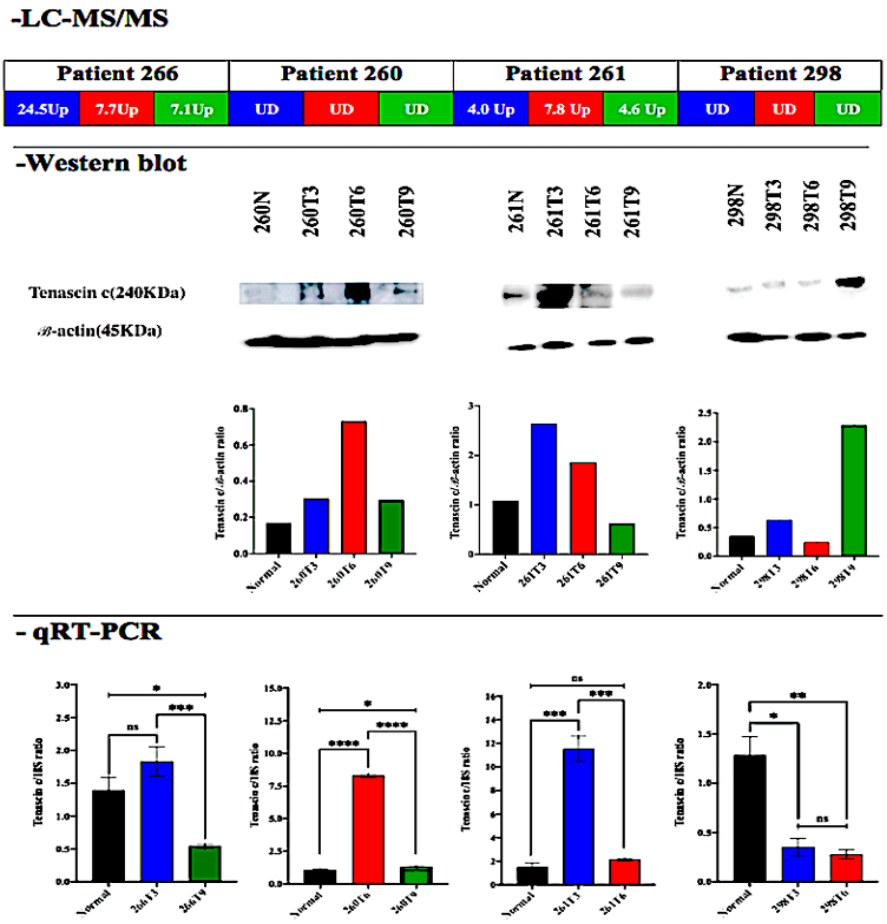

Figure 3.6. Tenascin c heterogeneity validation. **A**: Tenascin c protein abundance in three regions per tumour compared to the surrounding normal tissues per patient by LC-MS/MS (n=3 technical repeats), **B**: Tenascin c protein abundance in the tested trisects by western blot (n=1 technical repeats, ß-actin used as a loading control), **C**: qRT-PCR assessment of Tenascin c mRNA level (n=3 technical repeats, 18s used as a loading control). Black colour: normal lung tissue, Blue colour: tumour part T3-Q1, Red colour: tumour part T6-Q2, Green colour: tumour part T9-Q3. T3, T6, T9 are three biopsies taken from the same patient tumour, the number of patients n=4 (260, 261, 266, 298).

3.4.1.3.3. Enolase-1 (*c-Myc* promoter binding protein)

Western blot and qRT-PCR validation of enolase-1 expression in three selected parts per tumour; (Q1: blue, Q2: red, Q3: green), compared to matched control normal tissues in lung SqCC patients n=4 (coded 260, 261, 266, 298) for detecting intra-tumour gene expression heterogeneity is detailed in figure 3.7. **In patient 260**, LC-MS/MS has detected enolase-1 5.4, 4 and 2.8-fold elevated in T3-Q1, T6-Q2 and T9-Q3, respectively. Western blot also showed the same profile trend where it was 6-fold more abundant in T3-Q1 and T6-Q2 and 3-fold more in T9-Q3 compared to the normal tissue levels (Figure 3.7-B). qRT-PCR showed no difference in mRNA levels between T6-Q2 and T9-Q3 (Figure 3.7-C). Western blot and LC-MS/MS showed heterogeneity between T9-Q3 and the other tumour regions, while there was no difference at mRNA levels. **In patient 261**, the level of enolase-1 was upregulated by 2±0.5 fold in all tumour regions as detected by mass spectrometry. Western blot revealed an opposite profile, where it was 4-fold, 3-fold and 0.5-fold decreased in T3-Q1, T6-Q3 and T9-Q2, respectively (Figure 3.7-B). qRT-PCR revealed no change at the level of mRNA in T3-Q1, and a 50% decrease in enolase-1 mRNA in T6-Q2 compared to normal tissue was detected (Figure 3.7-C). **In patient 266**, qRT-PCR detected no significant change in enolase-1 mRNA levels in T9-Q3, while T3-Q1 had increased by 30% compared to the normal control tissue (not significant). qRT-PCR showed a significant difference within the two tested tumour regions, T3-Q1 and T9-Q3 (Figure 3.7-C). Western blot was not performed due to sample scarcity. **In patient 298**, the expression of enolase-1 was elevated in all tumour regions by 1.5, 1.8 and 1.6-fold in T3-Q1, T6-Q2 and T9-Q3, respectively as detected by LC-MS/MS. Western blot also showed increased enolase-1 abundance by 2X-fold, 3.5X-fold and 0.5X-fold in T3-Q1, T6-Q2 and

T9-Q3, respectively more than in control normal tissue (Figure 3.7-B). qRT-PCR revealed a decreased enolase-1 mRNA levels by 2X-fold in the two tested regions compared to the control normal tissue (Figure 3.7-C).

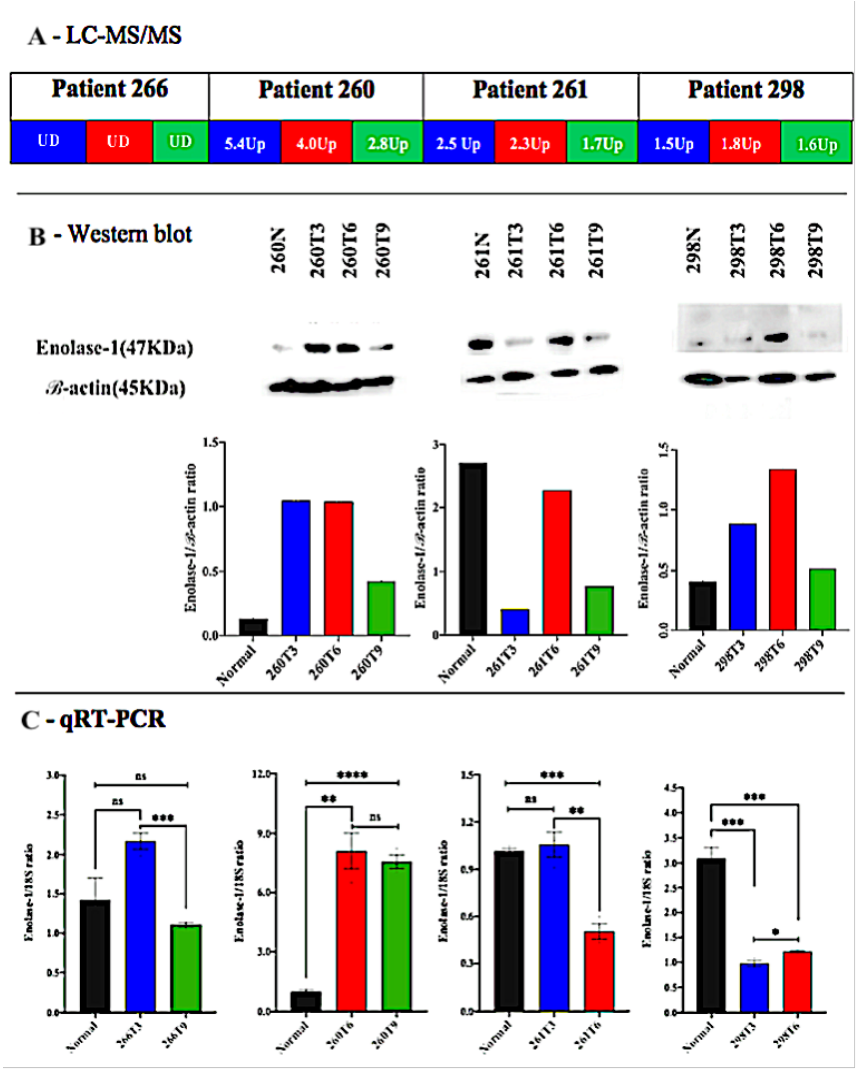

Figure 3.7. Enolase-1 heterogeneity validation. **A**: Enolase-1 protein abundance in three regions per tumour compared to the surrounding normal tissues per patient by LC-MS/MS (n=3 technical repeats), **B**: Enolase-1 protein abundance in the tested trisects by western blot (n=1 technical repeats, ß-actin used as a loading control), **C**: qRT-PCR assessment of enolase-1 mRNA level (n=3 technical repeats, 18s used as a loading control). Black colour: normal lung tissue, Blue colour: tumour part T3-Q1, Red colour: tumour part T6-Q2, Green colour: tumour part T9-Q3. T3, T6, T9 are three biopsies taken from the same patient tumour, the number of patients n=4 (260, 261, 266, 298).

3.4.1.3.4. ERO1-La

Validation of ERO1-La expression in the three selected parts per tumour (T3-Q1: blue, T6-Q2: red, T9-Q3: green) in reference to matched control normal tissues in lung SqCC patients n=4 (coded 260, 261, 266, 298) for detecting intra-tumour gene expression heterogeneity by western blot and qRT-PCR is detailed in figure 3.8.

In patient 260, LC-MS/MS detected elevated ERO1-La protein levels in the all regions, T9-Q3 had the least abundance of ERO1-La (4.2-fold) and T3-Q1 and T6-Q2 were 10.6 and 13.9-fold more than the normal tissue, respectively. Western blot also showed overexpression of the protein in T6-Q2 and T9-Q3 but was a little bit lowered in T3-Q1 (Figure 3.8-B). ERO1-La mRNA was also significantly increased, T6-Q2 exhibit amounts of mRNA exceeded 30X-fold more than the control tissue (Figure 3.8-C). **In patient 261**, by LC-MS/MS, T3-Q1 and T6-Q2 almost had the same levels and T9-Q3 had nearly half of their abundance. Western blot analysis showed minor decrease in ERO1-La in T3-Q1, while T6-Q2 and T9-Q3 were a little bit increased (by 10% and 40%, respectively) (Figure 3.8-B). No significant change in ERO1-La mRNA between control tissue and T6-Q2, and it was significantly decreased by 30% in T3-Q1 when compared to the control tissue (Figure 3.8-C). **In patient 266**, ERO1-La was not detected by LC-MS/MS in all regions. Western blot was not performed for *EROI-La* on this sample due to protein sample scarcity. qRT-PCR showed no significant change between normal and T3-Q1, while the mRNA levels of ERO1-La was slightly decreased in T9-Q3 than in normal tissue and T3-Q1 (Figure 3.8-C). **In patient 298**, ERO1-La was also was not detected by LC-MS/MS (within the cut-off value: 1.2-fold). Western blot revealed increased abundance of the protein by 2X and 1.5X-fold in T3-Q1 and T9-Q3, respectively, while T6-Q2 exhibited only a little increase in the protein

abundance compared to normal tissue (Figure 3.8-B). qRT-PCR showed a significant decrease in the mRNA levels in both T3-Q1 and T6-Q2, the latter had decreased by 50% compared to the matched normal tissue (Figure 3.8-C).

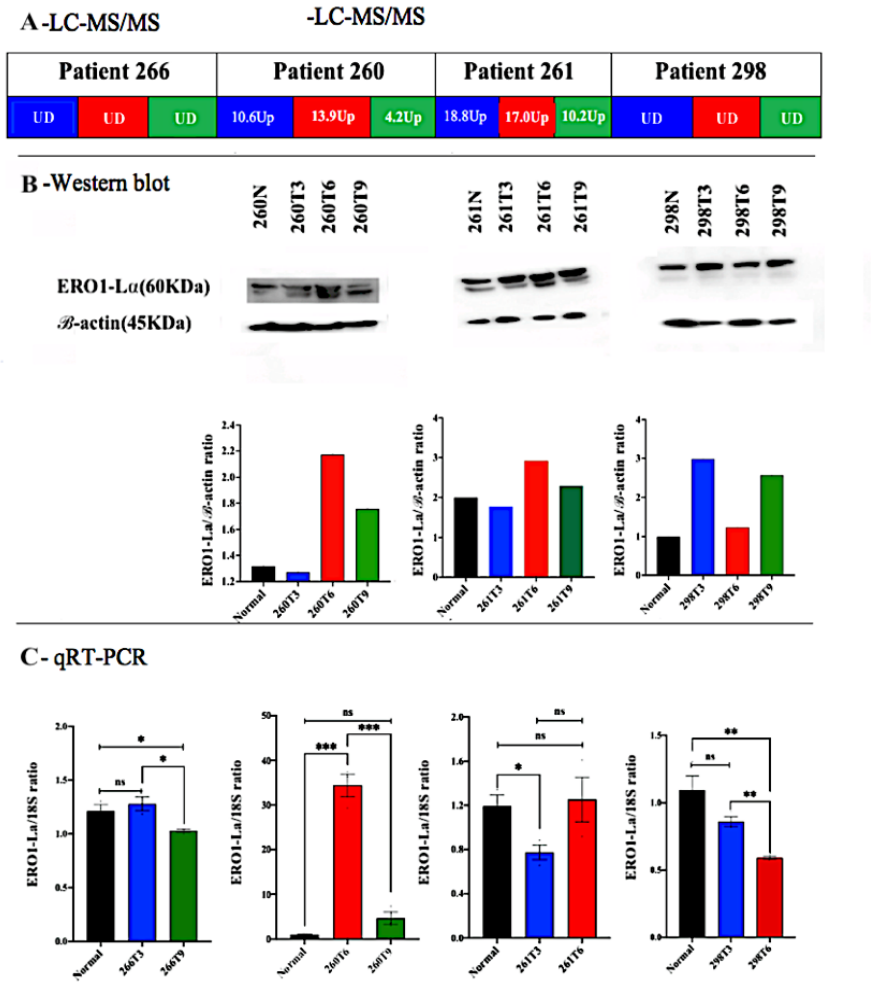

Figure 3.8. ERO1-La heterogeneity validation. **A**: EROI-La protein abundance in three regions per tumour compared to the surrounding normal tissues per patient by LC-MS/MS (n=3 technical repeats), **B**: EROI-La protein abundance in the tested trisects by western blot (n=1 technical repeats, ß-actin used as a loading control), **C**: qRT-PCR assessment of EROI-La mRNA level (n=3 technical repeats, 18s used as a loading control). Black colour: normal lung tissue, Blue colour: tumour part T3-Q1, Red colour: tumour part T6-Q2, Green colour: tumour part T9-Q3. T3, T6, T9 are three biopsies taken from the same patient tumour, the number of patients n=4 (260, 261, 266, 298).

3.4.2. Assessment of PI3K/AKT and JAK/STAT pathway activation in LSqCC patients specimens

In this part, *PI3K-AKT/PKB* and *JAK/STAT* signalling pathways were assessed in the three tumour regions and the matched normal tissue of the four LSqCC patients by PathScan® Intracellular Signalling Array Kit (Chemiluminescent Readout) (Cat No.7323). The phosphorylation of some key proteins (including *AKT* and its affected downstream signalling molecules (*GSK*, m-*TOR*, *ERK*, *P53*, *BAD*), marked in red (Figure 3.9) were quantified in the three regions of each tumour compared to their matched normal lung tissue (taken from same patient). As seen in Figure 3.9, *AKT* is a central downstream molecule that is phosphorylated by many receptor and non-receptor tyrosine kinases, including *JAK*/*STAT* and *PI3K*. Activation of the *JAK*/*STAT* pathway was examined by quantification of *STAT3* phosphorylation (Figures 3.10-3.14B). *PIM* 1/2/3 kinases are downstream targets of the *STAT3* transcription factor and their expression was also quantified (Figures 3.10-3.14A).

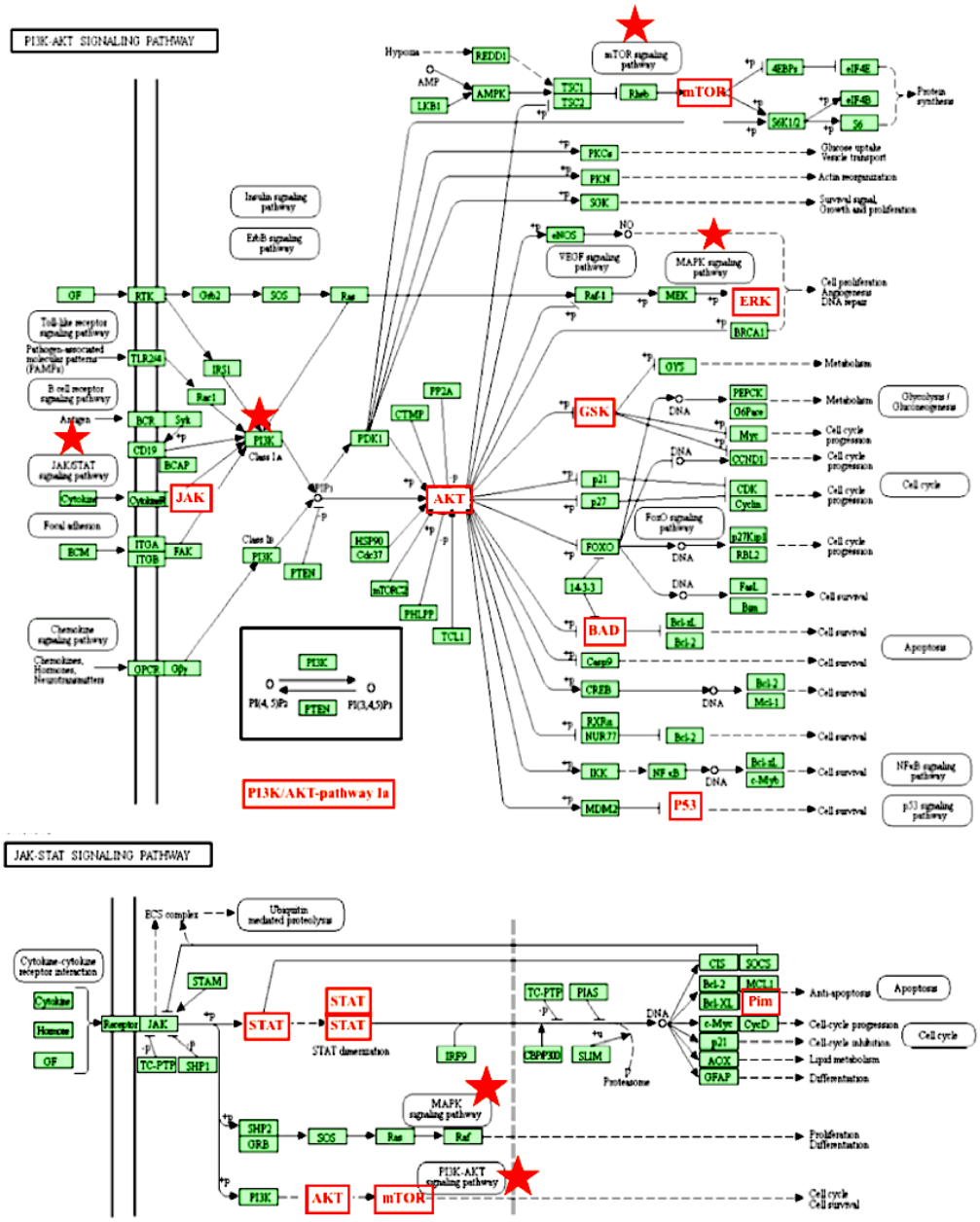

Figure 3.9. PI3K-AKT and JAK/STAT signalling pathways. Proteins in red were assessed for their phosphorylation variation within the tumour tissue specimen being studied. KEGG-signalling pathways with red stars were assessed and their activity was found variable.

3.4.2.1. JAK-STAT pathway assessment in patient 260

PIM1/2/3 kinase mRNA expression was measured by qRT-PCR in the tumour trisects Q1 and Q3 figure 3.10A. Phosphorylation of 18 target proteins, involved in the *PI3K/AKT* and *JAK/STAT* signalling pathways were quantified in each tumour trisect compared to matched normal lung tissue per 5µg total protein as depicted in figure 3.10B. Based on PCA analysis, T260-Q3 was different from the other two tumour regions in this patient (Figure 3.4A). *PIM 1* and *3* were downregulated in the two selected regions (Q1 and Q3) with no heterogeneous expression, while *PIM 2* was upregulated in both tumour regions, Q1 was double the abundance as in Q3 (Figure 3.10A). T260-Q3 had lower levels of phosphorylated proteins including *STAT1*, *AKT* Thr308/Ser437, *AMPKa*, *mTOR*, *HSP27*, *GSK-3b*, *P70S6K*, *SAPK*, *PRAS40*, *P38* compared to the other tumour regions although higher than matched normal tissue. T260-Q3 showed decreased phosphorylated proteins *PARP*, *S6RP*, *BAD*, *P53*, caspase-3 compared to matched normal tissue (Figure 3.10B). T260-Q1 had the highest signalling activity in *PI3K*/*AKT* and *JAK*/*STAT* pathways. *PIM2* mRNA expression was significantly elevated in patient 260 and the expression was heterogeneous. T260-Q3 had the lowest level of *pBAD* which might reflect the low levels of *PIM1* and *2* mRNA by qRT-PCR in this tumour region compared to T260-Q1 region (Figure 3.10A).

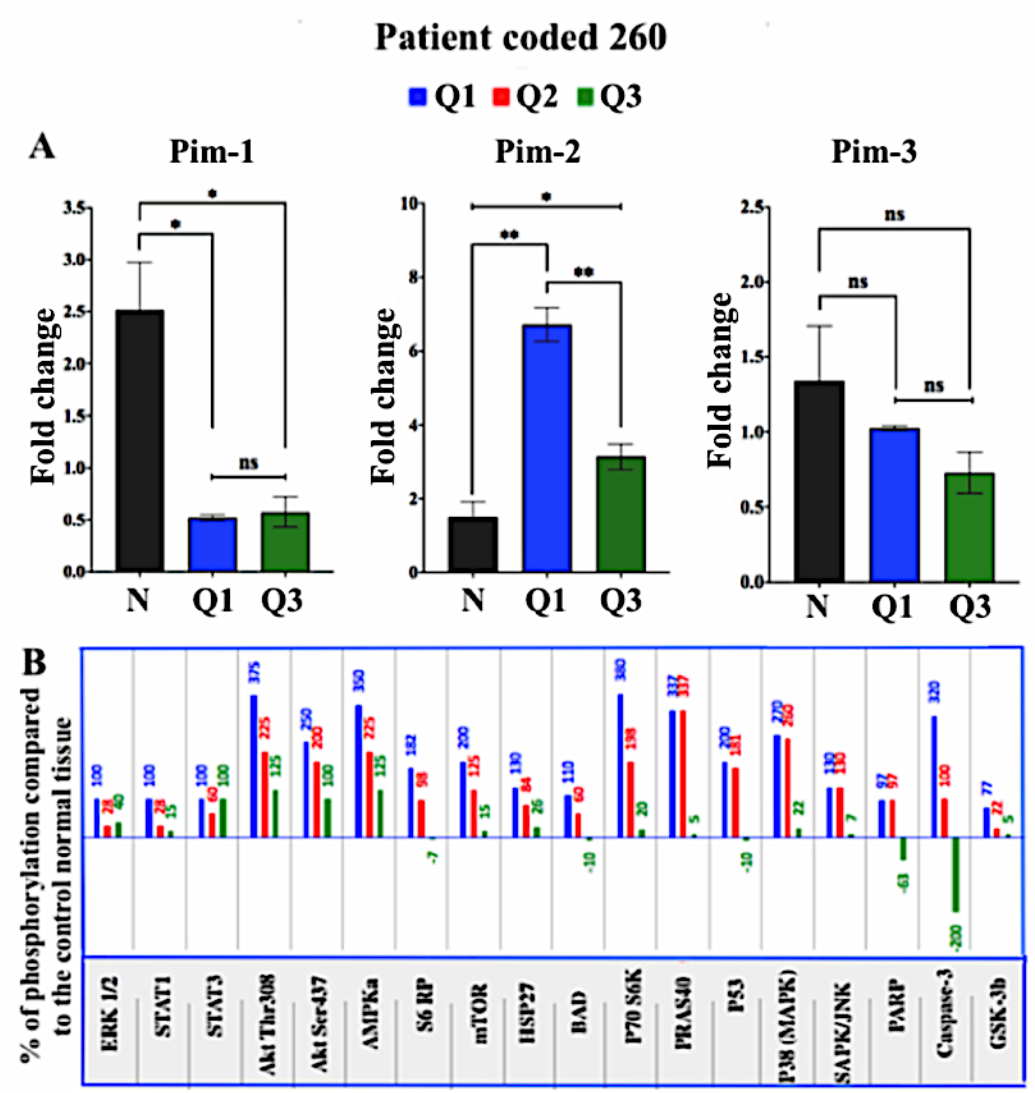

Figure 3.10. PI3K-AKT/mTOR and JAK-STAT pathways assessment in patient 260. A: assessment of JAK/STAT pathway by measuring the levels of PIM isoforms mRNA by qRT-PCR represented as Mean±STD (n=3 repeats). B: phosphorylation of 18 signalling molecules modulated via phosphorylation in JAK/STAT and PI3K/AKT and downstream pathways. Bars=% phosphorylation = (Tumour/Normal)X100.

3.4.2.2. JAK-STAT pathway assessment in patient 261

PIM 1/2/3 kinase mRNA expression was measured by qRT-PCR in the tumour trisects Q1 and Q3 figure 3.11A. Phosphorylation of 18 target proteins, involved in the *PI3K*/*AKT* and *JAK*/*STAT* signalling pathways were quantified in each tumour trisect compared to matched normal lung tissue per 5µg total protein as depicted in figure 3.11B. Based on PCA analysis, T261-Q1 was different from the other two tumour regions in this patient (Figure 3.4B). *PIM1* and *3* mRNA expression was elevated in Q1 as detected by qRT-PCR (Figure 3.11A).

Assessment of *PI3K*/*AKT* and *JAK*/*STAT* pathways showed T261-Q1 was different from the other tumour regions in the phosphorylation of several proteins including *mTOR*, *P70 S6K*, *P38* (*MAPK*), *PARP* and Caspase-3 which were lower than the matched normal tissue. T261-Q1 had similar phosphorylation levels as the matched normal tissue for proteins *AKT* Thr308, *SAPK*/*JNK* and *GSK*-3b (Figure 3.11B). p-BAD was elevated in the three tumour regions, with expression in T261-Q1 lower than Q3 and higher than Q2.

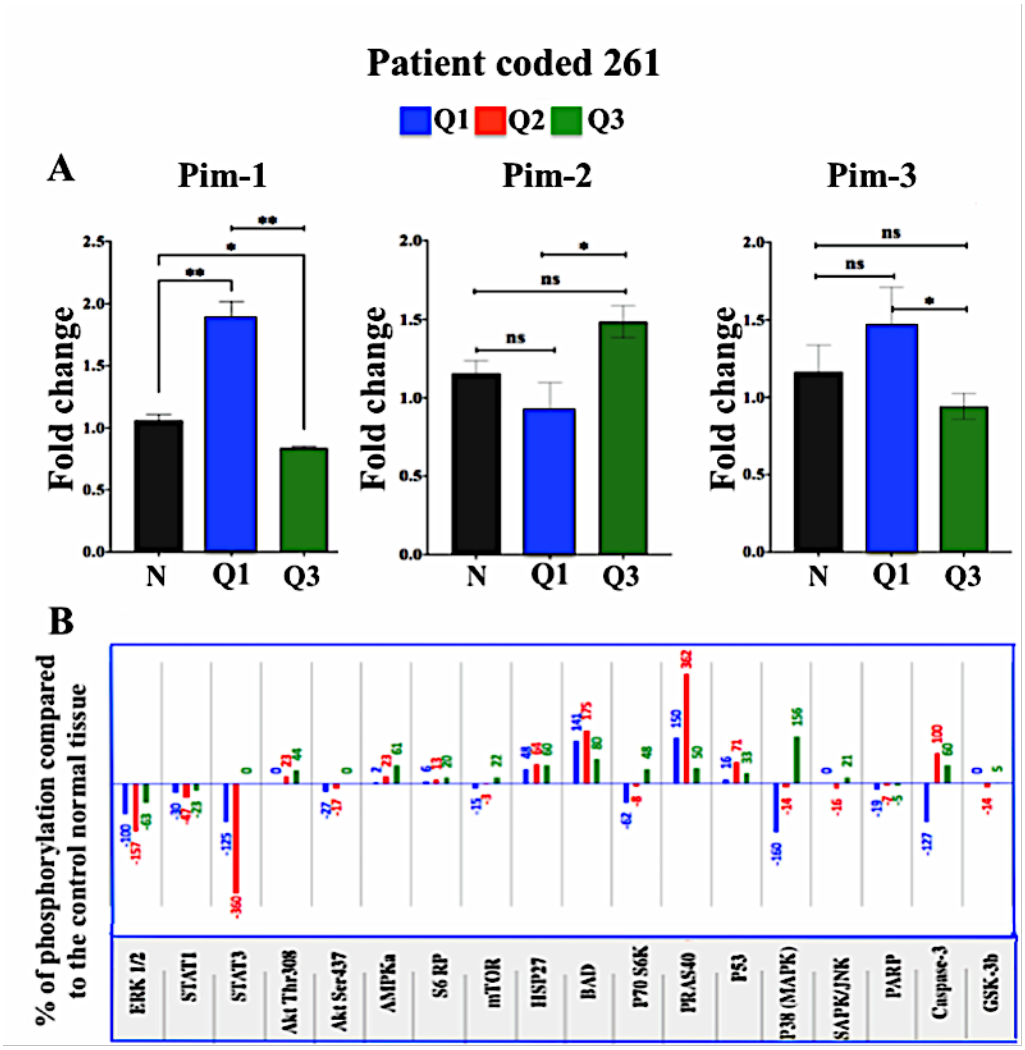

Figure 3.11. PI3K-AKT/mTOR and JAK-STAT pathways assessment in patient 261. A: assessment of JAK/STAT pathway by measuring the levels of PIM isoforms represented as Mean±STD (n=3 repeats). B: phosphorylation of 18 signalling molecules modulated via phosphorylation in JAK/STAT and PI3K/AKT and downstream pathways. Bars=% phosphorylation = (Tumour/Normal)X100.

3.4.2.3. JAK-STAT pathway assessment in patient 266

*PIM*1/2/3 kinase mRNA expression was measured by qRT-PCR in the tumour trisects Q1 and Q2 (Figure 12A). Phosphorylation of 18 target proteins, involved in the PI3K/AKT and JAK/STAT signalling pathways were quantified in each tumour trisect compared to matched normal lung tissue per 5µg total protein as depicted in figure 3.12B. Based on PCA analysis, T266-Q2 was different from the other two tumour regions (Figure 3.4C). As seen in figure 3.12A, *PIM1/2/3* mRNA expression was significantly upregulated in T266-Q1 compared to the normal control tissues. *PIM*1 and 2 were both downregulated in T266-Q2 but *PIM*3 was slightly increased, this might reflect the reduced levels of *BAD* phosphorylation (Figure 3.12A/B). T266-Q1 had the highest levels of phosphorylation of *AKT, AMPK, S6 RP, mTOR, HSP27, BAD, PRAS6K, P53, P38, SAPK, caspase-3* and *GSK-3b* (Figure 3.12B).

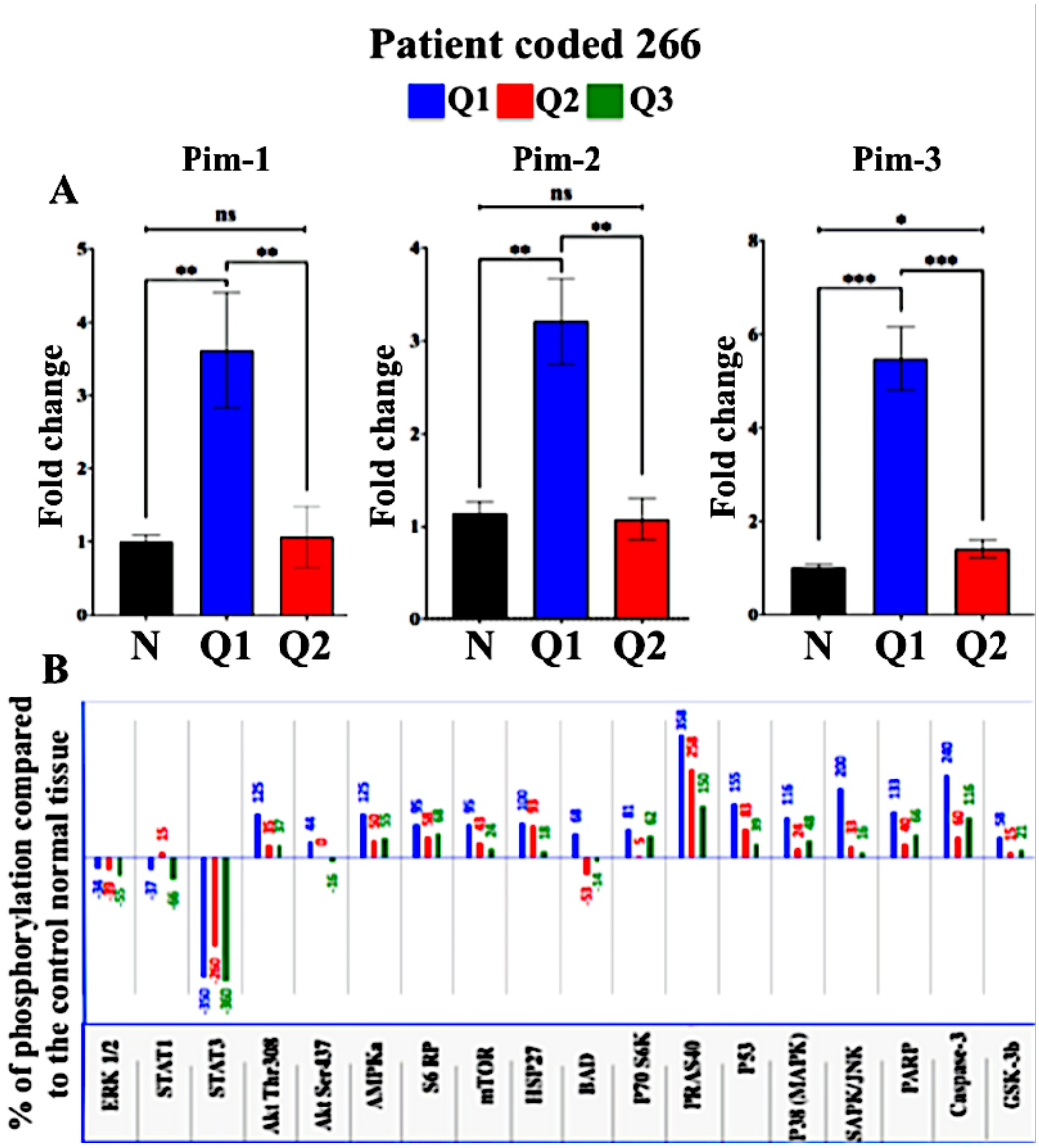

Figure 3.12. PI3K-AKT/mTOR and JAK-STAT pathways assessment in patient 266. A: assessment of JAK/STAT pathway by measuring the levels of PIM isoforms represented as Mean±STD (n=3 repeats). B: phosphorylation of 18 signalling molecules modulated via phosphorylation in JAK/STAT and PI3K/AKT and downstream pathways. Bars=% phosphorylation = (Tumour/Normal)X100.

3.4.2.4. JAK-STAT pathway assessment in patient 298

PIM1/2/3 kinase mRNA expression was measured by qRT-PCR in the tumour trisects Q1 and Q3 figure 3.13A. Phosphorylation of 18 target proteins, involved in the *PI3K*/*AKT* and *JAK*/*STAT* signalling pathways were quantified in each tumour trisect compared to matched normal lung tissue per 5µg total protein as depicted in figure 3.13B. Based on PCA analysis, T266-Q1 was different from the other two tumour regions (Figure 3.4D). *PIM1/2/3* kinases were elevated in T298-Q1 by 1.5, 2.5 and 3-fold more than the matched normal tissue (Figure 3.13A). *PIM*1 and 3 kinases were 2-fold reduced in T298-Q2 compared to the control normal tissue. All 18 phosphorylated proteins had higher expression in T298-Q2 than the two other tumour regions (Figure 3.13B). Phosphorylated *STAT3* expression was lower in T298-Q1 and T298-Q3 than matched normal tissue. *p-BAD* was elevated in all tumour regions and T298-Q1 had the lowest levels among the tumour regions (Figure 3.13B).

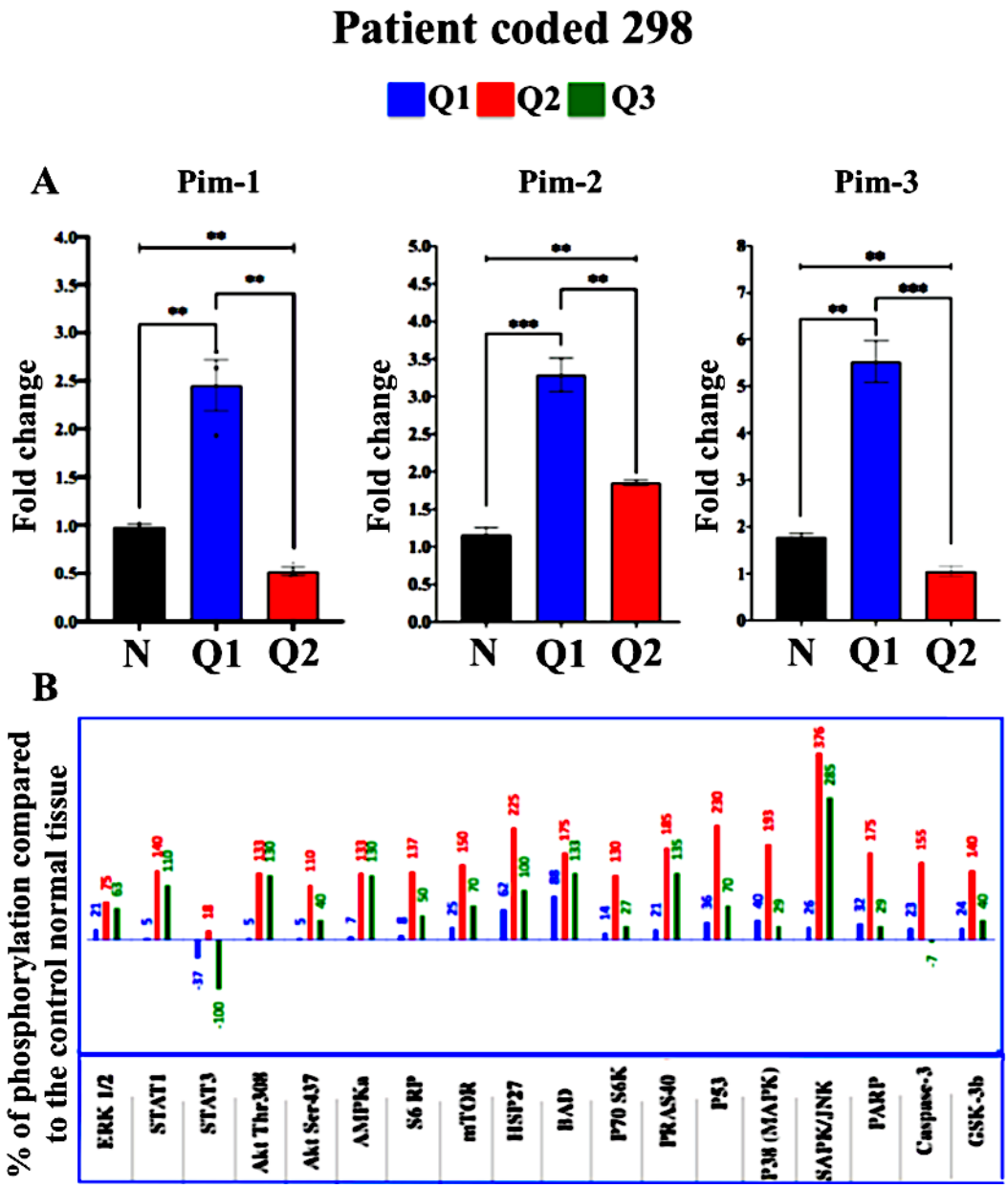

Figure 3.13. PI3K-AKT/mTOR and JAK-STAT pathways assessment in patient 298. A: assessment of JAK/STAT pathway by measuring the levels of PIM isoforms mRNA represented as Mean±STD *(*n=3 repeats*)*. B: phosphorylation of 18 signalling molecules modulated via phosphorylation in JAK/STAT and PI3K/AKT and downstream pathways. Bars=% phosphorylation = *(*Tumour/Normal*)* X100.

3.5. Discussion

Intra-tumour heterogeneity (ITH) presents a significant challenge to cancer therapy that leads to drug resistance and a poor prognosis for patients (McGranahan and Swanton, 2017). Even tumour nodules originating from the same primary lesion that have a similar histopathology can respond significantly different to treatment (Cusnir and Cavalcante, 2012). At present in our cancer centre, patients with a diagnosis of advanced lung cancer are screened for the presence of somatic mutations using the Oncomine Focus Assay before the clinician determines a personalised treatment protocol. This is a next-generation sequencing panel that allows the user to conduct concurrent RNA and DNA analysis from FFPE tumour biopsy samples and targets 52 genes relevant to solid tumours including SNVs, indels, CNVs and fusions. Tumour tissue will also be screened for *PD-L1* expression using immunohistochemical analysis to determine whether a patient is suitable for treatment with a checkpoint immunotherapy. There has been much debate in the literature over what the appropriate cut-off value for *PD-L1* expression should be for a tumour to be sensitive to treatment with a *PD1/PD-L1* inhibitor. Similar to other studies that have tested predictive biomarkers e.g. *EGFR*, *VEGF*, determining an appropriate cut-off value for high versus low protein expression is challenging due to ITH and a limited amount of tumour tissue in a biopsy sample. Phosphorylated proteins are an ideal indicator of whether a specific pathway is activated in a tumour and therefore have the potential to determine whether that tumour may respond to a targeted treatment. However, their expression is not routinely quantified in the clinic as due to their instability they have not proven to be robust biomarkers.

In this research study we aimed to: i- quantify the difference in protein expression within three different regions of four lung squamous cell carcinomas using matched normal tissue as a reference, ii- quantify 18 phosphorylated protein kinases involved in both the *JAK/STAT*-and *PI3K/AKT* pathway across different regions of the same tumour and iii- quantify *PIM*1/2/3 kinase mRNA expression within the different tumour regions to determine any variance of *JAK/STAT* signalling pathway that supported the presence of ITH.

Detection of intra-tumour heterogeneity using LC-MS/MS

Differentially expressed proteins (upregulated/downregulated) across three different regions of the same tumour for four patients was compared to matched normal tissue and the changes were filtered to a cut-off value of 1.2 fold change and significance at <0.05. The summary of the number of up and down regulated proteins was tabulated in table 3.6. Details on the changed proteins including; fold change in the three tumour regions, gene name and the full protein name were included in the results above (section 3.4.1.1.). The percentages of shared up and down regulated proteins in all three tumour regions (cut-off value of 1.2), in respective order were: in patient 260 68.5% pn=232) and 54% (n=144), in patient 261: 68% (n=184) and 60.4% (n=169), in patient 266: 72.2% (n=234) and 57.6% (n=132), in patient 298: 75.1% (n=201) and 59.7% (n=124). The heterogenous expression of up and down regulated proteins per patient are presented in the results under sections 3.4.1.2.1 to 3.4.1.2.4. Principal Component Analysis (PCA) has clustered region Q3 **in patient 260** as different from the other two tumour regions investigated in terms of protein abundance (Figure 3.4). In addition to the heterogeneous expression of shared protein in the three tumour regions, 13.8% (n=232) and 8.3% (n=144) of the upregulated and downregulated proteins were

uniquely expressed in Q3 region at the cut-off value 1.2-fold (increase/decrease). In contrast, the unique up/down regulated proteins were (1.7% and 8.3%) and (1.7% and 3.5%) in Q1 and Q2, respectively. Region Q3 of this patient tumour share a low percentage of the up and downregulated proteins with the other two regions, while Q1 and Q2 shared about 20.1% (n=144) of the down regulated proteins. **In patients 261** and **298**, the region T-Q1 had a different proteome expression profile than the other two tumour regions, while in patient 266, T-Q2 was different to the other two regions (Figure 3.4).

Based on the first PCA and Venn diagram analysis of the mass-spectrometry data, the tumour regions that clustered away from other tumour regions are assumed to have differential protein expression and may rely on different cell signalling pathways.

Validation of a panel of 4 (Desmoplakin, Tenascin C, ERO1-La and Enolase-1) differentially expressed proteins

A panel of 4 (Desmoplakin, Tenascin C, *Enolase-1* and *ERO1-La*) differentially expressed proteins identified by LC-MS/MS were chosen to validate further by western blot analysis. **Desmoplakin (***DSP*) is one of the desmosome components of the inner membrane of the endoplasmic reticulum. *DSP* is known to play a tumour suppressant role by inhibiting the Wnt/β-catenin signalling pathway and its downregulation was found associated with poor prognosis, tumour invasion and metastasis in patients with non-small cell lung cancer (Yang et al., 2012). In this research work, DSP was identified as a good example of intra-tumour heterogeneity and it was chosen for further validation by western blot analysis. It was significantly decreased in all tumour regions in patient 260 with fold change of 5.3, 5.2 and 21.6 in Q1, Q2, Q3, respectively (Figure 3.5). This highlights that Q3 is

different from the other two parts of the tumour as indicated by PCA (Figure 3.4). Western blot showed an opposite profile for patient 260, where it was up-regulated in all regions of the tumour using beta actin as a loading control, and Q3 had the lowest expression of protein compared to the other parts of the tumour specimen. qRT-PCR showed no difference in mRNA levels between Q2 and Q3 (Figure 3.5). Western blot is a more reliable methodology than mass-spectrometry, the latter is more sensitive and can sometimes be affected by the sample complexity. In patient 261, by LC-MS/MS, DSP was found significantly overexpressed in Q1, Q2 and Q3 with fold change of 138, 90 and 50, respectively (Figure 3.5). By western blot, DSP was detected overexpressed, and 261-Q2 was the most abundant region of the tumour. qRT-PCR revealed an increased level of mRNA in Q1 than in Q2, the translation machinery of mRNA into protein is defected here. In patient 298, DSP was not detected by mass spectrometry (i.e: it was not within the cut-off value), while mRNA and protein levels were matched by qRT-PCR and western blot, respectively. T298 Q1 and Q2 had less mRNA and higher protein abundance compared to the matched control normal tissues (Figure 3.5). mRNA was more abundant in tumour tissue regions Q1 and Q3, the later had double Q1 levels (Figure 3.5).

Tenascin c is an adhesion modulatory extracellular matrix molecule found overexpressed in solid tumours and associated with increased proliferation, migration and epithelial-mesenchymal transition (EMT) (Yoshida et al., 2015, Orend and Chiquet-Ehrismann, 2006). Tenascin c has been shown to have a role in resistance to chemotherapy in triple negative breast cancer (Popova et al., 2017). Tenascin c overexpression correlates to increased tumour invasion and angiogenesis and poor prognosis in many cancer types (Lowy and Oskarsson,

2015). In this research work, tenascin c was not detected by mass spectrometry in specimens coded 260 and 298, and was significantly upregulated in specimen coded 261 with fold change of 4.0, 7.8 and 4.6 in Q1, Q2 and Q3, respectively (Figure 3.6). Tenascin c was also detected elevated by 24.5, 7.7 and 7.1 in Q1, Q2 and Q3 in specimen coded 266, respectively (Figure 3.6). Western blot analysis detected increased tenascin c in all patient 260 tumour regions and Q2 had increased expression compared to Q1 and Q3. In patient 261, tenascin c was elevated in Q1 (highest) and Q2 while it was downregulated in Q3. The level of tenascin c mRNA in 260-Q3 and 261-Q2 was the same as in their matched normal tissue and was significantly increased (5-and 6 fold) in Q2 and Q1 in 260 and 261, respectively. Western blot for sample 298 detected elevated tenascin c expression in 298-Q1 and Q3 but not in Q2, and 298-Q3 had the highest elevation (7-fold higher than normal). qRT-PCR revealed a two-fold decrease in the two tumour regions and there was no difference between 298-Q1 and 298-Q2. In patient 266, tenascin c mRNA was elevated in 266-Q1 and was 2- fold more than in 266-Q3 (Figure 3.6).

Enolase alpha (**Enolase-1)** is a multi-subunit isoenzyme found to promote cell glycolysis, growth, migration and invasion in non-small lung cancer via PI3K/AKT pathway (Fu et al., 2015). Enolase-1 also has **a tumour suppressant** effect by binding to c-Myc promoter. Increased levels of enolase-1 was found associated with increased production of autoantibodies, a decline in the basal level of these autoantibodies was used as a prognostic marker in post-operative lung cancer (Hsiao et al., 2015). In this research work, LC-MS/MS has detected elevated enolase-1 in patients 260, 261, 298 and it was undetectable in patient 266 (Figure 3.7). Western blot revealed elevated levels of enolase-1 in patient 260 and the least amounts were detected in Q3. In patient 298, enolase-1 levels were correspondent

to that detected by LC-MS/MS and were heterogeneous across all tumour regions. In patient 266, enolase-1 showed an opposite profile to that in mass spectrometry, Q1 and Q3 were significantly decreased while Q2 had a little decrease (Figure 3.7). Enolase-1 mRNA expression was significantly elevated in patient 260 with no intra-tumour difference, down-regulated in patient 298 with no difference, heterogenous in patient 266 (Q1 double Q3 levels) and 261 (Q1 double Q2 levels).

Overexpression of endoplasmic reticulum oxidoreductase 1 alpha (ERO1-La**)** correlates with a poor prognosis and overall survival in breast cancer (Kutomi et al., 2013). ERO1-La expression is augmented by hypoxia to stimulate angiogenesis and to compensate for the loss of oxygen redox power this is modulated via activation of hypoxia –induced factor 1 (HIF-1) mediated pathway (Krock et al., 2011, Zimna and Kurpisz, 2015). **In patient 260**, the mass spectrometry data showed ERO1-La was significantly overexpressed compared to matched normal tissue with fold change of 10.6, 13.9 and 4.2 in Q1, Q2 and Q3, respectively. ERO1-La was also detected in patient 261 with fold change of 18.8, 17 and 10.2, in Q1, Q2, Q3, respectively (Figure 3.8). ERO1-La was undetectable in 266 and 298 within the cut-off value used in this study. qRT-PCR also showed heterogeneous mRNA expression between two tested regions (30-fold and 4-fold increase in Q2 and Q3, respectively compared to matched normal tissue.

In patient 261, PCA of the mass spectrometry data clustered Q1 away from the other two tumour regions. MS/MS detected Q1 and Q2 with *ERO1-La* protein levels close to each other with 18.8 and 17-fold more than in the normal tissue (Figure 3.8). Western blot and qRT-PCR detected a slight decrease in the levels of *ERO1-La* in Q1, while Q2 had increased *ERO1-La* expression compared to the normal tissue. In patient 266, Q2 was clustered away from the other two tumour regions by

whole proteome PCA analysis (Figure 3.4). No data on *ERO1-La* was obtained as its expression was not within the cut-off value and the protein samples were degraded (No western blot data). *ERO1-La* expression was detected slightly low in Q3 compared to the normal tissue while no change in the mRNA level of *ERO1-La* in Q1 was detected (Figure 3.8). In specimen coded 298, western blot revealed increased *ERO1-La* in all tumour regions and Q1 had the maximal increase while Q2 had the lowest. qRT-PCR showed decreased amounts of ERO1-La mRNA and Q2 had the lowest levels (approximately half the normal value).

Quantifying phosphorylated protein expression to determine ITH

Increased phosphorylated proteins correlate with the activation of a specific pathway and therefore have the potential to identify tumours that may respond to a corresponding targeted treatment (Ardito et al., 2017). Differences in protein phosphorylation within the tumour tissues would indicate heterogeneity and could predict treatment failure to targeted therapy (Lim and Ma, 2019). However, quantification of the phosphorylated form of a protein is not routinely quantified in the clinic as they are easily degraded and have not proven to be robust biomarkers. The aim of this study was to determine whether there is a high degree of intra-tumour heterogeneity associated with phosphorylated protein expression. A PathScan array approach was used that tested 18 different phosphorylated proteins. Several proteins involved in both the *JAK*/*STAT* and *PI3K* signalling pathways were included on the array and we were interested in quantifying their expression within the tumours as these proteins may be used as predictive biomarkers to stratify patients for treatment with a *PI3K-mTOR* inhibitor for example.

***JAK/STAT* signalling pathway** has been demonstrated to play a role in the tumourigenesis of non-small cell lung cancer due to either mutations in JAKs with

gain of function associated with increased expression of *PD-L1* (Li et al., 2017b, Xu et al., 2017), or due to increased oncogenes that activate the JAK/STAT signalling pathway (Leonard and O'Shea, 1998) leading to increased proliferation, metastasis and drug resistance (Yang et al., 2019b). JAKs are tyrosine kinases bound to the cytoplasmic part of many receptor tyrosine kinases, and occur as multimeric subunit forms e.g. cytokine receptor type I and II (Stark and Darnell, 2012), as homodimers e.g. growth hormones and erythropoietin receptors, or exist as heterodimers subunits e.g. interferons and interleukins receptors (Seif et al., 2017). Di/multimerization and activation of *JAKs* occur when *JAK* containing receptors bind to their ligands, *JAKs* then recruit and trans-phosphorylate *STATs* in order to activate and dimerize them so they can associate with other transcription regulators and translocate to the nucleus to bind to their specific DNA sequence to act as transcription activator or suppressor (Levy and Darnell, 2002). Serine phosphorylation of *STATs* might augment their transcription power as in *STAT1* or might counteract this as in *STAT3(Seif et al., 2017)*. *MAPK, JNK* and *ERK* have been well documented to be involved in serine phosphorylation of *STATs* (Seif et al., 2017). Two *JAK/STAT* signalling pathways have been recognized; the canonical pathway, involves phosphorylated JAKs and *STATs* through *PI3* Kinase (*PI3K*), Mitogen-activated kinase (*MAPK*) and intracellular receptor kinase (*ERK*) (Li, 2008), and the non-canonical pathway which involve the unphosphorylated *STATS* where they translocate to the nucleolus, binds to heterochromatin protein-1 (*HP1*), and play role in heterochromatin stability (Li, 2008). In this chapter, a panel of 18 phosphorylated proteins including those involved in *PI3K-AKT/PKB* and *JAK/STAT* signalling pathways were assessed in three tumour regions and matched

normal tissues of four LSqCC patients using a Pathscan® Array (Cell Signalling) (Figure 3.9).

HSP27 is an **oncogenic** heat shock protein, that is overexpressed in NSCLC and its phosphorylation is required for cell death inhibition (Benn et al., 2002). phosphorylated *HSP27* was heterogeneous among patient 260 and the least amount was detected in Q3 (26% more than normal tissue). Q2 and Q1 had 84% and 130% (doubled) more expression than normal tissue, respectively. ***MAPK*** is the major leading signalling pathway that phosphorylates HSP27 (Robitaille et al., 2010), and its expression was 2.5-times more than normal tissue in Q1 and Q2, and there was a 20% increase in Q3 (Figure 3.10). In patient 261, all regions had approximately the same amounts of phosphorylated HSP27 despite the big variation in *MAPK* phosphorylation (Figure 3.11). In patient 266, Q3 had the lowest amount of P-HSP27 compared to the other two regions of the tumour which were approximately double than in the normal tissue. *MAPK* phosphorylation was higher than the normal tissue and variable among tumour regions (Figure 3.12). In patient 298, phosphorylated *HSP27* was increased in all tumour regions, T6 had the highest increase (more than 2-fold increase than normal tissues), and *MAPK* phosphorylation was matching the phosphorylation level in HSP27 (Figure 3.13). Patient 260-Q3 and 266-Q3 are the least aggressive tumour parts as they had very low levels of phosphorylated HSP27 (the active oncogenic form).

P53 is phosphorylated and stabilized mainly by *AMPK* (Maclaine and Hupp, 2009), leading to overexpression of the *MDM2* gene which when phosphorylated complexes with P53 and leads to its ubiquitination, degradation and cell survival (Karni-Schmidt et al., 2016). Overexpression of mutated P53 with reduced tumour suppressant function is associated with many forms of drug resistance including

doxorubicin and cetuximab (*EGFR*-inhibitor) (Hientz et al., 2017). In this research work, *P53* was 2-fold more phosphorylated **in patient 260**-Q1 while it was 10% less than the normal tissue in Q3. This might indicate increased ubiquitination degradation of *P53* in Q3 than in other regions. *AMPK* phosphorylation was lowest in Q3 although was double that of normal tissue (Figure 3.10). **In patient 261**, *P53* was phosphorylated in all regions. Q3 had a 2-fold higher expression in Q1 with the latter lower than region Q2. *AMPK* phosphorylation levels in 261-Q1 was similar to the normal tissue (only 2% increase) (Figure 3.11). **In patient 266**, P53 phosphorylation was high in Q1, while Q2 and Q3 had lower expression. *AMPK* phosphorylation was 2-fold higher in Q1 than the other two tumour regions of patient 266 (Figure 3.12). **In patient 298**, the amount of phosphorylated *P53* was very high in Q2 (2-fold more than in normal tissue) and was increased by 36% and 70% in Q1 and Q3, respectively compared to normal tissue. *AMPK* phosphorylation was only 7% increase in Q1 compared to 100% increase (double) in Q2 and Q3 (Figure 3.13). Patient 260-Q3 has the lowest expression of phosphorylated proteins compared to the two other tumour regions.

Bcl-2 agonist of cell death (*BAD*) is a tumour suppressor gene (*TSG*) and can be antagonised when phosphorylated by *EGFR*, *MAPK*, *PI3K*, *JNK1/2, JAK/STAT* and others (Sunayama et al., 2005). *BAD*, when phosphorylated, interacts with *BCL-XL* and prevents the release of cytochrome c required for the induction of apoptosis (Downward, 1999, Hirai and Wang, 2001), therefore, interfering with BAD phosphorylation by dual inhibition of *EGFR*, *PI3K/AKT* is a therapeutic option for the treatment of cancer (She et al., 2005). In patient 260, phosphorylated *BAD* was 10% less in Q3 than the normal tissue and was doubled (1.1-fold) and 60% more in Q1 and Q2, so the tumour suppressant effect of *BAD* in these regions

is antagonized while maybe still active in Q3 (Figure 3.10). In patient 261, all tumour regions had a higher amount of phosphorylated *BAD* than in normal tissue, thus its tumour suppressant activity is silenced (Figure 3.11). In patient 266, only Q1 had approximately 70% more phosphorylated *BAD* than the normal tissue while the other two regions the *BAD* function is still active (Figure 3.12). In patient 298, all tumour regions had high expression of phosphorylated *BAD* where it could be working to interfere with apoptosis instead of *TSG* (Figure 3.13). The phosphorylated (active) form of tyrosine kinases, *AKT*, *MAPK*, *ERK1/2* were all heterogeneous across different tumour regions (Figures: 3.10-13). The overall assessment of *BAD* phosphorylation in the patients studied demonstrated that 260-Q3, 266-Q2 & Q3 may be less invasive and less aggressive.

Caspase-3 is a tumour suppressant cysteine protease that is downregulated in many solid tumours including lung cancer (Yoo et al., 2004). In NSCLC, increased caspase3 expression correlated with an increased survival, low lymph node metastasis and overall a good prognosis (Fennell, 2005). Phosphorylation of caspase-3 by *P38-MAPK* reduces its cleavage activity leading to cell survival (antagonises its tumour suppressant effect). In patient 260, the abundance of phosphorylated caspase-3 was 2-fold decreased in Q3 than the normal tissue while was increased 3-fold and double more in the other two regions, respectively (Figure 3.10). In patient 261, Q1 phosphorylated caspase-3 was less than in normal tissue by double, but was more abundant in the other two tumour regions (Figure 3.11). In patient 266, all tumour regions had more phosphorylated caspase-3 than the normal tissue and the least amount was detected in Q2 (Figure 3.12). In patient 298, the phosphorylation of caspase-3 was 23% less in Q3 than in the normal tissue, and was 23% and 155% more abundant in Q1 & Q2, respectively (Figure 3.13). The

overall assessment of caspase-3 phosphorylation in the studied patients revealed 260-Q3, 261-Q1 and 298-Q3 regions to be less invasive as well.

STAT1* and *3 can be phosphorylated mainly by JAK kinases, the phosphorylated levels of STATs reflects not only *JAK/STAT* pathway but also other tyrosine kinases mediated pathways such as *PI3K* and *MAPK* (Seif et al., 2017, Harrison, 2012). Intracellular signalling assessment of *JAK/STAT* pathway was done by quantifying STATs phosphorylation. In patient 260, *p-STAT1* levels were increased and heterogeneous among the tumour regions while Q3 had the lowest expression (Figure 3.10). *STAT1* was also increased in patient 298 in Q2 and Q3 (Figure 3.13). Phosphorylated *STAT1* expression was lower than the normal tissue in patients 261 and 266 in all tested tumour regions (Figures 3.11, 3.12). *pSTAT3* was only elevated in patient 260 and was lower than normal in the other three patients. Only patient 260 and 298 had an activated *JAK*/*STAT* pathway.

PIM1, 2 and 3 mRNA expression was also quantified by qRT-PCR. Results revealed a significant increase in *PIM2* mRNA levels in patient 260 in both tumour regions examined (Q1 and Q3), Q3 had double the amount of *PIM2* levels than Q1 and this might confirm an upstream genetic makeup heterogeneity, while *PIM1* and *3* were both downregulated in Q1 and Q3 (Figure 3.10). In patient 261, there was 2-fold more *PIM1* expression in Q1 than in Q2. *PIM*2 had no significant change compared to the normal tissue. *PIM3* mRNA was elevated in Q1 and lowered in Q2 compared to matched normal tissue. *PIM1* and *3* might demonstrate upstream genetic makeup differences in this patient (Figure 3.11). In patient 266, all three *PIM* kinases were upregulated in Q1 compared to the normal tissue and Q3, confirming the existence of heterogeneity within the tumour mass of this patient (Figure 3.12). In patient 298, all *PIM* kinases were also significantly elevated in

Q1 and were significantly downregulated in Q2 (except *PIM*2 in Q2). Again, heterogeneity existed in patient 298 (Figure 3.13).

Although vast resources have been spent in developing new therapies for cancer, many of the drugs have failed due to the emergence of drug resistance. Recent research has found that the majority of treatment failure is due to tumour heterogeneity (Fisher et al., 2013, Burrell and Swanton, 2014, Lim and Ma, 2019). This study quantified both proteomic and phospho-proteomic expression to determine the extent of intra-tumour heterogeneity that exists within lung squamous cell carcinomas. This tumour histology has less driver mutations and therefore less treatment options than adenocarcinomas. Although ITH was present across all of the tumours studied we showed that the majority of total proteins were expressed in all tumour regions albeit differentially expressed.

These data highlight the need for large multi-centre test and validation studies, across different tumour histology, to first identify and then validate robust prognostic and predictive biomarkers that can be used in the clinic to guide patient treatment. Further studies to validate representative cut-off values for immune-histochemistry tests are also crucial for implementing biomarkers into practice. On the other hand our data highlighted that the expression of phosphorylated proteins across tumour regions is more spurious. In some cases expression of known cancer pathway proteins was lower in the tumour tissue than in the matched normal tissue and this may in part be due to the instability of phosphorylated proteins rather than true differences in expression. To be effective in the clinical setting the quantification of phosphorylated protein can be best utilised where there is an option to have multiple tumour biopsies and where there is a system of preserving the tissue in an appropriate stabilising buffer immediately after collection. In

summary, well-validated robust biomarkers proven to be associated with a specific activated pathway and displaying very little intra-tumour heterogeneity are crucial to guide clinicians in the stratification of patients for targeted therapy.

4. **Chapter IV**: Intratumour heterogeneity (ITH) in lung adenocarcinomas defined by multi-region whole exome sequencing (WES) & microarray RNA analysis.

4.1. Introduction

Lung adenocarcinoma represents more than 50% of all lung carcinomas (Kim et al., 2006). Adenocarcinoma is the most common form of lung cancer in women, Asians, and people under the age of 45. It is more likely to occur in non-smokers (either never smokers or former smokers) than people who currently smoke. The main activated/mutated driver oncogenes in lung adenocarcinoma are *EGFR, KRAS, HER2, MYC, MET, EML4-ALK and BCL2* (Revannasiddaiah et al., 2014). *EGFR* and *ALK* tyrosine kinase inhibitors (TKIs) can be used as first line or second line treatment. The eligibility of the patient to be treated with and EGFR TKI as a first line treatment is the presence of sensitising mutations in the EGFR tyrosine kinase domain such as; exon 19 deletions or exon 21 L858R point mutation which are associated with increased kinase activity (gain of function) (Roeper and Griesinger, 2019, Greulich et al., 2005, Pao et al., 2005). Anaplastic lymphoma kinase (*ALK*) gene amplification (copy number), activation (point mutations) and chromosomal rearrangement has been documented in many patients with lung adenocarcinoma (Yano et al., 2003). The development of oral tyrosine kinases inhibitors such as gefitinib and erlotinib which interrupt *EGFR* signalling, and crizotinib, ceritinib and alectinib for treatment of positive *ALK* NSCLC are now FDA approved for the treatment of lung adenocarcinoma (Holla et al., 2017). Lung adenocarcinoma has been documented to have a great range of pathological and molecular heterogeneity (Stegmeier et al., 2010). Resistance to *EGFR* TKIs can be intrinsic (patient does not respond to treatment at start) due to *KRAS* activation and *PTEN* down-regulation, or can be acquired (patient becomes non-responding to *EGFR*-TKIs after sometime, i.e: initially responding). The most common acquired resistance to *EGFR*-TKI is T790M substitution mutation (methionine encoded

instead of threonine) in exon 20, this substitution changes the binding site of the TKI (loss of specificity) and increases ATP affinity leading to acquired resistance (Yun et al., 2008). *HGF*-receptor (*MET*) amplification is reported to be responsible for 20% of *EGFR*-TKI acquired resistance (Cappuzzo et al., 2009). When disease progression occurs while patients are on treatment with a TKI a second biopsy is required for the assessment of the causative mutation/amplification that is driving the acquired resistance (Arcila et al., 2011). *EGFR* mutations result in *PI3K* pathway activation which can be suppressed by using *EGFR* TKIs. Acquired resistance to *EGFR* TKIs can occur via the acquisition of a *PIK3CA* mutation. Therefore, targeting the *PI3K* pathway in *EGFR*- mutated lung cancer with acquired resistance to *EGFR* TKIs is a promising strategy (La Monica et al., 2009). This chapter aims to profile DNA mutations using whole genome sequencing (WES) and mRNA expression using microarray technology, within different regions of the same tumour compared to matched normal tissue in a cohort of patients with lung adenocarcinoma. These data will highlight the overall intra-tumour heterogeneity within the tumour specimens (mutation prevalence and gene expression). We will also examine *PIM* kinase expression in two regions per tumour in the three patients with lung adenocarcinoma studied in this chapter.

4.2 Experimental design

Three patients with lung adenocarcinoma (N=3) were included in this study. Patients were consented as part of the Thoracic Oncology Research biobank at St. James's Hospital. After the tumour was surgically resected along with surrounding normal lung tissue, the consultant pathologist isolated two pieces of tumour tissue from different regions of the same tumour and the tissues were immediately stabilized in All protect® Qiagen (Cat. #: 76405) overnight at 4°C. The buffer was

then removed, and the samples were bio banked at -80°C until use. RNA and DNA were extracted as previously detailed in chapter two (under section 3.3.1.2.1 and 3.3.1.2.2.). Total RNA samples for each patient were sent to ArrayStar™ Incorporation for mRNA expression analysis, and the DNA samples were sent to LC Sciences for whole exome sequencing (WES). The aims of this chapter are: i- to quantify changes in mRNA expression and the prevalence of mutations between tumour tissue and matched normal tissue, ii- to determine any molecular heterogeneity (RNA and DNA) between two different parts of the same tumour mass, iii- to correlate mutation profiles of the tumour tissue with mRNA expression and iv to compare *PIM* kinase and *DSP*, *TNC*, *ERO1-LA* and *ENO1* expression within two different regions of the tumour per patient.

4.3. Materials and Methods

4.3.1. Tumour tissue collection

Fresh lung adenocarcinoma tissue along with some surrounding normal tissues from a written consented, newly diagnosed and treatment naïve patients (Table 4.1) were harvested and handled as described earlier under section 3.3.1.1 (previous chapter). No specific criteria were put to choose the candidate tumour specimens as the main question of this research project was to confirm and stress the existence of heterogeneity within lung adenocarcinoma tissues. Haematoxylin and eosin staining were performed by the consultant pathologist to ensure the percentage of malignant cells within the resected tumour mass is >50%.

4.3.2. Nucleic acid isolation

All Prep-DNA/RNA/miRNA universal kit, Qiagen (Cat. #80224) was used to extract RNA and DNA from the tissue samples obtained from lung adenocarcinoma patients. The protocol procedure was detailed under materials and methods section

3.3.1.2 (previous chapter). The eluted RNA samples were measured by Nanodrop ND-1000. RNA qualitative and quantitative results are tabulated in appendix *4.1*.

4.3.3. Whole exome sequencing (WES)

Whole exome sequencing (WES) was conducted by LC Sciences. The procedure was carried out in three steps as follows: i- DNA fragmentation and library construction followed by hybridization (90 min) and capture/wash/amplification, ii- Illumina sequencing and iii- data extraction and analysis.

The extracted patients' DNA samples were sent to LC Sciences for whole exome sequencing. The DNA was subjected to a sonication fragmentation step, then the Library was constructed using pre-designed probes (Capture library) SureSelect® Human All Exon V6 kit (Cat.no. 5190-88863-Agilent technology). The kit covers 99% of RefSeq, *CCDS, GENCODe, HGMD*_cds and OMIM_cds databases. The sequencing was then performed using Illumina Hiseq X Ten 150-bp paired-end sequencing method.

Table 4.1. Samples coding and experimental design for whole exome sequencing.

Sample Name	Gender	Sample Type	Analysis_name
Patient _1_N		**Normal**	**Patient_1_ADC_T1_N**
Patient _1_T1	Female	Tumour	Patient_1_ADC_T1_T
Patient _1_T2		Tumour	Patient_1_ADC_T2_T
Patient _2_N		**Normal**	**Patient_2_ADC_T1_N**
Patient _2_T1	Female	Tumour	Patient_2_ADC_T1_T
Patient _2_T2		Tumour	Patient_2_ADC_T2_T
Patient_3_N		**Normal**	**Patient_3_ADC_T1_N**
Patient_3_T1	Male	Tumour	Patient_3_ADC_T1_T
Patient_3_T2		Tumour	Patient_3_ADC_T2_T

T: tumour, ADC: adenocarcinoma, N: Normal tissue.

4.3.4. Bioinformatics

The millions of paired-end generated reads of 150bp in FASTQ files were aligned to a reference genome utilizing Burrows-Wheeler Alignment (BWA) software. A post-alignment processing step, utilizing Picard tools, was undertaken to identify and mark duplicate reads from BAM files. Variant calling was generated by GATK Haplotype Caller, which examines the evidence for variation from reference via Bayesian inference. At the end, Ensembl Variant Effect Predictor (VEP) was utilized to add biological information to a set of variants.

4.3.5. Arraystar® Human Lnc-RNA Microarray V4.0

This experiment was designed to compare the expression of non-coding LncRNA and coding mRNA in two regions per tumour compared to matched normal lung tissue. The principle and procedure of the ArrayStar® microarray is detailed under 2.3.4.

4.3.6. q-RT PCR quantification of *PIM* kinase expression and *DSP*, *TNC*, *ERO1A* and *ENO1* in lung adenocarcinoma

PIM1/2/3 kinase (chapter 2) and *DSP*, *TNC*, *ERO1-La* and *ENO1*, the four candidate proteins that displayed intratumour heterogeneity (chapter 3), were also quantified in these lung adenocarcinoma samples. Expression in two different tumour regions was compared to matched normal lung tissue, and the results were represented as column graphs with +/-STD using GraphPad Prism software version 7.

4.3.6.1. Primer design

Forward and reverse primer sets for *DSP*, *TNC*, *ERO1A* and *ENO1* were designed in Primer3Plus software available online at http://www.bioinformatics.nl/cgi-bin/primer3plus/primer3plus.cgi using NCBI accession numbers IDs:

(>NM_004415.4), (>NM_014584.3), (>NM_001428.5), (>NM_002160.4), respectively. The position of the primers per gene and the flanked exons junctions were detailed under section 3.3.1.10.1-4. *PIM1/2/3* kinase primers are detailed under section 2.3.5.1.

4.3.6.2. q-PCR protocol

This experiment was performed to evaluate *DSP*, *TNC*, *ERO1A* and *ENO1* mRNA expression in a panel of lung cancer cell lines. The full protocol for the RNA isolation, synthesis of the first strand cDNA and q-PCR is detailed under section 3.3.1.10.5-7.

4.3.6.3. qRT-PCR protocol

qRT-PCR protocol for quantitative comparison of *DSP*, *TNC*, *ERO1A* and *ENO1* and *PIM1/2/3* kinase expression between matched normal lung tissue and two regions per tumour was carried out as described under section 3.3.1.10.7.

4.4. Results

4.4.1. Mutational analysis (Whole Exome Sequencing Study)

Three types of mutations were detected; insertions, deletions and point mutations, summarized in figure 4.1.

4.4.1.1. Insertion mutations

In patient 1, three genes; *SLC22A10*, *ERCC5* and *COL16A1*, in the matched normal tissue (N) had one nucleotide insertions in one of their exons. The deleterious one was located in the open reading frame of the excision repair cross-complementation group 5 endonuclease (*ERCC5*) gene at exon 13 leading to frame-shift and loss of amino acid sequence after this mutation. The other two genes; *SLC22A10* and *COL16A1* had insertions located in the untranslated regions (UTR) with no impact. The first tumour region (T1) had one insertion in the *COL16A1* gene at exon 71 with no impact as it was located in the 3'UTR. This mutation was also detected in the normal tissues . The second tumour region (T2) had one insertion in *SLC22A10* in exon 3 with no impact. The other insertion in this patient were located in genes introns with no impact on the encoded protein. The largest insertion (23nts) was detected in the low density lipoprotein receptor (*LRP1B*) gene with no impact on the encoded protein (*appendix* 4.2).

In patient 2, two genes with exonic insertions were detected in the matched normal tissue (N); single nucleotide insertion in *KIAA1731* gene with frame-shift, three nucleotide in-frame insertion in *ERBB2* gene with moderate effect on the gene amino acid sequence. In the (T1), 4 genes were detected with exonic insertions, two were shared with the normal tissue (*KIAA1731* and *ERBB2*), and the other two (*GNY* and *ZNF500*) had insertions in their 3-UTR sequence, thus no impact on the encoded gene resulted. In (T2) of this patient, the *NOTCH1* gene was detected with

an insertion at the 5-UTR sequence of exon 1. Other mutations in this patient were detected in some gene introns which have no impact on the encoded genes (*appendix* 4.3).

In patient 3, 16 genes were detected with insertions; 10 in the matched normal tissue (9 with high impact, 1 moderate impact), 11 in T1 (10 with high impact and 1 modifier) and three unique in T2. The normal tissue shared 9 genes with high impact insertion mutations with while the others are unique. Intronic insertions were neglected as they have no impact on the encoded protein structure. The longest insertion was detected in the cytochrome *P450* family A7 (*CPA7*) gene (38 nts) which was shared between the normal tissue and the first analysed tumour region (*appendix* 4.4).

4.4.1.2. Deletion mutations

In patient 1, the normal tissue only had three mutated genes with frame-shift (*SULT6B1, PTPRZ1* and *RLTPR* with high impact) deletions. T1 had two genes with deletions, *CHAF1A* which had three in-frame nucleotides deletion with high impact on the gene structure, and *ELAVL3* had an 8 nucleotide deletion in the 3-prime UTR sequence with no impact. T2 had 5 genes (*LRP4, FOXF1, ZFHX3, ELAVL3* and *CHAF1A*) with deletions in their exons, the last two detected are shared with T1 as well. 13, 6 and 10 genes were detected with intronic deletions with no impact on the encoded proteins in N, T1or T2, respectively (*appendix* 4.5).

In patient 2, twelve genes in the matched normal tissue had exonic deletions (eight with high impact). *IFR2BPL* gene had a 79 nucleotide deletion in the first exon, *MED13* had a 21nucleotide deletion in exon 20 and *CD55* had a 14 nucleotide deletion, all lead to a frame-shift consequence with high impact on the encoded protein. T1 had 10 genes with exonic deletions, six lead to frame-shift with high

impact, 3 genes with in-frame-deletions and 1 with a deletion in the 5-prime UTR. Eight deletions were detected shared between N and T1, six of them were with high impact and resulted in a frame shift effect. T2 had two genes with exonic deletions. Six genes were detected in N with intronic deletions, while 16 and 15 genes (7 out of them shared between region 1 and 2 of the tumour) were detected in T1 and T2 (*appendix* 4.6). **In patient 3,** 30 genes in N (26 with high impact, 3 moderate impact, 1 modifier) had exonic deletions (3 unique, 27 shared with region 1, none was shared with region 2). *ARMC5*, *SCL30A2, WWC3* and *RTL1* genes were detected uniquely mutated in N with 38, 21, 18 and 17 nucleotides deletions in their exons number 1, 8, 19, 1, respectively. T1 had 33 genes (30 with high impact, 3 moderate) with exonic deletions (4 unique, 2 shared with tumour region 2, and 27 were detected shared with the normal tissue). T2 had 5 genes (1 with high impact and 1 moderate) with exonic deletions (two unique and three shared with T1). However, the genes with intronic deletions in this patient were 11, 33 and 28 in N, T1 or T2, respectively (*appendix* 4.7).

4.4.1.3. Point mutations

In patient 1, 24 genes had exonic point mutations (single nucleotide substitution): {1 with high impact "stop codon gained", 9 with low impact "synonymous variants", 12 moderate "missense variants" and 2 exon modifier mutation "3'-UTR variant"}. T1 had 33 genes with exonic point mutations {3 with high impact ("1 stop lost", "1 stop gained", 1 "start lost"), 12 with low impact "synonymous variants", 15 moderate "missense variants" and 3 modifiers "1 3'UTR and 1 5'UTR variants"}. T2 had 32 genes with exonic point mutations {2 with high impact ("1 stop lost and 1 stop gained", 12 low "synonymous variant", 13 moderate "missense variant" and 5 modifiers "three 3'-UTR and two 5'-UTR variants"} (appendix 4.8).

POTEC, KMT2C and *FAM153C* point mutations were shared between N and T1. *GOLGA6B1* is the only point mutation shared between N and T2. 16 exonic point mutations were shared between T1 and T2. 8 and 9 exonic point mutations were unique to T1 and T2, respectively. T1 and T2 also share 13 intronic point mutations and each had three unique intronic point mutations. The total intronic point mutations in N, T1 and T2 were 17, 20 and 16, respectively (*appendix* 4.8).

In patient 2, N had 188 point mutations in the protein coding genes; 118 in the exon regions {5 with high impact "stop codon gained", 31 low impact "1 splice region variant" and 30 "synonymous variants", 9 "modifiers" 4 "3'UTR and 5 5'UTR variants" and 73 moderate "missense variants"}, and 70 were intronic {1 high "splice acceptor variant", 4 low "splice region variant", 65 modifiers "intron variants"}. T1 had 167 genes with point mutations (appendix 4.9); 118 were exonic {5 high "4 stop gained", 1 "stop lost", 10 modifiers 5 "3'UTR and 5 5'UTR variants", 25 low 2 "splice region variant" and 23 "synonymous variants", and 78 moderate "missense variants"}, and 47 were intronic {1 high "splice acceptor variant", 3 low "splice region variant" and 43 modifiers "intron variants"}. T2 had 65 SNPs in the protein coding genes; 50 were exonic {1 high "stop gained", 6 low 1 "splice region variant" and 5 "synonymous variants", 3 modifiers "3'UTR variants" and 40 moderate "missense variants"}, and 15 were intronic {1 low "splice region variant" and 14 modifiers "intron variants"}. One gene exon and one intron point mutation were shared between N and T2, while no mutations were found shared between T1 and T2 or between N and T1 (*appendix* 4.9).

In patient 3, 1346 genes had point mutations in N, 866 were detected in the protein coding genes exons {53 with high impact (51 "stop codon gained" and 1 "stop codon lost", 598 with moderate impact "missense variants", 172 with low impact

“4 splice region variants” and 168 “synonymous variants”) and 48 modifiers (26 “3-prime-UTR variants” and 22 “5-prime UTR variants”)}, and 454 SNPs were in the protein coding introns {11 with high impact (6 “splice acceptor variants” and 5 “splice donor variants”), 416 modifiers (all are “intron variants” and 27 with low impact “splice region variants”)}. T1 had 1464 genes with SNPs; {939 of which were in exons (54 with high impact “2 stop lost and 52 stop gained”, 643 with moderate impact SNPs “missense variants”, 53 were modifiers 22 “5-prime UTR” and 31 “3-prime UTR variants”, and 189 with low impact effect “synonymous variants”)}, and 525 SNPs were located in the gene coding introns {13 with high impact (5 “splice donor variants” and 8 “splice acceptor variants”), 482 modifiers “intron variants” and 30 with low impact “splice region variants”)}. T2 had 75 genes with SNPs; 43 in the exons {1 with high impact “stop codon gained”, 13 low impact SNPs 1 “splice region variant” and 12 “synonymous variants”, 26 with moderate impact “missense variants” and 3 modifiers 2 with “3-‘UTR variant” and 1 with “5-‘UTR variant”)}, and 32 intronic located SNPs {3 with low impact “splice region variants” and 29 modifiers “intron variants”} (*appendix* 4.10).

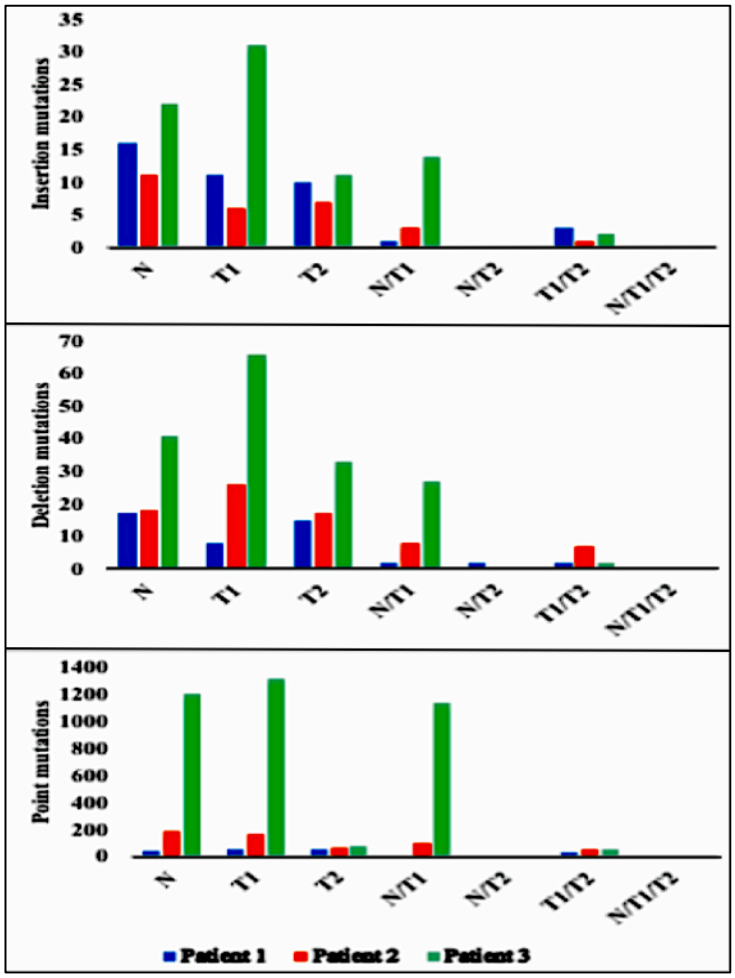

Figure 4.1. Whole exome sequencing mutation analysis. Whole exome sequencing of 3 lung adenocarcinoma patients, N: normal tissue, T1: tumour region 1, T2: tumour region 2, (/): denote shared mutations between the indicated tissue regions.

4.4.2. ArrayStar® microarray mRNA study.

The Venn diagrams show shared, opposing and uniquely expressed mRNAs in two tumour regions per patient (T1, T2) compared to the matched normal tissue in three patients with lung adenocarcinoma (Figure 4.2A, B and C, respectively). **The pattern for patient 1** was; 2167 mRNAs transcripts were upregulated in the T1 region compared to matched normal lung tissue (fold change >2) (Figure 4.2-A). Among these mRNAs, 1613 were uniquely upregulated in T1 (*appendix* 4.11). There were also 2523 mRNAs downregulated, 1311 of them were uniquely down regulated in this part of the tumour (*appendix* 4.12).

In the T2 region , 1938 mRNAs were upregulated compared to matched normal tissue (fold change >2); 1236 were uniquely upregulated (*appendix* 4.13). Also, there were 1622 mRNAs downregulated in T2, with 558 unique for this region (*appendix* 4.14). Patient 1, had 483 mRNAs shared upregulated in both T1 and T2 tumour regions (*appendix* 4.15), and 993 mRNAs shared downregulated in both T1 and T2 (*appendix* 4.16). 71 mRNAs were upregulated in T1 but downregulated in T2 (fold change >2) (*appendix* 4.17). Also, 219 mRNAs were upregulated in T2 and downregulated in T1 (fold change >2) (*appendix* 4.18).

The pattern for patient 2 was; 914 mRNAs were upregulated and 1407 mRNAs were downregulated with 298 mRNAs uniquely upregulated (*appendix* 4.19) and 191 mRNAs uniquely downregulated (*appendix* 4.20) in the T1 region. The T2 region had 1531 upregulated mRNAs and 2593 downregulated mRNAs with 919 uniquely upregulated (*appendix* 4.21) and 1373 uniquely downregulated (*appendix* 4.22). 606 upregulated mRNAs (*appendix* 4.23) and 1210 down regulated mRNAs (*appendix* 4.24) were shared between T1 and T2 regions. 10 mRNAs (*appendix* 4.25) were up-regulated in T1 and down-regulated in T2 and 6 mRNAs (*appendix* 4.26) were up-regulated in T2 and down-regulated in T1. **The pattern for patient 3** was; 2106 and 2079 mRNAs were upregulated and downregulated, respectively in T1 compared to matched normal tissue (fold change >2). Among these mRNAs 824 were uniquely upregulated (*appendix* 4.27) and 225 were uniquely down-regulated (*appendix* 4.28) in T1 region. In T2, 1580 and 2682 mRNAs were upregulated and downregulated, respectively. Among these mRNAs 317 were uniquely upregulated (*appendix* 4.29) and 809 were uniquely downregulated (*appendix* 4.30). 1854 mRNAs were downregulated (*appendix* 4.31) and 1263

mRNAs were upregulated in both T1 and T2 regions (*appendix* 4.32). 19 mRNAs were upregulated in T1 but downregulated in T2 (*appendix* 4.33).

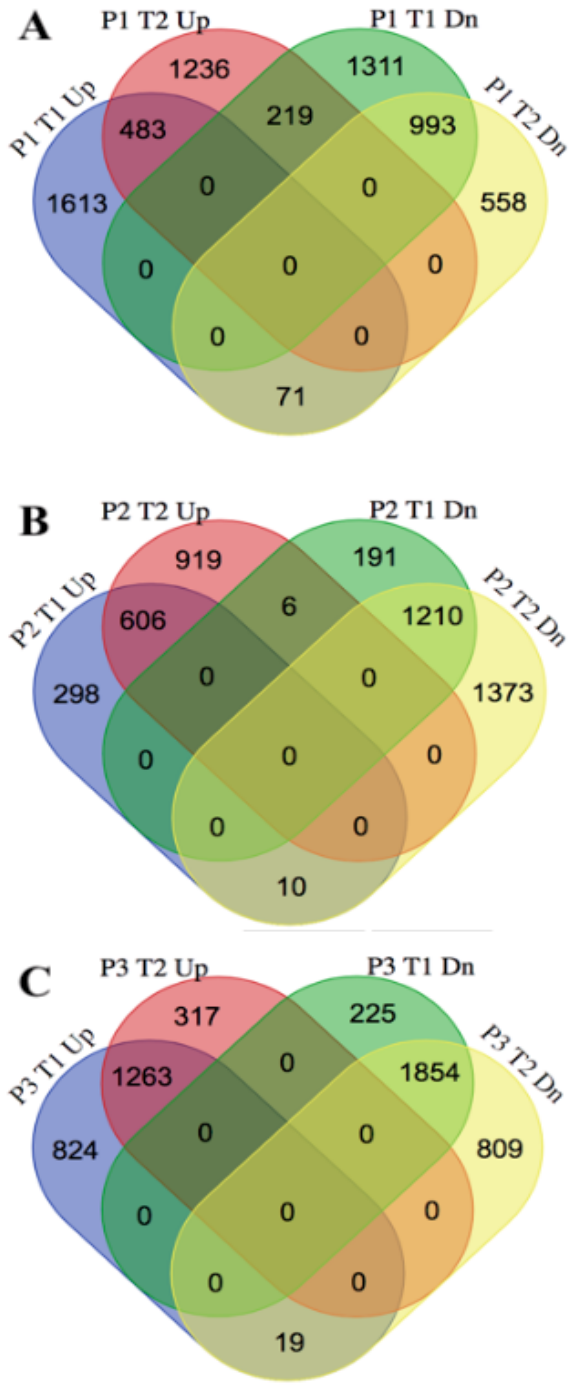

Figure 4.2. Venn diagrams of up and down-regulated mRNAs in two regions per patient in three patients diagnosed with lung adenocarcinoma. P1/P2/P3: three patients coded 1,2,3. T1/T2 are two selected regions of the tumour analysed compared to normal lung tissues harvested from the same patient. Up: upregulated in the malignant tissue compared to the normal tissues, Dn: downregulated in the tumour tissues compared to the normal lung tissue. Intersections showed the shared genes with same or opposite expression profiles.

4.4.2.1. Quantification of *DSP* gene and desmoplakin protein expression.

DSP mRNA expression was quantified by qRT-PCR in RNA isolated from the three patients analysed by WES and microarray technologies above. *DSP* expression within the two tumour regions (T1 -blue and T2 -red) was compared to matched normal tissue (N) (Figure 4.3-A) (n=2). No protein samples were available from the above patients, therefore, desmoplakin was assessed in another set of three patients with lung adenocarcinoma (Figure 4.3-B). The comparison was done in two regions (T1 -red and T2 -blue) from the same tumour mass per patient compared to the normal tissue (green). To minimize technical pipetting and loading errors, results were normalized for their alpha/beta tubulin (in western blot) and S18 gene expression (in qRT-PCR) as internal loading control and expressed as relative expression.

In patient 1, qRT-PCR showed that the level of *DSP* mRNA was elevated in T1 and T2 compared to the control normal tissue but no heterogeneous expression was observed between T1 and T2 (Figure 4.3-A). *DSP* protein expression was decreased 10.7-fold and increased 1.9-fold in T1 and T2, respectively by microarray analysis (Figure 4.3-B). **In patient 2**, *DSP* mRNA expression by qRT-PCR, was significantly elevated in T1 and T2 (with no heterogeneity) compared to the normal tissue (Figure 4.3-A). *DSP* protein level was 1.1 and 3.3-fold elevated in T1 and T2, respectively compared to the matched normal tissue (Figure 4.3-B). **In patient 3,** *DSP* expression was increased 3.3 and 3.8-fold in T1 and T2 compared to the normal tissue by the microarray analysis, while qRT-PCR detected no mRNA levels differences between T1 and T2 (Figure 4.3-A). Western blot showed elevated desmoplakin in two patients (P1, P3) (Figure 4.3-B) with heterogeneous pattern (T2 -red) in the two patients had half the amount of desmoplakin in T1 -blue. In patient

2, desmoplakin was unchanged in T2 -red compared to the normal tissues, while it was downregulated in T1 -blue. The expression was heterogeneous in this patient's tumour regions as well.

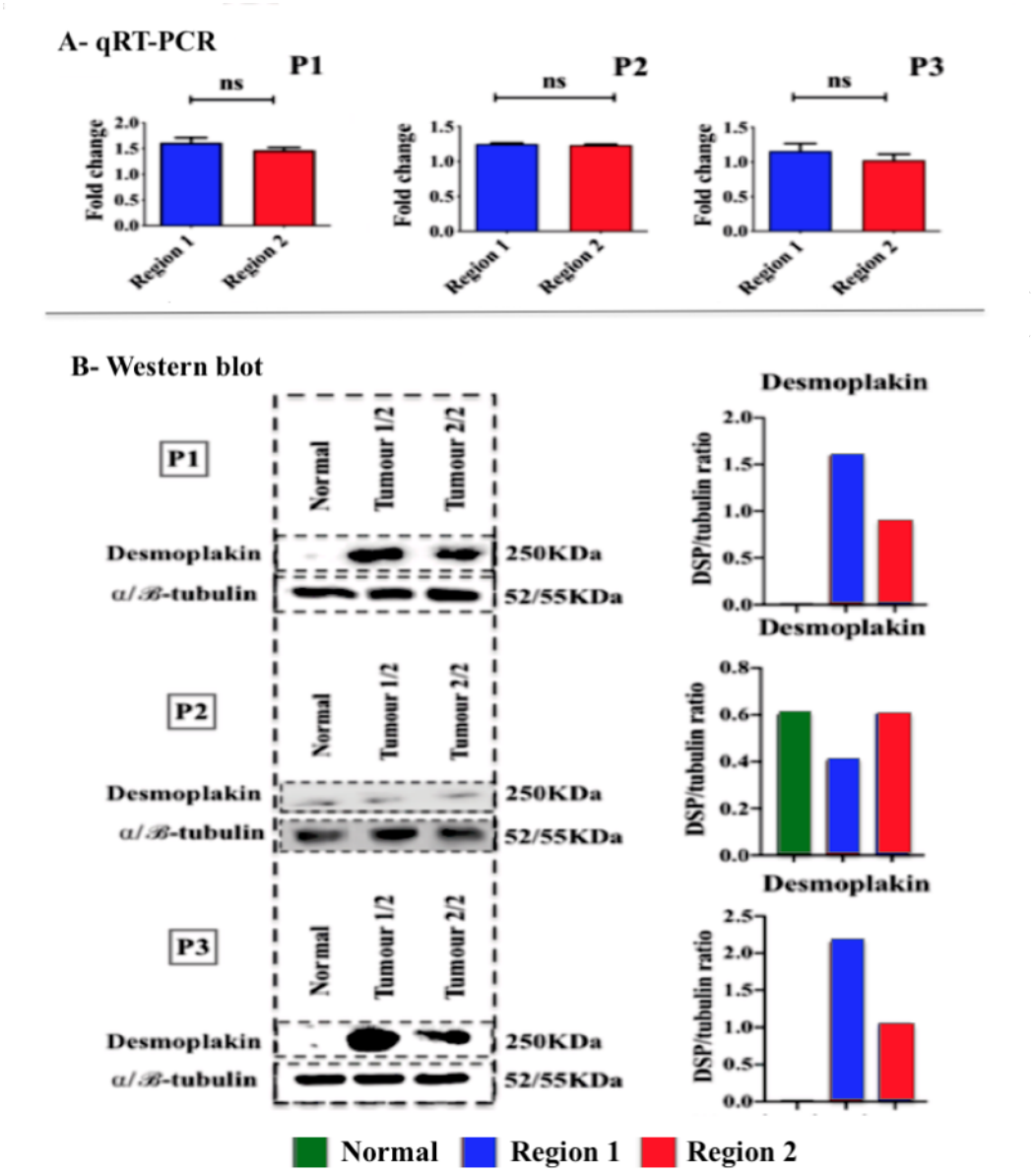

Figure 4.3. Comparative analysis of desmoplakin in the malignant tissue compared to their matched control normal tissues in three patients with lung adenocarcinoma (P1, P2, P3). A. by qRT-PCR, **B**. by western blot in three patient in the patients analyzed by arrayStar® and WES. Green denotes desmoplakin protein relative expression levels in the control normal tissues per patient, red and blue denote desmoplakin protein/mRNA relative expression levels in two different regions per tumour per patient.

4.4.2.2. Quantification of *TNC* gene expression.

TNC antibodies fail to detect *TNC-c* in all the tested samples. *TNC-c* mRNA expression was upregulated 9.2 and 1.3-fold in T1 and T2 of patient 1, down-regulated 1.3 and 1.1-fold in T1 and T2, respectively in patient 2, and upregulated 3.6 and 2.3-fold in patient 3, by microarray analysis. *TNC* expression was validated further by qRT-PCR in the three lung adenocarcinoma patients (P1, P2 and P3). Expression in the two tumour regions (T1 -blue) and T2 -red) from the same tumour mass per patient were compared to the matched normal tissue (N). To minimize technical pipetting and loading errors, results were normalized for their S18 gene expression (in qRT-PCR) as internal loading control and expressed as fold change. In patient 1, 2 and 3, *TNC-c* mRNA was upregulated by 0.8-fold, in T1 and T2 in patients 1 and 2 compared to their matched normal tissue. In patient 3, *TNC-c* was 1.3-fold elevated. No intra-tumour heterogeneity was seen in the three patients among their two tested tumour regions (Figure 4.4). No protein samples were left to assess TNC protein abundance in the tested samples.

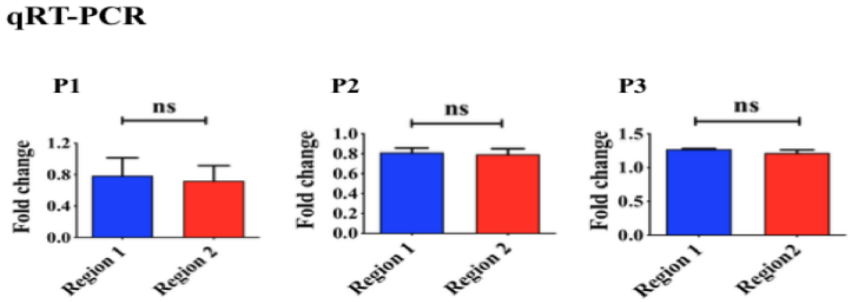

Figure 4.4. Comparative analysis of TNC-c levels in the malignant tissue (T1 and T2) compared to their matched normal tissue (N) in three patients with lung adeno-carcinoma (P1, P2, P3). Red and blue denote TNC-c mRNA relative expression levels in the two different regions per tumour per patient.

4.4.2.3 Quantification of *ENO1* gene and Enolase-1 protein expression.

The microarray analysis showed *ENO1* gene expression was downregulated 1.1-fold in T1 and upregulated 1.1-fold in T2 compared to matched normal tissue in patient 1. *ENO1* was elevated 1.8 and 2.1-fold in T1 and T2, respectively in patient 2. *ENO1* was elevated 2.5-fold and 1.8-fold in T1 and T2, respectively in patient 3. *ENO1* expression was validated further by quantitative qRT-PCR in the three lung adenocarcinoma patients (P1, P2 and P3). *ENO1* expression within the two tumour regions (T1 -red and T2 -blue) was compared to matched normal tissue (N -green) (Figure 4.5-A). As no protein samples were available from these patients, enolase-1 was assessed in another three lung adenocarcinoma patients. The comparison was also done in two regions (blue and red) from the same tumour mass per patient compared to the normal tissue (green) (Figure 4.5-B). To minimize technical pipetting and loading errors, results were normalized for their alpha/beta tubulin (in western blot) and S18 gene expression (in qRT-PCR) as internal loading control and expressed as relative expression. qRT-PCR showed a significant upregulation, by approximately 1.4-fold, 1.1-fold and 1.4-fold, of enolase-1 mRNA expression in patient 1, 2 and 3, respectively. The enolase-1 expression exhibited no heterogeneous expression pattern among the two tumour regions per patient in all the three patients included in this study. In three lung adenocarcinoma patients, enolase-1 was detected down-regulated in region 1 of the three patients (blue). In patient 1 and 2, enolase-1 was unchanged in the second analysed regions (red).

In the patient 3, region 2 was detected 2X times upregulated in than in the control normal tissue (red).

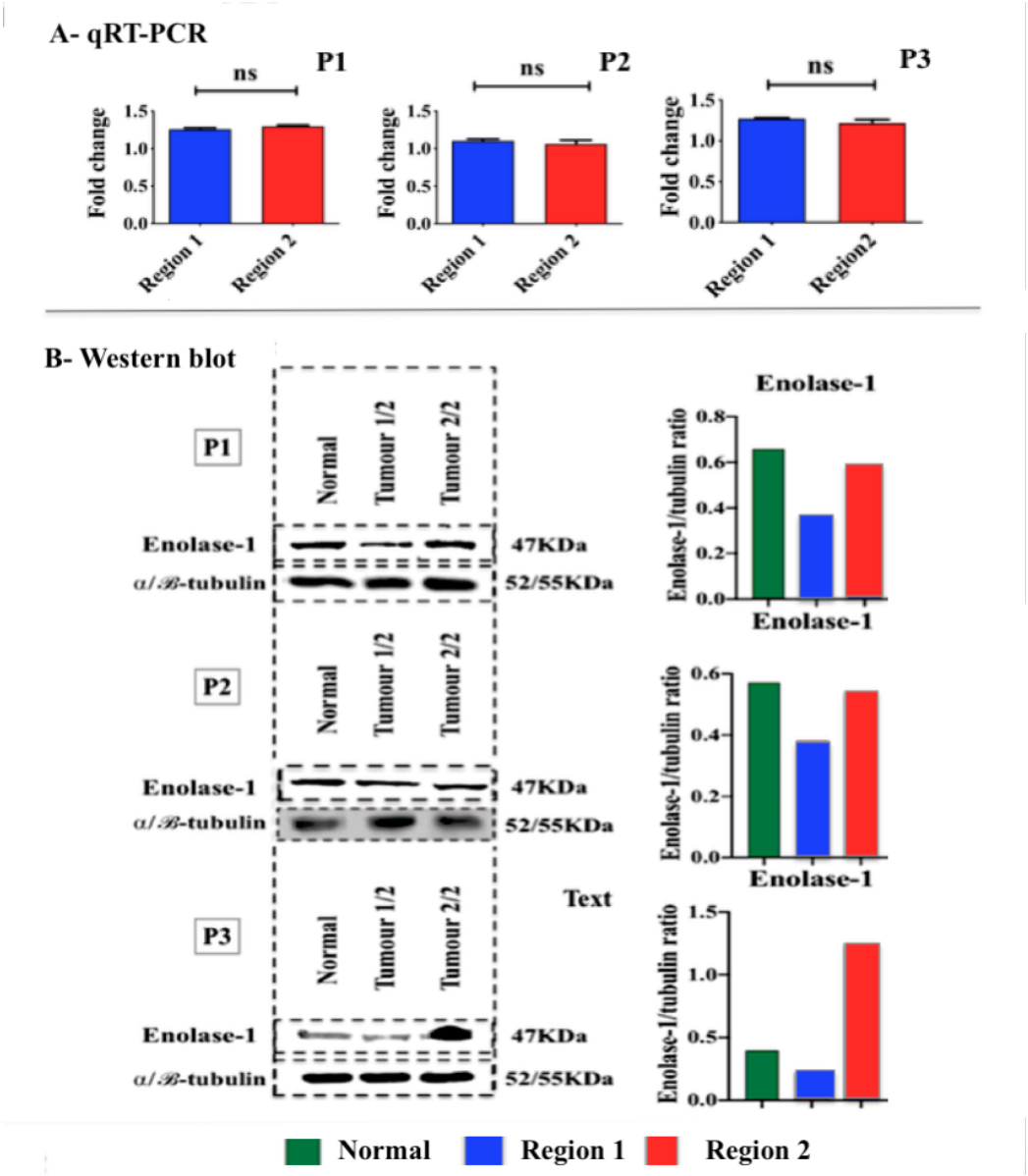

Figure 4.5. Comparative analysis of enolase-1 in the malignant tissue compared to their matched control normal tissues in three patients with lung adenocarcinoma (P1, P2, P3). A. by qRT-PCR **B**. by western blot in the patients analysed by arrayStar® and WES. Green denotes enolase-1 protein relative expression levels in the control normal tissues per patient, blue and red denote enolase-1 protein/mRNA relative expression levels in two different regions per tumour per patient.

4.4.2.4. Quantification of *ERO1A* gene and ERO1-LA protein expression.

ERO1A gene expression was validated in RNA from the three patients diagnosed with lung adenocarcinoma (P1, P2 and P3), analysed by WES and microarray technologies using qRT-PCR. No protein samples were available to assess ERO1-La in these patients therefore, ERO1-La was assessed in another set of three patients diagnosed with adenocarcinoma. *ERO1A* expression within the two tumour regions (T1 -red and T2 -blue) was compared to matched normal tissue (N -green). To minimize technical pipetting and loading errors, results were normalized for their alpha/beta tubulin (in western blot) and S18 gene expression (in qRT-PCR) as internal loading control and expressed as relative expression. In patient 1 *ERO1A* expression was increased 2.1-fold in T1 and 1.7-fold in T2 compared to the matched normal tissue. In patient 2, *ERO1A* expression was elevated 1.1 and 1.6-fold in T1 and T2, respectively compared to matched normal tissue. In patient 3, *ERO1A* expression was elevated by 2.1 and 1.1-fold in T1 and T2, respectively. By qRT-PCR, *ERO1A* mRNA levels were significantly elevated in the two tumour regions compared to the normal tissue in all patients, and no heterogeneous expression pattern was observed (Figure 4.6A). Figure 4.6-B shows western blot analysis of ERO1-La protein expression in three patients diagnosed with lung adenocarcinoma. Both patient 1 (P1) and 2 (P2) malignant tissues (two regions) had elevated *ERO1-La* protein levels compared to the control normal tissue. The level was heterogeneous among the two tumour regions. In patient 3, the two regions of the tumour (blue and red) had a lower level of ERO1-La compared to their matched control tissue with differential expression between the two tumour regions.

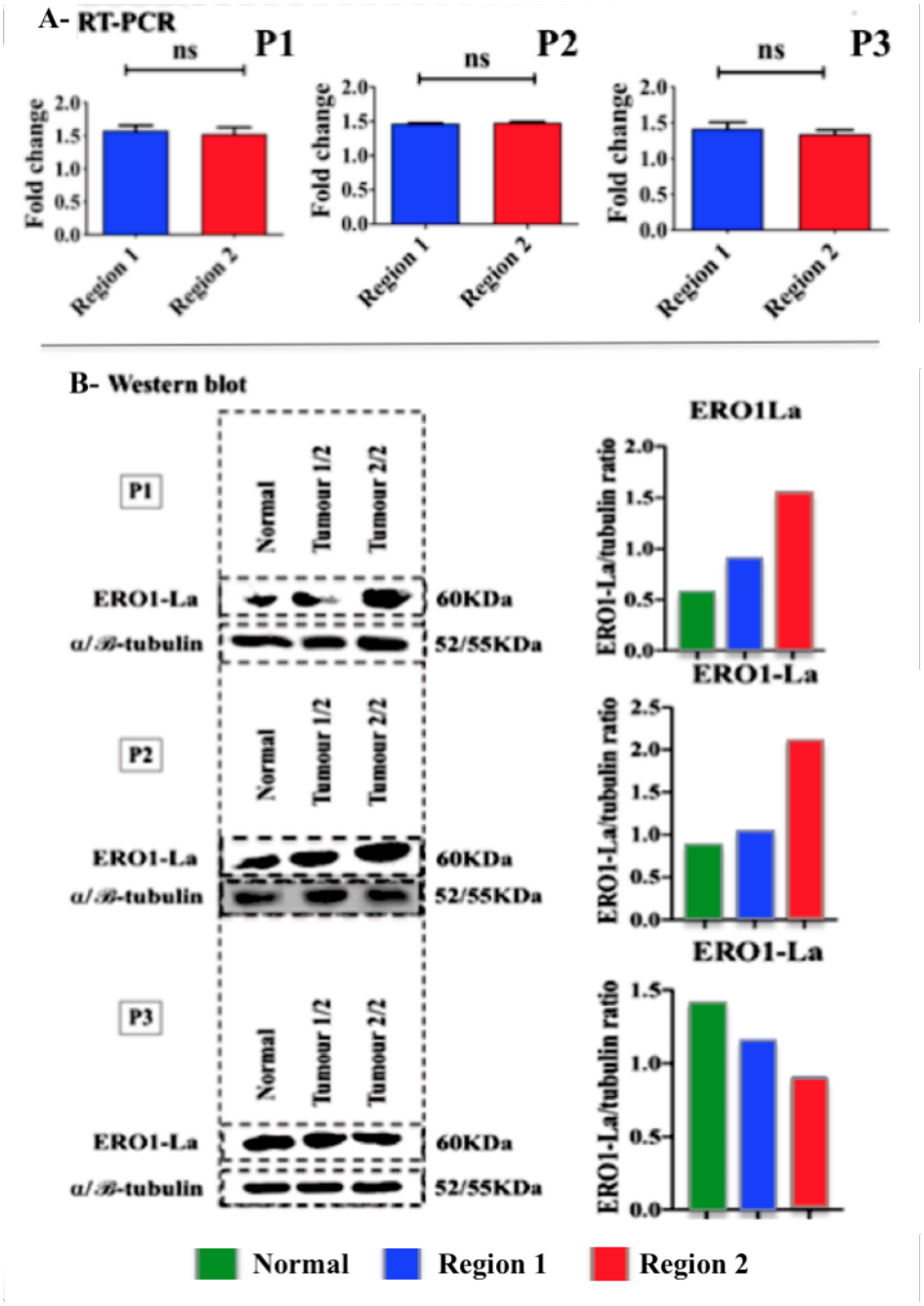

Figure 4.6. Comparative analysis of ERO1-La in the malignant tissue compared to their matched control normal tissues in three patients with lung adenocarcinoma (P1, P2, P3). A. by qRT-PCR, **B**. by western blot in three patients analysed by arrayStar® and WES. Green denotes ERO1-La protein relative expression levels in the control normal tissues per patient, red and blue denote ERO1-La protein/mRNA relative expression levels in two different regions per tumour per patient.

4.4.3. Bioinformatic analysis of microarray expression data

4.4.3.1. Expression of protein tyrosine kinases

In patient 1, *ROR2* and *FLT3* receptor tyrosine kinases (RTKs) were 4.2 and 3.1-fold elevated, respectively in T1 and were unchanged in T2. *KIT* and *LTK* were 2.4 and 3.5-fold decreased, respectively in T1 and unchanged in T2. In respective order, *ERBB 2* and *3* were 2.8 and 3.4-fold down-regulated in T1 and 2.3 and 6.1-fold upregulated in T2 compared to N. *DDR1* was unchanged in T1 and was upregulated in T2. There were also five non-receptor tyrosine kinases (NRTKs) including *ITK*, *CSK*, *BLK*, *ZAP70* and *LCK* (fold change: 2.3, 2.5, 2.1, 2.2, 2.4, respectively) upregulated in T1 and unchanged in T2. In contrast, there were two non-receptor tyrosine kinases upregulated FER and FRK (fold change: 3.4, 5.7, respectively) and two tyrosine kinases *BTK* and *MATK* downregulated (fold change: 2.1 and 3.3, respectively) in T2 while unchanged in T1 (Table 4.2). **In patient 2**, tyrosine kinase with immunoglobulin-like and EGF-like domains 1 (*TIE1*) was upregulated in both T1 and T2 of this patient. Three RTKs; *ROR1 ROR2*, and *DDR2* were down-regulated in both T1 and T2. Two RTKs *MUSK* and *EGFR* were upregulated in T2 but were unchanged in T1. There were also three RTKs down-regulated in T2 but unchanged in T1 (Table 4.2). The expression of NTRKs in this patient were as follows: *CSK*, *BTK*, *MATK* and *BLK* were unchanged in T1 and down-regulated in T2. *JAK2* was down-regulated in both T1 and T2. *ITK* was upregulated in T1 and unchanged in T2, while *FRK* was upregulated in T2 and unchanged in T1 (Table 4.2).

Table 4.2. Expression of protein tyrosine kinases in three lung AD patients.

	Description	GeneSymbol	FC	
			R1	R2
	Patient 1			
RTK	Receptor tyrosine kinase-like orphan receptor 2	ROR2	4.2	0
	Fms-related tyrosine kinase 3	FLT3	3.1	0
	V-kit Hardy-Zuckerman 4 feline sarcoma viral oncogene homolog	KIT	-2.4	0
	Leukocyte receptor tyrosine kinase	LTK	-3.5	0
	Erb-b2 receptor tyrosine kinase 2	ERBB2	-2.8	2.3
	Erb-b2 receptor tyrosine kinase 3	ERBB3	-3.4	6.1
	Discoidin domain receptor tyrosine kinase 1	DDR1	0	2.7
NRTK	IL2-inducible T-cell kinase	ITK	2.3	0
	C-src tyrosine kinase	CSK	2.5	0
	BLK proto-oncogene, Src family tyrosine kinase	BLK	2.1	0
	Zeta chain of T cell receptor associated protein kinase 70kDa	ZAP70	2.2	0
	LCK proto-oncogene, Src family tyrosine kinase	LCK	2.4	0
	Fer (fps/fes related) tyrosine kinase	FER	0	3.4
	Fyn-related Src family tyrosine kinase	FRK	0	5.7
	Bruton tyrosine kinase	BTK	0	-2.1
	Megakaryocyte-associated tyrosine kinase	MATK	0	-3.3
	Patient 2			
RTK	Tyrosine kinase with immunoglobulin-like and EGF-like domains 1	TIE1	2.2	2.4
	Receptor tyrosine kinase-like orphan receptor 2	ROR2	-2.8	-4.6
	Discoidin domain receptor tyrosine kinase 2	DDR2	-3.0	-3.3
	Receptor tyrosine kinase-like orphan receptor 1	ROR1	-2.0	-2.4
	Muscle, skeletal, receptor tyrosine kinase	MUSK	0	2.7
	Epidermal growth factor receptor	EGFR	0	2.4
	Fms-related tyrosine kinase 3	FLT3	0	-2.4
	Fibroblast growth factor receptor 2	FGFR2	0	-2.1
	V-kit Hardy-Zuckerman 4 feline sarcoma viral oncogene homolog	KIT	0	-2.5
NRTK	IL2-inducible T-cell kinase	ITK	2.8	0
	Janus kinase 2	JAK2	-2.1	-3.4
	Fyn-related Src family tyrosine kinase	FRK	0	2.3
	C-src tyrosine kinase	CSK	0	-2.2
	Bruton tyrosine kinase	BTK	0	-4.1
	Megakaryocyte-associated tyrosine kinase	MATK	0	-3.8
	BLK proto-oncogene, Src family tyrosine kinase	BLK	0	-3.0
	Patient 3			
RTK	Protein tyrosine kinase 7 (inactive)	PTK7	2.4	0
	MET proto-oncogene, receptor tyrosine kinase	MET	-2.2	-2.1
	Discoidin domain receptor tyrosine kinase 2	DDR2	-3.7	-3.6
	Leukocyte receptor tyrosine kinase	LTK	-3.2	-3.2
	Fibroblast growth factor receptor 2	FGFR2	0	2.1
	Erb-b2 receptor tyrosine kinase 2	ERBB2	0	-2.0
NRTK	BLK proto-oncogene, Src family tyrosine kinase	BLK	3.1	2.5
	Fyn-related Src family tyrosine kinase	FRK	2.8	0
	IL2-inducible T-cell kinase	ITK	11.2	0
	Janus kinase 3	JAK3	2.3	0
	FES proto-oncogene, tyrosine kinase	FES	-2.2	-2.4
	Megakaryocyte-associated tyrosine kinase	MATK	-4.0	-3.4

RTK: receptor tyrosine kinase, NRTK: non-receptor tyrosine kinase, FC: fold change, R1: tumour region 1, R2: tumour region 2. (-) and (+) values: down-regulated and up-regulated, respectively, in the tumour tissues compared to the control normal tissue.

In patient 3, three RTKs were down-regulated in both T1 and T2 including *MET*, *DDR2* and *LTK*. *ERBB2* was down-regulated in T2 and unchanged in T1, *FGFR2* was upregulated in T2 but unchanged in T1, while *PTK7* was upregulated in T1 and unchanged in T2. In contrast two NRTKs; *FES* and *MATK* were down-regulated in both T1 and T2, and *FRK*, *ITK*, and *JAK3* were upregulated in T1 and unchanged in T2, while *BLK* was upregulated in both tumour regions (Table 4.2).

4.4.3.2. Mutations associated with protein tyrosine kinases

In patient 1, whole exome sequencing detected four RTKs (*AXL, EGFR, EPHA10* AND *TIE1*) mutated in the normal tissue. *AXL* and *EPHA10* were also mutated in T1. *ERBB4* was mutated with two nucleotide deletions in intron 7 in T2, and *ROR2* was mutated in exon 9 in the normal tissue. The two tumour regions of this patient are heterogeneous in two NTRKs *ABL* had 3 nucleotide deletions in T1 and *YES1* had a point mutation in T2 (Table 4.3). **In patient 2**, the normal tissue and T1 shared two RTKs with the same mutations. *EGFR* had two point mutations in exon 7 and 21, and *ERBB2* had three nucleotide insertions in exon 8. In the normal tissue, *ERBB2* also had a point mutation in intron 8, and *RET* had a point mutation in exon 5. *ERBB2* and *EPHB*6 had point mutation, and *FGFR4* had two nucleotide deletions in intron 8, 7, and 2, respectively. Normal tissue had a unique point mutation in NTRK *LYN*. T1 and T2 both had a point mutation in exon 10 of *TXK* and a single nucleotide insertion in intron 12 of *SYK*. T2 had a unique single nucleotide deletion in the *YES1* tyrosine kinase. T1 and T2 had *INSRR*, *ERBB4* with a point mutation in intron 7 and 5, respectively and *EGFR* had a two nucleotide deletion in intron 25. *MUSK* was mutated only in T1 with a single nucleotide insertion in intron 13 and with point mutation in the exon 15 (Table 4.3). **In patient 3**, the *ALK* receptor tyrosine kinase had a point mutation in intron 11 in N, T1 and T2. Normal tissue and T1 also shared two mutated RTKs *ERBB4* had a substitution in exon 27 and *FGFR4* had two nucleotide deletions in intron 2. *EPHA10* had insertion in intron 10 in the normal tissue. *FGFR1* had a three nucleotide deletion in exon 5 in both T1 and T2. T2 had three mutated receptor tyrosine kinases including *ERBB4* with a single insertion at intron 14, *CSF1R* with a point mutation at intron 13, *AXL* with a three nucleotide deletion in intron 14 (Table 4.3). T1 and T2 both had a single

nucleotide deletion at intron 1 of *BMX*, while T1 and the normal tissue had mutated *ZAP70* and *FYN* genes (Table 4.3).

Table 4.3. WES-detected mutated protein tyrosine kinases.

	Chrom	Pos	Ref	Alt	Symbol	Type	Exon/Intron	Conseq.	Impact	
	Patient 1									
Normal	Chr9	94486025	TTCC	T	ROR2	Deletion	E9	ID	MT	RTK
	Chr19	41758161	GTGA	G	AXL	Deletion	I14	IV	MR	
	Chr7	55269062	GTC	G	EGFR	Deletion	I25	IV	MR	
	Chr1	38187802	CA	C	EPHA10	Deletion	I10	IV	MR	
	Chr1	43774445	C	A	TIE1	SNV	I7	IV	MR	
	Chr9	133759489	CAAG	C	ABL1	deletion	E11	ID	MT	NRTK
Region 1	Chr1	38187802	C	CA	EPHA10	insertion	I10	IV	MR	RTK
	Chr19	41758161	GTGA	G	AXL	Deletion	I14	IV	MR	
	Chr18	747929	T	C	YES1	SNV	E4	MV	MT	NRTK
Region 2	Chr2	212578379	TAA	T	ERBB4	Deletion	I7	SRV	Low	RTK
	Patient 2									
Normal	chr7	55221744	C	T	EGFR	SNV	E7	MV	MT	RTK
	chr7	55259515	T	G	EGFR	SNV	E21	MV	MT	
	chr17	37868202	T	TGGG	ERBB2	insertion	E8	II	MT	
	chr10	43601921	A	G	RET	SNV	E5	MV	MT	
	chr7	142563186	G	T	EPHB6	SNV	I7	IV	MR	
	chr17	37868551	C	A	ERBB2	SNV	I8	IV	MR	
	chr5	176517099	TTG	T	FGFR4	deletion	I2	IV	MR	
	chr8	56866308	C	A	LYN	SNV	I7	IV	MR	NRTK
Region 1	chr7	55221744	C	T	EGFR	SNV	E7	MV	MT	RTK
	chr7	55259515	T	G	EGFR	SNV	E21	MV	MT	
	chr17	37868202	T	TGGG	ERBB2	insertion	E8	II	MT	
	chr9	113562939	A	C	MUSK	SNV	E15	MV	MT	
	chr7	55269062	GTC	G	EGFR	deletion	I25	IV	MR	
	chr2	212589964	G	C	ERBB4	SNV	I5	IV	MR	
	chr1	156818703	C	T	INSRR	SNV	I7	IV	MR	
	chr9	113548014	G	GA	MUSK	insertion	I13	IV	MR	
	chr4	48088631	C	G	TXK	SNV	E10	MV	MT	NRTK
	chr9	93650758	T	TA	SYK	insertion	I12	IV	MR	
Region 2	chr1	156818703	C	T	INSRR	SNV	I7	IV	MR	RTK
	chr2	212589964	G	C	ERBB4	SNV	I5	IV	MR	
	chr7	55269062	GTC	G	EGFR	deletion	I25	IV	MR	
	chr4	48088631	C	G	TXK	SNV	E10	MV	MT	
	chr9	93650758	T	TA	SYK	insertion	I12	IV	MR	NRTK
	chr18	751880	CA	C	YES1	deletion	I2	IV	MR	
	Patient 3									
Normal	chr2	212251640	CT	TA	ERBB4	substitution	E27	MV	MT	RTK
	chr1	38187802	C	CA	EPHA10	insertion	I10	IV	MR	
	chr2	29497959	C	A	ALK	SNV	I11	IV	Low	
	chr5	176516968	CGT	C	FGFR4	deletion	I2	IV	MR	
	chr2	98349522	G	C	ZAP70	SNV	I5	IV	MR	NRTK
	chr6	111995610	G	A	FYN	SNV	I13	IV	MR	
	chr9	93629399	G	A	SYK	SNV	I6	IV	MR	
Region 1	chr2	212251640	CT	TA	ERBB4	substitution	E27	MV	MT	RTK
	chr8	38285913	GTCA	G	FGFR1	deletion	E5	ID	MT	
	chr2	29497959	C	A	ALK	SNV	I11	IV	Low	
	chr5	176516968	CGT	C	FGFR4	deletion	I2	IV	MR	
	chr2	98349522	G	C	ZAP70	SNV	I5	IV	MR	NRTK
	chr6	111995610	G	A	FYN	SNV	I13	IV	MR	
	chrX	15509448	CA	C	BMX	deletion	I1	IV	MR	
Region 2	chr8	38285913	GTCA	G	FGFR1	deletion	E5	ID	MT	RTK
	chr2	29497959	C	A	ALK	SNV	I11	IV	Low	
	chr2	212530218	G	GA	ERBB4	insertion	I14	IV	MR	
	chr5	149440964	T	C	CSF1R	SNV	I13	IV	MR	
	chr19	41758161	GTGA	G	AXL	deletion	I14	IV	MR	
	chrX	15509448	CA	C	BMX	deletion	I1	IV	MR	NRTK

RTK: receptor tyrosine kinase, NRTK: non-receptor tyrosine kinase, POS: located on the positive strand, Ref: reference sequence, Alt: detected alteration, Conseq: consequence of such mutation, SNV: single nucleotide variant, E: exon, I: intron, MT: moderate, MR: modifier, IV: intron variant, MV: missense variant, ID: Inframe deletion, II: intron variant, SRV: splice region variant.

4.4.3.3. Functional mapping of differentially expressed genes

All significantly ($p<0.05$) upregulated genes (T1: 2167, and T2: 1938) and down-regulated genes (T1: 2524, and T2: 1623) using a cut off value of 2-fold in **patient 1** were uploaded to Panther GO-Slim biological process classification. Genes were classified into the following biological functions: biological adhesion (46, 29, 60, 42), biological regulation (498, 365, 588, 381), cell population proliferation (28, 17, 26, 23), cellular component organisation or biogenesis (242, 213, 316, 186), cellular process (790, 675, 489, 570), developmental process (150, 112, 198, 128), growth (10, 4, 10, 4), immune system process (102, 29, 37,42), localization (232, 213, 276, 164), locomotion (59, 40, 80, 56), 11: metabolic process (475, 418, 489, 288), multi-organism process (60, 27, 30, 31), multicellular organism process (170, 102, 174, 124), response to stimuli (327, 230, 342, 225) and signalling (244, 161, 270, 188). The order of gene numbers between brackets is (up in T1 -red, up in T2 -blue, down in T1 -dark green, down in T2 -light green), respectively (Figure 4.7: P1). Panther biological classification of the significantly upregulated genes (T1: 867, and T2: 1531) and down-regulated genes (T1: 1462, and T2: 2593) using a 2-fold cut off value in **patient 2** was as following: biological adhesion (13, 21, 40, 62), biological regulation (188, 347, 347, 568), cell population proliferation (6, 12, 17, 29), cellular component organisation or biogenesis (82, 207, 170, 297), cellular process (292, 579, 531, 918), developmental process (59, 98, 141, 197), growth (1, 6, 12, 15), immune system process (23, 23, 35,73), localization (80, 163, 160,273), locomotion (22, 29, 45, 87), metabolic process (182, 368, 286, 481), multi-organism process (11, 15, 31, 51), multicellular organismal process (49, 89, 149, 199), response to stimuli (113, 203, 230, 383), 15: signalling (80, 143, 178, 292). Gene number order is the same as in patient 1 (Figure 4.7: P2). **In patient 3**, the

significantly upregulated genes (T1: 2190, and T2: 1650) and down-regulated genes (T1: 2179 and T2: 2789) using a 2-fold cut off value were classified by Panther GO-Slim biological process to the following categories: biological adhesion (33, 26, 57, 66), biological regulation (466, 373, 509, 652), cell population proliferation (13, 16, 20, 30), cellular component organisation or biogenesis (307, 236, 215, 316), cellular process (856, 634, 751, 1015), developmental process (117, 99, 171, 222), growth (4, 3, 5, 10), immune system process (63, 52, 55,60), localization (228, 187, 207, 291), locomotion (42, 37, 59, 87), metabolic process (523, 368, 406, 568), multi-organism process (27, 25, 39, 47), multicellular organismal process (121, 95, 166, 201), response to stimuli (308, 245, 337, 432), signalling (197, 160, 262, 326) with the same order used in patient 1 and 2 (Figure 4.7-P3). Further analysis of the significantly upregulated and down regulated genes at 2-fold cut-off value per tumour region per patient was performed by KEGG pathway analysis and the top 15 pathways are listed in table: 4.4. *PI3K/AKT and JAK/STAT* pathways were studied in further detail.

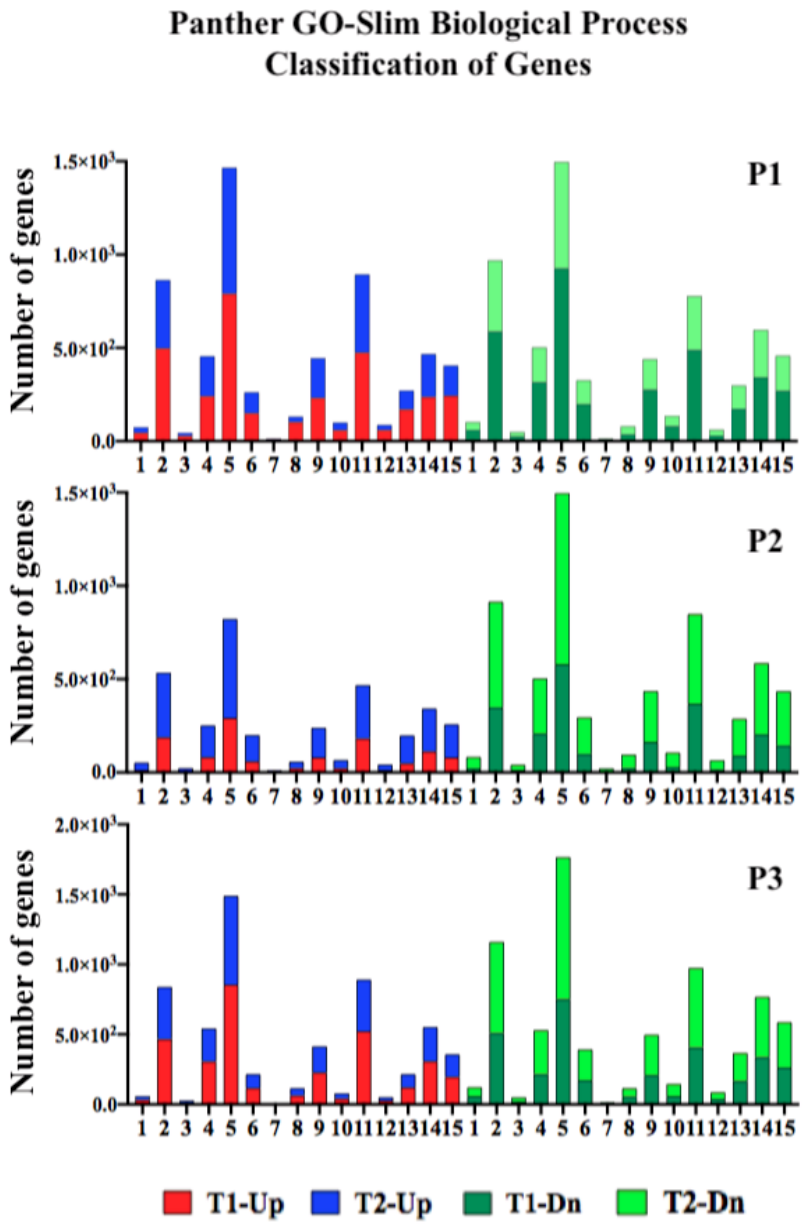

Figure 4.7. Panther GO-Slim Biological Process classification of differentially up and down regulated genes. 1: biological adhesion, 2: biological regulation, 3: cell population proliferation, 4: cellular component organisation or biogenesis, 5: cellular process, 6: developmental process, 7: growth, 8: immune system process, 9: localization, 10: locomotion, 11: metabolic process, 12: multi-organism process, 13: multicellular organismal process, 14: response to stimuli, 15: signalling. Red (T1-Up): up in region 1, blue (T2-Up): up in region 2, dark green (T1-Dn): down in region 1 and light green (T2-Dn): down in region 2.

KEGG pathway analysis of the differentially expressed genes (DEGs) (either upregulated or down-regulated), using a 2-fold cut off value, categorised the DEGs into specific signalling pathways which are listed in table 4.2. **In patient 1,** 8.7% (n=188) of the upregulated mRNAs T1 were involved in metabolic pathways, while 11.5% (n=224) of T2 upregulated genes were operating in metabolic pathways. On the other hand, 6.7% (n=146) and 4.7% (n=77) of the down regulated genes in T1 and T2, respectively were involved in metabolic pathways. The second top pathway was cytokine-cytokine receptor interaction, where 2.5% (n=58), 1.5% (n=38) of the upregulated and 1.8% (n=34), 1.9% (n=31) of the downregulated genes in T1 and T2, respectively were operating in this pathway. The third top clustering of genes was in known cancer pathways; 2.5% (n=54), 1.9% (n=49) of the upregulated genes and 5% (n=98), 3.4% (n=55) of the down regulated genes in T1 and T2, respectively were involved in such pathways. **In patient 2,** the percentage of genes that were involved in metabolic pathways was 9.3% (n=81) and 9.7% (149) of the upregulated genes in T1 and T2, respectively. On the other hand, 7.2% (n=105) and 6.6% (n=172) of the down-regulated genes of T1 and T2, respectively were involved in metabolism pathways. 2.2% (n=19), 1.9% (n=29) of the upregulated genes in T1 and T2, respectively were involved in the cytokine-cytokine receptor interaction, also 2.2% (n=32) and 2.0% (n=51) of the downregulated genes were involved in this signalling pathway. Upregulated genes involved in cancer pathways were 2.7% (n=23) and 2.5% (n=39), while the down regulated genes were 4.6% (n=67) and 4.5% (n=117). **In patient 3,** the percentage of upregulated genes involved in metabolic pathways was 9.3% (n=204) and 7% (n=116), while 6.5% (n=142) and 7% (n=197) of the downregulated genes were involved in cell metabolism. 1.8% (n=39), 2.2% (n=37) of the upregulated genes and 2.6% (n=57),

2.3% (n=64) of the downregulated genes in T1 and T2 were operating in cytokine-cytokine receptor interaction. The genes linked to cancer pathways were 2.5% (n=55), 2.6% (n=43) of the upregulated genes in T1 and T2, respectively and 4.4% (n=96), 4.5% (n=125) of the down-regulated genes in T1 and T2, respectively. The *PI3K/AKT* and *JAK/STAT* pathways were studied further to define any differences in signalling between the two tumour regions (T1 and T2) per patient.

Table 4.4. KEGG pathway analysis of the significantly up and down regulated mRNA per tumour region per patient.

		Patient 1				Patient 2				Patient 3			
		Upregulated		Down-regulated		Upregulated		Down-regulated		Upregulated		Down-regulated	
		Region 1	Region 2	Region 1	Region 2	Region 1	Region 2	Region 1	Region 2	Region 1	Region 2	Region 1	Region 2
hsa01100	Metabolic pathways	188	224	146	77	81	149	105	172	204	116	142	197
hsa04060	Cytokine-cytokine receptor interaction	58	38	34	31	19	29	32	51	39	37	57	64
hsa05200	Pathways in cancer	54	49	98	55	23	39	67	117	55	43	96	125
hsa04151	PI3K-Akt signaling pathway	50	30	62	38	15	26	45	66	35	30	54	66
hsa04062	Chemokine signaling pathway	34	14	26	26	10	12	25	42	20	14	39	50
hsa04010	MAPK signaling pathway	33	25	43	31	10	21	28	41	21	18	55	64
hsa04514	Cell adhesion molecules (CAMs)	32	11	24	30	6	9	18	39	21	16	22	28
hsa04510	Focal adhesion	28	14	48	26	5	13	37	51	19	14	39	54
hsa04810	Regulation of actin cytoskeleton	28	11	37	22	3	14	26	40	17	13	32	40
hsa04662	B cell receptor signaling pathway	24	3	8	11	2	5	6	16	9	6	11	10
hsa04014	Ras signaling pathway	22	15	30	24	6	17	24	42	4	2	42	52
hsa04512	ECM-receptor interaction	22	8	27	17	4	6	21	29	12	12	16	23
hsa04630	JAK-STAT signaling pathway	20	14	21	14	4	9	14	24	12	13	24	30
hsa04064	NF-kappa B signaling pathway	20	7	14	13	5	9	7	12	6	6	19	18
hsa05235	PDL1 expression and PD1	18	2	10	10	1	5	10	16	3	4	11	13

4.4.3.4. PI3K-AKT signalling pathway in patient 1.

Four genes (*CDK4, COL1A1, EIF4EBP1, and SPP1*) were upregulated in both T1 and T2, listed at the top of table 4.5. The secreted phosphoprotein (*SPP1*) was increased 199-fold in T1 and 6.2-fold in T2; Collagen type 1 alpha 1 (*COL1A1*) was increased 6.9-fold in T1 compared to 2.4-fold in T2, both are extracellular matrix proteins. Twenty three genes (Table 4.5 -line5) were detected down-regulated in both T1 and T2. Among these 23 genes are ECM structural proteins including *COL4C3/4, COL5C6, ITGA1, LAMB2/G3, TNC-XB* and von Willebrand factor. Among the 23 down-regulated genes are several cytokines and cytokine receptors including *IL 4, IL2/7R*. Several growth factors were also down-regulated in both tumour regions of this patient such as *VEGFR*, *PGF*, *PDGFA*, *NGF* (Table 4.5). On the other hand, some genes encoding for ECM structural proteins such as *LAMA3/B3, ITGB4/6*, and some receptor tyrosine kinases such as *ERBB2*, *ERBB3*, *FGF4* and *AMPK*, were down-regulated in T1 while they were uniquely upregulated in T2 (Table 4.5). Genes that were uniquely upregulated in T1 include; ECM genes such as *COLs, ITGs, THBS1*, in addition to *TNC-c* and *VTN*. There were several growth factors detected upregulated only in T1 e.g. *FGF 1, 5, 10, 16, 17, 19,* and also growth factor receptors such as *FLT1R* and *FLT3R*, ILGF and ANGPT. In contrast, the unique down regulated genes in T1 include; *COL4, ITGs, LAMG*, and *PP2* catalytic and regulatory subunits in addition to some cytokines and growth factors (Table 4.5). There were also some cytokines such as *IFNA1R* and *IL2RB* found down-regulated in T1 but unchanged in T2 (Table 4.5). T2 had 17 uniquely upregulated genes which include ECM genes, cytokines, growth factors. T2 also had 12 down-regulated genes on top of them *TNC-n* and *EREG* (Table 4.5). The overall differences between T1 and T2 of this patient are summarized in figure

4.8. Both tumour regions have upregulated and down regulated GFs, CKs, ECM encoding genes, RTKs and GPCR (indicated as red fill for the upregulated and red line above the boxes for the down-regulated genes) (Figure 4.8). Upstream to the *PIP2/PIP3* end point, T1 differs from T2 in some genes encoding for cell membrane receptors including *TLR2/3, CD19, CKR, and ITGA* (Figure 4.8). *PI3K-B* and T cell leukaemia 1B (*TCL1*) were also upregulated in T1 in addition to lower levels of *PTEN* and *PI3K-A*. Downstream to *AKT*, T2 had more elevated genes (yellow) including *GYS*, cyclins, *Bcl2*, *SGK*, *LKB1* and *AMPK* while both regions shared *CREB*, *CDK* and *4EBPs* upregulated (red-fill). Shared down-regulated are marked as red line above gene name. Down-regulated in T1 marked as green line above the gene while in T2 marked in yellow line above the gene name (Figure 4.8).

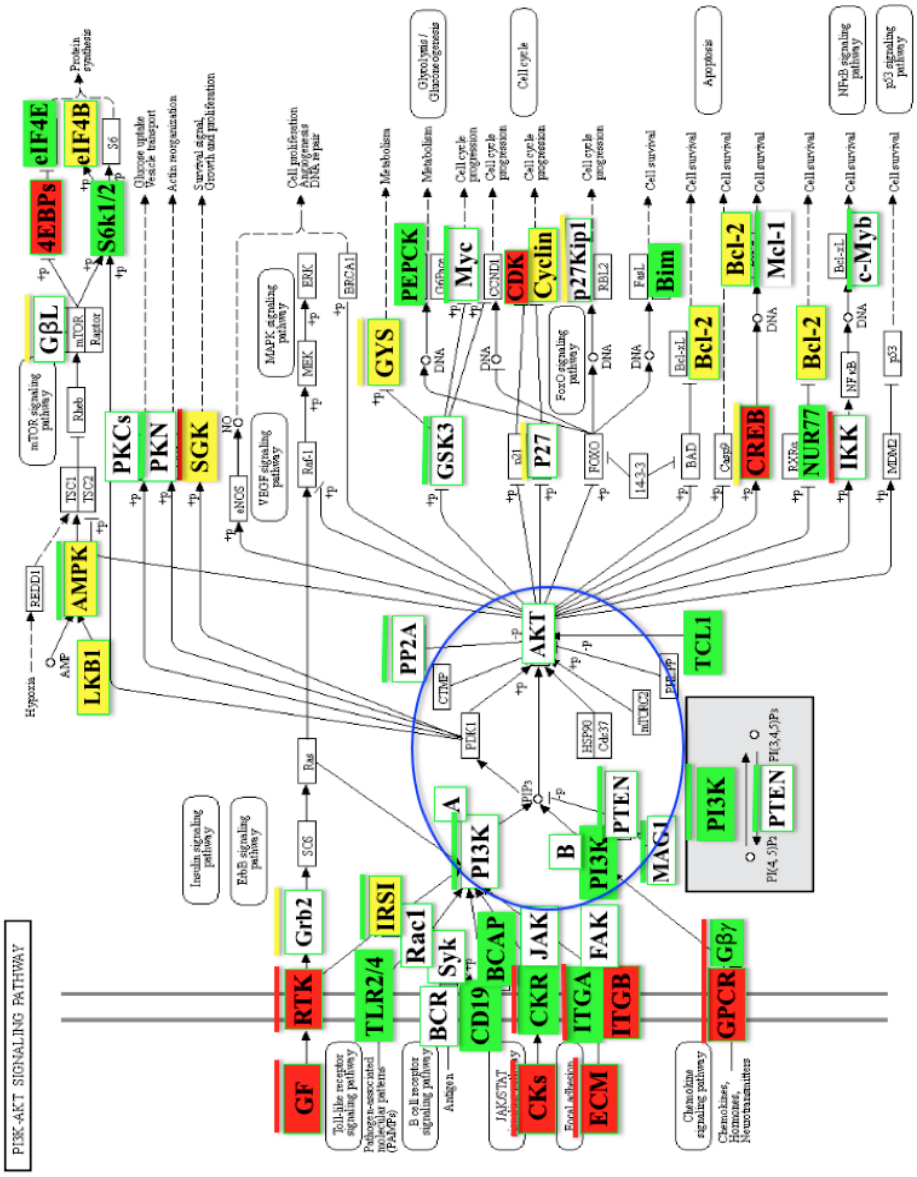

Figure 4.8. PI3K/AKT signalling pathway in patient 1. Red-fill: upregulated genes in both tumour regions, green-fill: upregulated in region 1, yellow-fill: upregulated in region 2, red line above gene name: downregulated in both tumour regions, green line above gene name: downregulated in T1, yellow line under gene name: down regulated inT2.

Table 4.5. Expression of genes involved in PI3K/AKT pathway in patient 1.

KEGG Entry	Symbol	Description	T1	T2
hsa:1019	CDK4	cyclin dependent kinase 4	2.2	2.1
hsa:1277	COL1A1	collagen type I alpha 1 chain	6.9	2.4
hsa:1978	EIF4EBP1	eukaryotic translation initiation factor 4E binding protein 1	2.7	2.4
hsa:6696	SPP1	secreted phosphoprotein 1	199.0	6.2
hsa:1285	COL4A3	collagen type IV alpha 3 chain	-4.2	-6.4
hsa:1286	COL4A4	collagen type IV alpha 4 chain	-2.1	-2.6
hsa:131873	COL6A6	collagen type VI alpha 6 chain	-5.6	-2.6
hsa:2791	GNG11	G protein subunit gamma 11	-4.8	-4.1
hsa:2997	GYS1	glycogen synthase 1	-14.1	-20.8
hsa:3551	IKBKB	inhibitor of nuclear factor kappa B kinase subunit beta	-4.3	-2.5
hsa:3559	IL2RA	interleukin 2 receptor subunit alpha	-7.8	-3.5
hsa:3565	IL4	interleukin 4	-11.0	-4.4
hsa:3575	IL7R	interleukin 7 receptor	-2.4	-2.0
hsa:3672	ITGA1	integrin subunit alpha 1	-6.4	-3.9
hsa:3791	KDR	kinase insert domain receptor	-5.3	-3.1
hsa:4254	KITLG	KIT ligand	-14.3	-19.8
hsa:3913	LAMB2	laminin subunit beta 2	-2.2	-2.2
hsa:10319	LAMC3	laminin subunit gamma 3	-6.6	-6.0
hsa:57121	LPAR5	lysophosphatidic acid receptor 5	-2.7	-3.0
hsa:64223	MLST8	MTOR associated protein, LST8 homolog	-7.9	-9.1
hsa:4803	NGF	nerve growth factor	-2.9	-4.0
hsa:5154	PDGFA	platelet derived growth factor subunit A	-21.0	-2.3
hsa:5228	PGF	placental growth factor	-16.7	-19.3
hsa:7060	THBS4	thrombospondin 4	-4.4	-3.4
hsa:7148	TNXB	tenascin XB	-5.1	-2.2
hsa:7422	VEGFA	vascular endothelial growth factor A	-3.9	-3.4
hsa:7450	VWF	von Willebrand factor	-5.1	-4.2
hsa:2064	ERBB2	erb-b2 receptor tyrosine kinase 2	-2.8	2.3
hsa:2065	ERBB3	erb-b2 receptor tyrosine kinase 3	-3.4	6.1
hsa:2264	FGFR4	fibroblast growth factor receptor 4	-3.3	3.0
hsa:3667	IRS1	insulin receptor substrate 1	-2.5	3.1
hsa:3691	ITGB4	integrin subunit beta 4	-2.3	2.8
hsa:3694	ITGB6	integrin subunit beta 6	-20.8	2.4
hsa:3909	LAMA3	laminin subunit alpha 3	-2.6	2.0
hsa:3914	LAMB3	laminin subunit beta 3	-6.9	2.8
hsa:5563	PRKAA2	protein kinase AMP-activated catalytic subunit alpha 2	-3.4	2.1

Table 4.5-continued

hsa:51378	ANGPT4	angiopoietin 4	**2.2**	/
hsa:10018	BCL2L11	BCL2 like 11	**2.7**	/
hsa:930	CD19	CD19 molecule	**10.4**	/
hsa:1278	COL1A2	collagen type I alpha 2 chain	**2.2**	/
hsa:1291	COL6A1	collagen type VI alpha 1 chain	**3.0**	/
hsa:1292	COL6A2	collagen type VI alpha 2 chain	**2.3**	/
hsa:1293	COL6A3	collagen type VI alpha 3 chain	**4.1**	/
hsa:1311	COMP	cartilage oligomeric matrix protein	**3.1**	/
hsa:1385	CREB1	cAMP responsive element binding protein 1	**2.2**	/
hsa:1436	CSF1R	colony stimulating factor 1 receptor	**4.6**	/
hsa:1977	EIF4E	eukaryotic translation initiation factor 4E	**2.8**	/
hsa:2246	FGF1	fibroblast growth factor 1	**3.5**	/
hsa:2255	FGF10	fibroblast growth factor 10	**2.4**	/
hsa:8823	FGF16	fibroblast growth factor 16	**2.2**	/
hsa:8822	FGF17	fibroblast growth factor 17	**3.0**	/
hsa:9965	FGF19	fibroblast growth factor 19	**7.5**	/
hsa:2250	FGF5	fibroblast growth factor 5	**4.2**	/
hsa:2321	FLT1	fms related receptor tyrosine kinase 1	**2.1**	/
hsa:2322	FLT3	fms related receptor tyrosine kinase 3	**3.0**	/
hsa:2335	FN1	fibronectin 1	**4.5**	/
hsa:2788	GNG7	G protein subunit gamma 7	**3.4**	/
hsa:3381	IBSP	integrin binding sialoprotein	**2.8**	/
hsa:3439	IFNA1	interferon alpha 1	**9.9**	/
hsa:3481	IGF2	insulin like growth factor 2	**24.2**	/
hsa:3560	IL2RB	interleukin 2 receptor subunit beta	**3.1**	/
hsa:22801	ITGA11	integrin subunit alpha 11	**8.5**	/
hsa:3676	ITGA4	integrin subunit alpha 4	**3.0**	/
hsa:3695	ITGB7	integrin subunit beta 7	**2.4**	/
hsa:284217	LAMA1	laminin subunit alpha 1	**6.0**	/
hsa:3911	LAMA5	laminin subunit alpha 5	**2.6**	/
hsa:1902	LPAR1	lysophosphatidic acid receptor 1	**2.4**	/
hsa:2846	LPAR4	lysophosphatidic acid receptor 4	**2.2**	/
hsa:5105	PCK1	phosphoenolpyruvate carboxykinase 1	**8.4**	/
hsa:56034	PDGFC	platelet derived growth factor C	**3.0**	/
hsa:5156	PDGFRA	platelet derived growth factor receptor alpha	**2.4**	/
hsa:118788	PIK3AP1	phosphoinositide-3-kinase adaptor protein 1	**3.8**	/
hsa:5294	PIK3CG	phosphatidylinositol-4,5-bisphosphate 3-kinase catalytic subunit gamma	**3.1**	/
hsa:23533	PIK3R5	phosphoinositide-3-kinase regulatory subunit 5	**2.4**	/
hsa:6199	RPS6KB2	ribosomal protein S6 kinase B2	**2.3**	/
hsa:8115	TCL1A	T cell leukemia/lymphoma 1A	**2.2**	/
hsa:7057	THBS1	thrombospondin 1	**3.0**	/
hsa:7058	THBS2	thrombospondin 2	**28.0**	/
hsa:7097	TLR2	toll like receptor 2	**4.5**	/
hsa:3371	TNC	tenascin C	**9.2**	/
hsa:7448	VTN	vitronectin	**3.5**	/

Table 4.5-continued

hsa:284	ANGPT1	angiopoietin 1	-11.9	/
hsa:374	AREG	amphiregulin	-4.4	/
hsa:1129	CHRM2	cholinergic receptor muscarinic 2	-4.3	/
hsa:1282	COL4A1	collagen type IV alpha 1 chain	-2.1	/
hsa:1284	COL4A2	collagen type IV alpha 2 chain	-2.6	/
hsa:1288	COL4A6	collagen type IV alpha 6 chain	-3.3	/
hsa:2690	GHR	growth hormone receptor	-2.6	/
hsa:2932	GSK3B	glycogen synthase kinase 3 beta	-3.0	/
hsa:3447	IFNA13	interferon alpha 13	-3.1	/
hsa:3569	IL6	interleukin 6	-3.5	/
hsa:3673	ITGA2	integrin subunit alpha 2	-4.5	/
hsa:3675	ITGA3	integrin subunit alpha 3	-2.5	/
hsa:8516	ITGA8	integrin subunit alpha 8	-17.0	/
hsa:3696	ITGB8	integrin subunit beta 8	-2.1	/
hsa:3815	KIT	KIT proto-oncogene, receptor tyrosine kinase	-2.4	/
hsa:3918	LAMC2	laminin subunit gamma 2	-5.1	/
hsa:9223	MAGI1	membrane associated guanylate kinase, WW and PDZ domain containing 1	-3.2	/
hsa:4170	MCL1	MCL1 apoptosis regulator, BCL2 family member	-2.8	/
hsa:4602	MYB	MYB proto-oncogene, transcription factor	-2.6	/
hsa:4609	MYC	MYC proto-oncogene, bHLH transcription factor	-7.9	/
hsa:8503	PIK3R3	phosphoinositide-3-kinase regulatory subunit 3	-2.1	/
hsa:5586	PKN2	protein kinase N2	-3.4	/
hsa:5516	PPP2CB	protein phosphatase 2 catalytic subunit beta	-2.1	/
hsa:5523	PPP2R3A	protein phosphatase 2 regulatory subunit B''alpha	-2.1	/
hsa:28227	PPP2R3B	protein phosphatase 2 regulatory subunit B''beta	-5.3	/
hsa:5525	PPP2R5A	protein phosphatase 2 regulatory subunit B'alpha	-3.2	/
hsa:5529	PPP2R5E	protein phosphatase 2 regulatory subunit B'epsilon	-2.0	/
hsa:5728	PTEN	phosphatase and tensin homolog	-2.1	/
hsa:5649	RELN	reelin	-3.1	/
hsa:6446	SGK1	serum/glucocorticoid regulated kinase 1	-2.6	/
hsa:1027	CDKN1B	cyclin dependent kinase inhibitor 1B	-2.7	/

Table 4.5-continued

hsa:596	BCL2	BCL2 apoptosis regulator	/	2.2
hsa:898	CCNE1	cyclin E1	/	13.6
hsa:1297	COL9A1	collagen type IX alpha 1 chain	/	87.7
hsa:148327	CREB3L4	cAMP responsive element binding protein 3 like 4	/	4.5
hsa:1942	EFNA1	ephrin A1	/	2.0
hsa:1943	EFNA2	ephrin A2	/	2.3
hsa:1975	EIF4B	eukaryotic translation initiation factor 4B	/	3.3
hsa:1969	EPHA2	EPH receptor A2	/	2.1
hsa:26281	FGF20	fibroblast growth factor 20	/	4.5
hsa:2998	GYS2	glycogen synthase 2	/	4.5
hsa:3574	IL7	interleukin 7	/	3.4
hsa:22798	LAMB4	laminin subunit beta 4	/	2.7
hsa:9170	LPAR2	lysophosphatidic acid receptor 2	/	4.5
hsa:10161	LPAR6	lysophosphatidic acid receptor 6	/	2.1
hsa:80310	PDGFD	platelet derived growth factor D	/	2.3
hsa:10110	SGK2	serum/glucocorticoid regulated kinase 2	/	16.6
hsa:6794	STK11	serine/threonine kinase 11	/	2.2
hsa:9586	CREB5	cAMP responsive element binding protein 5	/	-2.4
hsa:2069	EREG	epiregulin	/	-2.3
hsa:59345	GNB4	G protein subunit beta 4	/	-2.1
hsa:2793	GNGT2	G protein subunit gamma transducin 2	/	-3.3
hsa:2885	GRB2	growth factor receptor bound protein 2	/	-2.3
hsa:3561	IL2RG	interleukin 2 receptor subunit gamma	/	-2.0
hsa:3563	IL3RA	interleukin 3 receptor subunit alpha	/	-3.4
hsa:3678	ITGA5	integrin subunit alpha 5	/	-3.0
hsa:3679	ITGA7	integrin subunit alpha 7	/	-2.6
hsa:23678	SGK3	serum/glucocorticoid regulated kinase family member 3	/	-2.5
hsa:63923	TNN	tenascin N	/	-2.3
hsa:7424	VEGFC	vascular endothelial growth factor C	/	-3.4

T1: tumour region 1, T2: tumour region 2. (+): denotes upregulated, (-): denotes down-regulated. Colour code: from red to yellow: from the highest to the lowest upregulated fold change values, dark to light green: the highest to the lowest downregulated fold change values.

4.4.3.5. PI3K-AKT signalling pathway in patient 2.

The number of down-regulated genes is triple the number of upregulated ones. Fifteen versus forty five and twenty six versus sixty six genes were up and down - regulated in T1 and T2, respectively. Eight genes were upregulated in both T1 and T2 including *SGK2, CCNE2, OSMR*, *EFG*, *CD19*, *IL2RA*, *COL2A1* and *SSP1* (27 and 80-fold increased in T1 and T2, respectively) (Table 4.6). Forty-one genes were downregulated in T1 and T2 by microarray analysis. Among these genes are *COL4/6*, *FGF*, laminin, *TNC*, *AKT*, ILs and *JAK2* (Table 4.6). Six genes were upregulated in T1 and unchanged in T2, the most abundant was *FGF5* which was 14-fold higher than matched normal tissue (Table 4.6). Next are the genes that showed an opposite expression profile i.e. unchanged in T1 and upregulated in T2; these genes include *GFs*, hormones, genes encoding for *ECM* proteins, *ILs*, *MYC* transcription factor and *PI3K* adaptor and regulatory subunits. *MYB* transcription factor was up-regulated in T1 and down-regulated in T2. Four genes were uniquely down-regulated in T1 but not affected in T2 including *FGF9*, *PDGF-D*, *IFNA1* and *ITGA3* (Table 4.6). Twenty-four genes that were down-regulated in T2 and unchanged in T1 including *PPs*, *ECM* genes, *ILs, GFs* (Table 4.6). Upstream to PIP2/PIP3, both T1 and T2 had *ECM, GF*, *CD19* and *CKR* genes up and down-regulated. T2 had elevated *RTK*, cytokines and ITGA which were unique to this region. *PI3K-B* was also upregulated in T2 only with lower levels of *PTEN* (Figure 4.9). Downstream of *PIP2/PIP3*, cyclins and *SGK* were elevated in both regions, *MYC* transcription factor, *CREB* and *IKK* as well as *Rheb* were uniquely elevated in T2 while the *GYS* was uniquely elevated in T1 (Figure 4.9).

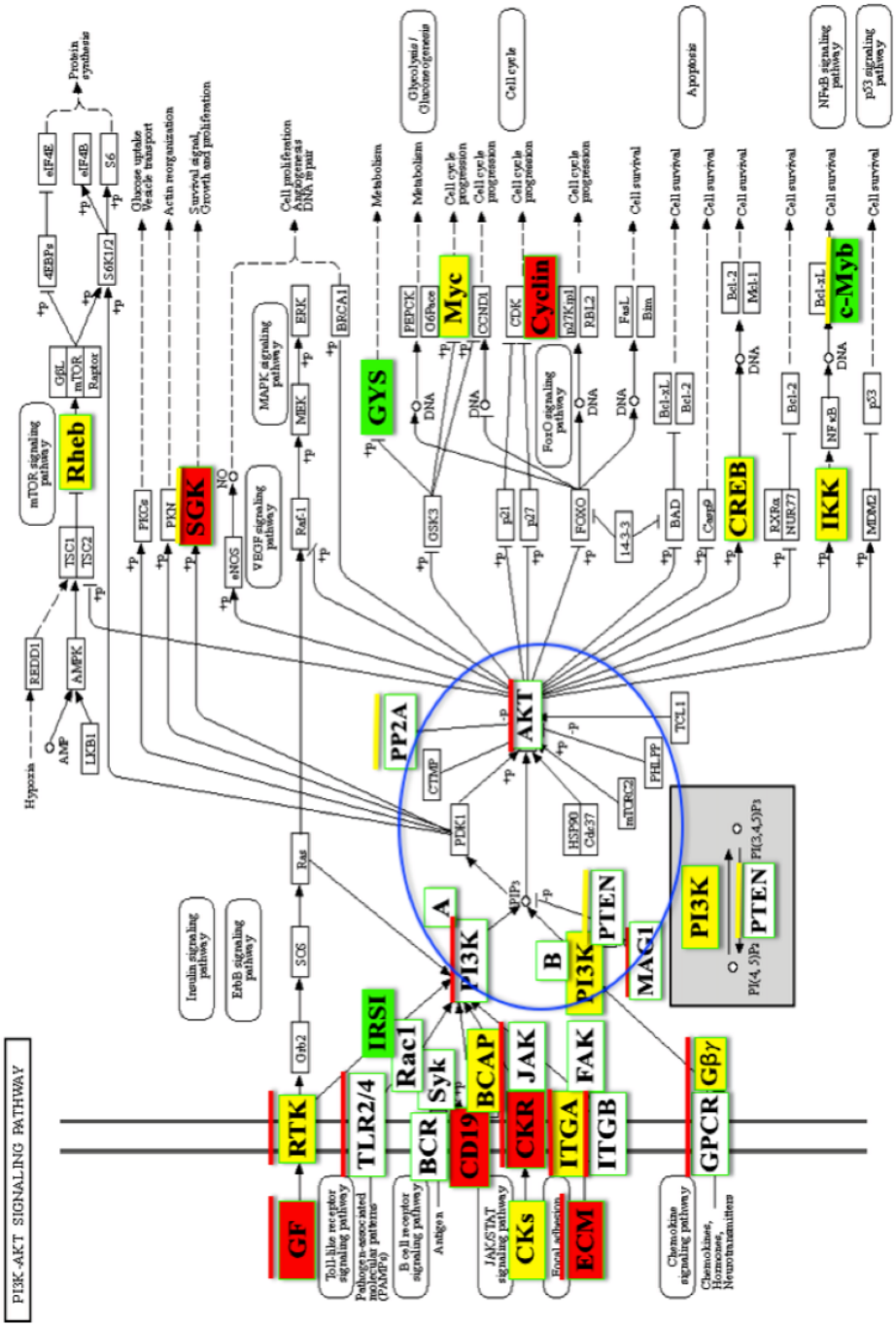

Figure 4.9. PI3K/AKT signalling pathway in patient 2. Red-fill: upregulated genes in both tumour regions, green-fill: upregulated in region 1, yellow-fill: upregulated in region 2, red line above gene name: downregulated in both tumour regions, green line above gene name: downregulated in region 1, yellow line under gene name: down regulated in region 2.

Table 4.6. Expression of the genes involved in PI3K/AKT pathway in patient 2.

KEGG Entry	Symbol	Description	T1	T2
hsa:9134	CCNE2	cyclin E2	**2.5**	**4.1**
hsa:930	CD19	CD19 molecule	**3.0**	**4.1**
hsa:1280	COL2A1	collagen type II alpha 1 chain	**2.7**	**3.7**
hsa:1950	EGF	epidermal growth factor	**3.4**	**4.0**
hsa:3559	IL2RA	interleukin 2 receptor subunit alpha	**2.6**	**2.4**
hsa:9180	OSMR	oncostatin M receptor	**3.1**	**4.2**
hsa:10110	SGK2	serum/glucocorticoid regulated kinase 2	**4.5**	**3.2**
hsa:6696	SPP1	secreted phosphoprotein 1	**27.3**	**80.6**
hsa:10000	AKT3	AKT serine/threonine kinase 3	-2.1	-2.7
hsa:284	ANGPT1	angiopoietin 1	-2.5	-6.3
hsa:1282	COL4A1	collagen type IV alpha 1 chain	-2.3	-3.1
hsa:1284	COL4A2	collagen type IV alpha 2 chain	-2.7	-2.7
hsa:1285	COL4A3	collagen type IV alpha 3 chain	-2.0	-2.8
hsa:1286	COL4A4	collagen type IV alpha 4 chain	-2.1	-3.8
hsa:1287	COL4A5	collagen type IV alpha 5 chain	-3.4	-8.0
hsa:1288	COL4A6	collagen type IV alpha 6 chain	-3.5	-13.0
hsa:1291	COL6A1	collagen type VI alpha 1 chain	-2.9	-2.5
hsa:1292	COL6A2	collagen type VI alpha 2 chain	-2.4	-3.1
hsa:131873	COL6A6	collagen type VI alpha 6 chain	-2.4	-4.6
hsa:1943	EFNA2	ephrin A2	-2.4	-3.1
hsa:8817	FGF18	fibroblast growth factor 18	-2.6	-3.2
hsa:2247	FGF2	fibroblast growth factor 2	-2.9	-7.9
hsa:2252	FGF7	fibroblast growth factor 7	-2.6	-5.0
hsa:2264	FGFR4	fibroblast growth factor receptor 4	-3.6	-10.1
hsa:2690	GHR	growth hormone receptor	-2.4	-2.4
hsa:59345	GNB4	G protein subunit beta 4	-2.2	-3.3
hsa:2791	GNG11	G protein subunit gamma 11	-2.2	-8.4
hsa:3082	HGF	hepatocyte growth factor	-2.2	-3.1
hsa:3563	IL3RA	interleukin 3 receptor subunit alpha	-2.1	-4.5
hsa:3569	IL6	interleukin 6	-3.3	-3.6
hsa:3673	ITGA2	integrin subunit alpha 2	-3.7	-4.1
hsa:8516	ITGA8	integrin subunit alpha 8	-3.5	-9.3
hsa:3717	JAK2	Janus kinase 2	-2.1	-3.4
hsa:3791	KDR	kinase insert domain receptor	-2.4	-2.5
hsa:284217	LAMA1	laminin subunit alpha 1	-2.2	-3.1
hsa:3908	LAMA2	laminin subunit alpha 2	-2.8	-4.0
hsa:3912	LAMB1	laminin subunit beta 1	-2.3	-3.6
hsa:22798	LAMB4	laminin subunit beta 4	-2.4	-6.3
hsa:3918	LAMC2	laminin subunit gamma 2	-2.6	-2.5
hsa:10161	LPAR6	lysophosphatidic acid receptor 6	-2.2	-3.1
hsa:9863	MAGI2	membrane associated guanylate kinase, WW and PDZ d	-2.9	-5.0
hsa:4915	NTRK2	neurotrophic receptor tyrosine kinase 2	-3.4	-16.4
hsa:5156	PDGFRA	platelet derived growth factor receptor alpha	-3.5	-3.6
hsa:5290	PIK3CA	phosphatidylinositol-4,5-bisphosphate 3-kinase catalytic	-2.1	-2.4
hsa:5295	PIK3R1	phosphoinositide-3-kinase regulatory subunit 1	-2.3	-2.9
hsa:8503	PIK3R3	phosphoinositide-3-kinase regulatory subunit 3	-3.8	-3.8
hsa:5649	RELN	reelin	-4.0	-4.7
hsa:7097	TLR2	toll like receptor 2	-2.0	-2.4
hsa:7148	TNXB	tenascin XB	-3.2	-3.8

Table 4.6-continued

hsa:2250	FGF5	fibroblast growth factor 5	**14.0**	/
hsa:2997	GYS1	glycogen synthase 1	**2.7**	/
hsa:3667	IRS1	insulin receptor substrate 1	**3.4**	/
hsa:4254	KITLG	KIT ligand	**3.3**	/
hsa:5228	PGF	placental growth factor	**3.5**	/
hsa:7060	THBS4	thrombospondin 4	**2.5**	/
hsa:4602	MYB	MYB proto-oncogene, transcription factor	**3.6**	-2.1
hsa:898	CCNE1	cyclin E1	/	**3.6**
hsa:1277	COL1A1	collagen type I alpha 1 chain	/	**3.5**
hsa:148327	CREB3L4	cAMP responsive element binding protein 3 like 4	/	**2.2**
hsa:1956	EGFR	epidermal growth factor receptor	/	**2.4**
hsa:2056	EPO	erythropoietin	/	**2.1**
hsa:26281	FGF20	fibroblast growth factor 20	/	**2.1**
hsa:2783	GNB2	G protein subunit beta 2	/	**2.1**
hsa:2786	GNG4	G protein subunit gamma 4	/	**2.4**
hsa:3551	IKBKB	inhibitor of nuclear factor kappa B kinase subunit beta	/	**2.9**
hsa:3565	IL4	interleukin 4	/	**2.1**
hsa:3678	ITGA5	integrin subunit alpha 5	/	**2.4**
hsa:3911	LAMA5	laminin subunit alpha 5	/	**2.0**
hsa:4609	MYC	MYC proto-oncogene, bHLH transcription factor	/	**2.7**
hsa:4803	NGF	nerve growth factor	/	**2.0**
hsa:118788	PIK3AP1	phosphoinositide-3-kinase adaptor protein 1	/	**2.4**
hsa:146850	PIK3R6	phosphoinositide-3-kinase regulatory subunit 6	/	**2.1**
hsa:6009	RHEB	Ras homolog, mTORC1 binding	/	**2.8**
hsa:7423	VEGFB	vascular endothelial growth factor B	/	**2.2**
hsa:80310	PDGFD	platelet derived growth factor D	-2.3	/
hsa:3690	ITGB3	integrin subunit beta 3	-2.1	/
hsa:3439	IFNA1	interferon alpha 1	-2.0	/
hsa:2254	FGF9	fibroblast growth factor 9	-4.6	/
hsa:374	AREG	amphiregulin	/	-2.0
hsa:1436	CSF1R	colony stimulating factor 1 receptor	/	-2.1
hsa:2263	FGFR2	fibroblast growth factor receptor 2	/	-2.1
hsa:2322	FLT3	fms related receptor tyrosine kinase 3	/	-2.4
hsa:2335	FN1	fibronectin 1	/	-2.1
hsa:3479	IGF1	insulin like growth factor 1	/	-2.3
hsa:3560	IL2RB	interleukin 2 receptor subunit beta	/	-2.9
hsa:3570	IL6R	interleukin 6 receptor	/	-3.6
hsa:3574	IL7	interleukin 7	/	-2.7
hsa:3672	ITGA1	integrin subunit alpha 1	/	-2.3
hsa:3676	ITGA4	integrin subunit alpha 4	/	-2.7
hsa:3693	ITGB5	integrin subunit beta 5	/	-2.2
hsa:3815	KIT	KIT proto-oncogene, receptor tyrosine kinase	/	-2.5
hsa:3909	LAMA3	laminin subunit alpha 3	/	-2.5
hsa:3910	LAMA4	laminin subunit alpha 4	/	-3.1
hsa:10319	LAMC3	laminin subunit gamma 3	/	-2.4
hsa:1902	LPAR1	lysophosphatidic acid receptor 1	/	-2.7
hsa:5154	PDGFA	platelet derived growth factor subunit A	/	-2.8
hsa:5521	PPP2R2B	protein phosphatase 2 regulatory subunit Bbeta	/	-2.3
hsa:5525	PPP2R5A	protein phosphatase 2 regulatory subunit B'alpha	/	-2.2
hsa:5526	PPP2R5B	protein phosphatase 2 regulatory subunit B'beta	/	-2.0
hsa:5728	PTEN	phosphatase and tensin homolog	/	-2.7
hsa:6446	SGK1	serum/glucocorticoid regulated kinase 1	/	-2.4
hsa:7450	VWF	von Willebrand factor	/	-3.4

T1: tumour region 1, T2: tumour region 2. (+): denotes upregulated, (-): denotes down-regulated. Colour code: from red to yellow: from the highest to the lowest upregulated fold change values, dark to light green: the highest to the lowest downregulated fold change values.

4.4.3.6. PI3K-AKT signalling pathway in patient 3

Twenty three genes, involved in the PI3K-AKT pathway, were upregulated in both T1 and T2 including extracellular matrix encoding genes such as *COL1A1, COL2A1, COL9A1*, *TNC*, *LAMA1*, *LAMC1* and *ITGD8*. In addition *CCNE1/2*, *BCL2* and growth hormones such as *NGF* and *PDGFD* as well as cytokines such as *IFNα2* were elevated in both T1 and T2 (Table 4.7). Thirty eight genes were down-regulated in both T1 and T2 compared to normal tissue. Among these genes are *COL4/5, ITGA1, 2, 3, 8* and *B6*, and also *LAMA 2,4* and *G3*, *TNXB*. Some growth factors were also down-regulated in both T1 and T2 including *FGF2*, *FGF5*, *FGF9*, *FGF4*, *GHR*, *HGF*, in addition to cytokines such as *IL4, IL2* and *IL3* receptors subunit alpha. *PIK3RI*, *PTEN*, *PKC* (Table 4.7). *EGF* was upregulated in T1 and down regulated in T2 with a 6.3-fold difference. T1 had 11 genes uniquely upregulated including phosphatase 2, *JAK3*, *IGF*, *FGF3*, *ITG* and *MYB* (Table 4.7). Six genes were downregulated in T1 including protein kinase N2, *NTF3*, *FGF18*, *LPAR5/6*. T2 had seven genes upregulated including *IFNα1*, *IL6R*, *FGF19, FGFR2*, *EIF4E* and *COL4*. Also there were seventeen uniquely downregulated genes in T2 including *COL4*, *FOXO3*, *IL6*, *ITGs, RELN, TSP4* and others (Table 4.7). All the above mentioned genes that showed similarity or differences in their expression profile among T1 and T2 are summarized in figure 4.10. Shared upregulated and downregulated genes detected in both tumour regions are listed in red-fill boxes and red-lines, respectively. Upregulated and down-regulated genes in T1 are in green-fill boxes and green lines, respectively, while upregulated and down-regulated genes in T2 are in yellow-fill boxes and yellow lines, respectively (Figure 4.10).

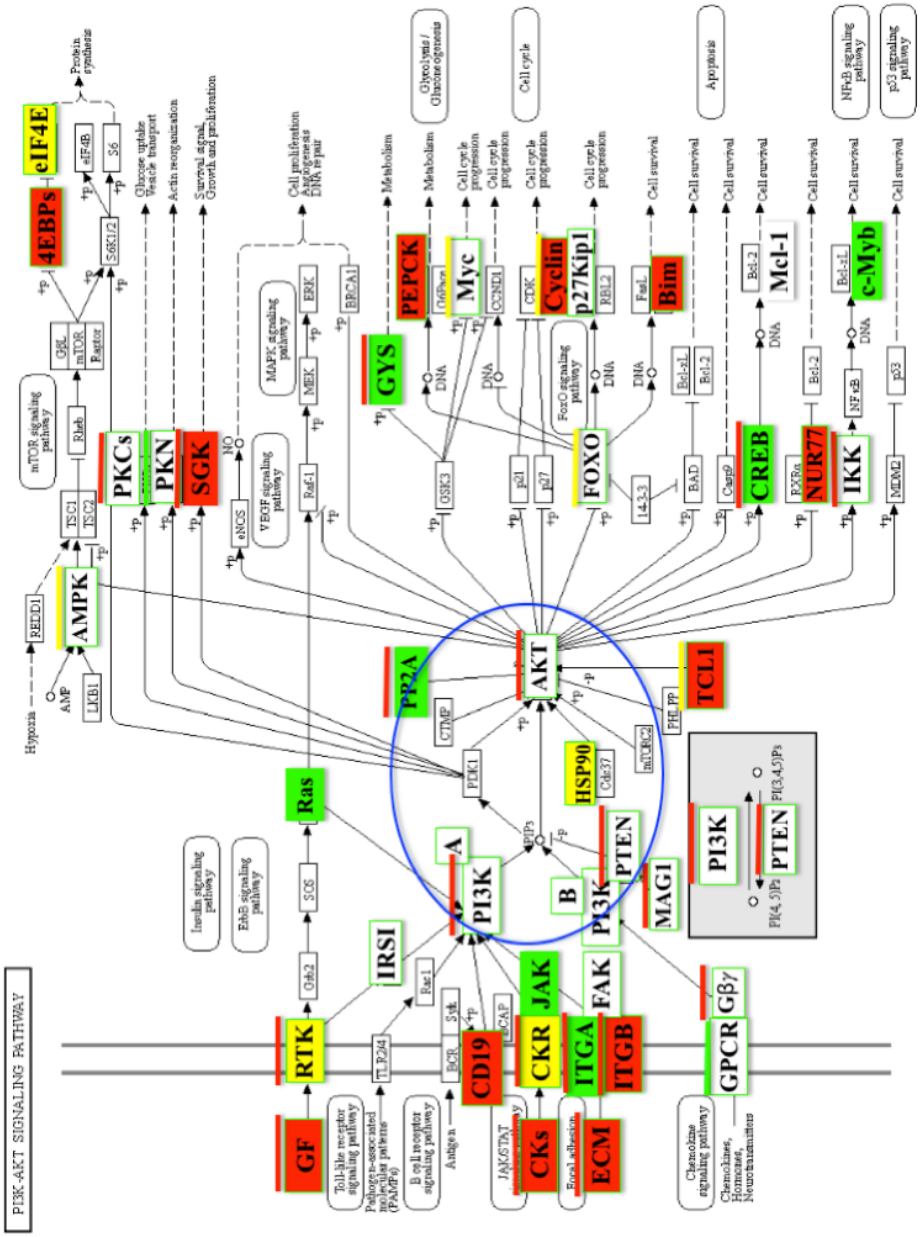

Figure 4.10. PI3K/AKT signalling pathway in patient 3. Red-fill: upregulated genes in both tumour regions, green-fill: upregulated in region 1, yellow-fill: upregulated in region 2, red line above gene name: downregulated in both tumour regions, green line above gene name: downregulated in region 1, yellow line under gene name: down regulated in region 2.

Table 4.7. Expression of the genes involved in PI3K/AKT in patient 3.

KEGG Entry	Symbol	Description	T1	T2
hsa:10018	BCL2L11	BCL2 like 11	3.2	2.0
hsa:898	CCNE1	cyclin E1	6.9	4.5
hsa:9134	CCNE2	cyclin E2	5.1	2.9
hsa:930	CD19	CD19 molecule	16.1	15.8
hsa:1277	COL1A1	collagen type I alpha 1 chain	3.5	4.5
hsa:1280	COL2A1	collagen type II alpha 1 chain	16.2	11.1
hsa:1297	COL9A1	collagen type IX alpha 1 chain	31.0	8.0
hsa:1943	EFNA2	ephrin A2	2.1	2.5
hsa:1945	EFNA4	ephrin A4	3.5	2.6
hsa:1978	EIF4EBP1	eukaryotic translation initiation factor 4E binding protein 1	5.7	6.2
hsa:3440	IFNA2	interferon alpha 2	3.1	2.2
hsa:3696	ITGB8	integrin subunit beta 8	4.0	2.3
hsa:284217	LAMA1	laminin subunit alpha 1	5.3	11.3
hsa:3915	LAMC1	laminin subunit gamma 1	2.1	2.2
hsa:4803	NGF	nerve growth factor	3.5	4.0
hsa:3164	NR4A1	nuclear receptor subfamily 4 group A member 1	2.2	2.4
hsa:5105	PCK1	phosphoenolpyruvate carboxykinase 1	2.6	2.3
hsa:80310	PDGFD	platelet derived growth factor D	2.8	2.4
hsa:10110	SGK2	serum/glucocorticoid regulated kinase 2	2.8	2.1
hsa:6696	SPP1	secreted phosphoprotein 1	46.3	12.3
hsa:8115	TCL1A	T cell leukemia/lymphoma 1A	2.8	2.1
hsa:7058	THBS2	thrombospondin 2	3.2	2.7
hsa:3371	TNC	tenascin C	3.6	2.3
hsa:10000	AKT3	AKT serine/threonine kinase 3	-2.3	-2.3
hsa:284	ANGPT1	angiopoietin 1	-9.0	-7.8
hsa:1287	COL4A5	collagen type IV alpha 5 chain	-4.4	-5.9
hsa:1288	COL4A6	collagen type IV alpha 6 chain	-10.0	-9.2
hsa:131873	COL6A6	collagen type VI alpha 6 chain	-4.5	-4.5
hsa:9586	CREB5	cAMP responsive element binding protein 5	-4.7	-4.6
hsa:1435	CSF1	colony stimulating factor 1	-3.0	-3.3
hsa:1442	CSH1	chorionic somatomammotropin hormone 1	-2.5	-2.5
hsa:1969	EPHA2	EPH receptor A2	-2.2	-2.2
hsa:2246	FGF1	fibroblast growth factor 1	-2.1	-3.0

Table 4.7-continued

hsa:2247	FGF2	fibroblast growth factor 2	-2.1	-3.5
hsa:2250	FGF5	fibroblast growth factor 5	-2.9	-2.9
hsa:2254	FGF9	fibroblast growth factor 9	-4.1	-5.1
hsa:2264	FGFR4	fibroblast growth factor receptor 4	-5.5	-7.1
hsa:2324	FLT4	fms related receptor tyrosine kinase 4	-2.1	-2.3
hsa:2690	GHR	growth hormone receptor	-3.4	-4.6
hsa:2791	GNG11	G protein subunit gamma 11	-10.0	-9.4
hsa:2997	GYS1	glycogen synthase 1	-3.7	-3.4
hsa:3082	HGF	hepatocyte growth factor	-2.1	-2.7
hsa:3551	IKBKB	inhibitor of nuclear factor kappa B kinase subunit beta	-2.6	-2.2
hsa:3559	IL2RA	interleukin 2 receptor subunit alpha	-4.9	-2.3
hsa:3563	IL3RA	interleukin 3 receptor subunit alpha	-2.9	-4.1
hsa:3565	IL4	interleukin 4	-3.9	-2.9
hsa:3575	IL7R	interleukin 7 receptor	-4.1	-4.0
hsa:3672	ITGA1	integrin subunit alpha 1	-4.5	-4.4
hsa:3673	ITGA2	integrin subunit alpha 2	-4.7	-5.0
hsa:3675	ITGA3	integrin subunit alpha 3	-2.1	-2.1
hsa:8516	ITGA8	integrin subunit alpha 8	-14.7	-14.7
hsa:3694	ITGB6	integrin subunit beta 6	-2.7	-2.6
hsa:3791	KDR	kinase insert domain receptor	-8.0	-12.5
hsa:4254	KITLG	KIT ligand	-4.0	-3.9
hsa:3908	LAMA2	laminin subunit alpha 2	-3.7	-4.2
hsa:3910	LAMA4	laminin subunit alpha 4	-2.4	-2.4
hsa:10319	LAMC3	laminin subunit gamma 3	-10.6	-9.3
hsa:9863	MAGI2	membrane associated guanylate kinase, WW and PDZ 2	-5.1	-6.3
hsa:4233	MET	MET proto-oncogene, receptor tyrosine kinase	-2.2	-2.1
hsa:4915	NTRK2	neurotrophic receptor tyrosine kinase 2	-16.1	-26.1
hsa:5154	PDGFA	platelet derived growth factor subunit A	-5.7	-5.4
hsa:5228	PGF	placental growth factor	-4.1	-4.5
hsa:8503	PIK3R3	phosphoinositide-3-kinase regulatory subunit 3	-2.3	-4.7
hsa:5525	PPP2R5A	protein phosphatase 2 regulatory subunit B'alpha	-2.2	-3.0
hsa:5526	PPP2R5B	protein phosphatase 2 regulatory subunit B'beta	-2.5	-3.6
hsa:5578	PRKCA	protein kinase C alpha	-3.8	-2.5
hsa:5728	PTEN	phosphatase and tensin homolog	-3.7	-4.7
hsa:23678	SGK3	serum/glucocorticoid regulated kinase family member 3	-2.1	-2.3
hsa:7148	TNXB	tenascin XB	-3.3	-4.0
hsa:7424	VEGFC	vascular endothelial growth factor C	-2.0	-2.6
hsa:7450	VWF	von Willebrand factor	-7.6	-4.6

Table 4.7-continued

hsa:1950	EGF	epidermal growth factor	2.0	-4.3
hsa:148327	CREB3L4	cAMP responsive element binding protein 3 like 4	2.5	/
hsa:2248	FGF3	fibroblast growth factor 3	2.9	/
hsa:2998	GYS2	glycogen synthase 2	2.2	/
hsa:3479	IGF1	insulin like growth factor 1	2.1	/
hsa:22801	ITGA11	integrin subunit alpha 11	2.6	/
hsa:3718	JAK3	Janus kinase 3	2.3	/
hsa:4602	MYB	MYB proto-oncogene, transcription factor	2.9	/
hsa:4893	NRAS	NRAS proto-oncogene, GTPase	2.6	/
hsa:5519	PPP2R1B	protein phosphatase 2 scaffold subunit Abeta	2.2	/
hsa:5522	PPP2R2C	protein phosphatase 2 regulatory subunit Bgamma	3.5	/
hsa:5523	PPP2R3A	protein phosphatase 2 regulatory subunit B"alpha	2.9	/
hsa:256076	COL6A5	collagen type VI alpha 5 chain	/	3.5
hsa:1977	EIF4E	eukaryotic translation initiation factor 4E	/	2.1
hsa:9965	FGF19	fibroblast growth factor 19	/	2.1
hsa:2263	FGFR2	fibroblast growth factor receptor 2	/	2.1
hsa:3320	HSP90AA1	heat shock protein 90 alpha family class A member 1	/	2.0
hsa:3452	IFNA21	interferon alpha 21	/	2.2
hsa:3570	IL6R	interleukin 6 receptor	/	2.1
hsa:57121	LPAR5	lysophosphatidic acid receptor 5	-2.4	/
hsa:10161	LPAR6	lysophosphatidic acid receptor 6	-2.3	/
hsa:1129	CHRM2	cholinergic receptor muscarinic 2	-3.0	/
hsa:8817	FGF18	fibroblast growth factor 18	-2.1	/
hsa:4908	NTF3	neurotrophin 3	-2.2	/
hsa:5586	PKN2	protein kinase N2	-2.1	/
hsa:374	AREG	amphiregulin	/	-4.5
hsa:896	CCND3	cyclin D3	/	-2.2
hsa:1282	COL4A1	collagen type IV alpha 1 chain	/	-2.3
hsa:1285	COL4A3	collagen type IV alpha 3 chain	/	-2.5
hsa:2064	ERBB2	erb-b2 receptor tyrosine kinase 2	/	-2.0
hsa:2309	FOXO3	forkhead box O3	/	-2.3
hsa:3569	IL6	interleukin 6	/	-9.1
hsa:3688	ITGB1	integrin subunit beta 1	/	-2.1
hsa:3690	ITGB3	integrin subunit beta 3	/	-2.4
hsa:9223	MAGI1	membrane associated guanylate kinase, WW and PDZ domain	/	-2.2
hsa:4609	MYC	MYC proto-oncogene, bHLH transcription factor	/	-2.1
hsa:5516	PPP2CB	protein phosphatase 2 catalytic subunit beta	/	-2.0
hsa:5562	PRKAA1	protein kinase AMP-activated catalytic subunit alpha 1	/	-2.3
hsa:5649	RELN	reelin	/	-2.4
hsa:6446	SGK1	serum/glucocorticoid regulated kinase 1	/	-2.8
hsa:9623	TCL1B	T cell leukemia/lymphoma 1B	/	-2.2
hsa:7060	THBS4	thrombospondin 4	/	-2.4

T1: tumour region 1, T2: tumour region 2. (+): denotes upregulated, (-): denotes down-regulated. Colour code: from red to yellow: from the highest to the lowest upregulated fold change values, dark to light green: the highest to the lowest downregulated fold change values.

4.4.3.7. JAK/STAT signalling pathway in patient 1

The two tumour regions (T1 and T2) shared an increased *IL23R* and suppressor of cytokine signalling 1 (*SOCS1*). T1 and T2 also shared eight downregulated genes including *IL4, IL2*, *IL5* and *IL7* receptors, and *PDGFA* (Table 4.8). Two interleukin receptors; *IL13RA2* and *IL20RA* were down regulated in T1 and upregulated in T2. T1 had 18 upregulated genes, which were unchanged T2, including interferons, interferon receptors, cytokines, thrombopoietin growth factor, and *STATs 1, 4, 5* as well as platelet derived growth factor receptor alpha. In contrast, T2 had ten upregulated genes, unchanged in T1, including *STAT6*, *PIM1* and some cytokines and cytokines receptors (Table 4.8). T1 had 11 uniquely down-regulated genes including *SOCS 2* and *3*, *PIK3R3*, *MYC* and *IL6* and its signal transducer (*IL6ST*), in addition to growth factor receptors. In contrast, six genes were uniquely downregulated in T2 from this patient, four of them are cytokines receptors (Table 4.8). The overall differences between the two tumour regions detected by the arrays are summarized in figure 4.11-A. Both regions had elevated and lowered expression of cytokines/cytokines receptor. *STATs* were elevated in both tumour regions in addition to *SOCS*. T2 possesses elevated *Bcl-2* and *PIM1*, while T1 has some elevated growth factors *PIM1/2/3* were elevated in both tumour regions by microarray analysis (Figure 4.11-B). *PIM1/2/3* were also elevated by qRT-PCR in both tumour regions (Figure 4.11-C). Increased *PIM1* and *2* were observed in T2 compared to T1 but this was not statistically significant. *PIM3* expression was higher in T1 compared to T2 ($p=0.04$).

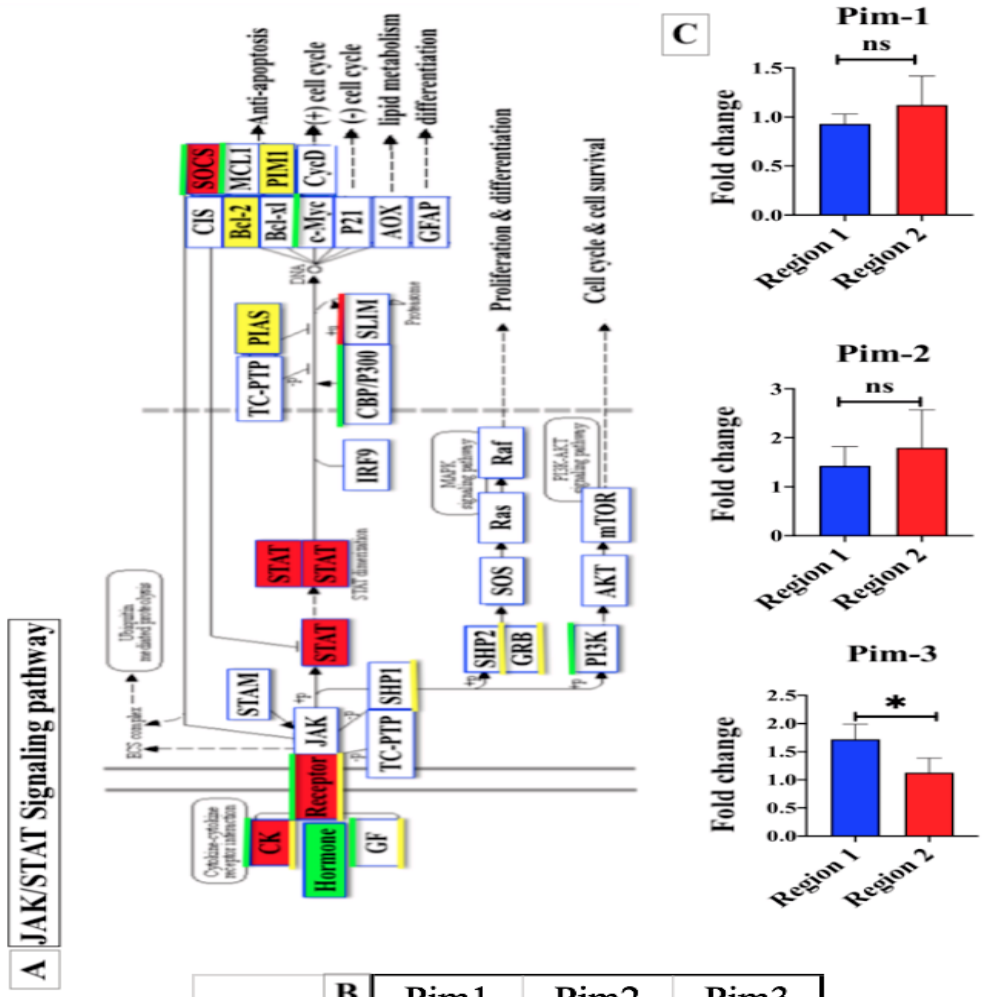

B	Pim1	Pim2	Pim3
Region 1	1.5	6.6	1.3
Region 2	2.6	1.3	1.8

Figure 4.11. JAK/STAT signalling pathway in patient 1. A. genes detected dysregulated in JAK/STAT pathway by arrayStar®: Red fill: upregulated in both regions, red line above gene name: down-regulated in both tumour regions, green fill: upregulated in T1, green line above gene symbol: down-regulated in T1, yellow fill: upregulated in T2, yellow line under gene symbol: down-regulated in T2. **B**. PIM1/2/3expression in the two tumour regions as detected by ArrayStar®. **C**. qRT-PCR validation of PIM1/2/3 in the two tumour regions of patient 1, *: (p=0.04).

Table 4.8. Expression of genes involved in JAK/STAT pathway in patient 1.

KEGG Entry	Symbol	Description	T1	T2
hsa:149233	IL23R	interleukin 23 receptor	2.1	2.5
hsa:8651	SOCS1	suppressor of cytokine signaling 1	2.8	2.5
hsa:2273	FHL1	four and a half LIM domains 1	-3.0	-2.0
hsa:3559	IL2RA	interleukin 2 receptor subunit alpha	-7.8	-3.5
hsa:3565	IL4	interleukin 4	-11.0	-4.4
hsa:3568	IL5RA	interleukin 5 receptor subunit alpha	-2.1	-2.0
hsa:3575	IL7R	interleukin 7 receptor	-2.4	-11.0
hsa:3953	LEPR	leptin receptor	-6.1	-3.6
hsa:3977	LIFR	LIF receptor subunit alpha	-19.4	-3.3
hsa:5154	PDGFA	platelet derived growth factor subunit A	-21.0	-2.3
hsa:3598	IL13RA2	interleukin 13 receptor subunit alpha 2	-2.8	3.2
hsa:53832	IL20RA	interleukin 20 receptor subunit alpha	-6.8	6.9
hsa:1438	CSF2RA	colony stimulating factor 2 receptor subunit alpha	3.6	/
hsa:1489	CTF1	cardiotrophin 1	2.9	/
hsa:3439	IFNA1	interferon alpha 1	9.9	/
hsa:3458	IFNG	interferon gamma	4	/
hsa:3460	IFNGR2	interferon gamma receptor 2	3.1	/
hsa:56832	IFNK	interferon kappa	2	/
hsa:282617	IFNL3	interferon lambda 3	2.4	/
hsa:3586	IL10	interleukin 10	2.5	/
hsa:51561	IL23A	interleukin 23 subunit alpha	2.4	/
hsa:9466	IL27RA	interleukin 27 receptor subunit alpha	2.5	/
hsa:3560	IL2RB	interleukin 2 receptor subunit beta	3.1	/
hsa:3952	LEP	leptin	2.1	/
hsa:4352	MPL	MPL proto-oncogene, thrombopoietin receptor	3.3	/
hsa:5156	PDGFRA	platelet derived growth factor receptor alpha	2.4	/
hsa:6772	STAT1	signal transducer and activator of transcription 1	5.3	/
hsa:6775	STAT4	signal transducer and activator of transcription 4	2.1	/
hsa:6776	STAT5A	signal transducer and activator of transcription 5A	5.3	/
hsa:7066	THPO	thrombopoietin	6.6	/

Table 4.8-continued

hsa:1387	CREBBP	CREB binding protein	**-2.1**	/
hsa:2690	GHR	growth hormone receptor	**-2.6**	/
hsa:3447	IFNA13	interferon alpha 13	**-3.1**	/
hsa:3569	IL6	interleukin 6	**-3.5**	/
hsa:3572	IL6ST	interleukin 6 signal transducer	**-3.5**	/
hsa:4170	MCL1	MCL1 apoptosis regulator, BCL2 family member	**-2.8**	/
hsa:4609	MYC	MYC proto-oncogene, bHLH transcription factor	**-7.9**	/
hsa:8503	PIK3R3	phosphoinositide-3-kinase regulatory subunit 3	**-2.1**	/
hsa:8835	SOCS2	suppressor of cytokine signaling 2	**-4.7**	/
hsa:9021	SOCS3	suppressor of cytokine signaling 3	**-2.2**	/
hsa:8027	STAM	signal transducing adaptor molecule	**-3.1**	/
hsa:596	BCL2	BCL2 apoptosis regulator	/	**2.2**
hsa:1437	CSF2	colony stimulating factor 2	/	**2.1**
hsa:3596	IL13	interleukin 13	/	**3.2**
hsa:58985	IL22RA1	interleukin 22 receptor subunit alpha 1	/	**17.9**
hsa:3574	IL7	interleukin 7	/	**3.4**
hsa:3976	LIF	LIF interleukin 6 family cytokine	/	**7.1**
hsa:10401	PIAS3	protein inhibitor of activated STAT 3	/	**2.8**
hsa:5292	PIM1	Pim-1 proto-oncogene, serine/threonine kinase	/	**2.6**
hsa:6778	STAT6	signal transducer and activator of transcription 6	/	**2.4**
hsa:85480	TSLP	thymic stromal lymphopoietin	/	**4.0**
hsa:2885	GRB2	growth factor receptor bound protein 2	/	**-2.3**
hsa:3601	IL15RA	interleukin 15 receptor subunit alpha	/	**-2.2**
hsa:3561	IL2RG	interleukin 2 receptor subunit gamma	/	**-2.0**
hsa:3563	IL3RA	interleukin 3 receptor subunit alpha	/	**-3.4**
hsa:5781	PTPN11	protein tyrosine phosphatase non-receptor type 11	/	**-2.0**
hsa:5777	PTPN6	protein tyrosine phosphatase non-receptor type 6	/	**-2.3**

T1: tumour region 1, T2: tumour region 2. (+): denotes upregulated, (-): denotes down-regulated. Colour code: from red to yellow: from the highest to the lowest upregulated fold change values, dark to light green: the highest to the lowest downregulated fold change values.

4.4.3.8. JAK/STAT signalling pathway in patient 2

The ratio of upregulated and down-regulated genes involved in the JAK/STAT pathway was 1 to 3 in T1 and T2, respectively. Upregulated genes in T2 were approximately triple that in T1 (9:4), also T2 had approximately double the number of down-regulated genes than in T1 (24:14). Three genes including epidermal growth factor receptor (*EGFR*), IL2 receptor (*IL2RA*) and Oncostatin M receptor (*OSMR*) were upregulated in both T1 and T2 with no significant difference (Table 4.9). Thirteen genes involve in the JAK/STAT pathway were down-regulated in both T1 and T2, including *JAK2* , *AKT* and *PI3K* (marked with red line above their gene symbols) (Figure 4.12-A). *PIM1/2/3* were decreased in T1, while in T2; *PIM1* was increased, *PIM2* decreased and *PIM3* expression was unchanged by microarray analysis (Figure 4.12-B). Validation of *PIM1/2/3* by quantitative RT-PCR showed a less than two-fold increase in the *PIM1*, *PIM2* and *PIM3* compared to normal tissue. *PIM3* expression was significantly different between T1 and T2 ($p=0.03$) (Figure 4.12-C).

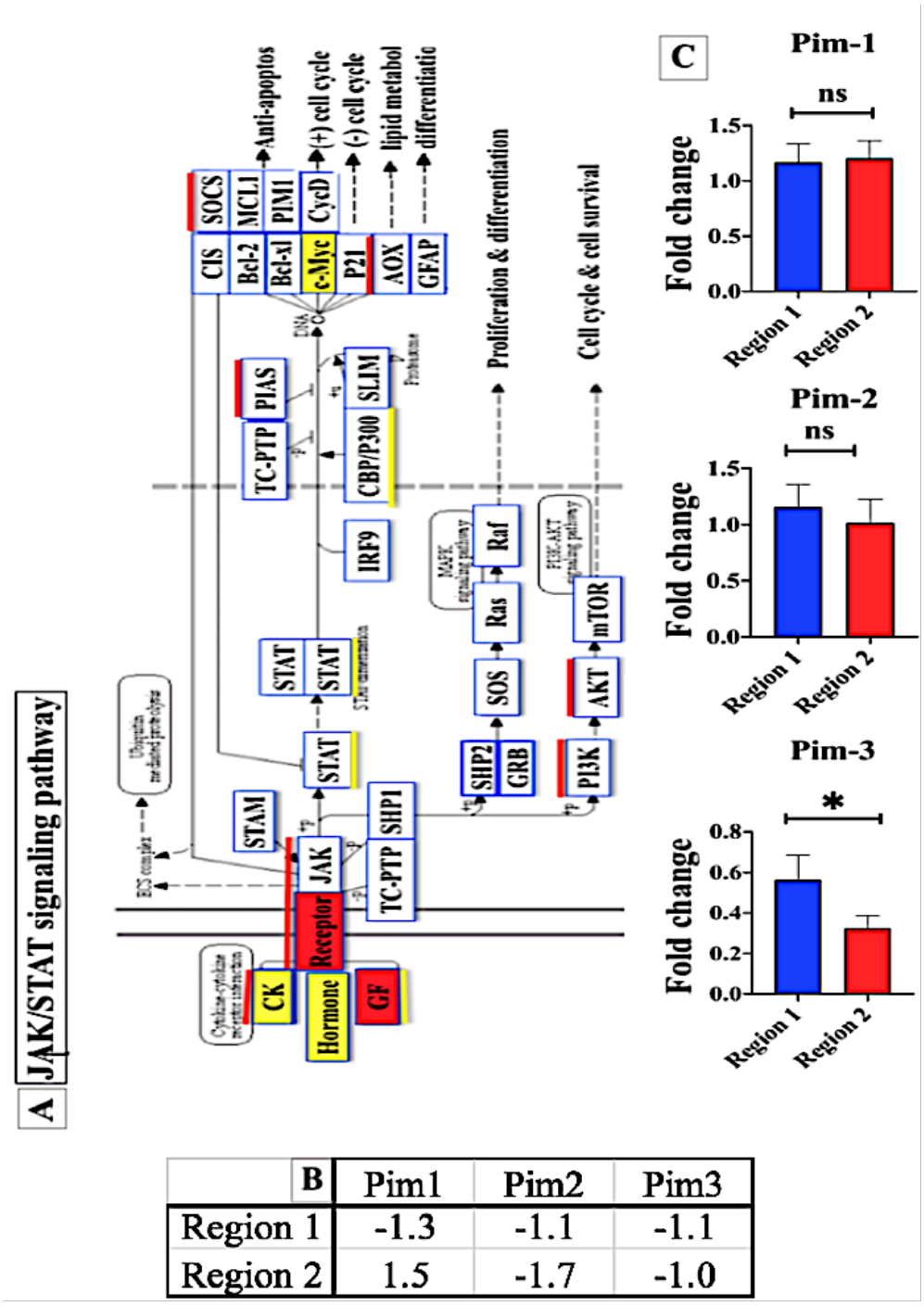

B	Pim1	Pim2	Pim3
Region 1	-1.3	-1.1	-1.1
Region 2	1.5	-1.7	-1.0

Figure 4.12. JAK/STAT signalling pathway in patient 2. A. genes detected dysregulated in JAK/STAT pathway by arrayStar®: Red fill: upregulated in both regions, red line above gene name: down-regulated in both tumour regions, yellow fill: upregulated in region 2, yellow line under gene symbol: down-regulated in region 2. **B**. PIM1/2/3 levels in the two tumour regions as detected by arrayStar®. **C**. qRT-PCR assessment of PIM1/2/3 in the two tumour regions of patient 2, *: (p=0.03).

Table 4.9. Expression of the genes involved in the JAK/STAT pathway in patient 2.

KEGG Entry	Symbol	Description	T1	T2
hsa:1950	EGF	epidermal growth factor	3.4	4.0
hsa:3559	IL2RA	interleukin 2 receptor subunit alpha	2.6	2.4
hsa:9180	OSMR	oncostatin M receptor	3.1	4.2
hsa:10000	AKT3	AKT serine/threonine kinase 3	-2.1	-2.7
hsa:316	AOX1	aldehyde oxidase 1	-3.3	-5.5
hsa:2690	GHR	growth hormone receptor	-2.4	-2.4
hsa:3563	IL3RA	interleukin 3 receptor subunit alpha	-2.1	-4.5
hsa:3569	IL6	interleukin 6	-3.3	-3.7
hsa:3717	JAK2	Janus kinase 2	-2.1	-3.4
hsa:3953	LEPR	leptin receptor	-2.5	-14.9
hsa:5156	PDGFRA	platelet derived growth factor receptor alpha	-3.5	-3.6
hsa:10401	PIAS3	protein inhibitor of activated STAT 3	-2.4	-3.0
hsa:5290	PIK3CA	phosphatidylinositol-4,5-bisphosphate 3-kinase catalytic sub. alpha	-2.1	-2.4
hsa:5295	PIK3R1	phosphoinositide-3-kinase regulatory subunit 1	-2.3	-2.9
hsa:8503	PIK3R3	phosphoinositide-3-kinase regulatory subunit 3	-3.8	-3.8
hsa:8651	SOCS1	suppressor of cytokine signaling 1	-4.0	-2.4
hsa:116379	IL22RA2	interleukin 22 receptor subunit alpha 2	3.4	/
hsa:3439	IFNA1	interferon alpha 1	-2.0	/
hsa:1271	CNTFR	ciliary neurotrophic factor receptor	/	2.1
hsa:1956	EGFR	epidermal growth factor receptor	/	2.4
hsa:2056	EPO	erythropoietin	/	2.1
hsa:3601	IL15RA	interleukin 15 receptor subunit alpha	/	3.1
hsa:3565	IL4	interleukin 4	/	2.1
hsa:4609	MYC	MYC proto-oncogene, bHLH transcription factor	/	2.7
hsa:1387	CREBBP	CREB binding protein	/	-2.2
hsa:3458	IFNG	interferon gamma	/	-3.0
hsa:3600	IL15	interleukin 15	/	-2.0
hsa:3560	IL2RB	interleukin 2 receptor subunit beta	/	-2.9
hsa:3570	IL6R	interleukin 6 receptor	/	-3.6
hsa:3574	IL7	interleukin 7	/	-2.7
hsa:5154	PDGFA	platelet derived growth factor subunit A	/	-2.8
hsa:8835	SOCS2	suppressor of cytokine signaling 2	/	-2.4
hsa:6775	STAT4	signal transducer and activator of transcription 4	/	-2.8
hsa:6777	STAT5B	signal transducer and activator of transcription 5B	/	-2.2
hsa:85480	TSLP	thymic stromal lymphopoietin	/	-2.5

T1: tumour region 1, T2: tumour region 2. (+): denotes upregulated, (-): denotes downregulated. Colour code: from red to yellow: from the highest to the lowest upregulated fold change values, dark to light green: the highest to the lowest downregulated fold change values.

4.4.3.9. JAK/STAT signalling pathway in patient 3

Microarray analysis identified nine genes involved in the JAK/STAT pathway upregulated in both T1 and T2 including *IL10*, *IL22RA2*, *PTPN2*, *THPO*, *IFNA2*, *IFNL3*, *STAM2* and *STAT5A*, *SOCS1* (Table 4.10) (Figure 4.13-A). 22 genes were downregulated in both T1 and T2 including CK, GF, PI3K receptor and *AKT3* in addition to *SOCS3* (Table 4.10), denoted as red line above gene symbols in figure 4.13-A. T1 had uniquely elevated *JAK3*, *SOCS4* and *EGF*, and decreased levels of *FHL1* and cytokine inducible SH2 containing protein (Table 4.10). T2 had elevated IFA/G, IL20 and IL6R, and also by decreased levels of STAT6/5B, *CYCD3*, *EGF,* IL6 and IL6 signal transducer (Table 4.10). In figure 4.13-A, genes that were upregulated/downregulated in T1 are denoted by green fill and green line above gene names, respectively. Genes that were up/downregulated in T2 are denoted by yellow fill and yellow lines below gene names, respectively. *PIM* kinase expression is a marker for activated JAK/STAT pathway and was assessed by the microarray followed by qRT-PCR in both T1 and T2 compared to N. Figure 4.13-B shows the expression profile of *PIM1/2/3* as detected by the microarray. qRT-PCR showed *PIM1*, *2, 3* were elevated less than 2-fold in both T1 and T2 and *PIM3* showed a significant difference between these regions ($p=0.01$) (Figure 4.13-C).

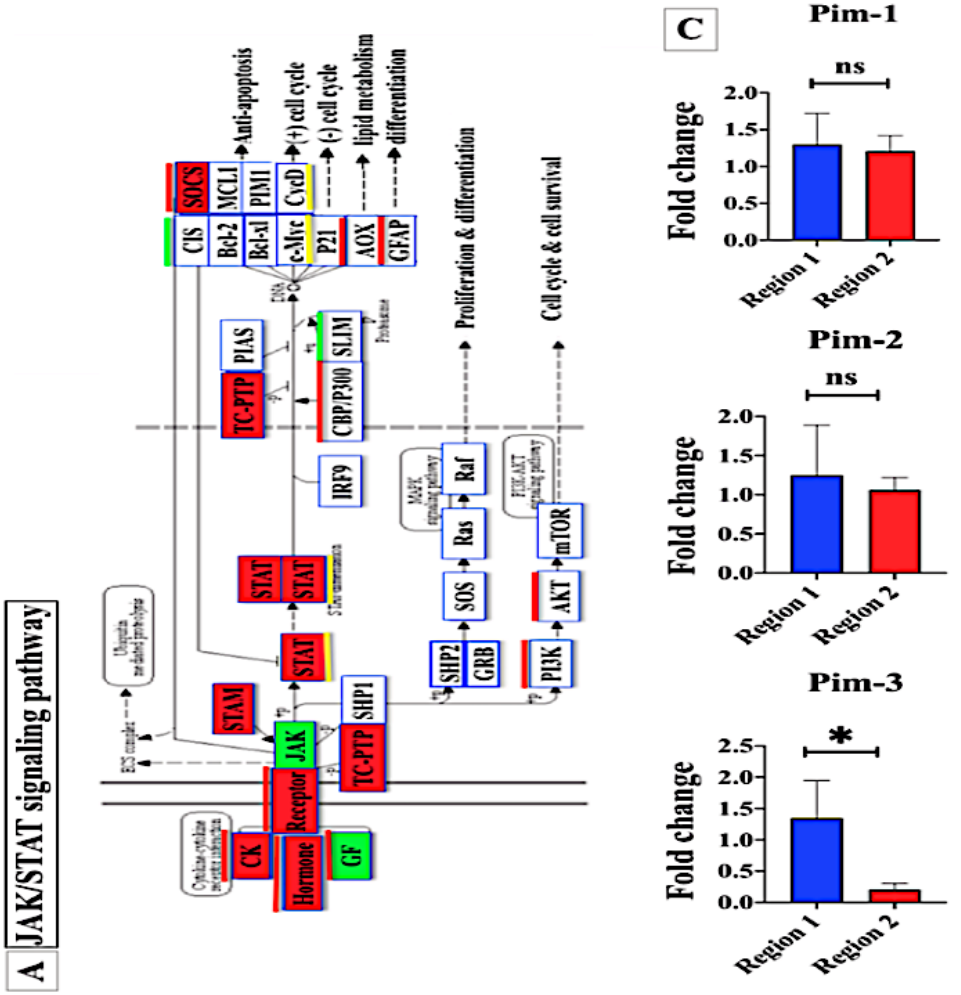

B	Pim1	Pim2	Pim3
Region 1	1.6	3.3	-1.1
Region 2	1.1	2.2	-1.8

Figure 4.13. JAK/STAT signalling pathway in patient 3. A. genes detected dysregulated in JAK/STAT pathway by arrayStar®: Red fill: upregulated in both regions, red line above gene name: down-regulated in both tumour regions, yellow fill: upregulated in region 2, yellow line under gene symbol: down-regulated in region 2. **B**. PIM1/2/3expression in the two tumour regions as detected by arrayStar®. **C**. qRT-PCR validation of PIM1/2/3 in the two tumour regions of patient 2, *: (p=0.01).

Table 4.10. Expression of the genes involved in JAK/STAT pathway in patient 3.

KEGG Entry	Symbol	Description	T1	T2
hsa:3440	IFNA2	interferon alpha 2	3.1	2.2
hsa:282617	IFNL3	interferon lambda 3	2.2	2.2
hsa:3586	IL10	interleukin 10	3.1	2.4
hsa:116379	IL22RA2	interleukin 22 receptor subunit alpha 2	3.8	2.8
hsa:5771	PTPN2	protein tyrosine phosphatase non-receptor type 2	3.8	2.7
hsa:8651	SOCS1	suppressor of cytokine signaling 1	2.4	2.9
hsa:10254	STAM2	signal transducing adaptor molecule 2	3.0	2.6
hsa:6776	STAT5A	signal transducer and activator of transcription 5A	3.0	2.3
hsa:7066	THPO	thrombopoietin	3.0	6.2
hsa:10000	AKT3	AKT serine/threonine kinase 3	-2.3	-2.3
hsa:316	AOX1	aldehyde oxidase 1	-6.3	-8.2
hsa:1387	CREBBP	CREB binding protein	-2.4	-3.0
hsa:1442	CSH1	chorionic somatomammotropin hormone 1	-2.5	-2.5
hsa:2670	GFAP	glial fibrillary acidic protein	-2.7	-2.7
hsa:2690	GHR	growth hormone receptor	-3.4	-4.6
hsa:3459	IFNGR1	interferon gamma receptor 1	-2.5	-3.3
hsa:3596	IL13	interleukin 13	-2.3	-2.3
hsa:3598	IL13RA2	interleukin 13 receptor subunit alpha 2	-3.1	-3.1
hsa:3600	IL15	interleukin 15	-2.3	-2.4
hsa:53832	IL20RA	interleukin 20 receptor subunit alpha	-18.8	-24.6
hsa:3559	IL2RA	interleukin 2 receptor subunit alpha	-4.9	-2.3
hsa:3563	IL3RA	interleukin 3 receptor subunit alpha	-2.9	-4.1
hsa:3565	IL4	interleukin 4	-3.9	-2.9
hsa:3575	IL7R	interleukin 7 receptor	-4.1	-4.0
hsa:3952	LEP	leptin	-2.1	-2.7
hsa:3953	LEPR	leptin receptor	-2.1	-9.8
hsa:3976	LIF	LIF interleukin 6 family cytokine	-2.2	-4.1
hsa:3977	LIFR	LIF receptor subunit alpha	-7.1	-16.1
hsa:5154	PDGFA	platelet derived growth factor subunit A	-5.7	-5.4
hsa:8503	PIK3R3	phosphoinositide-3-kinase regulatory subunit 3	-2.3	-4.7
hsa:9021	SOCS3	suppressor of cytokine signaling 3	-2.1	-2.6

Table 4.10-continued

hsa:1950	EGF	epidermal growth factor	**2.0**	**/**
hsa:3718	JAK3	Janus kinase 3	**2.3**	/
hsa:122809	SOCS4	suppressor of cytokine signaling 4	**3.4**	/
hsa:2273	FHL1	four and a half LIM domains 1	**-2.3**	/
hsa:1154	CISH	cytokine inducible SH2 containing protein	**-2.2**	/
hsa:3452	IFNA21	interferon alpha 21	/	**2.2**
hsa:3458	IFNG	interferon gamma	/	**2.3**
hsa:50604	IL20	interleukin 20	/	**2.4**
hsa:3570	IL6R	interleukin 6 receptor	/	**2.1**
hsa:896	CCND3	cyclin D3	/	**-2.2**
hsa:1950	EGF	epidermal growth factor	/	**-4.3**
hsa:3569	IL6	interleukin 6	/	**-9.1**
hsa:3572	IL6ST	interleukin 6 signal transducer	/	**-3.0**
hsa:4609	MYC	MYC proto-oncogene, bHLH transcription factor	/	**-2.1**
hsa:6777	STAT5B	signal transducer and activator of transcription 5B	/	**-2.1**
hsa:6778	STAT6	signal transducer and activator of transcription 6	/	**-2.2**
hsa:85480	TSLP	thymic stromal lymphopoietin	/	**-2.9**

T1: tumour region 1, T2: tumour region 2. (+): denotes upregulated, (-): denotes down-regulated. Colour code: from red to yellow: from the highest to the lowest upregulated fold change values, dark to light green: the highest to the lowest downregulated fold change values.

4.4.3.10. Mutated genes operating in *JAK*/*STAT* and *PI3K*/*AKT* pathways in patient 1.

Whole exome sequencing showed patient 1 had mutations in genes involved in *JAK*/*STAT* pathway signalling. Two mutations (intronic) were detected in the normal tissue only. One exonic mutation was detected in the *MCL1* gene (exon 1) in both; normal tissue and T1. Another mutation detected in intron 2 of *IL22RA1* was shared between the normal and T2. Two intronic mutations, in *STAT4* and *SOCS2*, were detected only in T1, while one was unique to T2 in the *STAM* gene. Only one mutation (intronic) in *PTPN6* gene was shared between T1 and T2 (Table 4.11). Twenty four genes involved in *PI3K*/*AKT* pathway signalling were mutated in patient 1, six of which were shared between T1 and T2and not found N. One intronic mutation in the *COMP* gene was detected in both T1 and T2 and N. The normal tissue had eight unique mutations, T1 had four unique mutations, while T2 had six unique mutations in the *PI3K*/*AKT* signalling pathway (Table 4.11). No correlation between the detected mutations and gene expression of the mutated genes was observed.

Table 4.11. Mutations associated with genes involved in PI3K/AKT and JAK/STAT pathways in patient 1.

		ArrayStar		Whole exome sequencing		
	Symbol	Region 1	Region 2	Normal	Region 1	Region 2
JAK/STAT	LEPR	-6.1	-3.6	I-19 AT SNP MR	/	/
	STAT4	2.1	/	/	I4 A:G SNP MR	/
	STAT5A	5.3	/	I12 T:TA I MR	/	/
	MCL1	-2.8	/	E1 GTCC:G D MT	E1 GTCC:G D MT	/
	SOCS2	-4.7	/	/	I2 C:A SNP MR	/
	IL22RA1	/	17.9	I2 A:C SNP MR	/	I2 A:C SNP MR
	PTPN6	/	-2.3	/	/	I13 G:C SNP MR
	PTPN6	/	-2.3	/	I12 T:G SNP MR	/
	STAM	-3.1	/	/	/	I11 TA:T D MR
PI3K/AKT	COL4A3	-4.2	-6.4	/	I9 ACT:A D MR	/
	COL4A4	-2.1	-2.6	I12 T:TA I low	/	/
	LAMB2	-2.2	-2.2	/	E7 T:C SNP MT	E7 T:C SNP MT
	VEGFA	-3.9	-3.4	/	E1 A:C SNP low	E1 A:C SNP low
	VWF	-5.1	-4.2	E28 T:G SNP low	E28 T:G ANP low	/
	IRS1	-2.5	3.1	E1 TTGC:T D MT	/	/
	LAMA3	-2.6	2.0	/	I12 ACT:A D MR	I12 ACT:A D MR
	COMP	3.1	/	I8 G:C SNP MR	/	I8 G:C SNP MR
	COMP	3.1	/		I13 A:C SNP MR	
	COMP	3.1	/	/	/	I8 T:C SNP MR
	COMP	3.1	/	/	/	I8 A:C SNP Low
	FGF10	2.4	/	E1 AAGC:A D MT	/	/
	FLT1	2.1	/	/	I14 TATG: T D MR	I14 TATG:T D MR
	FN1	4.5	/	/	I36 G:T SNP low	/
	LAMA1	6.0	/	/	I16 GA:G D MR	/
	PIK3AP1	3.8	/	E4 T:C SNP MT	/	/
	COL9A1	/	87.7	I32 GA:G D MR	/	/
	ANGPT1	-11.9	/	I8A:G SNP MR	/	/
	COL4A2	-2.6	/	/	E48 TA:T D MR	/
	COL4A6	-3.3	/	/	I3 CA:C D MR	I3 CA:C D MR
	ITGA2	-4.5	/	/	E17 G:A SNP MT	E17 G:A SNP MT
	MAGI1	-3.2	/	I4 TGA:T D MR	/	/
	MCL1	-2.8	/	E1 GTCC:G D MT	E1 GTCC:G D MT	/
	GNB4	/	-2.1	I9 G:GA I low	/	/
	KDR	-5.3	-3.1	/	/	I22 C:CA I MR
	RELN	-3.1	/	/	/	I33 G:GA I low
	PTEN	-2.1	/	/	/	I4 G:GT I MR
	PTEN	-2.1	/	/	/	E9 CT:C D MR

I-followed by a number: intron-located mutations, E-followed by a number: exon-located mutations, SNP: single nucleotide polymorphism / (point mutation), D: deletion, I: insertion, MR: modifier, mutation have no impact as it located in the introns, MT: moderate, mutation moderately affecting the gene structure. Low: mutations had a low impact on the gene structure. Letters in red: exonic mutations found only in one region, blue letters: intronic mutations found in one tumour region, green letters: shared mutations.

4.4.3.11. Mutated genes involved in *JAK/STAT* and *PI3K/AKT* pathways in patient 2.

Whole exome sequencing showed patient 2 had mutations in certain genes signalling via *JAK/STAT* pathway. Two intronic mutations in *IL6R* and *IL2RA* were detected in the normal tissue only. T1 had two exonic SNP mutations; in *EGFR* gene exons 7 and 21 with moderate impact on the structure of the gene. T2 had one unique mutation in exon 21 of *PIK3CA* gene (Table 4.12). Both tumour regions share a *PIK3R1* mutation in exon 10 with no impact on the gene structure. Fourteen genes involved in the *PI3K/AKT* signalling pathway were mutated in patient 2 (Table 4.12). Only five of them had exonic mutations including *SPP1*and *FGFR4* only in the normal tissue, *IL6R T/G SNP in exon28 was shared between normal tissue and tumour region 1 (not found in region 2), PIK3CA* and *PIK3R1* in both T1 and T2 (Table 4.12). The other nine mutations were intronic and had no impact on the gene structure. No correlation between the detected mutations and gene expression of the mutated genes was observed.

Table 4.12. Mutations associated with genes involved in PI3K/AKT and JAK/STAT pathways in patient 2.

		ArrayStar		Whole exome sequencing		
	Symbol	Region 1	Region 2	Normal	Region 1	Region 2
JAK/STAT	EGFR	/	**2.4**	/	I25 GTC:C D MR	I25 GTC:C D MR
	EGFR	/	**2.4**	/	E7 C:T SNP MT	/
	EGFR	/	**2.4**	/	E21 T:G SNP MT	/
	PIK3R1	**-2.3**	**-2.9**	/	E10 T:C SNP MR	E10 T:C SNP MR
	PIK3CA	**-2.1**	**-2.4**	/	/	E21 T:TA I MR
	IL6R	/	**-3.6**	I5 C:A SNP MR	/	/
	IL2RA	**2.6**	**2.4**	I7 A:T SNP MR	/	/
PI3K/AKT	EGFR	/	**2.4**	/	I25 GTC:C D MR	I25 GTC:C D MR
	EGFR	/	**2.4**	/	E7 C:T SNP MT	/
	EGFR	/	**2.4**	/	E21 T:G SNP MT	/
	PIK3R1	**-2.3**	**-2.9**	/	E10 T:C SNP MR	E10 T:C SNP MR
	PIK3CA	**-2.1**	**-2.4**	/	/	E21 T:TA I MR
	IL6R	/	**-3.6**	I5 C:A SNP MR	/	/
	IL2RA	**2.6**	**2.4**	I7 A:T SNP MR	/	/
	SPP1	/	-3.1	E1 TTGC:T D MT	/	/
	FGFR4	/	**2.0**	E1 AAGC:A D MT	/	/
	TNXB	**2.6**	**2.4**	I8 G:C SNP MR	/	I8 G:C SNP MR
	TNXB	**2.6**	**2.4**	/	I13 A:C SNP MR	/
	LAMA3	-2.1	-3.8	/	I14 TATG: T D MR	I14 TATG:T D MR
	LAMA4	-3.6	-10.1	/	I36 G:T SNP low	/
	LAMA5	/	-2.0	/	I12 ACT:A D MR	I12 ACT:A D MR
	COL4A4	/	**-3.6**	/	/	I8 T:C SNP MR
	PPP2R5B	/	**2.4**	/	I9 ACT:A D MR	/
	VWF	/	-3.4	/	I16 GA:G D MR	/

I-followed by a number: intron-located mutations, E-followed by a number: exon-located mutations, SNP: single nucleotide polymorphism /(point mutation), D: deletion, I: insertion, MR: modifier, mutation have no impact as it located in the introns, MT: moderate, mutation moderately affecting the gene structure. Low: mutations had a low impact on the gene structure. Letters in red: exonic mutations found only in one region, blue letters: intronic mutations found in one tumour region, green letters: shared mutations.

4.4.3.12. Mutated genes involved in *JAK*/*STAT* and *PI3K*/*AKT* pathways in patient 3.

Whole exome sequencing showed that patient 3 had four mutated genes involved in the JAK/STAT pathway. *CREBBP* had a SNP mutation in exon 27 in both T1 and T2with moderate impact on the gene structure, *STAT5A* also was mutated in both T1 and T2 in the intron 12 with no impact. One SNP mutation was detected in T1 in the *CISH* gene with high impact (affecting splicing donor sequence). Another mutation was detected in the normal tissue in intron 2 of the *PDGFA* gene with no impact on the amino acid sequence of the encoded protein (Table 4.13). There were 32 genes mutated in this patient, *SGK2*/exon 10 SNP was shared in N, T1 and T2, *PKN2*/exon 13 SNP was shared in T1 and T2. T1 had four unique mutations that were not detected either in the normal tissue or in T2 (Table 4.13). These four mutations had no impact on the encoded protein as located in the introns. T2 had seven unique mutations, only one of them had a moderate impact on the encoded *RELN* protein. The normal tissue had nine unique mutations including, *FGF5*/exon1, *KDR*/exon4, *PPP2R5B* and were associated with moderate impact on the encoded protein. Fifteen mutations were shared between N and T1, four with high impact including, *PKN2*/exon14, *THBS2*/exon10, *CSF1*/exon6, and *COL9A1*/exon5, another four with moderate impact in *ITGA8*/exon30, *KDR*/exon14, *MAG12*/exon15 and *COL6A5*/exon32 while the rest had low or no impact on the encoded proteins (Table 4.13).

Table 4.13. Mutations associated with genes involved in PI3K/AKT and JAK/STAT pathways in patient 3.

		ArrayStar		Whole exome sequencing		
	Symbol	Region 1	Region 2	Normal	Region 1	Region 2
JAK/STAT	PDGFA	-5.7	-5.4	I2 A:C SNP MR	/	/
	CISH	-2.2	/	/	I3 C:A SNP High	/
	STAT5A	3.0	2.3	/	I12 C:CA I MR	I12 C: CA I MR
	CREBBP	-2.4	-3.0	/	E27 T:G SNP MT	E27 T:G SNP MT
PI3K/AKT	SGK2	2.8	2.1	E10 G:T SNP High	E10 G:T SNP High	E10 G:T SNP High
	PKN2	-2.1	/	/	E13 T:C SNP Low	E13 T:C SNP Low
	PKN2	-2.1	/	E14 G:T SNP High	E14 G:T SNP High	/
	ITGA8	-14.7	-14.7	E30 T:G SNP MT	E30 T:G SNP MT	/
	SPP1	46.3	12.3	I6 A:T SNP MR	I6 A:T SNP MR	/
	THBS2	3.2	2.7	E10 C:CG I High	E10 C:CG I High	/
	TNC	3.6	2.3	I17 G:C SNP MR	I17 G:C SNP MR	/
	CSF1	-3.0	-3.3	E6 A:T SNP High	E6 A:T SNP High	/
	COL9A1	31.0	8.0	E5 CT:C D High	E5 CT:C D High	/
	COL9A1	31.0	8.0	E5 T:A SNP Low	E5 T:A SNP Low	/
	FGFR4	-5.5	-7.1	I2 CGT:C D MR	I2 CGT:C D MR	/
	KDR	-8.0	-12.5	E14 G:T SNP MT	E14 G:T SNP MT	/
	LAMA2	-3.7	-4.2	I16 C:T SNP MR	I16 C:T SNP MR	/
	LAMC3	-10.6	-9.3	E10 A:C SNP Low	E10 A:C SNP Low	/
	LAMC3	-10.6	-9.3	I19 G:C SNP MR	I19 G:C SNP MR	/
	MAGI2	-5.1	-6.3	E15 C:A SNP MT	E15 C:A SNP MT	/
	COL6A5	/	3.5	E32 G:T SNP MT	E32 G:T SNP MT	/
	CCNE2	5.1	2.9	E9 A:G SNP Low	/	/
	LAMA1	5.3	11.3	I16 CT:C D MR	/	/
	LAMC1	2.1	2.2	I7 G:GA I MR	/	/
	FGF5	-2.9	-2.9	E1 TTCC:T D MT	/	/
	KDR	-8.0	-12.5	E4 G:T SNP MT	/	/
	PDGFA	-5.7	-5.4	I2 A:C SNP MR	/	/
	PPP2R5B	-2.5	-3.6	E2 GC:G D MT	/	/
	PRKCA	-3.8	-2.5	I11 C:T SNP MR	/	/
	ITGA11	2.6	/	I7 CT:C D MR	/	/
	KITLG	-4.0	-3.9	/	I2 CA:C D MR	/
	EIF4E	5.7	6.2	/	I7 G:GA I Low	/
	COL4A3	/	-2.5	/	I4 GT:G D MR	/
	MAGI1	/	-2.2	/	I14 TTC:T D MR	/
	ITGA8	-14.7	-14.7	/	/	I8 AAC:A D MR
	BCL2L11	3.2	2.0	/	/	I1 A:T SNP MR
	COL1A1	3.5	4.5	/	/	I41 CAG: C D Low
	RELN	/	-2.4	/	/	E12 T:G SNP MT
	PTEN	-3.7	-4.7	/	/	E9 C:CT I MR
	VWF	-7.6	-4.6	/	/	E28 T:G SNP Low
	HSP90AA1	/	2.0	/	/	I8 C:A SNP MR

I-followed by a number: intron-located mutations, E-followed by a number: exon-located mutations, SNP: single nucleotide polymorphism /(point mutation), D: deletion, I: insertion, MR: modifier, mutation have no impact as it located in the introns, MT: moderate, mutation moderately affecting the gene structure. Low: mutations had a low impact on the gene structure. Letters in red: exonic mutations found only in one region, blue letters: intronic mutations found in one tumour region, green letters: shared mutations.

4.5. Discussion

Molecular heterogeneity is a frequent event in tumours and is responsible for several critical issues in the diagnosis and treatment of patients with cancer. Previous studies have shown that lung tumours are characterized by a high degree of molecular heterogeneity. Intra-tumour heterogeneity (ITH) plays a role in drug resistance and directly affects the treatment outcome of patients with lung cancer. At diagnosis tumour sections are microscopically examined by a pathologist, and the tumour cells based on their location in the tumour mass, central or sub-marginal, exhibit a range of variance in their levels of differentiation and gene expression regardless of their genetic evolution (Hlubek et al., 2007, Bertucci et al., 2004). The recent paradigm shift in the treatment of patients to a more personalised or targeted approach has resulted in molecular profiling of tumours becoming part of the standard diagnostic protocol. Cancer molecular diagnostics using next generation sequencing panels of known somatic mutations and translocations, such as the Oncomine panel used at St. James's Hospital, is now recommended for all patients with lung cancer. Screening tumours allows the clinician to stratify patients for targeted therapies and has become the standard of care as the number of molecular targeted drugs especially small molecule inhibitors has expanded (Van Hoeck et al., 2019).

Genomics and personalised medicine

About 1.5% of the protein coding genes, approximately 350 genes, have been reported to have recurrent somatic mutations that are proven to have a role in the development of cancer (Futreal et al., 2004).

DNA variants are called as differences in comparison to a reference and in a sequencing project Single Nucleotide Polymorphisms (SNPs) and DNA mutations

are defined as DNA variants detectable in >1 % or <1 % of the population, respectively. The term point mutation includes single base pair substitutions in the DNA while small insertions and deletions are collectively called (InDels) (Bardelli et al., 2003, Maquat, 2001). Single nucleotide substitution, if located in gene introns, usually has no impact on the overall gene product unless it affects the splicing donors. If located in an exon it may be silent with no impact or alternatively have high impact if it is affecting start and stop codons. It may also have an impact if it is located in the splicing acceptors in the UTR leading to failure to eject the intron during splicing (Iengar, 2012). Insertions and deletions can be deleterious if they occur in the exons and lead to either frame-shift or loss of the encoded amino acids, or result in splicing/termination codon issues (Cong et al., 2012).

The presence of genes with different sequences within the same tumour biopsy indicates tumour complexity or heterogeneity (Burkhart-Schultz and Jones, 1997). The most important mutations in the tumour biopsy are the driver mutations i.e. those present in genes whose function is required for growth and proliferation of tumour cells (Stratton et al., 2009). These mutations might lead to either activation or inactivation of genes that play a role in cancer and the susceptibility to cancer (Carvalho et al., 2009, Miki et al., 1994). Next generation sequencing is a sophisticated analytical tool that provides a full mutational signature that can improve diagnosis, allow patient stratification for treatment and predict the success of that treatment (Davies et al., 2017). The aim of this chapter was to quantify both genomic and transcriptomic heterogeneity in different areas of the same tumour compared to the match normal tissue. DNA and RNA were extracted simultaneously from two different tumour regions and matched normal tissue from three patients with lung adenocarcinoma. Whole exome sequencing (WES) was

used for genomic profiling and the ArrayStar microarray was used for the transcriptomic profiling.

Whole-Exome Sequencing for Assessing Intratumour Genetic Heterogeneity

There were a number of shared mutations (~13.2%) between the matched normal tissue (N) and T1 in patient 1. However, there was no overlap between mutations in the normal tissue and T2. Therefore this overlap between N and T1 may be the result of sequencing artifacts. A study by Shi et al., demonstrated that sequencing artifacts are common with WES, in particular when using tumour biopsies where the actual tumour content is <50%. They suggest excluding mutations in low-mappability regions or in certain mutational contexts could help improve the false detection rate of sub-clonal mutations. In this study, resected tumour tissue was used and the tumour content was checked by a pathologist to be >50%. After removing the 13.2% of mutated genes in T1 that were shared with the normal tissue, the number of mutations in T1 and T2 are similar (51-5 and 44) i.e. only 2 mutations difference. In patient 2, the overlap was a lot larger and accounts for 57.9% of the mutations between the normal and T1, while only 1.3% overlap were detected between the normal tissue and T2. After removing the 57.9% of genes (shared between normal and T1), the number of mutations in T1 and T2 become almost the same (159-92 and 57) i.e. only 10 mutations difference. In patient 3, the overlap was also large between the normal tissue and T1 accounting for 86.4% of the detected mutations. After removing these genes in addition to the 1% shared mutations between the normal tissue and T2, the mutation ratio between T1 and T2 becomes 179: 63 almost 3:1.

Genomic and Transcriptomic intra-tumour heterogeneity

To determine intra-tumour heterogeneity the number of mutated genes that were unique to T1 or T2 as well as those shared by both tumour regions were enumerated. In addition the number of differentially expressed genes that were unique to T1 or T2 as well as those shared by both tumour regions were enumerated. In patient 1, 14 (30.4%) and 12 (27.2%) mutations were unique to T1 and T2, respectively. There was no correlation between the number/type of mutations and the overall gene expression signature. Transcriptomic intra-tumour heterogeneity was demonstrated by T1 expressing 77.7% of the upregulated genes (74.4% of the upregulated genes unique to T1 and a further 3.3% were downregulated in T2), and 60.7% of the down-regulated genes (52% of downregulated genes unique to T1 and a further 8.7% upregulated in T2). T2 expressed 67.5% of the upregulated genes (57.3% of the upregulated genes were unique to T2 and a further 10.2% were downregulated in T1), and 38.8% of the down-regulated genes (34.4% were unique down-regulated in T2 and 4.4% were upregulated in T1). In patient 2, genomic intra-tumour heterogeneity was low as there were only 8 (5%) and 4 (6.3%) mutated genes unique in T1 and T2, respectively. T2 shared 90.5% of the point mutations with T1. Transcriptomic intra-tumour heterogeneity was high in this patient. T1 expressed 33.7% of the upregulated genes (32.6% uniquely upregulated in T1 and 1.1% were down-regulated in T2), and 14% of the down-regulated genes (13.57% uniquely downregulated in T1 and 0.43% were upregulated in T2). T2 expressed 60.4% of the upregulated genes (60% uniquely upregulated in T2 and 0.4% genes were down-regulated in T1), and 46.7% of the down-regulated genes (all 46.7% were uniquely downregulated in T2). **In patient 3**, 119 (9.1%) and 15 (20%) point mutations were unique to T1 and T2, respectively. Genomic intra-tumour

heterogeneity in this patient was very high and the total number of point mutations in T1 which was 20 times more than in T2. Excluding the shared point substitutions between the T1 and T2 and the ones that overlap with the normal tissue (1134 genes), the heterogeneity between the two tumour regions was still high as T1 contain 7-times more point mutations than in T2. Differentially upregulated genes unique to T1 and T2 was 824 (39%) and 225 (14%), respectively (2.6 times more unique genes in T1 than T2). Also there were 317 (15%) and 809 (30%) genes uniquely down-regulated in T1 and T2, respectively (2.5 times more down-regulated genes in T2 than in T1). In addition to that when we compared the expression of the shared up and down-regulated mRNA transcripts (1263 and 1854 up/down shared in T1/T2, respectively) we found the majority of them vary in their level of expression.

After taking into consideration sequencing artifacts that are an inevitable limitation of WES, the genomic and transcriptomic data combined provide evidence that there are variations in both the mutation and gene expression profiles between different regions of the same tumour. This intra-tumour heterogeneity may play a role in the stratification of patients for targeted treatments. A more rigorous approach to determining whether a specific tumour will benefit from a targeted inhibitor may be the combination of both genomic and transcriptomic or proteomic testing of the tumour biopsy. Therefore in samples where the presence of a driver mutation is not detected but is present, an activated pathway may be detected by mRNA or protein expression analysis. The combined data will predict whether the tumour will benefit from a specific targeted therapy.

Deregulation of tyrosine kinase activity in lung adenocarcinoma

In this chapter, tyrosine kinases were examined as a major target for treatment of many solid tumours including non-small cell lung cancers was taken as an example for the importance of tracking their heterogeneity in three patients diagnosed with lung adenocarcinoma.

Protein tyrosine kinases are the most important proteins modulating cell to cell as well as intracellular communications. There are 90 tyrosine kinases in the cells; 58 are transmembrane tyrosine kinase receptors categorized in 20 sub-families, and 32 are non-receptor protein tyrosine kinases (NTRKs) (Robinson et al., 2000). All receptor tyrosine kinases (RTKs) consist of an extracellular ligand-binding domain (activator), transmembrane domain and an intracellular cytoplasmic catalytic domain (Hubbard and Till, 2000).

Examples of some common mutations in cancer that affect the receptor-ligand response include: mutations in EGFR tyrosine kinase domain which interfere with the auto-inhibitory regulation mechanism of the receptor leading to persistent tyrosine kinase activity in NSCLC (Sharma et al., 2007).

Mutations in the juxtamembrane region are also linked to increased tyrosine kinase activity (Red Brewer et al., 2009). Point mutations in domain I, II, III of the extracellular part of EGFR receptor and deletions in domains I and II were also found in glioblastoma patients (Libermann et al., 1985).

FGFRs (I, II, III) activation mutations were detected in multiple myeloma, cervical and bladder carcinoma eg. domain 3 of the extracellular region of FGFR2 was linked to sustained dimerization and activation of the receptor. Other activating mutations were detected in the cytoplasmic part of FGFR2 and 3 leading to increased tyrosine kinase activity (Lemmon and Schlessinger, 2010).

The NTRKs interact with the receptor tyrosine kinases, thus are involved in the downstream signalling transduction originating from outside the cells. There are 32 enzymes classified into 10 subfamilies including: *ABL, ACK, CSK, FAK, FES, FRK, JAK, SRC-A/B, TEC,* and *SYK* (Robinson et al., 2000). All signalling pathways regulating cells proliferation, apoptosis, survival and cell differentiation function through protein tyrosine kinases. Mutations in RTKs and NTRKS that cause increased expression are well-known to be linked to malignant transformation in many cancers therefore targeting these tyrosine kinases with specific inhibitors has proven very beneficial to patients (Gocek et al., 2014). Here we examined the three tumours for the presence of known driver mutations associated with lung adenocarcinoma in the following genes *EGFR* and *HER-2* (exon20 mutation) *BRAF* (V600E), *FGFR1-4*, *K-RAS*, *MET*, neuregulin-1, *NRTK*, *PIK3CA,* ,*RET* and *ROS1* (Chu, 2020).

In the normal tissue of **patient 1**, *RTK*; *AXL*, *EGFR*, *EPHA10* and *TIE1* had intronic mutations, and *ROR2* had a three nucleotide deletion in exon 9 leading to a frame-shift that moderately affected the tyrosine kinase structure. ROR2 has 1386 amino acids, the binding and active sites are located in the amino acid number 507 and 615, respectively. The mutation found in this patient was located in the 9th exon (ast exon) which starts from 550 and 1386 meaning that the activity and the substrate binding site of the enzyme might be affected. Microarray analysis showed *ROR2* was upregulated in T1 and T2 compared to the normal tissue and was more abundant in T1 than in T2. The normal tissue also had a three nucleotide deletion in the cytoplasmic tyrosine kinase *ABL1* which moderately impacts the structure of the kinase.

ABL1 was not differentially expressed between the normal and malignant tissues. RTKs *EPHA10* and *AXL*, had two mutated introns both were shared with the normal tissue. The cytoplasmic TK *YES1* had a point mutation in exon 4 with moderate impact in T1. YES1 belongs to Scr family tyrosine kinases and found to play a major role in tumour cells proliferation, survival and metastasis (Bilal et al., 2010, Patel et al., 2013, Singh et al., 2019). *YES1* was not differentially expressed within the tumour tissues by microarray analysis. *ERBB4* (*HER3*) was mutated (in intron 7) with no impact in T2. *LTK, EPHB6, ERBB2/3/4* and *DDR1* receptor tyrosine kinases were upregulated and more abundant in T2 compared T1. *PDGFRA*, *CSF1R*, *ROR2*, *AXL* and *RET* were more abundant in T1 than T2. NRTKs *ITK*, *CSK*, *BLK*, *ZAP70* and *LCK* were upregulated in T1 and in T2 *FER* and *FRK* were upregulated while *BTK* and *MATK* were down-regulated. When the genomic and transcriptomic data were compared, no impact of mutations on corresponding gene expression was observed.

In patient 2, the normal tissue and T2 had four RTKs with exonic mutations and four with intronic mutations *EGFR* (exon 7 SNP), *EGFR* (exon 21 SNP) and *ERBB2* (exon 8 3NT insertion) were shared. *RET* (exon 5 SNP) and *MUSK* (exon 15 SNP) were unique to the normal tissue and T1, respectively. The other mutations were in the introns of RTKs in either normal tissue (*EPHB6*, *ERBB2*, *FGFR4*) or T1 (*EGFR*, *ERBB4*, *INSRR*, *MUSK*) and had no impact on the receptor structure. *LYN* and (*TXK* and *SYK*) were the only mutated NRTKs in the normal tissue and T1, respectively. T1 and T2 shared intron mutated RTKs; *INSRR*, *ERBB4* and *EGFR*. T1 and T2 also shared mutated NRTKs *SYK* and *TXK*. *NRTK YES1* was uniquely mutated in T2.

Microarray data showed upregulated *TIE1* in both T1 and T2. *DDR2*, *ROR1*, *ROR2* were all down-regulated in both tumour regions and had no mutations in either the normal or tumour regions. *FLT3*, *KIT* and *FGFR2* were all down-regulated in T2 and unchanged in T1 and no mutations detected in any region. *EGFR* was upregulated in T2 but unchanged in T1 and it had two exon mutations shared in normal tissue and T1, and also had a two nucleotide deletion in intron 25 in T1 and T2 but not in the normal tissue. *MUSK* was up-regulated in T2 and unchanged in T1, and was only mutated in T1 in exon 15 and intron 13. Four NRTKs; *BLK, MATK, BTK and CSK* were down-regulated in T2 and unchanged in T1, while *FRK* was upregulated in T2 only, and *ITK* was upregulated in T1 but unchanged T2. None of these four NRTKs were mutated in all tissues analyzed from this patient. This heterogeneity in the expression among the tumour regions would impact on the selection of the tyrosine kinases inhibitor-based treatment and how likely the patient would be put under surveillance. The overall observation cannot conclude that there is a link between mutations and the level of expression.

In patient 3, *ALK* (SNP) and *FGFR4* (2 nts Del) RTK had intronic mutations in both normal tissue and in T1, ALK was also detected in the T2. Two RTKs were mutated in T1 *ERBB4* (two nucleotide substitution) and *FGFR1* (3 nts Del). *ERBB4* also was detected in normal tissue, while *FGFR1* was shared with the T2. Three uniquely mutated RTKs *ERBB4* (single nucleotide insertion), *CSF1R* (SNP) and *AXL* (3 nts Del) were detected in T2.

NTRKs *ZAP70* and *FYN* had single nucleotide intronic substitutions in T1 and in normal tissue of this patient. *SYK* had a SNP in intron 6 in T1 only, while *BMX* had a single nucleotide deletion in both T1 and T2. RTK *EPHA10* was up-regulated in T1 and down-regulated T2. Among the non-receptor tyrosine kinases, the IL2-

inducible T-cell kinase was 11.2-fold upregulated in T1 compared to normal tissue, and downregulated in T2.

When it comes to the point of selecting the best tyrosine kinase inhibitor for each patient, information about all tyrosine kinases (receptor and non-receptor) including mutations and their impact on the enzyme activity and also their expression profile in multiple regions per tumour, are needed.

Functional classification of the significantly differentially expressed genes

Panther GO-Slim Biological Process classification of differentially expressed genes, per patient, showed that the genes are involved in biological adhesion, biological regulation, cell population proliferation, cellular component organisation or biogenesis, cellular process, developmental process, growth, immune system process, localization, locomotion, metabolic process, multi-organism process, multicellular organismal process, response to stimuli, signalling were not the same (Figure 4.7).

The protein tyrosine kinases in addition to cytokines and hormones, that were found differentially expressed with a heterogeneous pattern across the tumour regions in the three patients, along with their receptors, are very important in malignancy transformation including the control of cell survival, cell cycle, metabolism, proliferation as well as antagonizing programmed cell death. Therefore, in some patients, combination of more than one tyrosine kinase inhibitor/antagonist could be a good option to overcome tumour relapse. Otherwise targeting a specific pathway would be the best once identified perhaps by pathway signalling arrays.

The aim of this chapter was to elucidate the extent of genomic and transcriptomic intra-tumour heterogeneity within lung adenocarcinoma tumours and determine whether profiling both may be more advantageous than genomic profiling alone. If

the levels of intra-tumour heterogeneity are high and driver mutations are not detected in a biopsy at diagnosis, even when they are present in some parts of the tumour, perhaps when combined with transcriptomic profiling the activated pathway driven by the mutation may be detected and the patient will be stratified to the appropriate targeted therapy.

Deregulation of the JAK/STAT and PI3K-mTOR signalling pathways in lung adenocarcinoma

KEGG analysis identified the *PI3K-mTOR* pathway having a large number of differentially expressed genes. The *PI3K-mTOR* signalling pathway can be activated by several triggers including 1: focal adhesion by extracellular matrix molecules (ECM) such as collagen, integrins, laminins (Xia et al., 2004), 2: receptor tyrosine kinases including: growth factors such as epidermal growth factors, platelets derived growth factors, fibroblast growth factors, hormones such as erythropoietin, angiopoietin (Fruman et al., 2017), 3: cytokines such as interleukins and interferons (Xie et al., 2014), 4: activation of G-protein coupled receptors by hormones, chemokines and neurotransmitters (Manning and Toker, 2017). Sections 4.4.4.4-6 summarize all the differences between the two tumour sections of the three patients and highlighted the unique lists of genes that can activate *PI3K/AKT* pathway with different mechanism listed above. The more genes upregulated/activated in the tumour tissue the higher the tumour chance to tolerate and bypass the effect *PI3K/AKT* targeted therapy. The clinically important genes, when *PI3K* targeted therapy used, are those involved in the conversion of *PIP2* to *PIP3*, i.e. upstream to *PIP3* including cell surface receptors/their activators, genes bypass them by affecting *PTEN* activity. **In patient 1**, T2 had 8 upregulated ECMs and receptor kinases (*LAMA3, LAMB3, IGNB4, IGNB6, ERBB2, ERBB3, FGF4,*

and AMPK) while were detected down-regulated in T1. In contrast T1 possesses unique upregulated growth factors and growth factors receptors (*FGF1, 5, 10, 16, 17, 19, FLT1R, FLT3R, ILGF* and angiopoietin). T1 also had *PI3KA*, *PTEN* down-regulated. *PI3KB* was detected upregulated in T1, along with lowered *PTEN* and elevated *TCL1* (*AKT* co-activator which bypass *PI3K* signalling pathway) makes it more aggressive than T2. The overall conclusion is that this patient cannot be treated by targeting *PI3K* alone, combination therapy would be preferable to avoid tumour relapse. **In patient 2**, T2 also had lowered *PTEN* levels and elevated *PI3KB* levels, which were found with an opposite profile in T1. T2 also had more upregulated hormones, growth factors, cytokines *RTK*, cytokines, and integrins than in T1. The overall picture is that when using *PI3K* targeted therapy, the dose should be carefully adjusted as the response would be varied; good at the beginning and slower later in T2. **In patient 3**, epidermal growth factor was upregulated in T1 and down-regulated in T2. T2 had more elevated collagen, interferons and fibroblast growth factors than T1. T1 had 11 unique upregulated genes including *IGF, FGF3, IGN, MYB, JAK3* and phosphatase 2. Combination of PI3K inhibitors with *EGFR* inhibitors would be an advantage as *EGF* was high in T1. With *PI3K* targeted therapy, we might see tumour relapse (T1 region) as *PI3K* is more activated than in T2.

However, the results of chapter 2 highlighted that an activated *STAT3* pathway including the downstream *PIM* kinases drive resistance to *PI3K-mTOR* targeted therapy in NSCLC. Here, KEGG pathway analysis was used to examine the differentially expressed genes and determine whether either the *PI3K-mTOR* or *JAK/STAT* signalling pathways showed differences between two tumour regions of the patients involved in this study (Table 4.2).

In patient 1, a total of 69 genes involved in the *JAK/STAT* pathway were differentially expressed in the tumour region compared to the normal tissue. Forty-one genes in T1, 20 were upregulated and 21 were down-regulated. In contrast twenty-eight in T2; half of them were upregulated and half were down-regulated. Several cytokines were detected uniquely upregulated in T1 include: IFNα/γ, *IFNγR, IL10/23, IL2/27R*, and several hormones which *are CSF2RA, PDGFRA*, thrombopoietin, and thrombopoietin receptor, leptin, and cardiotrophin. Some cytokines and growth hormones were uniquely down-regulated in T1 includes *IL6*, *IL6R, IFNβ, STAM, SOCs2/3, CREBBP, c-Myc, MCL1* and *PI3KR3*. Two interleukin receptors, *IL20RA* and *IL13RA2* were down-regulated in region 1 and upregulated in region 2. In contrast T2 also possesses unique cytokines and growth hormones that modulate *JAK/STAT* pathway including; *IL13, IL7, LIF, IL22RA1*, *PIM1, STAT6, PIAS3*, *CSF2, TSLP*, cell surface receptor B-cell receptor 2 were upregulated, and *IL2, IL3, IL15R, GFR*-bound protein 2 and *PTPN6* and 11 (Table 4.5). Using *PIM*-kinases to evaluate the activation of *JAK/STAT* pathway, both tumour regions had activated pathway with *PIM*2 (5-times) more abundant in T2 and *PIM*1/3 were more elevated in T1.

In patient 2, 35 genes involved in JAK/STAT pathway were significantly differentially expressed; *IL22RA2* was uniquely upregulated in T1, six (*NTFR, EGFR, EPO, IL15RA, IL4, MYC*) were uniquely upregulated in T2. IFNα1 was uniquely down-regulated in T1, while 11 were uniquely down-regulated in T2 (Table 4.6). In this patient, T2 of the tumour would have more chance to tolerate targeted therapy to PI3K as concluded in chapter 2.

In patient 3, 48 genes involved in *JAK/STAT* pathway were detected differentially expressed in the two tumour regions; (*EGF, JAK3, SOCs4*) and (*IFNα21, IFNγ,*

IL20, IL6R) were uniquely upregulated in T1 and T2, respectively. In contrast (*FHL1, CISH*) and (*EGF, IL6, IL6ST, MYC, STAT5B, STAT6, TSLP, CCND3)* were down-regulated in T1 and T2, respectively. Each single gene affect the *JAK/STAT* pathway level of activation and T1 is expected to have more *JAK/STAT* activation in this patient (Table 4.7).

***PIM* kinases** can be induced by cytokines such as IL4 and 6 and IFNγ (Lilly et al., 1992). *PIM* kinases were selected from the microarray data as a marker for activated JAK/STAT pathway and were validated by qRT-PCR in the two tumour regions in reference to the control normal tissue per patient. In patient 1, the microarray detected activation of all three *PIM* kinases which was confirmed by qRT-PCR. The expression pattern between the two regions was heterogeneous with no significance except *PIM3* which was greater in T1 than in T2 (p=0.04) (Figure 4.9C/B). In patient 2, the three *PIM* kinases were elevated with no differences except *PIM3* which was elevated by 55% in T1 and 30% in T2 with p value of 0.03 (Figure 4.11C/B). In patient 3, all three *PIM* kinases were elevated with heterogeneous patterns by the microarray (Figure 4-13C/B). *PIM1* and 2 were doubled and both regions had almost the same levels, *PIM3* had seven times more expression in T1 than in T2 (p=0.01). *PIM* kinases are known to play a role in cancer cell proliferation, and evasion of apoptosis in many malignancies (Santio and Koskinen, 2017). *PIM* kinases were found to suppress apoptosis, maintain PI3K/AKT/mTORC1 and regulate *cMyc* oncogenicity (Rebello et al., 2018). In chapter 2, GDC-0980 resistance was found associated with activation of the JAK/STAT pathway and increased *PIM* kinases were validated by western blot to support such hypothesis (unpublished data).

TNC, *DSP*, *ERO1A* and *ENO1* expression in adenocarcinoma patients

Tenascin is an extracellular glycoprotein derived from myofibroblasts in the cancer microenvironment, and has been shown to promote cancer metastasis via regulation of epithelial-mesenchymal transition. Increased levels was found to be a good predictor of patient survival in lung adenocarcinoma regardless of age, sex, mutational profile and smoking history (Takahashi et al., 2013, Gocheva et al., 2017). Tenascin c was shown to be overexpressed in all major types of lung cancer (Silacci et al., 2006) and influenced doxorubicin cytotoxicity via interfering with apoptosis, therefore targeting tenascin c was proposed as an adjuvant chemotherapy (Oskarsson et al., 2011, Shi et al., 2015).

Desmoplakin upregulation was linked to epithelial-mesenchymal transition (EMT) and PI3K/AKT activation, while decreased levels of desmoplakin was found associated with PI3K/AKT deactivation and mesenchymal to epithelial transition (*MET*) (Silacci et al., 2006). *DSP* was downregulated 10.7-fold in T1 and upregulated 1.9-fold in T2 of patient 1 by microarray. In patient 2 *DSP* was upregulated 1.1-fold and 3.3-fold in T1 and T2, respectively. In patient 3, it was upregulated3.3-fold and 3.8-fold compared to the control normal tissues. *DSP* was further evaluated by qRT-PCR and the results showed no difference between the two tumours regions tested per patient. In patient 1, *DSP* was elevated by 1.5-fold while in the other two patients it was elevated by one fold (Figure 4.3A). Expression of **tenascin c** is modulated by *PDGF* via PI3K-AKT signalling pathway (Jinnin et al., 2006). *TNC* mRNA in the three patients, was upregulated by 9.2 and 1.3-fold in T1 and T2 respectively in patient 1, down-regulated 1.3 and 1.1-fold in region T1 and T2, respectively in patient 2, and upregulated 3.6 and 2.3-fold in T1 and T2 respectively in patient 3 by microarray. In the three patients, *TNC* was

elevated by 80% in patient 1 and 2 and by 1.25 fold in patient 3 as detected by qRT-PCR. There was no difference in *TNC* levels among the two tumour regions per patient (Figure 4.4).

In patient 1, *ENO1* was down-regulated 1.1-fold in T1 and upregulated 1.1-fold T2. By qRT-PCR, *ENO1* was elevated by 20% with no difference between the two regions (Figure 4.5A). In patient 2, *ENO1* was upregulated 1.8 and 2.1 in region T1 and T2, respectively by microarray. By qRT-PCR, *ENO1* was unchanged compared to the normal tissue (Figure 4.5A). In patient 3, *ENO1* was upregulated 2.5 and 1.8-fold in T1 and T2, respectively. By qRT-PCR, *ENO1* was increased by 20% in the two regions and no difference between the two tumour regions (Figure 4.5A).

In patient 1, the expression of *ERO1a* was 2.1 and 2.7-fold upregulated compared to the normal tissue. qRT-PCR showed 1.5-fold upregulation but no difference was detected (Figure 4.6A). In patient 2, *ERO1a* was upregulated by 1.1 and 1.6-fold in T1 and T2, respectively by the micro-array. By qRT-PCR, *ERO1a* was 20% elevated in the tumour tissues compared to the normal tissue (Figure 4.6A).

In patient 3, *ERO1a* was upregulated 2.1 and 1.1-fold compared to the normal tissue by microarray. By qRT-PCR, *ERO1a* was upregulated 1.5-fold in the two regions with no difference (Figure 4.6A).

Desmoplakin, *enolase-1* and *ERO1-La* were evaluated by western blot in a separate set of three patients. *Desmoplakin* was, elevated by 1.5 fold and 1-fold in region T1 and T2 of patient 1, downregulated in T1 and unchanged in T2 of patient 2 and elevated in both tumour regions by two and one-fold, respectively in patient 3 (Figure 4.3B).

The difference in *EROI-La* protein abundance between the two tumour regions analysed from patient 1 in patient 1 was detected 3.5-fold. In patient 2, *ERO1-la* was unchanged in region 1 and was increased by 2-fold in region 2 (Figure 4.6B). In patient 3, by western blot *EROI-La* was detected down-regulated by 10% and 30% in region 1 and 2, respectively (Figure 4.4B). Western blot has detected enolase-1 down-regulated by 40% and 10% in region 1 and 2, respectively. In patient 2, enolase-1 was detected 30% down-regulated in region 1 and unchanged in region 2. In patient 3, enolase-1 was detected 40% down-regulated in region 1 and was detected 2-fold upregulated in region 2 (Figure 4.5B).

These findings support our hypothesis of intra-tumour heterogeneity and stress the importance of studying more than tumour region at patient diagnosis in order to better management of patient treatment and optimal patient surveillance. Good knowledge of the activated pathways during acquired drug resistance would offer the option of drug combination. Good knowledge of the possible activation of AKT that intersect with and bypass PI3K/AKT pathway, in addition to investigating several tumour parts would guide us predict the treatment success. Therefore, it is highly recommended to intensively investigate different tumour regions and highlight the differences at the level of gene expression/mutations and level of phosphorylation in order to better understanding of cancer patient management.

5. **Chapter V**: General discussion/ Conclusion/Future plan

5.1. Discussion

Lung cancer is the leading cause of cancer death among both men and women. Each year, more people die of lung cancer than of colon, breast, and prostate cancers combined. Lung tumours are heterogeneous with diverse molecular profiles between patients, making them difficult to treat. We now understand that we must exploit these differences by characterising each patient's distinct molecular signature and design treatment protocols that target specific tumours more effectively with reduced toxicities. Although a personalised medicine approach to treatment has increased response rates and overall survival in patients with NSCLC, intrinsic or acquired drug resistance is the inevitable endpoint to treatment for patients. Although our understanding of the molecular biology of lung carcinogenesis and the mechanisms involved in drug resistance to treatment is constantly evolving, we still have much to learn in order to significantly reduce the burden caused by this devastating disease. The focus of our research was to elucidate the drug resistance mechanisms involved in PI3K-mTOR inhibition and investigate intra-tumour genomic, transcriptomic and proteomic heterogeneity in NSCLC.

Advances in scientific research from the last two decades has facilitated the identification of genes involved in drug resistant and their molecular signalling mechanisms as a result we are now able to understand how the cancer cell adapts by making subtle molecular changes in order to protect itself from anti-cancer drugs. Thus, a better understanding of fundamental drug resistance mechanisms is of utmost importance to develop new treatment strategies to tackle the problem (Shanker et al., 2010).

Reports on the recent cancer research have stated that there have been many drugs evolved and are now in clinical trials, in an aim to control drug resistance and to improve drug efficacy. According to advance lung cancer research, drug resistance can be classified as three different levels, they include: cellular, molecular or pathological. More specifically drug resistance is driven by alteration in the expression of drug transporters, enhance activity of pro-survival, and anti-apoptotic pathways, as well as non-intrinsic influences of the tumour microenvironment. Several research as proved that tumours comprises a heterogeneous population of cells with various genetic, epigenetic, and phenotypic attribute leading to diverse responses to therapy, and underlies the emergence of resistant clones. The tumour heterogeneity is directed by specialised subpopulations of tumour cells called cancer stem cells (CSCs) that are highly self-renewing, have the capacity to initiate tumour, and retain the ability for multi-lineage differentiation. All of them have notably contributed to the evolution and acquisition of drug resistance in clinic (Chen et al., 2019). Our work mainly focused on intra tumour heterogeneity and bypass signalling as a result of pathway crosstalk which are two major hurdles for targeted therapy.

Both intrinsic and acquired drug resistance is caused by intra tumour heterogeneity. ITH is a phenomenon where a solid tumour consists of distinct sub-clonal populations of cells with distinct genomic modifications. This difference between cells results in some cells being resistant to treatment due to divergent biological behaviour. This genetic complexity of tumour cells is now better understood with the help of advances in next generation sequencing and genomic techniques like fluorescent in situ hybridisation (FISH) and G-banding karyotyping. In-depth DNA and RNA profiling of lung tumours to define both spatial and temporal

heterogeneity has highlighted the implications of ITH on response to treatment (Zito Marino et al., 2019). Recent studies have also investigated the effect of ITH on the immune response, and have revealed that ITH in combination with mutational load can predict response to checkpoint inhibitors (Goto, 2018).

Acquired drug resistance is often caused by the emergence of resistance mutations or the activation of bypass signalling pathways that allow the tumour cells to escape the effects of the treatment. Once biomarkers correlating to these parallel mechanisms of resistance are elucidated patients receiving treatment can be monitored for their activation. Once detected in patients undergoing treatments like immunotherapy, chemotherapy and targeted therapy, the clinician can then decide on a second line treatment that may overcome treatment resistance. This study focussed on the validation of biomarkers of acquired resistance to PI3K-mTOR pathway inhibition. Over the last two decades, extensive research has been carried out on PI3K pathway. This pathway plays a vital role in regulating cell growth and proliferation and has been shown to be deregulated in lung cancer. Previous studies have identified specific aberrations in the PI3K/AKT/mTOR pathway that result in its activation and that can be used as a predictive biomarkers such as copy number gains of *PIK3CA* and *RICTOR* as well as *PIK3CA* mutations (Tan and Yu, 2013). Consequently, many drugs have been studied and designed to target this pathway, some of these drugs have entered preclinical and clinical studies. The drug which we have tested in our study was GDC0980 (Apitolisib). It is a potent class-I *PI3K* inhibitor that has a dual catalytic site for *PI3K* and *mTOR* inhibiting downstream signals of both. Previous data has shown that it has greatest potency in lung, breast and prostate cancer (Wallin et al., 2011). When the cancer cells are treated with GDC0980 they causes G1 cell cycle arrest and in case of *mTOR* they lead to

apoptosis in some cancer cells including those with direct pathway activation via *PI3K* and *PTEN*. In our project we mainly focused on *PI3K-mTOR* in drug resistance and also molecular profiling for intra tumour heterogeneity. In our experiments we have used H1975GR and GP cells. Cells resistant to GDC-0980 (Apitolisib) were previously developed in lab by treated with different concentrations of *PI3K-mTOR* dual inhibitor GDC-0980 and the IC50 concentration was then calculated using the BrdU proliferation assay. The IC50 for the H1975 cells was 0.58μM GDC-0980. Both the parental cells and resistant cells were cultured in RPMI media. For the resistant cells 0.58μM GDC-0980 was added all the time. Looking at the data obtained from the chapter II we believe that the IL6/STAT3 plays significant role in escape mechanism in H1975 cells when treated with GDC0980. At first total RNA extraction was carried out using H1975GP and H1975GR cells which had attained 80% confluency. Arraystar® Human Lnc-RNA Microarray V4.0 was performed to analyse the differentially expressed mRNAs between the H1975GR1 or H1975GR6 and H1975GP and to quantify LncRNA. We observed that mRNA expression of a large group of genes was upregulated in resistance cell lines when compared to parental cell line and the expression was even more high in H1975GR6 cells. Changes in these mRNAs expression in H1975GR1 cells may highlight those mRNAs that are involved in the early development of resistance to GDC-0980. Considering the fact that lncRNAs are expressed aberrantly in all the cancers especially in the resistance cells it will be advantage if we target lncRNAs as they have no side effect on normal tissues. Although most of the studies on lncRNA targeting are still in the preclinical stage, research into mitochondrial long non-coding RNA (mtlncRNA) has progressed rapidly. Owing to the lack of sufficient data on clinical trials, the efficacy and safety

of lncRNA drugs in humans remain inconclusive. One of the lncRNA which was traced in literature is HOTAIR, it has entered early phase study to evaluate the potentiality of lncRNAs as biomarkers in thyroid cancer.

Further advances in lncRNA-targeted drugs for lung cancer are clearly dependent on the in-depth basic research into the function and mechanisms of lncRNAs. Of course, accurate approaches to the lncRNAs targeting and efficient delivery systems can significantly speed up this progress. LncRNA-targeted drug design provides a plethora of opportunities and challenges for the drug industry.

Later Panther-Slim biological process analysis also showed the upregulation of genes in H1975GR1 and these genes were said to be involved in cellular response to external stimuli, the genes were doubled in H1975GR6. While 55 down regulated in H1975GR1 and they were involved in the cell response to the external stimuli as well. These genes were increased to 78 genes in H1975GR6. Analysis of *PIM* Kinases pathway and its regulator was demonstrated by qRT-PCR and western blot. The results showed that *PIM1* and *PIM2* were significantly elevated (low ΔCt) in H1975GR compared to the H1975 sensitive cells and *PIM3* was also elevated but had statistical insignificance. This is because *PIM2* plays a major role in cancer cell proliferation in hematopoietic tumours and lung cancer (Liu et al., 2018).

Results from the western blot confirmed that protein expression was high in resistant cells when compared with parental cells which again aligned with the previous data. The evaluation of *MACC1* and *PIM* kinases was carried out by inhibiting siRNA expression using DharmaFECT as a transfection agent. One of the major findings in our project was the detection of *MACC1* as early marker for resistance event. According to the best of our knowledge, for the very first time in the lung cancer research we have demonstrated the role of *MACC1* in resistance to

PI3K-mTOR inhibition which in turn regulate the induction of *CMTM6*, *cMYC* and *PIM* kinases. Different classes of *CMTM* protein was analysed but later *CMTM6* was chosen for further qRT-PCR and western blot validation. According to the analysis *CMTM6* level was very high in the resistance cell line when compared to parental cells. A study by Mamessier et al., *showed that CMTM6 plays a role* in limiting antitumour immunity (Mamessier et al., 2018). When the cells were treated with AZD1208 we observed an upregulation of *c-MET*, *cMYC* and *PIM* kinases suggesting that they may play a role as an escape signalling mechanism that leads to drug resistance. The literature suggests that AZD1208 treatment alone does not induce considerable cell death whereas when combined with an Akt inhibitor there is a synergistic antitumour effect through regulation of the DNA damage repair pathway.

In addition the result of evaluation of *DSP, TNC, ERO1A* and *ENO1* genes obtained as expected and they also supported all the previous findings connecting the increased or decreased expression of these genes with drug resistance. Therefore from our chapter II and also from the relevant research we can conclude that targeting *PIM* kinases and *PI3K-mTOR* pathway as a potential strategy to treat NSCLC patient with activated *PI3K-mTOR*.

The second part of the project (Chapter III) focused on proteomic and phospho-proteomic expression analysis in LSqCC tumours. Protein expression was quantified within three regions per tumour from four patients with lung squamous cell carcinomas using matched normal tissue as a reference. Protein expression were quantified using Label-free L-C/MS-MS comparative proteomics and although the results obtained supported previous findings (the existence of intra-tumour heterogeneity) i.e. the tumour regions clustered apart from each other

tumour regions, for the most part protein expression was identified in all tumour regions albeit differentially expressed. Principle component analysis was then performed to demonstrate the heterogeneous expression of proteins between the different areas of the same tumour mass. Enolase-1, desmoplakin, tenascin C and *EROI-La* proteins were then selected for further validation by western blot analysis using the same protein samples. All the four proteins found heterogeneous in their expression by MS therefore it matched the other literature and the result was obtained as anticipated. On the other hand, *PIM* kinase expression was used to show the variance of *JAK/STAT* signalling pathway within the analysed tumours and support the existence of ITH and this was accomplished by qRT-PCR and the result suggested that heterogeneity existed within the tumour cells and at the end *PI3K-mTOR* and *JAK*/*STAT* activation was analysed using path scan array phosphor-protein analysis. From our study we can conclude that it is always better to consider previously validated biomarker which is well described with specific activated pathway and it is the easiest way to detect ITH and therefore it allows for better guidance for selection of patient customized targeted therapy. We also observed that use of GDC-0980, the PI3K-mTOR dual inhibitor wasn't a best match to treat these patients as *PIM* kinases were elevated in some tumour regions indicating functionally active *JAK/STAT* pathway.

The last part of the project (Chapter IV) focused on whole exome sequencing and microarray analysis of ITH present in the lung adenocarcinomas. Three patients with lung adenocarcinoma were considered in this study and the tumour was resected along with surrounding normal lung tissue. RNA and DNA were extracted. Total RNA samples for each patient were sent to ArrayStar™ Incorporation for mRNA expression analysis, and the DNA samples were sent to LC Sciences for

whole exome sequencing (WES). According to the data obtained, the three major mutation detected are insertion, deletion and point mutation.

There was no impact of the detected mutations on their genes' expression. However, looking at the percentage of the number of unique mutated genes per tumour region we can infer that all the three samples had high level of total heterogeneity. In patient 1, the unique mutations detected in T1 and T2 were 30.4% and 27.2%, respectively. At the gene expression level, heterogeneity score accounts for 77.7% of the upregulated genes in T1 (74.4% unique up and 3.3% detected down in T2) in addition to 60.7% of the down-regulated genes were unique in T1. T2 of patient 1 67.5% and 38.8% of the upregulated and down-regulated genes, respectively, were detected unique in this tumour region. In patient 2, the mutations shared between the two tumour regions was very high, accounting for 90.5%. At the gene expression levels, 33.7% of the upregulated genes and 14% of the down-regulated genes in T1 were unique, while 60.4% and 46.7% of the up and down-regulated genes in T2 were unique. Heterogeneity within patient 2 tumour sections were more obvious at gene expression levels than in mutations. In patient 3, 9.1% and 20% of the point mutations were detected unique in T1 and T2, respectively. There were 20-times more SNPs in T1 than in T2. 39% and 15% of the up and down-regulated genes in T1 were unique, while, 14% and 30% of the up and down-regulated genes in T2 were unique. Covering the most frequent and well known event in lung cancer is tumour heterogeneity which is responsible for several major issues like tumour relapse and treatment implication. Heterogeneity could be mainly because of cell population with varied expression of cell markers to the genetic or epigenetic alterations (Kreso and Dick, 2014). Several different types of heterogeneity have been noticed in lung cancer such as inter tumour, intratumour

and interpatient variability. Out of the three heterogeneity intra tumour place a major role in lung cancer leading to difference in the treatment response in each individual resulting in drug resistance therefore altering the treatment outcome in patients. Furthermore, significant genetic diversity between the primary tumour and corresponding metastatic lesions could play a pivotal role in the therapeutic context of lung cancer patients (Marusyk et al., 2012). Hence there is more scope for personalised and targeted therapy where the molecular profiling of tumour being a part of the standard diagnostic protocol. Screening tumour allows clinician to distinguish patients for targeted therapies.

Diagnostics and therapeutics have been combined meaningfully to achieve a personalised medicine approach to treatment that is now common place in the clinic. Targeted therapy is a new option for treating patients made possible by screening tumours for predictive biomarkers. Targeted therapy is said to be the best approach to treatment and has revolutionized the field as the targeted drugs work differently from standard chemotherapy with less side effects and great efficacy. FDA have approved targeted therapy for lung cancer tumours showing characteristics of abnormalities in *EGFR, ALK, ROS-1, NTRK, MET, RET* and *BRAF V600E*. The *PI3K*/*AKT*/*mTOR* pathway is commonly activated in non-small-cell lung cancer. In addition they mediate resistance to *EGF* receptor tyrosine kinase inhibitors. Although the mechanism of resistance to *PI3K* is the active area of research, activation of parallel signalling pathway have been observed and have suggested to play a major role. Hence, significant strategy to improve the treatment outcome is by combination therapy where the targeted therapy efficacy is enhanced by additional co-targeting the potential bypass tracts (Heavey et al., 2014). For instance to overwhelm the activation of *EGFR/ MEK* pathway by *PI3K* inhibitors,

combination therapy with both *PI3K* and *EGFR/ MEK* inhibitor has been tested in preclinical trials.

Increased cell signalling towards cell survival and proliferation is very important for cancer cells. Molecules responsible for cell signalling are kinases in nature and operate through phosphorylation events. In the last part of this chapter, KEGG analysis was used to examine the differentially expressed genes and determine whether either the *PI3K-mTOR* or *JAK/STAT* signalling pathways showed differences between two tumour regions of the patients involved in this study. This helps us to understand the possible activation of *AKT* that intersect with and bypass *PI3K/AKT* pathway. We focus on tyrosine kinases and their role in *PI3K/AKT* and *JAK/STAT* pathway. The former is one of GDC-0980 targets and the latter is the pathway involved in acquired resistance to the inhibitor. *RTK/PI3K/mTORC2/AKT* signalling cascade can be attributed as being the underlying cause of dysregulated *AKT* activation in a high proportion of these cancers. However, majority of cancer do not exhibit *RTK/PI3K* pathway aberrations but they possess activated *AKT* expression.

The genomic and transcriptomic data outlined in this research work combined provide evidence that there are variations in both the mutation and gene expression profiles between the two examined regions of the same tumour. In summary, in addition to the principle of intra-tumour heterogeneity role in development of treatment adaptation by cancer cells, we must be aware of choosing the right candidate for targeted therapy as well as planning for a good drug combination (eg. tumours with *EGFR* overexpression /mutation with gain of function plus activated *PI3K* kinase cannot be treated by PI3K monotherapy inhibitors but combination of *EGFR* and *PI3K* inhibitors would be more effective in suppressing tumour growth otherwise cross-talk of the increased *EGFR* signalling with other pathways would lead to bypass and adapt *PI3K* inhibition).

Prior knowledge of activated pathways associated with drug resistance to the proposed targeted inhibitor in combination with scanning for these pathways to assess their activation in multiple tumour regions by phospho-proteomics, mass-spectrometry, microarray scanning, WES with accurate in-depth bioinformatic analysis would make us more competent in planning the patient-customised treatment protocol.

5.2. Conclusion

This study confirms that tumour cells respond to targeted pathway inhibition by activation of bypass signalling pathways to hamper the effect of drug treatments. We demonstrated that activation of *PIM* kinase and its co-regulators c-Myc and *MACC1* occurs in response to *PI3K-mTOR* inhibition in NSCLC. *MACC1* activation was an early event in *PI3K-mTOR* drug resistance and may have regulated the induction of *c-Myc*, *PIM* kinases and EMT-related genes. Further studies targeting the *PIM* kinase pathway are warranted to delineate the interplay between it and *MACC1*, *c-Myc* and also *CMTM6* which were all activated in response to *PI3K-mTOR* inhibition. These results, together with previous data in other cancer types highlight the potential for dual targeting of both the *PI3K-mTOR* and *PIM* kinase pathways as a promising strategy for the future treatment of patients with *PI3K-mTOR* activated NSCLC.

Our profiling studies on intra-tumour heterogeneity (ITH) showed that there are differences in protein and phosphoprotein expression between different regions of tumour. However, for most proteins some expression was detected in all regions of the tumour examined albeit at different amounts. Therefore if possible multiple biopsies should be screened to determine biomarker expression where feasible and cut-off values for predictive biomarkers must be carefully considered when assigning patients to specific targeted treatments. Our panel of biomarkers *DSP,*

TNC, ERO1A and *ENO1* were differentially expressed in different regions of the tumour and further studies in a larger cohort of NSCLC patients are warranted to determine their use as potential biomarkers in NSCLC.

The main limitation of our ITH studies was the small sample size analysed, and this was due to the cost involved in the next generation sequencing technologies used and Our results therefore may not reflect what happens in all tumours but it does give an insight into the amount and types of ITH that are present across NSCLC tumours.

our dataset has identified lncRNA expression profiles in lung cancer and further investigations on lncRNA expression and its involvement in molecular regulatory mechanisms may be a critical step in personalized treatment. The targeting of dysregulated lncRNAs could provide a new therapeutic approach for NSCLC treatment.

Overall tumour heterogeneity hampers drug efficacy and leads to tumour relapse due to multiple parallel drug resistance mechanisms that result in poor treatment outcomes for patients. In-depth analysis of the results of this research study supports our initial hypothesis that the elucidation of the mechanisms of resistance to *PI3K-mTOR* inhibition will provide a rationale for co-targeting treatment strategies for patients with tumours that have a dysregulated *PI3K-mTOR* pathway. Furthermore comparison of DNA mutation profiles and RNA, protein and phosphorylated protein expression profiles, within different regions of the same tumour has highlighted the potential limitations of tumour tissue biopsies to accurately predict molecular or proteomic profiles which could interfere with patient stratification for personalised targeted treatment.

5.3. Future Plan

The future plan would include the following research studies to:

1- Delineate further the precise interplay between *PIM* kinases, *MACC1*, CMTM6, *c-Myc* and *c-Met* in both NSCLC cells and cell lines resistant to GDC-0980.

2- Validate *PIM* kinases, *MACC1*, *CMTM6*, *c-Myc* and *c-Met* in the two other cell lines resistant to GDC-0980; i.e: A549GR and H460GR.

3- Test further drug combinations in order to overcome the resistance to *PI3K-mTOR* inhibition (e.g. *PIM*-447 (pan-*PIM* kinase inhibitor) + GDC-0980, or *MACC1* inhibitor + GDC-0980).

4- Validate the non-coding RNAs found associated with the resistance to GDC-0980 in H1975GR cells.

5- Validation of our panel of biomarkers in a larger cohort of NSCLC patients and correlate to overall survival to determine their use as prognostic markers.

References

ABE, Y., OHNISHI, Y., YOSHIMURA, M., OTA, E., OZEKI, Y., OSHIKA, Y., TOKUNAGA, T., YAMAZAKI, H., UEYEMA, Y., OGATA, T., TAMAOKI, N. & NAKAMURA, M. 1996. P-glycoprotein-mediated acquired multidrug resistance of human lung cancer cells in vivo. *Br J Cancer,* 74**,** 1929-34.

ABERLE, D. R., ADAMS, A. M., BERG, C. D., BLACK, W. C., CLAPP, J. D., FAGERSTROM, R. M., GAREEN, I. F., GATSONIS, C., MARCUS, P. M., SICKS, J. D. & TEAM, N. L. S. T. R. 2011. Reduced lung-cancer mortality with low-dose computed tomographic screening. *N Engl J Med,* 365**,** 395-409.

AKINLEYE, A., AVVARU, P., FURQAN, M., SONG, Y. & LIU, D. 2013. Phosphatidylinositol 3-kinase (PI3K) inhibitors as cancer therapeutics. *J Hematol Oncol,* 6**,** 88.

AKSAMITIENE, E., KIYATKIN, A. & KHOLODENKO, B. N. 2012. Cross-talk between mitogenic Ras/MAPK and survival PI3K/Akt pathways: a fine balance. *Biochem Soc Trans,* 40**,** 139-46.

ALBAUGH, P., FAN, Y., MI, Y., SUN, F., ADRIAN, F., LI, N., JIA, Y., SARKISOVA, Y., KREUSCH, A., HOOD, T., LU, M., LIU, G., HUANG, S., LIU, Z., LOREN, J., TUNTLAND, T., KARANEWSKY, D. S., SEIDEL, H. M. & MOLTENI, V. 2012. Discovery of GNF-5837, a Selective TRK Inhibitor with Efficacy in Rodent Cancer Tumour Models. *ACS Med Chem Lett,* 3**,** 140-5.

ALSAAB, H. O., SAU, S., ALZHRANI, R., TATIPARTI, K., BHISE, K., KASHAW, S. K. & IYER, A. K. 2017. PD-1 and PD-L1 Checkpoint Signaling Inhibition for Cancer Immunotherapy: Mechanism, Combinations, and Clinical Outcome. *Front Pharmacol,* 8**,** 561.

ALSINA, M., MARCOS-GRAGERA, R., CAPDEVILA, J., BUXÓ, M., ORTIZ, R. M., BARRETINA, P., VILARDELL, L., BRUNET, J., BELTRAN, M. & IZQUIERDO, Á. 2011. Neuroendocrine tumours: a population-based study of incidence and survival in Girona Province, 1994-2004. *Cancer Epidemiol,* 35**,** e49-54.

AMEDEE, R. G. & DHURANDHAR, N. R. 2001. Fine-needle aspiration biopsy. *Laryngoscope,* 111**,** 1551-7.

ANTELOPE, O., VELLORE, N. A., POMICTER, A. D., PATEL, A. B., VAN SCOYK, A., CLAIR, P. M., DEININGER, M. W. & O'HARE, T. 2019. BCR-ABL1 tyrosine kinase inhibitor K0706 exhibits preclinical activity in Philadelphia chromosome-positive leukemia. *Exp Hematol,* 77**,** 36-40.e2.

ARCILA, M. E., OXNARD, G. R., NAFA, K., RIELY, G. J., SOLOMON, S. B., ZAKOWSKI, M. F., KRIS, M. G., PAO, W., MILLER, V. A. & LADANYI, M. 2011. Rebiopsy of lung cancer patients with acquired resistance to EGFR inhibitors and enhanced detection of the T790M mutation using a locked nucleic acid-based assay. *Clin Cancer Res,* 17**,** 1169-80.

ARDITO, F., GIULIANI, M., PERRONE, D., TROIANO, G. & LO MUZIO, L. 2017. The crucial role of protein phosphorylation in cell signaling and its use as targeted therapy (Review). *Int J Mol Med,* 40**,** 271-280.

B'CHIR, F., LAOUANI, A., KSIBI, S., ARNAUD, M. J. & SAGUEM, S. 2007. Cigarette filter and the incidence of lung adenocarcinoma among Tunisian population. *Lung Cancer,* 57**,** 26-33.

BAGULEY, B. C. 2016. Classical and Targeted Anticancer Drugs: An Appraisal of Mechanisms of Multidrug Resistance. *Methods Mol Biol,* 1395**,** 19-37.

BARDELLI, A., PARSONS, D. W., SILLIMAN, N., PTAK, J., SZABO, S., SAHA, S., MARKOWITZ, S., WILLSON, J. K., PARMIGIANI, G., KINZLER, K. W.,

VOGELSTEIN, B. & VELCULESCU, V. E. 2003. Mutational analysis of the tyrosine kinome in colorectal cancers. *Science,* 300**,** 949.

BARTA, J. A., HENSCHKE, C. I., FLORES, R. M., YIP, R., YANKELEVITZ, D. F. & POWELL, C. A. 2017. Lung Cancer Diagnosis by Fine Needle Aspiration Is Associated With Reduction in Resection of Nonmalignant Lung Nodules. *Ann Thorac Surg,* 103**,** 1795-1801.

BEAN, J., BRENNAN, C., SHIH, J. Y., RIELY, G., VIALE, A., WANG, L., CHITALE, D., MOTOI, N., SZOKE, J., BRODERICK, S., BALAK, M., CHANG, W. C., YU, C. J., GAZDAR, A., PASS, H., RUSCH, V., GERALD, W., HUANG, S. F., YANG, P. C., MILLER, V., LADANYI, M., YANG, C. H. & PAO, W. 2007. MET amplification occurs with or without T790M mutations in EGFR mutant lung tumours with acquired resistance to gefitinib or erlotinib. *Proc Natl Acad Sci U S A,* 104**,** 20932-7.

BELLO, M. J. & REY, J. A. 1995. (Neurologic diseases due to alterations in oncogenes and tumour suppressing genes). *Neurologia,* 10 Suppl 1**,** 20-31.

BENN, S. C., PERRELET, D., KATO, A. C., SCHOLZ, J., DECOSTERD, I., MANNION, R. J., BAKOWSKA, J. C. & WOOLF, C. J. 2002. Hsp27 upregulation and phosphorylation is required for injured sensory and motor neuron survival. *Neuron,* 36**,** 45-56.

BERGER, W., SETINEK, U., HOLLAUS, P., ZIDEK, T., STEINER, E., ELBLING, L., CANTONATI, H., ATTEMS, J., GSUR, A. & MICKSCHE, M. 2005. Multidrug resistance markers P-glycoprotein, multidrug resistance protein 1, and lung resistance protein in non-small cell lung cancer: prognostic implications. *J Cancer Res Clin Oncol,* 131**,** 355-63.

BERTINO, E. M., CONFER, P. D., COLONNA, J. E., ROSS, P. & OTTERSON, G. A. 2009. Pulmonary neuroendocrine/carcinoid tumours: a review article. *Cancer,* 115**,** 4434-41.

BERTUCCI, F., SALAS, S., EYSTERIES, S., NASSER, V., FINETTI, P., GINESTIER, C., CHARAFE-JAUFFRET, E., LORIOD, B., BACHELART, L., MONTFORT, J., VICTORERO, G., VIRET, F., OLLENDORFF, V., FERT, V., GIOVANINNI, M., DELPERO, J. R., NGUYEN, C., VIENS, P., MONGES, G., BIRNBAUM, D. &

HOULGATTE, R. 2004. Gene expression profiling of colon cancer by DNA microarrays and correlation with histoclinical parameters. *Oncogene,* 23**,** 1377-91.

BILAL, E., ALEXE, G., YAO, M., CONG, L., KULKARNI, A., GINJALA, V., TOPPMEYER, D., GANESAN, S. & BHANOT, G. 2010. Identification of the YES1 Kinase as a Therapeutic Target in Basal-Like Breast Cancers. *Genes Cancer,* 1**,** 1063-73.

BOARDMAN, L. A. 2009. Overexpression of MACC1 leads to downstream activation of HGF/MET and potentiates metastasis and recurrence of colorectal cancer. *Genome Med,* 1**,** 36.

BOUSSIOTIS, V. A. 2016. Molecular and Biochemical Aspects of the PD-1 Checkpoint Pathway. *N Engl J Med,* 375**,** 1767-1778.

BRASÓ-MARISTANY, F., FILOSTO, S., CATCHPOLE, S., MARLOW, R., QUIST, J., FRANCESCH-DOMENECH, E., PLUMB, D. A., ZAKKA, L., GAZINSKA, P., LICCARDI, G., MEIER, P., GRIS-OLIVER, A., CHEANG, M. C., PERDRIX-ROSELL, A., SHAFAT, M., NOËL, E., PATEL, N., MCEACHERN, K., SCALTRITI, M., CASTEL, P., NOOR, F., BUUS, R., MATHEW, S., WATKINS, J., SERRA, V., MARRA, P., GRIGORIADIS, A. & TUTT, A. N. 2016. PIM1 kinase regulates cell death, tumour growth and chemotherapy response in triple-negative breast cancer. *Nat Med,* 22**,** 1303-1313.

BRAULT, L., GASSER, C., BRACHER, F., HUBER, K., KNAPP, S. & SCHWALLER, J. 2010. PIM serine/threonine kinases in the pathogenesis and therapy of hematologic malignancies and solid cancers. *Haematologica,* 95**,** 1004-15.

BRIGGS, S. & TOMLINSON, I. 2013. Germline and somatic polymerase ε and δ mutations define a new class of hypermutated colorectal and endometrial cancers. *J Pathol,* 230**,** 148-53.

BRODY, A. R. 2005. The brush cell. *Am J Respir Crit Care Med,* 172**,** 1349.

BROWN, K. A. L., D.T. 2018. *Histology, Lung.*

BROWN, N. F., WILLIAMS, M., ARKENAU, H. T., FLEMING, R. A., TOLSON, J., YAN, L., ZHANG, J., SWARTZ, L., SINGH, R., AUGER, K. R., LENOX, L., COX, D., LEWIS, Y., PLISSON, C., SEARLE, G., SALEEM, A., BLAGDEN, S. &

MULHOLLAND, P. 2018. A study of the focal adhesion kinase inhibitor GSK2256098 in patients with recurrent glioblastoma with evaluation of tumour penetration of (11C)GSK2256098. *Neuro Oncol,* 20**,** 1634-1642.

BRUGGE, J., HUNG, M. C. & MILLS, G. B. 2007. A new mutational AKTivation in the PI3K pathway. *Cancer Cell,* 12**,** 104-7.

BUCHANAN, S. G., HENDLE, J., LEE, P. S., SMITH, C. R., BOUNAUD, P. Y., JESSEN, K. A., TANG, C. M., HUSER, N. H., FELCE, J. D., FRONING, K. J., PETERMAN, M. C., AUBOL, B. E., GESSERT, S. F., SAUDER, J. M., SCHWINN, K. D., RUSSELL, M., ROONEY, I. A., ADAMS, J., LEON, B. C., DO, T. H., BLANEY, J. M., SPRENGELER, P. A., THOMPSON, D. A., SMYTH, L., PELLETIER, L. A., ATWELL, S., HOLME, K., WASSERMAN, S. R., EMTAGE, S., BURLEY, S. K. & REICH, S. H. 2009. SGX523 is an exquisitely selective, ATP-competitive inhibitor of the MET receptor tyrosine kinase with antitumour activity in vivo. *Mol Cancer Ther,* 8**,** 3181-90.

BURGER, J. A. & BUGGY, J. J. 2013. Bruton tyrosine kinase inhibitor ibrutinib (PCI-32765). *Leuk Lymphoma,* 54**,** 2385-91.

BURKHART-SCHULTZ, K. J. & JONES, I. M. 1997. Deletion and insertion in vivo somatic mutations in the hypoxanthine phosphoribosyltransferase (hprt) gene of human T-lymphocytes. *Environ Mol Mutagen,* 30**,** 371-84.

BURRELL, R. A. & SWANTON, C. 2014. Tumour heterogeneity and the evolution of polyclonal drug resistance. *Mol Oncol,* 8**,** 1095-111.

CABILI, M. N., TRAPNELL, C., GOFF, L., KOZIOL, M., TAZON-VEGA, B., REGEV, A. & RINN, J. L. 2011. Integrative annotation of human large intergenic noncoding RNAs reveals global properties and specific subclasses. *Genes Dev,* 25**,** 1915-27.

CABRERA CÉSAR, E., FERNÁNDEZ AGUIRRE, M. D. C., REINA MARFIL, N. & VELASCO GARRIDO, J. L. 2018. Diagnosis of Adrenocortical Carcinoma by Flexible Bronchoscopy. *Arch Bronconeumol,* 54**,** 171-172.

CAI, J., DU, S., WANG, H., XIN, B., WANG, J., SHEN, W., WEI, W., GUO, Z. & SHEN, X. 2017. Tenascin-C induces migration and invasion through JNK/c-Jun signalling in pancreatic cancer. *Oncotarget,* 8**,** 74406-74422.

CAPLIN, M. E., BAUDIN, E., FEROLLA, P., FILOSSO, P., GARCIA-YUSTE, M., LIM, E., OBERG, K., PELOSI, G., PERREN, A., ROSSI, R. E., TRAVIS, W. D. & PARTICIPANTS, E. C. C. 2015. Pulmonary neuroendocrine (carcinoid) tumours: European Neuroendocrine Tumour Society expert consensus and recommendations for best practice for typical and atypical pulmonary carcinoids. *Ann Oncol,* 26**,** 1604-20.

CAPPELLI, L. C., SHAH, A. A. & BINGHAM, C. O. 2017. Immune-Related Adverse Effects of Cancer Immunotherapy- Implications for Rheumatology. *Rheum Dis Clin North Am,* 43**,** 65-78.

CAPPUZZO, F., JÄNNE, P. A., SKOKAN, M., FINOCCHIARO, G., ROSSI, E., LIGORIO, C., ZUCALI, P. A., TERRACCIANO, L., TOSCHI, L., RONCALLI, M., DESTRO, A., INCARBONE, M., ALLOISIO, M., SANTORO, A. & VARELLA-GARCIA, M. 2009. MET increased gene copy number and primary resistance to gefitinib therapy in non-small-cell lung cancer patients. *Ann Oncol,* 20**,** 298-304.

CARRACEDO, A., MA, L., TERUYA-FELDSTEIN, J., ROJO, F., SALMENA, L., ALIMONTI, A., EGIA, A., SASAKI, A. T., THOMAS, G., KOZMA, S. C., PAPA, A., NARDELLA, C., CANTLEY, L. C., BASELGA, J. & PANDOLFI, P. P. 2008. Inhibition of mTORC1 leads to MAPK pathway activation through a PI3K-dependent feedback loop in human cancer. *J Clin Invest,* 118**,** 3065-74.

CARRIAGA, M. T. & HENSON, D. E. 1995. The histologic grading of cancer. *Cancer,* 75**,** 406-21.

CARVALHO, M., PINO, M. A., KARCHIN, R., BEDDOR, J., GODINHO-NETTO, M., MESQUITA, R. D., RODARTE, R. S., VAZ, D. C., MONTEIRO, V. A., MANOUKIAN, S., COLOMBO, M., RIPAMONTI, C. B., ROSENQUIST, R., SUTHERS, G., BORG, A., RADICE, P., GRIST, S. A., MONTEIRO, A. N. & BILLACK, B. 2009. Analysis of a set of missense, frameshift, and in-frame deletion variants of BRCA1. *Mutat Res,* 660**,** 1-11.

CASTRO, M. A., DAL-PIZZOL, F., ZDANOV, S., SOARES, M., MÜLLER, C. B., LOPES, F. M., ZANOTTO-FILHO, A., DA CRUZ FERNANDES, M., MOREIRA, J. C., SHACTER, E. & KLAMT, F. 2010. CFL1 expression levels as a prognostic and drug resistance marker in nonsmall cell lung cancer. *Cancer,* 116**,** 3645-55.

CAVALIERE, A., PROBST, K. C., WESTWELL, A. D. & SLUSARCZYK, M. 2017. Fluorinated nucleosides as an important class of anticancer and antiviral agents. *Future Med Chem,* 9**,** 1809-1833.

CEN, B., MAHAJAN, S., WANG, W. & KRAFT, A. S. 2013. Elevation of receptor tyrosine kinases by small molecule AKT inhibitors in prostate cancer is mediated by Pim-1. *Cancer Res,* 73**,** 3402-11.

CERSOSIMO, R. J. 2002. Lung cancer: a review. *Am J Health Syst Pharm,* 59**,** 611-42.

CHALHOUB, N. & BAKER, S. J. 2009. PTEN and the PI3-kinase pathway in cancer. *Annu Rev Pathol,* 4**,** 127-50.

CHANDARLAPATY, S., SAWAI, A., SCALTRITI, M., RODRIK-OUTMEZGUINE, V., GRBOVIC-HUEZO, O., SERRA, V., MAJUMDER, P. K., BASELGA, J. & ROSEN, N. 2011. AKT inhibition relieves feedback suppression of receptor tyrosine kinase expression and activity. *Cancer Cell,* 19**,** 58-71.

CHATTERJEE, N. & WALKER, G. C. 2017. Mechanisms of DNA damage, repair, and mutagenesis. *Environ Mol Mutagen,* 58**,** 235-263.

CHAUHAN, S. S., TOTH, R. K., JENSEN, C. C., CASILLAS, A. L., KASHATUS, D. F. & WARFEL, N. A. 2020. PIM kinases alter mitochondrial dynamics and chemosensitivity in lung cancer. *Oncogene,* 39**,** 2597-2611.

CHEN, J. M., CHIU, S. C., CHEN, K. C., HUANG, Y. J., LIAO, Y. A. & YU, C. R. 2020. Enolase 1 differentially contributes to cell transformation in lung cancer but not in esophageal cancer. *Oncol Lett,* 19**,** 3189-3196.

CHEN, L., YU, Z., LEE, Y., WANG, X., ZHAO, B. & JUNG, Y. M. 2012. Quantitative evaluation of proteins with bicinchoninic acid (BCA): resonance Raman and surface-enhanced resonance Raman scattering-based methods. *Analyst,* 137**,** 5834-8.

CHEN, W., ZHENG, R., BAADE, P. D., ZHANG, S., ZENG, H., BRAY, F., JEMAL, A., YU, X. Q. & HE, J. 2016. Cancer statistics in China, 2015. *CA Cancer J Clin,* 66**,** 115-32.

CHEN, W., ZHENG, R., ZENG, H. & ZHANG, S. 2015a. Epidemiology of lung cancer in China. *Thorac Cancer,* 6**,** 209-15.

CHEN, W., ZHENG, R., ZENG, H., ZHANG, S. & HE, J. 2015b. Annual report on status of cancer in China, 2011. *Chin J Cancer Res,* 27**,** 2-12.

CHEN, W. W., CHAN, D. C., DONALD, C., LILLY, M. B. & KRAFT, A. S. 2005. Pim family kinases enhance tumour growth of prostate cancer cells. *Mol Cancer Res,* 3**,** 443-51.

CHEN, Y., TANG, W. Y., TONG, X. & JI, H. 2019. Pathological transition as the arising mechanism for drug resistance in lung cancer. *Cancer Commun (Lond),* 39**,** 53.

CHEN, Z., FILLMORE, C. M., HAMMERMAN, P. S., KIM, C. F. & WONG, K. K. 2014. Non-small-cell lung cancers: a heterogeneous set of diseases. *Nat Rev Cancer,* 14**,** 535-46.

CHENG, H., SHCHERBA, M., PENDURTI, G., LIANG, Y., PIPERDI, B. & PEREZ-SOLER, R. 2014. Targeting the PI3K/AKT/mTOR pathway: potential for lung cancer treatment. *Lung Cancer Manag,* 3**,** 67-75.

CHENG, T. Y., CRAMB, S. M., BAADE, P. D., YOULDEN, D. R., NWOGU, C. & REID, M. E. 2016. The International Epidemiology of Lung Cancer: Latest Trends, Disparities, and Tumour Characteristics. *J Thorac Oncol,* 11**,** 1653-71.

CHIEN, J., KUANG, R., LANDEN, C. & SHRIDHAR, V. 2013. Platinum-sensitive recurrence in ovarian cancer: the role of tumour microenvironment. *Front Oncol,* 3**,** 251.

CHOI, C. M. & LEE, J. C. 2017. Staging Work-up for Early Lung Cancer: The More the Better? *Tuberc Respir Dis (Seoul),* 80**,** 403-404.

CHU, Q. S. 2020. Targeting non-small cell lung cancer: driver mutation beyond epidermal growth factor mutation and anaplastic lymphoma kinase fusion. *Ther Adv Med Oncol,* 12**,** 1758835919895756.

CLARK, M. B. & MATTICK, J. S. 2011. Long noncoding RNAs in cell biology. *Semin Cell Dev Biol,* 22**,** 366-76.

CLEMENS, G. R., SCHROEDER, R. E., MAGNESS, S. H., WEAVER, E. V., LECH, J. W., TAYLOR, V. C., MASUDA, E. S., BALUOM, M. & GROSSBARD, E. B. 2009. Developmental toxicity associated with receptor tyrosine kinase Ret inhibition in reproductive toxicity testing. *Birth Defects Res A Clin Mol Teratol,* 85**,** 130-6.

COLE, A. J., CLIFTON-BLIGH, R. & MARSH, D. J. 2015. Histone H2B monoubiquitination: roles to play in human malignancy. *Endocr Relat Cancer,* 22**,** T19-33.

CONG, P., YE, Y., WANG, Y., LU, L., YONG, J., YU, P., JOSEPH, K. K., JIN, F. & QI, M. 2012. A large deletion/insertion-induced frameshift mutation of the androgen receptor gene in a family with a familial complete androgen insensitivity syndrome. *Gene,* 500**,** 220-3.

COURTNEY, K. D., CORCORAN, R. B. & ENGELMAN, J. A. 2010. The PI3K pathway as drug target in human cancer. *J Clin Oncol,* 28**,** 1075-83.

CROOP, J. M., RAYMOND, M., HABER, D., DEVAULT, A., ARCECI, R. J., GROS, P. & HOUSMAN, D. E. 1989. The three mouse multidrug resistance (mdr) genes are expressed in a tissue-specific manner in normal mouse tissues. *Mol Cell Biol,* 9**,** 1346-50.

CROWDER, R. J., PHOMMALY, C., TAO, Y., HOOG, J., LUO, J., PEROU, C. M., PARKER, J. S., MILLER, M. A., HUNTSMAN, D. G., LIN, L., SNIDER, J., DAVIES, S. R., OLSON, J. A., WATSON, M. A., SAPORITA, A., WEBER, J. D. & ELLIS, M. J. 2009. PIK3CA and PIK3CB inhibition produce synthetic lethality when combined with estrogen deprivation in estrogen receptor-positive breast cancer. *Cancer Res,* 69**,** 3955-62.

CUADRAS, A., ROVIRA, E., MARCÉ, R. M. & BORRULL, F. 2016. Lung cancer risk by polycyclic aromatic hydrocarbons in a Mediterranean industrialized area. *Environ Sci Pollut Res Int,* 23**,** 23215-23227.

CUI, D., YU, C. H., LIU, M., XIA, Q. Q., ZHANG, Y. F. & JIANG, W. L. 2016. Long non-coding RNA PVT1 as a novel biomarker for diagnosis and prognosis of non-small cell lung cancer. *Tumour Biol,* 37**,** 4127-34.

CUSNIR, M. & CAVALCANTE, L. 2012. Inter-tumour heterogeneity. *Hum Vaccin Immunother,* 8**,** 1143-5.

D'AMICO, M. A., GHINASSI, B., IZZICUPO, P., MANZOLI, L. & DI BALDASSARRE, A. 2014. Biological function and clinical relevance of chromogranin A and derived peptides. *Endocr Connect,* 3**,** R45-54.

DANG, C. V., RESAR, L. M., EMISON, E., KIM, S., LI, Q., PRESCOTT, J. E., WONSEY, D. & ZELLER, K. 1999. Function of the c-Myc oncogenic transcription factor. *Exp Cell Res,* 253**,** 63-77.

DAVIES, H., GLODZIK, D., MORGANELLA, S., YATES, L. R., STAAF, J., ZOU, X., RAMAKRISHNA, M., MARTIN, S., BOYAULT, S., SIEUWERTS, A. M., SIMPSON, P. T., KING, T. A., RAINE, K., EYFJORD, J. E., KONG, G., BORG, Å., BIRNEY, E., STUNNENBERG, H. G., VAN DE VIJVER, M. J., BØRRESEN-DALE, A. L., MARTENS, J. W., SPAN, P. N., LAKHANI, S. R., VINCENT-SALOMON, A., SOTIRIOU, C., TUTT, A., THOMPSON, A. M., VAN LAERE, S., RICHARDSON, A. L., VIARI, A., CAMPBELL, P. J., STRATTON, M. R. & NIK-ZAINAL, S. 2017. HRDetect is a predictor of BRCA1 and BRCA2 deficiency based on mutational signatures. *Nat Med,* 23**,** 517-525.

DAVIS, A. A. & PATEL, V. G. 2019. The role of PD-L1 expression as a predictive biomarker: an analysis of all US Food and Drug Administration (FDA) approvals of immune checkpoint inhibitors. *J Immunother Cancer,* 7**,** 278.

DAVIS, M. I., HUNT, J. P., HERRGARD, S., CICERI, P., WODICKA, L. M., PALLARES, G., HOCKER, M., TREIBER, D. K. & ZARRINKAR, P. P. 2011. Comprehensive analysis of kinase inhibitor selectivity. *Nat Biotechnol,* 29**,** 1046-51.

DAVIS, S. L., ECKHARDT, S. G., DIAMOND, J. R., MESSERSMITH, W. A., DASARI, A., WEEKES, C. D., LIEU, C. H., KANE, M., CHOON TAN, A., PITTS, T. M. & LEONG, S. 2018. A Phase I Dose-Escalation Study of Linsitinib (OSI-906), a Small-Molecule Dual Insulin-Like Growth Factor-1 Receptor/Insulin Receptor Kinase Inhibitor, in Combination with Irinotecan in Patients with Advanced Cancer. *Oncologist,* 23**,** 1409-e140.

DE SOUSA E MELO, F., VERMEULEN, L., FESSLER, E. & MEDEMA, J. P. 2013. Cancer heterogeneity--a multifaceted view. *EMBO Rep,* 14**,** 686-95.

DEMPSEY, S., LYONS, S. & NOLAN, A. 2018. High Radon Areas and lung cancer prevalence: Evidence from Ireland. *J Environ Radioact,* 182**,** 12-19.

DHILLON, S. 2020. Delgocitinib: First Approval. *Drugs*.

DOWNWARD, J. 1999. How BAD phosphorylation is good for survival. *Nat Cell Biol,* 1**,** E33-5.

DRATKIEWICZ, E., SIMICZYJEW, A., PIETRASZEK-GREMPLEWICZ, K., MAZURKIEWICZ, J. & NOWAK, D. 2019. Characterization of Melanoma Cell Lines Resistant to Vemurafenib and Evaluation of Their Responsiveness to EGFR- and MET-Inhibitor Treatment. *Int J Mol Sci,* 21.

DU, Z. & LOVLY, C. M. 2018. Mechanisms of receptor tyrosine kinase activation in cancer. *Mol Cancer,* 17**,** 58.

DUAN, J., CHEN, L., ZHOU, M., ZHANG, J., SUN, L., HUANG, N., BIN, J., LIAO, Y. & LIAO, W. 2017. MACC1 decreases the chemosensitivity of gastric cancer cells to oxaliplatin by regulating FASN expression. *Oncol Rep,* 37**,** 2583-2592.

DUBIN, S. & GRIFFIN, D. 2020. Lung Cancer in Non-Smokers. *Mo Med,* 117**,** 375-379.

DUNNE, P. D., ALDERDICE, M., O'REILLY, P. G., RODDY, A. C., MCCORRY, A. M. B., RICHMAN, S., MAUGHAN, T., MCDADE, S. S., JOHNSTON, P. G., LONGLEY, D. B., KAY, E., MCART, D. G. & LAWLER, M. 2017. Cancer-cell intrinsic gene expression signatures overcome intratumoural heterogeneity bias in colorectal cancer patient classification. *Nat Commun,* 8**,** 15657.

DÍAZ-RAMOS, A., ROIG-BORRELLAS, A., GARCÍA-MELERO, A. & LÓPEZ-ALEMANY, R. 2012. α-Enolase, a multifunctional protein: its role on pathophysiological situations. *J Biomed Biotechnol,* 2012**,** 156795.

EDDY, H. A. & CASARETT, G. W. 1973. Development of the vascular system in the hamster malignant neurilemmoma. *Microvasc Res,* 6**,** 63-82.

EHRHART, N. 1998. Principles of tumour biopsy. *Clin Tech Small Anim Pract,* 13**,** 10-6.

ELKIS, Y., COHEN, M., YAFFE, E., SATMARY-TUSK, S., FELDMAN, T., HIKRI, E., NYSKA, A., FEIGLIN, A., OFRAN, Y., SHPUNGIN, S. & NIR, U. 2017. A novel Fer/FerT targeting compound selectively evokes metabolic stress and necrotic death in malignant cells. *Nat Commun,* 8**,** 940.

ENG, J., WOO, K. M., SIMA, C. S., PLODKOWSKI, A., HELLMANN, M. D., CHAFT, J. E., KRIS, M. G., ARCILA, M. E., LADANYI, M. & DRILON, A. 2015. Impact of Concurrent PIK3CA Mutations on Response to EGFR Tyrosine Kinase Inhibition in EGFR-Mutant Lung Cancers and on Prognosis in Oncogene-Driven Lung Adenocarcinomas. *J Thorac Oncol,* 10**,** 1713-9.

ENGELMAN, J. A., CHEN, L., TAN, X., CROSBY, K., GUIMARAES, A. R., UPADHYAY, R., MAIRA, M., MCNAMARA, K., PERERA, S. A., SONG, Y., CHIRIEAC, L. R., KAUR, R., LIGHTBOWN, A., SIMENDINGER, J., LI, T., PADERA, R. F., GARCÍA-ECHEVERRÍA, C., WEISSLEDER, R., MAHMOOD, U., CANTLEY, L. C. & WONG, K. K. 2008. Effective use of PI3K and MEK inhibitors to treat mutant Kras G12D and PIK3CA H1047R murine lung cancers. *Nat Med,* 14**,** 1351-6.

EVANS, M. J., VAN WINKLE, L. S., FANUCCHI, M. V. & PLOPPER, C. G. 2001. Cellular and molecular characteristics of basal cells in airway epithelium. *Exp Lung Res,* 27**,** 401-15.

FAES, S. & DORMOND, O. 2015. PI3K and AKT: Unfaithful Partners in Cancer. *Int J Mol Sci,* 16**,** 21138-52.

FANG, W. L., HUANG, K. H., LAN, Y. T., LIN, C. H., CHANG, S. C., CHEN, M. H., CHAO, Y., LIN, W. C., LO, S. S., LI, A. F., WU, C. W., CHIOU, S. H. & SHYR, Y. M. 2016. Mutations in PI3K/AKT pathway genes and amplifications of PIK3CA are associated with patterns of recurrence in gastric cancers. *Oncotarget,* 7**,** 6201-20.

FEDELE, C., TOTHILL, R. W. & MCARTHUR, G. A. 2014. Navigating the challenge of tumour heterogeneity in cancer therapy. *Cancer Discov,* 4**,** 146-8.

FENG, J. F., CHEN, S. & YANG, X. 2017. Combination of c-reactive protein and squamous cell carcinoma antigen in predicting postoperative prognosis for patients with squamous cell carcinoma of the esophagus. *Oncotarget*.

FENNELL, D. A. 2005. Caspase regulation in non-small cell lung cancer and its potential for therapeutic exploitation. *Clin Cancer Res,* 11**,** 2097-105.

FERON, O. 2009. Pyruvate into lactate and back: from the Warburg effect to symbiotic energy fuel exchange in cancer cells. *Radiother Oncol,* 92**,** 329-33.

FIELD, J. K., BRAMBILLA, C., CAPORASO, N., FLAHAULT, A., HENSCHKE, C., HERMAN, J., HIRSCH, F., LACHMANN, P., LAM, S., MAIER, S., MONTUENGA, L. M., MULSHINE, J., MURPHY, M., PULLEN, J., SPITZ, M., TOCKMAN, M., TYNDALE, R., WISTUBA, I. & YOUNGSON, J. 2002. Consensus statements from the Second International Lung Cancer Molecular Biomarkers Workshop: a European strategy for developing lung cancer molecular diagnostics in high risk populations. *Int J Oncol,* 21**,** 369-73.

FISHER, R., PUSZTAI, L. & SWANTON, C. 2013. Cancer heterogeneity: implications for targeted therapeutics. *Br J Cancer,* 108**,** 479-85.

FISSELER-ECKHOFF, A. & DEMES, M. 2012. Neuroendocrine tumours of the lung. *Cancers (Basel),* 4**,** 777-98.

FREEDMAN, M. 2004. State-of-the-art screening for lung cancer (part 1): the chest radiograph. *Thorac Surg Clin,* 14**,** 43-52.

FRUMAN, D. A., CHIU, H., HOPKINS, B. D., BAGRODIA, S., CANTLEY, L. C. & ABRAHAM, R. T. 2017. The PI3K Pathway in Human Disease. *Cell,* 170**,** 605-635.

FU, Q. F., LIU, Y., FAN, Y., HUA, S. N., QU, H. Y., DONG, S. W., LI, R. L., ZHAO, M. Y., ZHEN, Y., YU, X. L., CHEN, Y. Y., LUO, R. C., LI, R., LI, L. B., DENG, X. J., FANG, W. Y., LIU, Z. & SONG, X. 2015. Alpha-enolase promotes cell glycolysis, growth, migration, and invasion in non-small cell lung cancer through FAK-mediated PI3K/AKT pathway. *J Hematol Oncol,* 8**,** 22.

FUTREAL, P. A., COIN, L., MARSHALL, M., DOWN, T., HUBBARD, T., WOOSTER, R., RAHMAN, N. & STRATTON, M. R. 2004. A census of human cancer genes. *Nat Rev Cancer,* 4**,** 177-83.

GANDARA, D. R., HAMMERMAN, P. S., SOS, M. L., LARA, P. N. & HIRSCH, F. R. 2015. Squamous cell lung cancer: from tumour genomics to cancer therapeutics. *Clin Cancer Res,* 21**,** 2236-43.

GANESAN, S., COMSTOCK, A. T. & SAJJAN, U. S. 2013. Barrier function of airway tract epithelium. *Tissue Barriers,* 1**,** e24997.

GAO, X., LIU, X., LU, Y., WANG, Y., CAO, W., HU, H. & WANG, H. 2019a. PIM1 is responsible for IL-6-induced breast cancer cell EMT and stemness via c-myc activation. *Breast Cancer,* 26**,** 663-671.

GAO, Y. Q., CHENG, H. Y. & LIU, K. F. 2019b. Long non-coding RNA DANCR upregulates IGF2 expression and promotes ovarian cancer progression. *Eur Rev Med Pharmacol Sci,* 23**,** 3621-3626.

GIFFORD, A. J., HABER, M., WITT, T. L., WHETSTINE, J. R., TAUB, J. W., MATHERLY, L. H. & NORRIS, M. D. 2002. Role of the E45K-reduced folate carrier gene mutation in methotrexate resistance in human leukemia cells. *Leukemia,* 16**,** 2379-87.

GKOUNTAKOS, A., SARTORI, G., FALCONE, I., PIRO, G., CIUFFREDA, L., CARBONE, C., TORTORA, G., SCARPA, A., BRIA, E., MILELLA, M., ROSELL, R., CORBO, V. & PILOTTO, S. 2019. PTEN in Lung Cancer: Dealing with the Problem, Building on New Knowledge and Turning the Game Around. *Cancers (Basel),* 11.

GOCEK, E., MOULAS, A. N. & STUDZINSKI, G. P. 2014. Non-receptor protein tyrosine kinases signaling pathways in normal and cancer cells. *Crit Rev Clin Lab Sci,* 51**,** 125-37.

GOCHEVA, V., NABA, A., BHUTKAR, A., GUARDIA, T., MILLER, K. M., LI, C. M., DAYTON, T. L., SANCHEZ-RIVERA, F. J., KIM-KISELAK, C., JAILKHANI, N., WINSLOW, M. M., DEL ROSARIO, A., HYNES, R. O. & JACKS, T. 2017. Quantitative proteomics identify Tenascin-C as a promoter of lung cancer progression and contributor to a signature prognostic of patient survival. *Proc Natl Acad Sci U S A,* 114**,** E5625-E5634.

GONZÁLEZ-SANCHO, J. M., AGUILERA, O., GARCÍA, J. M., PENDÁS-FRANCO, N., PEÑA, C., CAL, S., GARCÍA DE HERREROS, A., BONILLA, F. & MUÑOZ, A. 2005. The Wnt antagonist DICKKOPF-1 gene is a downstream target of beta-catenin/TCF and is downregulated in human colon cancer. *Oncogene,* 24**,** 1098-103.

GOTO, T. 2018. Measuring Surgery Outcomes of Lung Cancer Patients with Concomitant Pulmonary Fibrosis: A Review of the Literature. *Cancers (Basel),* 10.

GREGG, J. P., LI, T. & YONEDA, K. Y. 2019. Molecular testing strategies in non-small cell lung cancer: optimizing the diagnostic journey. *Transl Lung Cancer Res,* 8**,** 286-301.

GREULICH, H., CHEN, T. H., FENG, W., JÄNNE, P. A., ALVAREZ, J. V., ZAPPATERRA, M., BULMER, S. E., FRANK, D. A., HAHN, W. C., SELLERS, W. R. & MEYERSON, M. 2005. Oncogenic transformation by inhibitor-sensitive and -resistant EGFR mutants. *PLoS Med,* 2**,** e313.

GRIDELLI, C., ROSSI, A., CARBONE, D. P., GUARIZE, J., KARACHALIOU, N., MOK, T., PETRELLA, F., SPAGGIARI, L. & ROSELL, R. 2015. Non-small-cell lung cancer. *Nat Rev Dis Primers,* 1**,** 15009.

GUIDETTI, G. F., ZARÀ, M., CANOBBIO, I., VISCONTE, C., DI NUNZIO, G. & TORTI, M. 2016. Novel pharmacological inhibitors demonstrate the role of the tyrosine kinase Pyk2 in adhesion and aggregation of human platelets. *Thromb Haemost,* 116**,** 904-917.

GULIS, G. & FUJINO, Y. 2015. Epidemiology, population health, and health impact assessment. *J Epidemiol,* 25**,** 179-80.

GUSTAFSSON, B. I., KIDD, M., CHAN, A., MALFERTHEINER, M. V. & MODLIN, I. M. 2008. Bronchopulmonary neuroendocrine tumours. *Cancer,* 113**,** 5-21.

GUTSCHNER, T., HÄMMERLE, M., EISSMANN, M., HSU, J., KIM, Y., HUNG, G., REVENKO, A., ARUN, G., STENTRUP, M., GROSS, M., ZÖRNIG, M., MACLEOD, A. R., SPECTOR, D. L. & DIEDERICHS, S. 2013. The noncoding RNA MALAT1 is a critical regulator of the metastasis phenotype of lung cancer cells. *Cancer Res,* 73**,** 1180-9.

HAAS, B., KLINGER, V., KEKSEL, C., BONIGUT, V., KIEFER, D., CASPERS, J., WALTHER, J., WOS-MAGANGA, M., WEICKHARDT, S., RÖHN, G., TIMMER, M., FRÖTSCHL, R. & ECKSTEIN, N. 2018. Inhibition of the PI3K but not the MEK/ERK pathway sensitizes human glioma cells to alkylating drugs. *Cancer Cell Int,* 18**,** 69.

HAERI, M. & KNOX, B. E. 2012. Endoplasmic Reticulum Stress and Unfolded Protein Response Pathways: Potential for Treating Age-related Retinal Degeneration. *J Ophthalmic Vis Res,* 7**,** 45-59.

HAGUET, H., DOUXFILS, J., CHATELAIN, C., GRAUX, C., MULLIER, F. & DOGNÉ, J. M. 2018. BCR-ABL Tyrosine Kinase Inhibitors: Which Mechanism(s) May Explain the Risk of Thrombosis? *TH Open,* 2**,** e68-e88.

HAJAT, C. 2011. An introduction to epidemiology. *Methods Mol Biol,* 713**,** 27-39.

HALLGRÍMSSON, J. G., JÓNSSON, T. & JÓHANNSSON, J. H. 1989. Bronchopulmonary carcinoids in Iceland 1955-1984. A retrospective clinical and histopathologic study. *Scand J Thorac Cardiovasc Surg,* 23**,** 275-8.

HANAHAN, D. & WEINBERG, R. A. 2011. Hallmarks of cancer: the next generation. *Cell,* 144**,** 646-74.

HANKER, A. B., KAKLAMANI, V. & ARTEAGA, C. L. 2019. Challenges for the Clinical Development of PI3K Inhibitors: Strategies to Improve Their Impact in Solid Tumours. *Cancer Discov,* 9**,** 482-491.

HARRIS, P. A., BOLOOR, A., CHEUNG, M., KUMAR, R., CROSBY, R. M., DAVIS-WARD, R. G., EPPERLY, A. H., HINKLE, K. W., HUNTER, R. N., JOHNSON, J. H., KNICK, V. B., LAUDEMAN, C. P., LUTTRELL, D. K., MOOK, R. A., NOLTE, R. T., RUDOLPH, S. K., SZEWCZYK, J. R., TRUESDALE, A. T., VEAL, J. M., WANG, L. & STAFFORD, J. A. 2008. Discovery of 5-((4-((2,3-dimethyl-2H-indazol-6-yl)methylamino)-2-pyrimidinyl)amino)-2-methyl-benzenesulfonamide (Pazopanib), a novel and potent vascular endothelial growth factor receptor inhibitor. *J Med Chem,* 51**,** 4632-40.

HARRISON, D. A. 2012. The Jak/STAT pathway. *Cold Spring Harb Perspect Biol,* 4.

HARROW, J., FRANKISH, A., GONZALEZ, J. M., TAPANARI, E., DIEKHANS, M., KOKOCINSKI, F., AKEN, B. L., BARRELL, D., ZADISSA, A., SEARLE, S., BARNES, I., BIGNELL, A., BOYCHENKO, V., HUNT, T., KAY, M., MUKHERJEE, G., RAJAN, J., DESPACIO-REYES, G., SAUNDERS, G., STEWARD, C., HARTE, R., LIN, M., HOWALD, C., TANZER, A., DERRIEN, T., CHRAST, J., WALTERS, N., BALASUBRAMANIAN, S., PEI, B., TRESS, M., RODRIGUEZ, J. M., EZKURDIA, I., VAN BAREN, J., BRENT, M., HAUSSLER, D., KELLIS, M., VALENCIA, A., REYMOND, A., GERSTEIN, M., GUIGÓ, R. & HUBBARD, T. J. 2012. GENCODE: the reference human genome annotation for The ENCODE Project. *Genome Res,* 22**,** 1760-74.

HASSAN, M. M., PHAN, A., LI, D., DAGOHOY, C. G., LEARY, C. & YAO, J. C. 2008. Risk factors associated with neuroendocrine tumours: A U.S.-based case-control study. *Int J Cancer,* 123**,** 867-73.

HAUSO, O., GUSTAFSSON, B. I., KIDD, M., WALDUM, H. L., DROZDOV, I., CHAN, A. K. & MODLIN, I. M. 2008. Neuroendocrine tumour epidemiology: contrasting Norway and North America. *Cancer,* 113**,** 2655-64.

HEAVEY, S., CUFFE, S., FINN, S., YOUNG, V., RYAN, R., NICHOLSON, S., LEONARD, N., MCVEIGH, N., BARR, M., O'BYRNE, K. & GATELY, K. 2016. In pursuit of synergy: An investigation of the PI3K/mTOR/MEK co-targeted inhibition strategy in NSCLC. *Oncotarget,* 7**,** 79526-79543.

HEAVEY, S., DOWLING, P., MOORE, G., BARR, M. P., KELLY, N., MAHER, S. G., CUFFE, S., FINN, S. P., O'BYRNE, K. J. & GATELY, K. 2018. Development and characterisation of a panel of phosphatidylinositide 3-kinase - mammalian target of rapamycin inhibitor resistant lung cancer cell lines. *Sci Rep,* 8**,** 1652.

HEAVEY, S., GODWIN, P., BAIRD, A. M., BARR, M. P., UMEZAWA, K., CUFFE, S., FINN, S. P., O'BYRNE, K. J. & GATELY, K. 2014. Strategic targeting of the PI3K-NFκB axis in cisplatin-resistant NSCLC. *Cancer Biol Ther,* 15**,** 1367-77.

HEIST, R. S., SEQUIST, L. V. & ENGELMAN, J. A. 2012. Genetic changes in squamous cell lung cancer: a review. *J Thorac Oncol,* 7**,** 924-33.

HENDIFAR, A. E., MARCHEVSKY, A. M. & TULI, R. 2017. Neuroendocrine Tumours of the Lung: Current Challenges and Advances in the Diagnosis and Management of Well-Differentiated Disease. *J Thorac Oncol,* 12**,** 425-436.

HIENTZ, K., MOHR, A., BHAKTA-GUHA, D. & EFFERTH, T. 2017. The role of p53 in cancer drug resistance and targeted chemotherapy. *Oncotarget,* 8**,** 8921-8946.

HIRAI, I. & WANG, H. G. 2001. Survival-factor-induced phosphorylation of Bad results in its dissociation from Bcl-x(L) but not Bcl-2. *Biochem J,* 359**,** 345-52.

HIROSHIMA, K., IYODA, A., SHIDA, T., SHIBUYA, K., IIZASA, T., KISHI, H., TANIZAWA, T., FUJISAWA, T. & NAKATANI, Y. 2006. Distinction of pulmonary large cell neuroendocrine carcinoma from small cell lung carcinoma: a morphological, immunohistochemical, and molecular analysis. *Mod Pathol,* 19**,** 1358-68.

HLUBEK, F., BRABLETZ, T., BUDCZIES, J., PFEIFFER, S., JUNG, A. & KIRCHNER, T. 2007. Heterogeneous expression of Wnt/beta-catenin target genes within colorectal cancer. *Int J Cancer,* 121**,** 1941-8.

HMMIER, A. 2018. *Identification of lung carcinoma biomarkers associated with tumour development and drug resistance.* PhD.

HOANG, T., MYUNG, S. K., PHAM, T. T. & PARK, B. 2020. Efficacy of Crizotinib, Ceritinib, and Alectinib in ALK-Positive Non-Small Cell Lung Cancer Treatment: A Meta-Analysis of Clinical Trials. *Cancers (Basel),* 12.

HOLLA, V. R., ELAMIN, Y. Y., BAILEY, A. M., JOHNSON, A. M., LITZENBURGER, B. C., KHOTSKAYA, Y. B., SANCHEZ, N. S., ZENG, J., SHUFEAN, M. A., SHAW, K. R., MENDELSOHN, J., MILLS, G. B., MERIC-BERNSTAM, F. & SIMON, G. R. 2017. ALK: a tyrosine kinase target for cancer therapy. *Cold Spring Harb Mol Case Stud,* 3**,** a001115.

HOLOHAN, C., VAN SCHAEYBROECK, S., LONGLEY, D. B. & JOHNSTON, P. G. 2013. Cancer drug resistance: an evolving paradigm. *Nat Rev Cancer,* 13**,** 714-26.

HORIUCHI, D., CAMARDA, R., ZHOU, A. Y., YAU, C., MOMCILOVIC, O., BALAKRISHNAN, S., CORELLA, A. N., EYOB, H., KESSENBROCK, K., LAWSON,

D. A., MARSH, L. A., ANDERTON, B. N., ROHRBERG, J., KUNDER, R., BAZAROV, A. V., YASWEN, P., MCMANUS, M. T., RUGO, H. S., WERB, Z. & GOGA, A. 2016. PIM1 kinase inhibition as a targeted therapy against triple-negative breast tumours with elevated MYC expression. *Nat Med,* 22**,** 1321-1329.

HOSSAIN, R., WU, C. C., DE GROOT, P. M., CARTER, B. W., GILMAN, M. D. & ABBOTT, G. F. 2018. Missed Lung Cancer. *Radiol Clin North Am,* 56**,** 365-375.

HSIAO, K. C., SHIH, N. Y., CHU, P. Y., HUNG, Y. M., LIAO, J. Y., CHOU, S. W., YANG, Y. Y., CHANG, G. C. & LIU, K. J. 2015. Anti-α-enolase is a prognostic marker in postoperative lung cancer patients. *Oncotarget,* 6**,** 35073-86.

HU, P., WONG, P. T., ZHOU, Q., SHENG, L., NIU, W., CHEN, S., XU, M. & LIN, Y. 2018. Clinical relevance of the multidrug resistance-associated protein 1 gene in non-small cell lung cancer: A systematic review and meta-analysis. *Oncol Rep,* 40**,** 3078-3091.

HU, X., BAO, J., WANG, Z., ZHANG, Z., GU, P., TAO, F., CUI, D. & JIANG, W. 2016. The plasma lncRNA acting as fingerprint in non-small-cell lung cancer. *Tumour Biol,* 37**,** 3497-504.

HU, Y., DAI, J., ZONG, G., XIAO, J., GUO, X., DAI, Y., LU, Z. & WAN, R. 2019. Restoration of p53 acetylation by HDAC inhibition permits the necrosis/apoptosis switch of pancreatic ainar cell during experimental pancreatitis in mice. *J Cell Physiol*.

HUBBARD, S. R. & TILL, J. H. 2000. Protein tyrosine kinase structure and function. *Annu Rev Biochem,* 69**,** 373-98.

HUBER, O. & PETERSEN, I. 2015. 150th Anniversary Series: Desmosomes and the Hallmarks of Cancer. *Cell Commun Adhes,* 22**,** 15-28.

HUNG, W. & ELLIOTT, B. 2001. Co-operative effect of c-Src tyrosine kinase and Stat3 in activation of hepatocyte growth factor expression in mammary carcinoma cells. *J Biol Chem,* 276**,** 12395-403.

IENGAR, P. 2012. An analysis of substitution, deletion and insertion mutations in cancer genes. *Nucleic Acids Res,* 40**,** 6401-13.

IMAMOVIC, D. & VRANIC, S. 2017. Novel regulators of PD-L1 expression in cancer: CMTM6 and CMTM4-a new avenue to enhance the therapeutic benefits of immune checkpoint inhibitors. *Ann Transl Med,* 5**,** 467.

INABA, H., GREAVES, M. & MULLIGHAN, C. G. 2013. Acute lymphoblastic leukaemia. *Lancet,* 381**,** 1943-55.

INAMURA, K. 2018. Update on Immunohistochemistry for the Diagnosis of Lung Cancer. *Cancers (Basel),* 10.

ISELLA, C., MELLANO, A., GALIMI, F., PETTI, C., CAPUSSOTTI, L., DE SIMONE, M., BERTOTTI, A., MEDICO, E. & MURATORE, A. 2013. MACC1 mRNA levels predict cancer recurrence after resection of colorectal cancer liver metastases. *Ann Surg,* 257**,** 1089-95.

ISLAM, M. S., KUSAKABE, M., HORIGUCHI, K., IINO, S., NAKAMURA, T., IWANAGA, K., HASHIMOTO, H., MATSUMOTO, S., MURATA, T., HORI, M. & OZAKI, H. 2014. PDGF and TGF-β promote tenascin-C expression in subepithelial myofibroblasts and contribute to intestinal mucosal protection in mice. *Br J Pharmacol,* 171**,** 375-88.

J.F. SAMBROOK AND D.W. RUSSELL, E. 2001. *Molecular Cloning: A Laboratory Manual*.

JACKMAN, D. M. & JOHNSON, B. E. 2005. Small-cell lung cancer. *Lancet,* 366**,** 1385-96.

JANSSEN, L. J. 2012. Airway smooth muscle as a target in asthma and the beneficial effects of bronchial thermoplasty. *J Allergy (Cairo),* 2012**,** 593784.

JENSEN, K., ANDERSON, J. A. & GLASS, E. J. 2014. Comparison of small interfering RNA (siRNA) delivery into bovine monocyte-derived macrophages by transfection and electroporation. *Vet Immunol Immunopathol,* 158**,** 224-32.

JIANG, D., LI, J., WANG, M., HAN, C., WANG, X., ZHAO, C. & YE, Y. 2017a. Combination of FGFR4 inhibitor Blu9931 and 5-fluorouracil effects on the biological characteristics of colorectal cancer cells. *Int J Oncol,* 51**,** 1611-1620.

JIANG, J., GUI, F., HE, Z., LI, L., LI, Y., LI, S., WU, X., DENG, Z., SUN, X., HUANG, X., HUANG, W., HAN, S., ZHANG, T., WANG, Z., JIAO, B., SONG, S., WANG, H., CHEN, L., ZHOU, D., LIU, Q., REN, R., ZHANG, J. & DENG, X. 2017b. Targeting BRK-Positive Breast Cancers with Small-Molecule Kinase Inhibitors. *Cancer Res,* 77**,** 175-186.

JIANG, N., DAI, Q., SU, X., FU, J., FENG, X. & PENG, J. 2020. Role of PI3K/AKT pathway in cancer: the framework of malignant behavior. *Mol Biol Rep,* 47**,** 4587-4629.

JINESH, G. G., MOKKAPATI, S., ZHU, K. & MORALES, E. E. 2016. Pim kinase isoforms: devils defending cancer cells from therapeutic and immune attacks. *Apoptosis,* 21**,** 1203-1213.

JINNIN, M., IHN, H., ASANO, Y., YAMANE, K., TROJANOWSKA, M. & TAMAKI, K. 2006. Platelet derived growth factor induced tenascin-C transcription is phosphoinositide 3-kinase/Akt-dependent and mediated by Ets family transcription factors. *J Cell Physiol,* 206**,** 718-27.

JOHNSON, B. D., GELDENHUYS, W. J. & HAZLEHURST, L. A. 2020. The Role of ERO1α in Modulating Cancer Progression and Immune Escape. *J Cancer Immunol (Wilmington),* 2**,** 103-115.

JOHNSON, R., TROCHA, S., MCLAWHORN, M., WORLEY, M., WHEELER, G., THOMPSON, L., SCHISLER, N., SCHAMMEL, D., SCHAMMEL, C., STEPHENSON, J. & BOLTON, W. 2011. Histology, not lymph node involvement, predicts long-term survival in bronchopulmonary carcinoids. *Am Surg,* 77**,** 1669-74.

JOKINEN, E. & KOIVUNEN, J. P. 2015. MEK and PI3K inhibition in solid tumours: rationale and evidence to date. *Ther Adv Med Oncol,* 7**,** 170-80.

JONES, F. S. & JONES, P. L. 2000. The tenascin family of ECM glycoproteins: structure, function, and regulation during embryonic development and tissue remodeling. *Dev Dyn,* 218**,** 235-59.

KALEMKERIAN, G. P., AKERLEY, W., BOGNER, P., BORGHAEI, H., CHOW, L. Q., DOWNEY, R. J., GANDHI, L., GANTI, A. K., GOVINDAN, R., GRECULA, J. C., HAYMAN, J., HEIST, R. S., HORN, L., JAHAN, T., KOCZYWAS, M., LOO, B. W.,

MERRITT, R. E., MORAN, C. A., NIELL, H. B., O'MALLEY, J., PATEL, J. D., READY, N., RUDIN, C. M., WILLIAMS, C. C., GREGORY, K., HUGHES, M. & NETWORK, N. C. C. 2013. Small cell lung cancer. *J Natl Compr Canc Netw,* 11**,** 78-98.

KARAKAS, B., BACHMAN, K. E. & PARK, B. H. 2006. Mutation of the PIK3CA oncogene in human cancers. *Br J Cancer,* 94**,** 455-9.

KARNI-SCHMIDT, O., LOKSHIN, M. & PRIVES, C. 2016. The Roles of MDM2 and MDMX in Cancer. *Annu Rev Pathol,* 11**,** 617-44.

KATO, Y., FERGUSON, T. B., BENNETT, D. E. & BURFORD, T. H. 1969. Oat cell carcinoma of the lung. A review of 138 cases. *Cancer,* 23**,** 517-24.

KAWAI, T., TOMINAGA, S., HIROI, S., KAMEDA, K., OGATA, S., NAKASHIMA, H., OZEKI, Y. & NAKANISHI, K. 2015. Expressions of Thyroid Transcription Factor-1, Napsin A, p40, p63, CK5/6 and Desmocollin-3 in Non-Small Cell Lung Cancer, as Revealed by Imprint Cytology Using a Malinol-Based Cell-Transfer Technique. *Acta Cytol,* 59**,** 457-64.

KAWANO, O., SASAKI, H., ENDO, K., SUZUKI, E., HANEDA, H., YUKIUE, H., KOBAYASHI, Y., YANO, M. & FUJII, Y. 2006. PIK3CA mutation status in Japanese lung cancer patients. *Lung Cancer,* 54**,** 209-15.

KAWANO, O., SASAKI, H., OKUDA, K., YUKIUE, H., YOKOYAMA, T., YANO, M. & FUJII, Y. 2007. PIK3CA gene amplification in Japanese non-small cell lung cancer. *Lung Cancer,* 58**,** 159-60.

KERR, K. M., BUBENDORF, L., EDELMAN, M. J., MARCHETTI, A., MOK, T., NOVELLO, S., O'BYRNE, K., STAHEL, R., PETERS, S., FELIP, E. & MEMBERS, P. 2014. Second ESMO consensus conference on lung cancer: pathology and molecular biomarkers for non-small-cell lung cancer. *Ann Oncol,* 25**,** 1681-90.

KHAN, K. H., WONG, M., RIHAWI, K., BODLA, S., MORGANSTEIN, D., BANERJI, U. & MOLIFE, L. R. 2016. Hyperglycemia and Phosphatidylinositol 3-Kinase/Protein Kinase B/Mammalian Target of Rapamycin (PI3K/AKT/mTOR) Inhibitors in Phase I Trials: Incidence, Predictive Factors, and Management. *Oncologist,* 21**,** 855-60.

KIM, H. S., I, H., CHOI, Y. S., KIM, K., SHIM, Y. M. & KIM, J. 2006. Surgical resection of recurrent lung cancer in patients following curative resection. *J Korean Med Sci,* 21**,** 224-8.

KIM, J. W., LEE, H. S., NAM, K. H., AHN, S., AHN, S. H., PARK, D. J., KIM, H. H. & LEE, K. W. 2017. mutations are associated with increased tumour aggressiveness and Akt activation in gastric cancer. *Oncotarget,* 8**,** 90948-90958.

KIM, W., YOUN, H., KWON, T., KANG, J., KIM, E., SON, B., YANG, H. J., JUNG, Y. & YOUN, B. 2013. PIM1 kinase inhibitors induce radiosensitization in non-small cell lung cancer cells. *Pharmacol Res,* 70**,** 90-101.

KITAGAWA, K., KOTAKE, Y. & KITAGAWA, M. 2009. Ubiquitin-mediated control of oncogene and tumour suppressor gene products. *Cancer Sci,* 100**,** 1374-81.

KLEMPNER, S. J., FABRIZIO, D., BANE, S., REINHART, M., PEOPLES, T., ALI, S. M., SOKOL, E. S., FRAMPTON, G., SCHROCK, A. B., ANHORN, R. & REDDY, P. 2020. Tumour Mutational Burden as a Predictive Biomarker for Response to Immune Checkpoint Inhibitors: A Review of Current Evidence. *Oncologist,* 25**,** e147-e159.

KNUDSEN, E. S., SHAPIRO, G. I. & KEYOMARSI, K. 2020. Selective CDK4/6 Inhibitors: Biologic Outcomes, Determinants of Sensitivity, Mechanisms of Resistance, Combinatorial Approaches, and Pharmacodynamic Biomarkers. *Am Soc Clin Oncol Educ Book,* 40**,** 115-126.

KRESO, A. & DICK, J. E. 2014. Evolution of the cancer stem cell model. *Cell Stem Cell,* 14**,** 275-91.

KRETZ, M., SIPRASHVILI, Z., CHU, C., WEBSTER, D. E., ZEHNDER, A., QU, K., LEE, C. S., FLOCKHART, R. J., GROFF, A. F., CHOW, J., JOHNSTON, D., KIM, G. E., SPITALE, R. C., FLYNN, R. A., ZHENG, G. X., AIYER, S., RAJ, A., RINN, J. L., CHANG, H. Y. & KHAVARI, P. A. 2013. Control of somatic tissue differentiation by the long non-coding RNA TINCR. *Nature,* 493**,** 231-5.

KRETZ, M., WEBSTER, D. E., FLOCKHART, R. J., LEE, C. S., ZEHNDER, A., LOPEZ-PAJARES, V., QU, K., ZHENG, G. X., CHOW, J., KIM, G. E., RINN, J. L., CHANG, H.

Y., SIPRASHVILI, Z. & KHAVARI, P. A. 2012. Suppression of progenitor differentiation requires the long noncoding RNA ANCR. *Genes Dev,* 26**,** 338-43.

KROCK, B. L., SKULI, N. & SIMON, M. C. 2011. Hypoxia-induced angiogenesis: good and evil. *Genes Cancer,* 2**,** 1117-33.

KUNG, J. T., COLOGNORI, D. & LEE, J. T. 2013. Long noncoding RNAs: past, present, and future. *Genetics,* 193**,** 651-69.

KUTOMI, G., TAMURA, Y., TANAKA, T., KAJIWARA, T., KUKITA, K., OHMURA, T., SHIMA, H., TAKAMARU, T., SATOMI, F., SUZUKI, Y., TORIGOE, T., SATO, N. & HIRATA, K. 2013. Human endoplasmic reticulum oxidoreductin 1-α is a novel predictor for poor prognosis of breast cancer. *Cancer Sci,* 104**,** 1091-6.

KWON, S. E. & CHAPMAN, E. R. 2011. Synaptophysin regulates the kinetics of synaptic vesicle endocytosis in central neurons. *Neuron,* 70**,** 847-54.

LA MONICA, S., GALETTI, M., ALFIERI, R. R., CAVAZZONI, A., ARDIZZONI, A., TISEO, M., CAPELLETTI, M., GOLDONI, M., TAGLIAFERRI, S., MUTTI, A., FUMAROLA, C., BONELLI, M., GENERALI, D. & PETRONINI, P. G. 2009. Everolimus restores gefitinib sensitivity in resistant non-small cell lung cancer cell lines. *Biochem Pharmacol,* 78**,** 460-8.

LA ROSA, S., CHIARAVALLI, A. M., PLACIDI, C., PAPANIKOLAOU, N., CERATI, M. & CAPELLA, C. 2010. TTF1 expression in normal lung neuroendocrine cells and related tumours: immunohistochemical study comparing two different monoclonal antibodies. *Virchows Arch,* 457**,** 497-507.

LAHIRY, P., TORKAMANI, A., SCHORK, N. J. & HEGELE, R. A. 2010. Kinase mutations in human disease: interpreting genotype-phenotype relationships. *Nat Rev Genet,* 11**,** 60-74.

LAMBE, G., DURAND, M., BUCKLEY, A., NICHOLSON, S. & MCDERMOTT, R. 2020. Adenocarcinoma of the lung: from BAC to the future. *Insights Imaging,* 11**,** 69.

LANTUEJOUL, S., MORO, D., MICHALIDES, R. J., BRAMBILLA, C. & BRAMBILLA, E. 1998. Neural cell adhesion molecules (NCAM) and NCAM-PSA expression in neuroendocrine lung tumours. *Am J Surg Pathol,* 22**,** 1267-76.

LATIMER, K. M. 2018. Lung Cancer: Clinical Presentation and Diagnosis. *FP Essent,* 464**,** 23-26.

LAWRENCE, H. R., MAHAJAN, K., LUO, Y., ZHANG, D., TINDALL, N., HUSEYIN, M., GEVARIYA, H., KAZI, S., OZCAN, S., MAHAJAN, N. P. & LAWRENCE, N. J. 2015. Development of novel ACK1/TNK2 inhibitors using a fragment-based approach. *J Med Chem,* 58**,** 2746-63.

LEBOULLEUX, S., DROMAIN, C., VATAIRE, A. L., MALKA, D., AUPÉRIN, A., LUMBROSO, J., DUVILLARD, P., ELIAS, D., HARTL, D. M., DE BAERE, T., GUIGAY, J., SCHLUMBERGER, M., DUCREUX, M. & BAUDIN, E. 2008. Prediction and diagnosis of bone metastases in well-differentiated gastro-entero-pancreatic endocrine cancer: a prospective comparison of whole body magnetic resonance imaging and somatostatin receptor scintigraphy. *J Clin Endocrinol Metab,* 93**,** 3021-8.

LEE, H. K., KIM, H. W., LEE, I. Y., LEE, J., JUNG, D. S., LEE, S. Y., PARK, S. H., HWANG, H., CHOI, J. S., KIM, J. H., KIM, S. W., KIM, J. K., COOLS, J., KOH, J. S. & SONG, H. J. 2014. G-749, a novel FLT3 kinase inhibitor, can overcome drug resistance for the treatment of acute myeloid leukemia. *Blood,* 123**,** 2209-19.

LEGRAS, A., PÉCUCHET, N., IMBEAUD, S., PALLIER, K., DIDELOT, A., ROUSSEL, H., GIBAULT, L., FABRE, E., LE PIMPEC-BARTHES, F., LAURENT-PUIG, P. & BLONS, H. 2017. Epithelial-to-Mesenchymal Transition and MicroRNAs in Lung Cancer. *Cancers (Basel),* 9.

LEMJABBAR-ALAOUI, H., HASSAN, O. U., YANG, Y. W. & BUCHANAN, P. 2015. Lung cancer: Biology and treatment options. *Biochim Biophys Acta,* 1856**,** 189-210.

LEMMON, M. A. & SCHLESSINGER, J. 2010. Cell signaling by receptor tyrosine kinases. *Cell,* 141**,** 1117-34.

LEONARD, W. J. & O'SHEA, J. J. 1998. Jaks and STATs: biological implications. *Annu Rev Immunol,* 16**,** 293-322.

LEVY, D. E. & DARNELL, J. E. 2002. Stats: transcriptional control and biological impact. *Nat Rev Mol Cell Biol,* 3**,** 651-62.

LI, C. H. & CHEN, Y. 2013. Targeting long non-coding RNAs in cancers: progress and prospects. *Int J Biochem Cell Biol,* 45**,** 1895-910.

LI, H., LIAO, X., LIU, Y., SHEN, Z., GAN, X. & HUANG, Z. 2015a. The expression of MACC1 and its role in the proliferation and apoptosis of salivary adenoid cystic carcinoma. *J Oral Pathol Med,* 44**,** 810-7.

LI, H., ZHANG, P., SUN, X., SUN, Y., SHI, C., LIU, H. & LIU, X. 2015b. MicroRNA-181a regulates epithelial-mesenchymal transition by targeting PTEN in drug-resistant lung adenocarcinoma cells. *Int J Oncol,* 47**,** 1379-92.

LI, J. H., LUO, N., ZHONG, M. Z., XIAO, Z. Q., WANG, J. X., YAO, X. Y., PENG, Y. & CAO, J. 2016. Inhibition of microRNA-196a might reverse cisplatin resistance of A549/DDP non-small-cell lung cancer cell line. *Tumour Biol,* 37**,** 2387-94.

LI, L., TIAN, T. & ZHANG, X. 2017a. The impact of radiation on the development of lung cancer. *J Theor Biol,* 428**,** 147-152.

LI, S. D., MA, M., LI, H., WALUSZKO, A., SIDORENKO, T., SCHADT, E. E., ZHANG, D. Y., CHEN, R. & YE, F. 2017b. Cancer gene profiling in non-small cell lung cancers reveals activating mutations in JAK2 and JAK3 with therapeutic implications. *Genome Med,* 9**,** 89.

LI, W. X. 2008. Canonical and non-canonical JAK-STAT signaling. *Trends Cell Biol,* 18**,** 545-51.

LIANG, W., LV, T., SHI, X., LIU, H., ZHU, Q., ZENG, J., YANG, W., YIN, J. & SONG, Y. 2016. Circulating long noncoding RNA GAS5 is a novel biomarker for the diagnosis of nonsmall cell lung cancer. *Medicine (Baltimore),* 95**,** e4608.

LIBERMANN, T. A., NUSBAUM, H. R., RAZON, N., KRIS, R., LAX, I., SOREQ, H., WHITTLE, N., WATERFIELD, M. D., ULLRICH, A. & SCHLESSINGER, J. 1985.

Amplification, enhanced expression and possible rearrangement of EGF receptor gene in primary human brain tumours of glial origin. *Nature,* 313**,** 144-7.

LILLY, M., LE, T., HOLLAND, P. & HENDRICKSON, S. L. 1992. Sustained expression of the pim-1 kinase is specifically induced in myeloid cells by cytokines whose receptors are structurally related. *Oncogene,* 7**,** 727-32.

LIM, S. M., XIE, T., WESTOVER, K. D., FICARRO, S. B., TAE, H. S., GURBANI, D., SIM, T., MARTO, J. A., JÄNNE, P. A., CREWS, C. M. & GRAY, N. S. 2015. Development of small molecules targeting the pseudokinase Her3. *Bioorg Med Chem Lett,* 25**,** 3382-9.

LIM, Z. F. & MA, P. C. 2019. Emerging insights of tumour heterogeneity and drug resistance mechanisms in lung cancer targeted therapy. *J Hematol Oncol,* 12**,** 134.

LIU, F., ZHANG, X., WEISBERG, E., CHEN, S., HUR, W., WU, H., ZHAO, Z., WANG, W., MAO, M., CAI, C., SIMON, N. I., SANDA, T., WANG, J., LOOK, A. T., GRIFFIN, J. D., BALK, S. P., LIU, Q. & GRAY, N. S. 2013a. Discovery of a selective irreversible BMX inhibitor for prostate cancer. *ACS Chem Biol,* 8**,** 1423-8.

LIU, H., WU, X., HUANG, J., PENG, J. & GUO, L. 2015. miR-7 modulates chemoresistance of small cell lung cancer by repressing MRP1/ABCC1. *Int J Exp Pathol,* 96**,** 240-7.

LIU, J., PAN, C., GUO, L., WU, M., GUO, J., PENG, S., WU, Q. & ZUO, Q. 2016. A new mechanism of trastuzumab resistance in gastric cancer: MACC1 promotes the Warburg effect via activation of the PI3K/AKT signaling pathway. *J Hematol Oncol,* 9**,** 76.

LIU, L., WAN, X., CHEN, G., MA, X., NING, B. & YANG, G. 2017. (Risk Factors of Lung Cancer in Xuanwei, Yunnan Province, China). *Zhongguo Fei Ai Za Zhi,* 20**,** 528-537.

LIU, Z., LIU, H., YUAN, X., WANG, Y., LI, L., WANG, G., SONG, J., SHAO, Z. & FU, R. 2018. Downregulation of Pim-2 induces cell cycle arrest in the G. *Oncol Lett,* 15**,** 4079-4086.

LIU, Z., SUN, M., LU, K., LIU, J., ZHANG, M., WU, W., DE, W., WANG, Z. & WANG, R. 2013b. The long noncoding RNA HOTAIR contributes to cisplatin resistance of human

lung adenocarcinoma cells via downregualtion of p21(WAF1/CIP1) expression. *PLoS One,* 8**,** e77293.

LODDENKEMPER, R. 1998. Thoracoscopy--state of the art. *Eur Respir J,* 11**,** 213-21.

LODDENKEMPER, R. & SCHÖNFELD, N. 1998. Medical thoracoscopy. *Curr Opin Pulm Med,* 4**,** 235-8.

LONGO-SORBELLO, G. S. & BERTINO, J. R. 2001. Current understanding of methotrexate pharmacology and efficacy in acute leukemias. Use of newer antifolates in clinical trials. *Haematologica,* 86**,** 121-7.

LOVERDOS, K., FOTIADIS, A., KONTOGIANNI, C., ILIOPOULOU, M. & GAGA, M. 2019. Lung nodules: A comprehensive review on current approach and management. *Ann Thorac Med,* 14**,** 226-238.

LOWY, C. M. & OSKARSSON, T. 2015. Tenascin C in metastasis: A view from the invasive front. *Cell Adh Migr,* 9**,** 112-24.

LU, T., WANG, Y., CHEN, D., LIU, J. & JIAO, W. 2018. Potential clinical application of lncRNAs in non-small cell lung cancer. *Onco Targets Ther,* 11**,** 8045-8052.

LUO, J., TANG, L., ZHANG, J., NI, J., ZHANG, H. P., ZHANG, L., XU, J. F. & ZHENG, D. 2014. Long non-coding RNA CARLo-5 is a negative prognostic factor and exhibits tumour pro-oncogenic activity in non-small cell lung cancer. *Tumour Biol,* 35**,** 11541-9.

LYNCH, T. J., BONDARENKO, I., LUFT, A., SERWATOWSKI, P., BARLESI, F., CHACKO, R., SEBASTIAN, M., NEAL, J., LU, H., CUILLEROT, J. M. & RECK, M. 2012. Ipilimumab in combination with paclitaxel and carboplatin as first-line treatment in stage IIIB/IV non-small-cell lung cancer: results from a randomized, double-blind, multicenter phase II study. *J Clin Oncol,* 30**,** 2046-54.

MA, X., DIAO, Y., GE, H., XU, F., ZHU, L., ZHAO, Z. & LI, H. 2020. Discovery and optimization of 2-aminopyridine derivatives as novel and selective JAK2 inhibitors. *Bioorg Med Chem Lett,* 30**,** 127048.

MACLAINE, N. J. & HUPP, T. R. 2009. The regulation of p53 by phosphorylation: a model for how distinct signals integrate into the p53 pathway. *Aging (Albany NY),* 1**,** 490-502.

MALHOTRA, J., MALVEZZI, M., NEGRI, E., LA VECCHIA, C. & BOFFETTA, P. 2016. Risk factors for lung cancer worldwide. *Eur Respir J,* 48**,** 889-902.

MALONE, T., SCHÄFER, L., SIMON, N., HEAVEY, S., CUFFE, S., FINN, S., MOORE, G. & GATELY, K. 2020. Current perspectives on targeting PIM kinases to overcome mechanisms of drug resistance and immune evasion in cancer. *Pharmacol Ther,* 207**,** 107454.

MAMESSIER, E., BIRNBAUM, D. J., FINETTI, P., BIRNBAUM, D. & BERTUCCI, F. 2018. CMTM6 stabilizes PD-L1 expression and refines its prognostic value in tumours. *Ann Transl Med,* 6**,** 54.

MANNING, B. D. & TOKER, A. 2017. AKT/PKB Signaling: Navigating the Network. *Cell,* 169**,** 381-405.

MANSOORI, B., MOHAMMADI, A., DAVUDIAN, S., SHIRJANG, S. & BARADARAN, B. 2017. The Different Mechanisms of Cancer Drug Resistance: A Brief Review. *Adv Pharm Bull,* 7**,** 339-348.

MANZANARES-MIRALLES, L., SARIKAYA-BAYRAM, Ö., SMITH, E. B., DOLAN, S. K., BAYRAM, Ö., JONES, G. W. & DOYLE, S. 2016. Quantitative proteomics reveals the mechanism and consequence of gliotoxin-mediated dysregulation of the methionine cycle in Aspergillus niger. *J Proteomics,* 131**,** 149-62.

MAQUAT, L. E. 2001. The power of point mutations. *Nat Genet,* 27**,** 5-6.

MARUSYK, A., ALMENDRO, V. & POLYAK, K. 2012. Intra-tumour heterogeneity: a looking glass for cancer? *Nat Rev Cancer,* 12**,** 323-34.

MATTSON, M. E., POLLACK, E. S. & CULLEN, J. W. 1987. What are the odds that smoking will kill you? *Am J Public Health,* 77**,** 425-31.

MCDERMOTT, M., EUSTACE, A. J., BUSSCHOTS, S., BREEN, L., CROWN, J., CLYNES, M., O'DONOVAN, N. & STORDAL, B. 2014. In vitro Development of

Chemotherapy and Targeted Therapy Drug-Resistant Cancer Cell Lines: A Practical Guide with Case Studies. *Front Oncol,* 4**,** 40.

MCGRANAHAN, N. & SWANTON, C. 2017. Clonal Heterogeneity and Tumour Evolution: Past, Present, and the Future. *Cell,* 168**,** 613-628.

MEMMOTT, R. M. & DENNIS, P. A. 2010. The role of the Akt/mTOR pathway in tobacco carcinogen-induced lung tumourigenesis. *Clin Cancer Res,* 16**,** 4-10.

MICKE, P., FALDUM, A., METZ, T., BEEH, K. M., BITTINGER, F., HENGSTLER, J. G. & BUHL, R. 2002. Staging small cell lung cancer: Veterans Administration Lung Study Group versus International Association for the Study of Lung Cancer--what limits limited disease? *Lung Cancer,* 37**,** 271-6.

MIKI, Y., SWENSEN, J., SHATTUCK-EIDENS, D., FUTREAL, P. A., HARSHMAN, K., TAVTIGIAN, S., LIU, Q., COCHRAN, C., BENNETT, L. M. & DING, W. 1994. A strong candidate for the breast and ovarian cancer susceptibility gene BRCA1. *Science,* 266**,** 66-71.

MILLER, D. M., THOMAS, S. D., ISLAM, A., MUENCH, D. & SEDORIS, K. 2012. c-Myc and cancer metabolism. *Clin Cancer Res,* 18**,** 5546-53.

MIYAKE, T., NAKAYAMA, T., NAOI, Y., YAMAMOTO, N., OTANI, Y., KIM, S. J., SHIMAZU, K., SHIMOMURA, A., MARUYAMA, N., TAMAKI, Y. & NOGUCHI, S. 2012. GSTP1 expression predicts poor pathological complete response to neoadjuvant chemotherapy in ER-negative breast cancer. *Cancer Sci,* 103**,** 913-20.

MOCHIZUKI, T., KITANAKA, C., NOGUCHI, K., MURAMATSU, T., ASAI, A. & KUCHINO, Y. 1999. Physical and functional interactions between Pim-1 kinase and Cdc25A phosphatase. Implications for the Pim-1-mediated activation of the c-Myc signaling pathway. *J Biol Chem,* 274**,** 18659-66.

MUKAIDA, N., NOSAKA, T., NAKAMOTO, Y. & BABA, T. 2018. Lung Macrophages: Multifunctional Regulator Cells for Metastatic Cells. *Int J Mol Sci,* 20.

MUNNIA, A., GIESE, R. W., POLVANI, S., GALLI, A., CELLAI, F. & PELUSO, M. E. M. 2017. Bulky DNA Adducts, Tobacco Smoking, Genetic Susceptibility, and Lung Cancer Risk. *Adv Clin Chem,* 81**,** 231-277.

NAGAHARU, K., ZHANG, X., YOSHIDA, T., KATOH, D., HANAMURA, N., KOZUKA, Y., OGAWA, T., SHIRAISHI, T. & IMANAKA-YOSHIDA, K. 2011. Tenascin C induces epithelial-mesenchymal transition-like change accompanied by SRC activation and focal adhesion kinase phosphorylation in human breast cancer cells. *Am J Pathol,* 178**,** 754-63.

NAKAMURA, H. & SAJI, H. 2014. Worldwide trend of increasing primary adenocarcinoma of the lung. *Surg Today,* 44**,** 1004-12.

NATHANSON, D. A., GINI, B., MOTTAHEDEH, J., VISNYEI, K., KOGA, T., GOMEZ, G., ESKIN, A., HWANG, K., WANG, J., MASUI, K., PAUCAR, A., YANG, H., OHASHI, M., ZHU, S., WYKOSKY, J., REED, R., NELSON, S. F., CLOUGHESY, T. F., JAMES, C. D., RAO, P. N., KORNBLUM, H. I., HEATH, J. R., CAVENEE, W. K., FURNARI, F. B. & MISCHEL, P. S. 2014. Targeted therapy resistance mediated by dynamic regulation of extrachromosomal mutant EGFR DNA. *Science,* 343**,** 72-6.

NETWORK, C. G. A. R. 2012. Comprehensive genomic characterization of squamous cell lung cancers. *Nature,* 489**,** 519-25.

NG, A. B. & HORAK, G. C. 1983. Factors significant in the diagnostic accuracy of lung cytology in bronchial washing and sputum samples. II. Sputum samples. *Acta Cytol,* 27**,** 397-402.

O'REILLY, K. E., ROJO, F., SHE, Q. B., SOLIT, D., MILLS, G. B., SMITH, D., LANE, H., HOFMANN, F., HICKLIN, D. J., LUDWIG, D. L., BASELGA, J. & ROSEN, N. 2006. mTOR inhibition induces upstream receptor tyrosine kinase signaling and activates Akt. *Cancer Res,* 66**,** 1500-8.

OHNO, H., KUBO, K., MUROOKA, H., KOBAYASHI, Y., NISHITOBA, T., SHIBUYA, M., YONEDA, T. & ISOE, T. 2006. A c-fms tyrosine kinase inhibitor, Ki20227, suppresses

osteoclast differentiation and osteolytic bone destruction in a bone metastasis model. *Mol Cancer Ther,* 5**,** 2634-43.

OKEGAWA, T., MORIMOTO, M., NISHIZAWA, S., KITAZAWA, S., HONDA, K., ARAKI, H., TAMURA, T., ANDO, A., SATOMI, Y., NUTAHARA, K. & HARA, T. 2017. Intratumour Heterogeneity in Primary Kidney Cancer Revealed by Metabolic Profiling of Multiple Spatially Separated Samples within Tumours. *EBioMedicine,* 19**,** 31-38.

OKUDELA, K., SUZUKI, M., KAGEYAMA, S., BUNAI, T., NAGURA, K., IGARASHI, H., TAKAMOCHI, K., SUZUKI, K., YAMADA, T., NIWA, H., OHASHI, R., OGAWA, H., MORI, H., KITAMURA, H., KANEKO, T., TSUNEYOSHI, T. & SUGIMURA, H. 2007. PIK3CA mutation and amplification in human lung cancer. *Pathol Int,* 57**,** 664-71.

OREND, G. & CHIQUET-EHRISMANN, R. 2006. Tenascin-C induced signaling in cancer. *Cancer Lett,* 244**,** 143-63.

OSKARSSON, T., ACHARYYA, S., ZHANG, X. H., VANHARANTA, S., TAVAZOIE, S. F., MORRIS, P. G., DOWNEY, R. J., MANOVA-TODOROVA, K., BROGI, E. & MASSAGUÉ, J. 2011. Breast cancer cells produce tenascin C as a metastatic niche component to colonize the lungs. *Nat Med,* 17**,** 867-74.

OZGENCLI, I., KILIC, D., GULLER, U., CIFTCI, M., KUFREVIOGLU, O. I. & BUDAK, H. 2018. A Comparison of the Inhibitory Effects of Anti-Cancer Drugs on Thioredoxin Reductase and Glutathione S-Transferase in Rat Liver. *Anticancer Agents Med Chem,* 18**,** 2053-2061.

PADDA, S. K., BURT, B. M., TRAKUL, N. & WAKELEE, H. A. 2014. Early-stage non-small cell lung cancer: surgery, stereotactic radiosurgery, and individualized adjuvant therapy. *Semin Oncol,* 41**,** 40-56.

PAO, W., MILLER, V. A., POLITI, K. A., RIELY, G. J., SOMWAR, R., ZAKOWSKI, M. F., KRIS, M. G. & VARMUS, H. 2005. Acquired resistance of lung adenocarcinomas to gefitinib or erlotinib is associated with a second mutation in the EGFR kinase domain. *PLoS Med,* 2**,** e73.

PAPADIMITRAKOPOULOU, V. 2012. Development of PI3K/AKT/mTOR pathway inhibitors and their application in personalized therapy for non-small-cell lung cancer. *J Thorac Oncol,* 7**,** 1315-26.

PAPADIMITRAKOPOULOU, V., LEE, J. J., WISTUBA, I. I., TSAO, A. S., FOSSELLA, F. V., KALHOR, N., GUPTA, S., BYERS, L. A., IZZO, J. G., GETTINGER, S. N., GOLDBERG, S. B., TANG, X., MILLER, V. A., SKOULIDIS, F., GIBBONS, D. L., SHEN, L., WEI, C., DIAO, L., PENG, S. A., WANG, J., TAM, A. L., COOMBES, K. R., KOO, J. S., MAURO, D. J., RUBIN, E. H., HEYMACH, J. V., HONG, W. K. & HERBST, R. S. 2016. The BATTLE-2 Study: A Biomarker-Integrated Targeted Therapy Study in Previously Treated Patients With Advanced Non-Small-Cell Lung Cancer. *J Clin Oncol,* 34**,** 3638-3647.

PAPAGERAKIS, S., SHABANA, A. H., POLLOCK, B. H., PAPAGERAKIS, P., DEPONDT, J. & BERDAL, A. 2009. Altered desmoplakin expression at transcriptional and protein levels provides prognostic information in human oropharyngeal cancer. *Hum Pathol,* 40**,** 1320-9.

PASTUSHENKO, I. & BLANPAIN, C. 2019. EMT Transition States during Tumour Progression and Metastasis. *Trends Cell Biol,* 29**,** 212-226.

PATEL, P. R., SUN, H., LI, S. Q., SHEN, M., KHAN, J., THOMAS, C. J. & DAVIS, M. I. 2013. Identification of potent Yes1 kinase inhibitors using a library screening approach. *Bioorg Med Chem Lett,* 23**,** 4398-403.

PAZ-ARES, L., MEZGER, J., CIULEANU, T. E., FISCHER, J. R., VON PAWEL, J., PROVENCIO, M., KAZARNOWICZ, A., LOSONCZY, G., DE CASTRO, G., SZCZESNA, A., CRINO, L., RECK, M., RAMLAU, R., ULSPERGER, E., SCHUMANN, C., MIZIARA, J. E., LESSA, Á., DEDIU, M., BÁLINT, B., DEPENBROCK, H., SOLDATENKOVA, V., KUREK, R., HIRSCH, F. R., THATCHER, N., SOCINSKI, M. A. & INVESTIGATORS, I. 2015. Necitumumab plus pemetrexed and cisplatin as first-line therapy in patients with stage IV non-squamous non-small-cell lung cancer (INSPIRE): an open-label, randomised, controlled phase 3 study. *Lancet Oncol,* 16**,** 328-37.

PHILP, A. J., CAMPBELL, I. G., LEET, C., VINCAN, E., ROCKMAN, S. P., WHITEHEAD, R. H., THOMAS, R. J. & PHILLIPS, W. A. 2001. The phosphatidylinositol 3'-kinase p85alpha gene is an oncogene in human ovarian and colon tumours. *Cancer Res,* 61**,** 7426-9.

POPOVA, O. P., BOGOMAZOVA, S. Y. & IVANOV, A. A. 2017. (Role of tenascin C in triple-negative breast cancer). *Arkh Patol,* 79**,** 10-15.

POWERS, B. E., HOOPES, P. J. & EHRHART, E. J. 1995. Tumour diagnosis, grading, and staging. *Semin Vet Med Surg (Small Anim),* 10**,** 158-67.

PROCTOR, R. N. 2001. Tobacco and the global lung cancer epidemic. *Nat Rev Cancer,* 1**,** 82-6.

QI, P. & DU, X. 2013. The long non-coding RNAs, a new cancer diagnostic and therapeutic gold mine. *Mod Pathol,* 26**,** 155-65.

QIAN, X., XU, W., XU, J., SHI, Q., LI, J., WENG, Y., JIANG, Z., FENG, L., WANG, X., ZHOU, J. & JIN, H. 2017. Enolase 1 stimulates glycolysis to promote chemoresistance in gastric cancer. *Oncotarget,* 8**,** 47691-47708.

QIU, M., XU, Y., YANG, X., WANG, J., HU, J., XU, L. & YIN, R. 2014. CCAT2 is a lung adenocarcinoma-specific long non-coding RNA and promotes invasion of non-small cell lung cancer. *Tumour Biol,* 35**,** 5375-80.

QUEK, K., LI, J., ESTECIO, M., ZHANG, J., FUJIMOTO, J., ROARTY, E., LITTLE, L., CHOW, C. W., SONG, X., BEHRENS, C., CHEN, T., WILLIAM, W. N., SWISHER, S., HEYMACH, J., WISTUBA, I. & FUTREAL, A. 2017. DNA methylation intratumour heterogeneity in localized lung adenocarcinomas. *Oncotarget,* 8**,** 21994-22002.

QUEKEL, L. G., GOEI, R., KESSELS, A. G. & VAN ENGELSHOVEN, J. M. 2003. (The limited detection of lung cancer on chest X-rays). *Ned Tijdschr Geneeskd,* 147**,** 1048-56.

QUINN, J. J. & CHANG, H. Y. 2016. Unique features of long non-coding RNA biogenesis and function. *Nat Rev Genet,* 17**,** 47-62.

RAHI, M. 2011. Human development report 2010: Changes in parameters and perspectives. *Indian J Public Health,* 55**,** 272-5.

RAUSCH, V., KRIEG, A., CAMPS, J., BEHRENS, B., BEIER, M., WANGSA, D., HESELMEYER-HADDAD, K., BALDUS, S. E., KNOEFEL, W. T., RIED, T. & STOECKLEIN, N. H. 2017. Array comparative genomic hybridization of 18 pancreatic ductal adenocarcinomas and their autologous metastases. *BMC Res Notes,* 10**,** 560.

REBELLO, R. J., HUGLO, A. V. & FURIC, L. 2018. PIM activity in tumours: A key node of therapy resistance. *Adv Biol Regul,* 67**,** 163-169.

RED BREWER, M., CHOI, S. H., ALVARADO, D., MORAVCEVIC, K., POZZI, A., LEMMON, M. A. & CARPENTER, G. 2009. The juxtamembrane region of the EGF receptor functions as an activation domain. *Mol Cell,* 34**,** 641-51.

REKHTMAN, N. 2010. Neuroendocrine tumours of the lung: an update. *Arch Pathol Lab Med,* 134**,** 1628-38.

REKHTMAN, N., PAIK, P. K., ARCILA, M. E., TAFE, L. J., OXNARD, G. R., MOREIRA, A. L., TRAVIS, W. D., ZAKOWSKI, M. F., KRIS, M. G. & LADANYI, M. 2012. Clarifying the spectrum of driver oncogene mutations in biomarker-verified squamous carcinoma of lung: lack of EGFR/KRAS and presence of PIK3CA/AKT1 mutations. *Clin Cancer Res,* 18**,** 1167-76.

REVANNASIDDAIAH, S., THAKUR, P., BHARDWAJ, B., SUSHEELA, S. P. & MADABHAVI, I. 2014. Pulmonary adenocarcinoma: implications of the recent advances in molecular biology, treatment and the IASLC/ATS/ERS classification. *J Thorac Dis,* 6**,** S502-25.

RICCIUTI, B., MENCARONI, C., PAGLIALUNGA, L., PACIULLO, F., CRINÒ, L., CHIARI, R. & METRO, G. 2016. Long noncoding RNAs: new insights into non-small cell lung cancer biology, diagnosis and therapy. *Med Oncol,* 33**,** 18.

RIZVI, N. A., MAZIÈRES, J., PLANCHARD, D., STINCHCOMBE, T. E., DY, G. K., ANTONIA, S. J., HORN, L., LENA, H., MINENZA, E., MENNECIER, B., OTTERSON, G. A., CAMPOS, L. T., GANDARA, D. R., LEVY, B. P., NAIR, S. G., ZALCMAN, G., WOLF, J., SOUQUET, P. J., BALDINI, E., CAPPUZZO, F., CHOUAID, C., DOWLATI, A., SANBORN, R., LOPEZ-CHAVEZ, A., GROHE, C., HUBER, R. M., HARBISON, C.

T., BAUDELET, C., LESTINI, B. J. & RAMALINGAM, S. S. 2015. Activity and safety of nivolumab, an anti-PD-1 immune checkpoint inhibitor, for patients with advanced, refractory squamous non-small-cell lung cancer (CheckMate 063): a phase 2, single-arm trial. *Lancet Oncol,* 16**,** 257-65.

ROBERTS, W. G., WHALEN, P. M., SODERSTROM, E., MORASKI, G., LYSSIKATOS, J. P., WANG, H. F., COOPER, B., BAKER, D. A., SAVAGE, D., DALVIE, D., ATHERTON, J. A., RALSTON, S., SZEWC, R., KATH, J. C., LIN, J., SODERSTROM, C., TKALCEVIC, G., COHEN, B. D., POLLACK, V., BARTH, W., HUNGERFORD, W. & UNG, E. 2005. Antiangiogenic and antitumour activity of a selective PDGFR tyrosine kinase inhibitor, CP-673,451. *Cancer Res,* 65**,** 957-66.

ROBINSON, D. R., WU, Y. M. & LIN, S. F. 2000. The protein tyrosine kinase family of the human genome. *Oncogene,* 19**,** 5548-57.

ROBITAILLE, H., SIMARD-BISSON, C., LAROUCHE, D., TANGUAY, R. M., BLOUIN, R. & GERMAIN, L. 2010. The small heat-shock protein Hsp27 undergoes ERK-dependent phosphorylation and redistribution to the cytoskeleton in response to dual leucine zipper-bearing kinase expression. *J Invest Dermatol,* 130**,** 74-85.

ROCHE, J. 2018. The Epithelial-to-Mesenchymal Transition in Cancer. *Cancers (Basel),* 10.

ROCK, J. R., ONAITIS, M. W., RAWLINS, E. L., LU, Y., CLARK, C. P., XUE, Y., RANDELL, S. H. & HOGAN, B. L. 2009. Basal cells as stem cells of the mouse trachea and human airway epithelium. *Proc Natl Acad Sci U S A,* 106**,** 12771-5.

ROEPER, J. & GRIESINGER, F. 2019. Epidermal growth factor receptor tyrosine kinase inhibitors in advanced nonsmall cell lung cancer: what is the preferred first-line therapy? *Curr Opin Oncol,* 31**,** 1-7.

ROMERO, D. 2018. Poziotinib for uncommon ERBB mutations. *Nat Rev Clin Oncol,* 15**,** 404.

ROSKOSKI, R. 2020. The role of fibroblast growth factor receptor (FGFR) protein-tyrosine kinase inhibitors in the treatment of cancers including those of the urinary bladder. *Pharmacol Res,* 151**,** 104567.

RUNGE, D. M., RUNGE, D., FOTH, H., STROM, S. C. & MICHALOPOULOS, G. K. 1999. STAT 1alpha/1beta, STAT 3 and STAT 5: expression and association with c-MET and EGF-receptor in long-term cultures of human hepatocytes. *Biochem Biophys Res Commun,* 265**,** 376-81.

RUSCH, V. W., ASAMURA, H., WATANABE, H., GIROUX, D. J., RAMI-PORTA, R., GOLDSTRAW, P. & COMMITTEE, M. O. I. S. 2009. The IASLC lung cancer staging project: a proposal for a new international lymph node map in the forthcoming seventh edition of the TNM classification for lung cancer. *J Thorac Oncol,* 4**,** 568-77.

SABBATINI, P., KORENCHUK, S., ROWAND, J. L., GROY, A., LIU, Q., LEPERI, D., ATKINS, C., DUMBLE, M., YANG, J., ANDERSON, K., KRUGER, R. G., GONTAREK, R. R., MAKSIMCHUK, K. R., SURAVAJJALA, S., LAPIERRE, R. R., SHOTWELL, J. B., WILSON, J. W., CHAMBERLAIN, S. D., RABINDRAN, S. K. & KUMAR, R. 2009. GSK1838705A inhibits the insulin-like growth factor-1 receptor and anaplastic lymphoma kinase and shows antitumour activity in experimental models of human cancers. *Mol Cancer Ther,* 8**,** 2811-20.

SAKURADA, A., TAKAHASHI, N., SATO, M., MIYAGAWA, Y., MATSUMURA, H. & MURAKAMI, G. 2005. Are difficulties during transbronchial lung biopsy/brushing through a fiberoptic bronchoscope based on the bronchial anatomy? *Surg Radiol Anat,* 27**,** 94-9.

SALVIANO-SILVA, A., LOBO-ALVES, S. C., ALMEIDA, R. C., MALHEIROS, D. & PETZL-ERLER, M. L. 2018. Besides Pathology: Long Non-Coding RNA in Cell and Tissue Homeostasis. *Noncoding RNA,* 4.

SAMPATH, D., CORTES, J., ESTROV, Z., DU, M., SHI, Z., ANDREEFF, M., GANDHI, V. & PLUNKETT, W. 2006. Pharmacodynamics of cytarabine alone and in combination

with 7-hydroxystaurosporine (UCN-01) in AML blasts in vitro and during a clinical trial. *Blood,* 107**,** 2517-24.

SAMUELS, Y., WANG, Z., BARDELLI, A., SILLIMAN, N., PTAK, J., SZABO, S., YAN, H., GAZDAR, A., POWELL, S. M., RIGGINS, G. J., WILLSON, J. K., MARKOWITZ, S., KINZLER, K. W., VOGELSTEIN, B. & VELCULESCU, V. E. 2004. High frequency of mutations of the PIK3CA gene in human cancers. *Science,* 304**,** 554.

SANDERS, H. R. & ALBITAR, M. 2010. Somatic mutations of signaling genes in non-small-cell lung cancer. *Cancer Genet Cytogenet,* 203**,** 7-15.

SANTIO, N. M. & KOSKINEN, P. J. 2017. PIM kinases: From survival factors to regulators of cell motility. *Int J Biochem Cell Biol,* 93**,** 74-85.

SANTO, E. E., STROEKEN, P., SLUIS, P. V., KOSTER, J., VERSTEEG, R. & WESTERHOUT, E. M. 2013. FOXO3a is a major target of inactivation by PI3K/AKT signaling in aggressive neuroblastoma. *Cancer Res,* 73**,** 2189-98.

SANTOS, F. P., KANTARJIAN, H., CORTES, J. & QUINTAS-CARDAMA, A. 2010. Bafetinib, a dual Bcr-Abl/Lyn tyrosine kinase inhibitor for the potential treatment of leukemia. *Curr Opin Investig Drugs,* 11**,** 1450-65.

SARRIS, E. G., SAIF, M. W. & SYRIGOS, K. N. 2012. The Biological Role of PI3K Pathway in Lung Cancer. *Pharmaceuticals (Basel),* 5**,** 1236-64.

SCHEFFLER, M., BOS, M., GARDIZI, M., KÖNIG, K., MICHELS, S., FASSUNKE, J., HEYDT, C., KÜNSTLINGER, H., IHLE, M., UECKEROTH, F., ALBUS, K., SERKE, M., GERIGK, U., SCHULTE, W., TÖPELT, K., NOGOVA, L., ZANDER, T., ENGEL-RIEDEL, W., STOELBEN, E., KO, Y. D., RANDERATH, W., KAMINSKY, B., PANSE, J., BECKER, C., HELLMICH, M., MERKELBACH-BRUSE, S., HEUKAMP, L. C., BÜTTNER, R. & WOLF, J. 2015. PIK3CA mutations in non-small cell lung cancer (NSCLC): genetic heterogeneity, prognostic impact and incidence of prior malignancies. *Oncotarget,* 6**,** 1315-26.

SCHILLER, J. H., HARRINGTON, D., BELANI, C. P., LANGER, C., SANDLER, A., KROOK, J., ZHU, J., JOHNSON, D. H. & GROUP, E. C. O. 2002. Comparison of four

chemotherapy regimens for advanced non-small-cell lung cancer. *N Engl J Med,* 346**,** 92-8.

SCHMIDT, L. H., SPIEKER, T., KOSCHMIEDER, S., SCHÄFFERS, S., HUMBERG, J., JUNGEN, D., BULK, E., HASCHER, A., WITTMER, D., MARRA, A., HILLEJAN, L., WIEBE, K., BERDEL, W. E., WIEWRODT, R. & MULLER-TIDOW, C. 2011. The long noncoding MALAT-1 RNA indicates a poor prognosis in non-small cell lung cancer and induces migration and tumour growth. *J Thorac Oncol,* 6**,** 1984-92.

SCHREIBER, G. & MCCRORY, D. C. 2003. Performance characteristics of different modalities for diagnosis of suspected lung cancer: summary of published evidence. *Chest,* 123**,** 115S-128S.

SCHROEDER, G. M., AN, Y., CAI, Z. W., CHEN, X. T., CLARK, C., CORNELIUS, L. A., DAI, J., GULLO-BROWN, J., GUPTA, A., HENLEY, B., HUNT, J. T., JEYASEELAN, R., KAMATH, A., KIM, K., LIPPY, J., LOMBARDO, L. J., MANNE, V., OPPENHEIMER, S., SACK, J. S., SCHMIDT, R. J., SHEN, G., STEFANSKI, K., TOKARSKI, J. S., TRAINOR, G. L., WAUTLET, B. S., WEI, D., WILLIAMS, D. K., ZHANG, Y., FARGNOLI, J. & BORZILLERI, R. M. 2009. Discovery of N-(4-(2-amino-3-chloropyridin-4-yloxy)-3-fluorophenyl)-4-ethoxy-1-(4-fluorophenyl)-2-oxo-1,2-dihydropyridine-3-carboxamide (BMS-777607), a selective and orally efficacious inhibitor of the Met kinase superfamily. *J Med Chem,* 52**,** 1251-4.

SEIF, F., KHOSHMIRSAFA, M., AAZAMI, H., MOHSENZADEGAN, M., SEDIGHI, G. & BAHAR, M. 2017. The role of JAK-STAT signaling pathway and its regulators in the fate of T helper cells. *Cell Commun Signal,* 15**,** 23.

SEQUIST, L. V., WALTMAN, B. A., DIAS-SANTAGATA, D., DIGUMARTHY, S., TURKE, A. B., FIDIAS, P., BERGETHON, K., SHAW, A. T., GETTINGER, S., COSPER, A. K., AKHAVANFARD, S., HEIST, R. S., TEMEL, J., CHRISTENSEN, J. G., WAIN, J. C., LYNCH, T. J., VERNOVSKY, K., MARK, E. J., LANUTI, M., IAFRATE, A. J., MINO-KENUDSON, M. & ENGELMAN, J. A. 2011. Genotypic and

histological evolution of lung cancers acquiring resistance to EGFR inhibitors. *Sci Transl Med,* 3**,** 75ra26.

SHAFER, S. H. & WILLIAMS, C. L. 2003. Non-small and small cell lung carcinoma cell lines exhibit cell type-specific sensitivity to edelfosine-induced cell death and different cell line-specific responses to edelfosine treatment. *Int J Oncol,* 23**,** 389-400.

SHANKER, M., WILLCUTTS, D., ROTH, J. A. & RAMESH, R. 2010. Drug resistance in lung cancer. *Lung Cancer (Auckl),* 1**,** 23-36.

SHARMA, S. V., BELL, D. W., SETTLEMAN, J. & HABER, D. A. 2007. Epidermal growth factor receptor mutations in lung cancer. *Nat Rev Cancer,* 7**,** 169-81.

SHE, Q. B., SOLIT, D. B., YE, Q., O'REILLY, K. E., LOBO, J. & ROSEN, N. 2005. The BAD protein integrates survival signaling by EGFR/MAPK and PI3K/Akt kinase pathways in PTEN-deficient tumour cells. *Cancer Cell,* 8**,** 287-97.

SHEIKH-ZEINEDDINI, N., SAFAROGHLI-AZAR, A., SALARI, S. & BASHASH, D. 2020. C-Myc inhibition sensitizes pre-B ALL cells to the anti-tumour effect of vincristine by altering apoptosis and autophagy: Proposing a probable mechanism of action for 10058-F4. *Eur J Pharmacol,* 870**,** 172821.

SHI, M., HE, X., WEI, W., WANG, J., ZHANG, T. & SHEN, X. 2015. Tenascin-C induces resistance to apoptosis in pancreatic cancer cell through activation of ERK/NF-κB pathway. *Apoptosis,* 20**,** 843-57.

SHI, W., SONG, J., WANG, W., ZHANG, Y. & ZHENG, S. 2017. MACC-1 antibody target therapy suppresses growth and migration of non-small cell lung cancer. *Mol Med Rep,* 16**,** 7329-7336.

SHIMOKAWA, H., URAMOTO, H., ONITSUKA, T., CHUNDONG, G., HANAGIRI, T., OYAMA, T. & YASUMOTO, K. 2011. Overexpression of MACC1 mRNA in lung adenocarcinoma is associated with postoperative recurrence. *J Thorac Cardiovasc Surg,* 141**,** 895-8.

SHUKUYA, T., YAMADA, T., KOENIG, M. J., XU, J., OKIMOTO, T., LI, F., AMANN, J. M. & CARBONE, D. P. 2019. The Effect of LKB1 Activity on the Sensitivity to PI3K/mTOR Inhibition in Non-Small Cell Lung Cancer. *J Thorac Oncol,* 14**,** 1061-1076.

SILACCI, M., BRACK, S. S., SPÄTH, N., BUCK, A., HILLINGER, S., ARNI, S., WEDER, W., ZARDI, L. & NERI, D. 2006. Human monoclonal antibodies to domain C of tenascin-C selectively target solid tumours in vivo. *Protein Eng Des Sel,* 19**,** 471-8.

SING, A., FREUDENBERG, N., KORTSIK, C., WERTZEL, H., KLOSA, B. & HASSE, J. 1997. Comparison of the sensitivity of sputum and brush cytology in the diagnosis of lung carcinomas. *Acta Cytol,* 41**,** 399-408.

SINGH, B. N., GONG, W., DAS, S., THEISEN, J. W. M., SIERRA-PAGAN, J. E., YANNOPOULOS, D., SKIE, E., SHAH, P., GARRY, M. G. & GARRY, D. J. 2019. Etv2 transcriptionally regulates Yes1 and promotes cell proliferation during embryogenesis. *Sci Rep,* 9**,** 9736.

SKULADOTTIR, H., HIRSCH, F. R., HANSEN, H. H. & OLSEN, J. H. 2002. Pulmonary neuroendocrine tumours: incidence and prognosis of histological subtypes. A population-based study in Denmark. *Lung Cancer,* 37**,** 127-35.

SLOT, A. J., MOLINSKI, S. V. & COLE, S. P. 2011. Mammalian multidrug-resistance proteins (MRPs). *Essays Biochem,* 50**,** 179-207.

SMITH, M. A., BATTAFARANO, R. J., MEYERS, B. F., ZOOLE, J. B., COOPER, J. D. & PATTERSON, G. A. 2006. Prevalence of benign disease in patients undergoing resection for suspected lung cancer. *Ann Thorac Surg,* 81**,** 1824-8; discussion 1828-9.

SOARES, H. P., NI, Y., KISFALVI, K., SINNETT-SMITH, J. & ROZENGURT, E. 2013. Different patterns of Akt and ERK feedback activation in response to rapamycin, active-site mTOR inhibitors and metformin in pancreatic cancer cells. *PLoS One,* 8**,** e57289.

SOCINSKI, M. A., EVANS, T., GETTINGER, S., HENSING, T. A., VANDAM SEQUIST, L., IRELAND, B. & STINCHCOMBE, T. E. 2013. Treatment of stage IV non-small cell lung cancer: Diagnosis and management of lung cancer, 3rd ed: American

College of Chest Physicians evidence-based clinical practice guidelines. *Chest,* 143**,** e341S-e368S.

SOLASSOL, I., PINGUET, F. & QUANTIN, X. 2019. FDA- and EMA-Approved Tyrosine Kinase Inhibitors in Advanced. *Biomolecules,* 9.

SON, Y., AN, Y., JUNG, J., SHIN, S., PARK, I., GWAK, J., JU, B. G., CHUNG, Y. H., NA, M. & OH, S. 2019. Protopine isolated from Nandina domestica induces apoptosis and autophagy in colon cancer cells by stabilizing p53. *Phytother Res*.

SONE, S., TAKASHIMA, S., LI, F., YANG, Z., HONDA, T., MARUYAMA, Y., HASEGAWA, M., YAMANDA, T., KUBO, K., HANAMURA, K. & ASAKURA, K. 1998. Mass screening for lung cancer with mobile spiral computed tomography scanner. *Lancet,* 351**,** 1242-5.

SOYER, T. 2016. The role bronchoscopy in the diagnosis of airway disease in children. *J Thorac Dis,* 8**,** 3420-3426.

SPITZ, M. R., WEI, Q., DONG, Q., AMOS, C. I. & WU, X. 2003. Genetic susceptibility to lung cancer: the role of DNA damage and repair. *Cancer Epidemiol Biomarkers Prev,* 12**,** 689-98.

SPIZZO, R., ALMEIDA, M. I., COLOMBATTI, A. & CALIN, G. A. 2012. Long non-coding RNAs and cancer: a new frontier of translational research? *Oncogene,* 31**,** 4577-87.

STACHLEWITZ, R. F., HART, M. A., BETTENCOURT, B., KEBEDE, T., SCHWARTZ, A., RATNOFSKY, S. E., CALDERWOOD, D. J., WAEGELL, W. O. & HIRST, G. C. 2005. A-770041, a novel and selective small-molecule inhibitor of Lck, prevents heart allograft rejection. *J Pharmacol Exp Ther,* 315**,** 36-41.

STANTA, G. & BONIN, S. 2018a. A Practical Approach to Tumour Heterogeneity in Clinical Research and Diagnostics. *Pathobiology,* 85**,** 7-17.

STANTA, G. & BONIN, S. 2018b. Overview on Clinical Relevance of Intra-Tumour Heterogeneity. *Front Med (Lausanne),* 5**,** 85.

STANTA, G., JAHN, S. W., BONIN, S. & HOEFLER, G. 2016. Tumour heterogeneity: principles and practical consequences. *Virchows Arch,* 469**,** 371-84.

STARK, G. R. & DARNELL, J. E. 2012. The JAK-STAT pathway at twenty. *Immunity,* 36**,** 503-14.

STEGMEIER, F., WARMUTH, M., SELLERS, W. R. & DORSCH, M. 2010. Targeted cancer therapies in the twenty-first century: lessons from imatinib. *Clin Pharmacol Ther,* 87**,** 543-52.

STEIN, U., WALTHER, W., ARLT, F., SCHWABE, H., SMITH, J., FICHTNER, I., BIRCHMEIER, W. & SCHLAG, P. M. 2009. MACC1, a newly identified key regulator of HGF-MET signaling, predicts colon cancer metastasis. *Nat Med,* 15**,** 59-67.

STRATTON, M. R., CAMPBELL, P. J. & FUTREAL, P. A. 2009. The cancer genome. *Nature,* 458**,** 719-24.

STURM, N., LANTUÉJOUL, S., LAVERRIÈRE, M. H., PAPOTTI, M., BRICHON, P. Y., BRAMBILLA, C. & BRAMBILLA, E. 2001. Thyroid transcription factor 1 and cytokeratins 1, 5, 10, 14 (34betaE12) expression in basaloid and large-cell neuroendocrine carcinomas of the lung. *Hum Pathol,* 32**,** 918-25.

SUN, M., LIU, X. H., WANG, K. M., NIE, F. Q., KONG, R., YANG, J. S., XIA, R., XU, T. P., JIN, F. Y., LIU, Z. J., CHEN, J. F., ZHANG, E. B., DE, W. & WANG, Z. X. 2014. Downregulation of BRAF activated non-coding RNA is associated with poor prognosis for non-small cell lung cancer and promotes metastasis by affecting epithelial-mesenchymal transition. *Mol Cancer,* 13**,** 68.

SUNAYAMA, J., TSURUTA, F., MASUYAMA, N. & GOTOH, Y. 2005. JNK antagonizes Akt-mediated survival signals by phosphorylating 14-3-3. *J Cell Biol,* 170**,** 295-304.

SUTHERLIN, D. P., BAO, L., BERRY, M., CASTANEDO, G., CHUCKOWREE, I., DOTSON, J., FOLKS, A., FRIEDMAN, L., GOLDSMITH, R., GUNZNER, J., HEFFRON, T., LESNICK, J., LEWIS, C., MATHIEU, S., MURRAY, J., NONOMIYA, J., PANG, J., PEGG, N., PRIOR, W. W., ROUGE, L., SALPHATI, L., SAMPATH, D., TIAN, Q., TSUI, V., WAN, N. C., WANG, S., WEI, B., WIESMANN, C., WU, P., ZHU, B. Y. & OLIVERO, A. 2011. Discovery of a potent, selective, and orally available class I

phosphatidylinositol 3-kinase (PI3K)/mammalian target of rapamycin (mTOR) kinase inhibitor (GDC-0980) for the treatment of cancer. *J Med Chem,* 54**,** 7579-87.

SÉGALINY, A. I., TELLEZ-GABRIEL, M., HEYMANN, M. F. & HEYMANN, D. 2015. Receptor tyrosine kinases: Characterisation, mechanism of action and therapeutic interests for bone cancers. *J Bone Oncol,* 4**,** 1-12.

TAKAHASHI, Y., SAWADA, G., KURASHIGE, J., MATSUMURA, T., UCHI, R., UEO, H., ISHIBASHI, M., TAKANO, Y., AKIYOSHI, S., IWAYA, T., EGUCHI, H., SUDO, T., SUGIMACHI, K., YAMAMOTO, H., DOKI, Y., MORI, M. & MIMORI, K. 2013. Tumour-derived tenascin-C promotes the epithelial-mesenchymal transition in colorectal cancer cells. *Anticancer Res,* 33**,** 1927-34.

TAN, A. C. 2020. Targeting the PI3K/Akt/mTOR pathway in non-small cell lung cancer (NSCLC). *Thorac Cancer,* 11**,** 511-518.

TAN, J. & YU, Q. 2013. Molecular mechanisms of tumour resistance to PI3K-mTOR-targeted therapy. *Chin J Cancer,* 32**,** 376-9.

TANAKA, K., HIRAIWA, N., HASHIMOTO, H., YAMAZAKI, Y. & KUSAKABE, M. 2004. Tenascin-C regulates angiogenesis in tumour through the regulation of vascular endothelial growth factor expression. *Int J Cancer,* 108**,** 31-40.

TANAKA, T., KUTOMI, G., KAJIWARA, T., KUKITA, K., KOCHIN, V., KANASEKI, T., TSUKAHARA, T., HIROHASHI, Y., TORIGOE, T., OKAMOTO, Y., HIRATA, K., SATO, N. & TAMURA, Y. 2017. Cancer-associated oxidoreductase ERO1-α promotes immune escape through up-regulation of PD-L1 in human breast cancer. *Oncotarget,* 8**,** 24706-24718.

TANIGUCHI, C. M., WINNAY, J., KONDO, T., BRONSON, R. T., GUIMARAES, A. R., ALEMÁN, J. O., LUO, J., STEPHANOPOULOS, G., WEISSLEDER, R., CANTLEY, L. C. & KAHN, C. R. 2010. The phosphoinositide 3-kinase regulatory subunit p85alpha can exert tumour suppressor properties through negative regulation of growth factor signaling. *Cancer Res,* 70**,** 5305-15.

TANTAI, J., HU, D., YANG, Y. & GENG, J. 2015. Combined identification of long non-coding RNA XIST and HIF1A-AS1 in serum as an effective screening for non-small cell lung cancer. *Int J Clin Exp Pathol,* 8**,** 7887-95.

THRESS, K., MACINTYRE, T., WANG, H., WHITSTON, D., LIU, Z. Y., HOFFMANN, E., WANG, T., BROWN, J. L., WEBSTER, K., OMER, C., ZAGE, P. E., ZENG, L. & ZWEIDLER-MCKAY, P. A. 2009. Identification and preclinical characterization of AZ-23, a novel, selective, and orally bioavailable inhibitor of the Trk kinase pathway. *Mol Cancer Ther,* 8**,** 1818-27.

THUN, M. J., LALLY, C. A., FLANNERY, J. T., CALLE, E. E., FLANDERS, W. D. & HEATH, C. W. 1997. Cigarette smoking and changes in the histopathology of lung cancer. *J Natl Cancer Inst,* 89**,** 1580-6.

THUNNISSEN, F. B. 2003. Sputum examination for early detection of lung cancer. *J Clin Pathol,* 56**,** 805-10.

TINTORI, C., LAURENZANA, I., LA ROCCA, F., FALCHI, F., CARRARO, F., RUIZ, A., ESTÉ, J. A., KISSOVA, M., CRESPAN, E., MAGA, G., BIAVA, M., BRULLO, C., SCHENONE, S. & BOTTA, M. 2013. Identification of Hck inhibitors as hits for the development of antileukemia and anti-HIV agents. *ChemMedChem,* 8**,** 1353-60.

TISSOT, T., THOMAS, F. & ROCHE, B. 2017. Non-cell-autonomous effects yield lower clonal diversity in expanding tumours. *Sci Rep,* 7**,** 11157.

TIWARI, R. K., BROWN, A., SADEGHIANI, N., SHIRAZI, A. N., BOLTON, J., TSE, A., VERKHIVKER, G., PARANG, K. & SUN, G. 2017. Design, Synthesis, and Evaluation of Dasatinib-Amino Acid and Dasatinib-Fatty Acid Conjugates as Protein Tyrosine Kinase Inhibitors. *ChemMedChem,* 12**,** 86-99.

TOKUMARU, S., SAYAMA, K., YAMASAKI, K., SHIRAKATA, Y., HANAKAWA, Y., YAHATA, Y., DAI, X., TOHYAMA, M., YANG, L., YOSHIMURA, A. & HASHIMOTO, K. 2005. SOCS3/CIS3 negative regulation of STAT3 in HGF-induced keratinocyte migration. *Biochem Biophys Res Commun,* 327**,** 100-5.

TOLCHER, A. W., KHAN, K., ONG, M., BANERJI, U., PAPADIMITRAKOPOULOU, V., GANDARA, D. R., PATNAIK, A., BAIRD, R. D., OLMOS, D., GARRETT, C. R., SKOLNIK, J. M., RUBIN, E. H., SMITH, P. D., HUANG, P., LEAROYD, M., SHANNON, K. A., MOROSKY, A., TETTEH, E., JOU, Y. M., PAPADOPOULOS, K. P., MORENO, V., KAISER, B., YAP, T. A., YAN, L. & DE BONO, J. S. 2015. Antitumour activity in RAS-driven tumours by blocking AKT and MEK. *Clin Cancer Res,* 21**,** 739-48.

TOMASHEFSKI, J. F., CONNORS, A. F., ROSENTHAL, E. S. & HSIUE, I. L. 1990. Peripheral vs central squamous cell carcinoma of the lung. A comparison of clinical features, histopathology, and survival. *Arch Pathol Lab Med,* 114**,** 468-74.

TOMIDA, M. & SAITO, T. 2004. The human hepatocyte growth factor (HGF) gene is transcriptionally activated by leukemia inhibitory factor through the Stat binding element. *Oncogene,* 23**,** 679-86.

TOWNSEND, D. M. & TEW, K. D. 2003. The role of glutathione-S-transferase in anti-cancer drug resistance. *Oncogene,* 22**,** 7369-75.

TRAVIS, W. D. 2014. Pathology and diagnosis of neuroendocrine tumours: lung neuroendocrine. *Thorac Surg Clin,* 24**,** 257-66.

TRAVIS, W. D., GIROUX, D. J., CHANSKY, K., CROWLEY, J., ASAMURA, H., BRAMBILLA, E., JETT, J., KENNEDY, C., RAMI-PORTA, R., RUSCH, V. W., GOLDSTRAW, P. & INSTITUTIONS, I. S. C. A. P. 2008. The IASLC Lung Cancer Staging Project: proposals for the inclusion of broncho-pulmonary carcinoid tumours in the forthcoming (seventh) edition of the TNM Classification for Lung Cancer. *J Thorac Oncol,* 3**,** 1213-23.

TSIM, S., O'DOWD, C. A., MILROY, R. & DAVIDSON, S. 2010. Staging of non-small cell lung cancer (NSCLC): a review. *Respir Med,* 104**,** 1767-74.

TUROVEROV, K. K., KUZNETSOVA, I. M. & UVERSKY, V. N. 2010. The protein kingdom extended: ordered and intrinsically disordered proteins, their folding, supramolecular complex formation, and aggregation. *Prog Biophys Mol Biol,* 102**,** 73-84.

UEMURA, T. & HIDA, T. 2017. Alectinib can replace crizotinib as standard first-line therapy for. *Ann Transl Med,* 5**,** 433.

UTERMARK, T., RAO, T., CHENG, H., WANG, Q., LEE, S. H., WANG, Z. C., IGLEHART, J. D., ROBERTS, T. M., MULLER, W. J. & ZHAO, J. J. 2012. The p110α and p110β isoforms of PI3K play divergent roles in mammary gland development and tumourigenesis. *Genes Dev,* 26**,** 1573-86.

VADDEPALLY, R. K., KHAREL, P., PANDEY, R., GARJE, R. & CHANDRA, A. B. 2020. Review of Indications of FDA-Approved Immune Checkpoint Inhibitors per NCCN Guidelines with the Level of Evidence. *Cancers (Basel),* 12.

VALDIGLESIAS, V., PÁSARO, E., MÉNDEZ, J. & LAFFON, B. 2011. Assays to determine DNA repair ability. *J Toxicol Environ Health A,* 74**,** 1094-109.

VAN GOOL, I. C., EGGINK, F. A., FREEMAN-MILLS, L., STELLOO, E., MARCHI, E., DE BRUYN, M., PALLES, C., NOUT, R. A., DE KROON, C. D., OSSE, E. M., KLENERMAN, P., CREUTZBERG, C. L., TOMLINSON, I. P., SMIT, V. T., NIJMAN, H. W., BOSSE, T. & CHURCH, D. N. 2015. POLE Proofreading Mutations Elicit an Antitumour Immune Response in Endometrial Cancer. *Clin Cancer Res,* 21**,** 3347-3355.

VAN HOECK, A., TJOONK, N. H., VAN BOXTEL, R. & CUPPEN, E. 2019. Portrait of a cancer: mutational signature analyses for cancer diagnostics. *BMC Cancer,* 19**,** 457.

VAN LOHUIZEN, M., VERBEEK, S., KRIMPENFORT, P., DOMEN, J., SARIS, C., RADASZKIEWICZ, T. & BERNS, A. 1989. Predisposition to lymphomagenesis in pim-1 transgenic mice: cooperation with c-myc and N-myc in murine leukemia virus-induced tumours. *Cell,* 56**,** 673-82.

VAN'T WESTEINDE, S. C. & VAN KLAVEREN, R. J. 2011. Screening and early detection of lung cancer. *Cancer J,* 17**,** 3-10.

VANSTEENKISTE, J. F., CANON, J. L., DE BRAUD, F., GROSSI, F., DE PAS, T., GRAY, J. E., SU, W. C., FELIP, E., YOSHIOKA, H., GRIDELLI, C., DY, G. K., THONGPRASERT, S., RECK, M., AIMONE, P., VIDAM, G. A., ROUSSOU, P., WANG, Y. A., DI TOMASO, E. & SORIA, J. C. 2015. Safety and Efficacy of Buparlisib (BKM120)

in Patients with PI3K Pathway-Activated Non-Small Cell Lung Cancer: Results from the Phase II BASALT-1 Study. *J Thorac Oncol,* 10**,** 1319-1327.

VARELA, G. & THOMAS, P. A. 2014. Surgical management of advanced non-small cell lung cancer. *J Thorac Dis,* 6 Suppl 2**,** S217-23.

VARGAS, L., HAMASY, A., NORE, B. F. & SMITH, C. I. 2013. Inhibitors of BTK and ITK: state of the new drugs for cancer, autoimmunity and inflammatory diseases. *Scand J Immunol,* 78**,** 130-9.

VASUDEVAN, S., VASQUEZ, J., CHEN, W., ZENG, S. & ARJOMANDI, M. 2018. Inflammatory Phenotypes Associated with Chronic Obstructive Pulmonary Disease Increase Susceptibility to Exacerbation. Lessons from Single Cell Analysis of Lung Macrophages. *Ann Am Thorac Soc,* 15**,** S289.

WALLIN, J. J., EDGAR, K. A., GUAN, J., BERRY, M., PRIOR, W. W., LEE, L., LESNICK, J. D., LEWIS, C., NONOMIYA, J., PANG, J., SALPHATI, L., OLIVERO, A. G., SUTHERLIN, D. P., O'BRIEN, C., SPOERKE, J. M., PATEL, S., LENSUN, L., KASSEES, R., ROSS, L., LACKNER, M. R., SAMPATH, D., BELVIN, M. & FRIEDMAN, L. S. 2011. GDC-0980 is a novel class I PI3K/mTOR kinase inhibitor with robust activity in cancer models driven by the PI3K pathway. *Mol Cancer Ther,* 10**,** 2426-36.

WANG, A., KUBO, J., LUO, J., DESAI, M., HEDLIN, H., HENDERSON, M., CHLEBOWSKI, R., TINDLE, H., CHEN, C., GOMEZ, S., MANSON, J. E., SCHWARTZ, A. G., WACTAWSKI-WENDE, J., COTE, M., PATEL, M. I., STEFANICK, M. L. & WAKELEE, H. A. 2015. Active and passive smoking in relation to lung cancer incidence in the Women's Health Initiative Observational Study prospective cohort. *Ann Oncol,* 26**,** 221-30.

WANG, J., ANDERSON, P. D., LUO, W., GIUS, D., ROH, M. & ABDULKADIR, S. A. 2012. Pim1 kinase is required to maintain tumourigenicity in MYC-expressing prostate cancer cells. *Oncogene,* 31**,** 1794-803.

WANG, J., KIM, J., ROH, M., FRANCO, O. E., HAYWARD, S. W., WILLS, M. L. & ABDULKADIR, S. A. 2010. Pim1 kinase synergizes with c-MYC to induce advanced prostate carcinoma. *Oncogene,* 29**,** 2477-87.

WANG, J., WANG, W., CAI, H., DU, B., ZHANG, L., MA, W., HU, Y., FENG, S. & MIAO, G. 2017a. MACC1 facilitates chemoresistance and cancer stem cell-like properties of colon cancer cells through the PI3K/AKT signaling pathway. *Mol Med Rep,* 16**,** 8747-8754.

WANG, L., HU, H., PAN, Y., WANG, R., LI, Y., SHEN, L., YU, Y., LI, H., CAI, D., SUN, Y. & CHEN, H. 2014a. PIK3CA mutations frequently coexist with EGFR/KRAS mutations in non-small cell lung cancer and suggest poor prognosis in EGFR/KRAS wildtype subgroup. *PLoS One,* 9**,** e88291.

WANG, L., SYN, N. L., SUBHASH, V. V., ANY, Y., THUYA, W. L., CHEOW, E. S. H., KONG, L., YU, F., PEETHALA, P. C., WONG, A. L., LALJIBHAI, H. J., CHINNATHAMBI, A., ONG, P. S., HO, P. C., SETHI, G., YONG, W. P. & GOH, B. C. 2018. Pan-HDAC inhibition by panobinostat mediates chemosensitization to carboplatin in non-small cell lung cancer via attenuation of EGFR signaling. *Cancer Lett,* 417**,** 152-160.

WANG, L., WU, Y., LIN, L., LIU, P., HUANG, H., LIAO, W., ZHENG, D., ZUO, Q., SUN, L., HUANG, N., SHI, M. & LIAO, Y. 2013. Metastasis-associated in colon cancer-1 upregulation predicts a poor prognosis of gastric cancer, and promotes tumour cell proliferation and invasion. *Int J Cancer,* 133**,** 1419-30.

WANG, Y., DUAN, J., CHEN, H., BAI, H., AN, T., ZHAO, J., WANG, Z., ZHUO, M., WANG, S. & WANG, J. 2017b. Analysis of EGFR mutation status in tissue and plasma for predicting response to EGFR-TKIs in advanced non-small-cell lung cancer. *Oncol Lett,* 13**,** 2425-2431.

WANG, Z., LI, Z., WU, C., WANG, Y., XIA, Y., CHEN, L., ZHU, Q. & CHEN, Y. 2014b. MACC1 overexpression predicts a poor prognosis for non-small cell lung cancer. *Med Oncol,* 31**,** 790.

WANG, Z., YIN, J., LI, M., SHEN, J., XIAO, Z., ZHAO, Y., HUANG, C., ZHANG, H., ZHANG, Z., CHO, C. H. & WU, X. 2019. Combination of shikonin with paclitaxel overcomes multidrug resistance in human ovarian carcinoma cells in a P-gp-independent manner through enhanced ROS generation. *Chin Med,* 14**,** 7.

WARNECKE-EBERZ, U., BOLLSCHWEILER, E., DREBBER, U., POHL, A., BALDUS, S. E., HOELSCHER, A. H. & METZGER, R. 2008. Frequent down-regulation of pim-1 mRNA expression in non-small cell lung cancer is associated with lymph node metastases. *Oncol Rep,* 20**,** 619-24.

WEBER, D. G., JOHNEN, G., CASJENS, S., BRYK, O., PESCH, B., JÖCKEL, K. H., KOLLMEIER, J. & BRÜNING, T. 2013. Evaluation of long noncoding RNA MALAT1 as a candidate blood-based biomarker for the diagnosis of non-small cell lung cancer. *BMC Res Notes,* 6**,** 518.

WEE, S., WIEDERSCHAIN, D., MAIRA, S. M., LOO, A., MILLER, C., DEBEAUMONT, R., STEGMEIER, F., YAO, Y. M. & LENGAUER, C. 2008. PTEN-deficient cancers depend on PIK3CB. *Proc Natl Acad Sci U S A,* 105**,** 13057-62.

WEI, M. M., ZHOU, Y. C., WEN, Z. S., ZHOU, B., HUANG, Y. C., WANG, G. Z., ZHAO, X. C., PAN, H. L., QU, L. W., ZHANG, J., ZHANG, C., CHENG, X. & ZHOU, G. B. 2016. Long non-coding RNA stabilizes the Y-box-binding protein 1 and regulates the epidermal growth factor receptor to promote lung carcinogenesis. *Oncotarget,* 7**,** 59556-59571.

WEINBLATT, M. E., KAVANAUGH, A., GENOVESE, M. C., MUSSER, T. K., GROSSBARD, E. B. & MAGILAVY, D. B. 2010. An oral spleen tyrosine kinase (Syk) inhibitor for rheumatoid arthritis. *N Engl J Med,* 363**,** 1303-12.

WHITE, N. M., CABANSKI, C. R., SILVA-FISHER, J. M., DANG, H. X., GOVINDAN, R. & MAHER, C. A. 2014. Transcriptome sequencing reveals altered long intergenic non-coding RNAs in lung cancer. *Genome Biol,* 15**,** 429.

WIESE, M. 2015. BCRP/ABCG2 inhibitors: a patent review (2009-present). *Expert Opin Ther Pat,* 25**,** 1229-37.

WILUSZ, J. E., SUNWOO, H. & SPECTOR, D. L. 2009. Long noncoding RNAs: functional surprises from the RNA world. *Genes Dev,* 23**,** 1494-504.

WOLOSHIN, S., SCHWARTZ, L. M. & WELCH, H. G. 2008. The risk of death by age, sex, and smoking status in the United States: putting health risks in context. *J Natl Cancer Inst,* 100**,** 845-53.

WONG, M. C. S., LAO, X. Q., HO, K. F., GOGGINS, W. B. & TSE, S. L. A. 2017. Incidence and mortality of lung cancer: global trends and association with socioeconomic status. *Sci Rep,* 7**,** 14300.

WRIGHT, M. W. 2014. A short guide to long non-coding RNA gene nomenclature. *Hum Genomics,* 8**,** 7.

WRIGHT, M. W. & BRUFORD, E. A. 2011. Naming 'junk': human non-protein coding RNA (ncRNA) gene nomenclature. *Hum Genomics,* 5**,** 90-8.

WU, J., JI, J., WENG, B., QIU, P., KANCHANA, K., WEI, T., WANG, Y., CAI, Y., LI, X. & LIANG, G. 2014. Discovery of novel non-ATP competitive FGFR1 inhibitors and evaluation of their anti-tumour activity in non-small cell lung cancer in vitro and in vivo. *Oncotarget,* 5**,** 4543-53.

WU, R., SU, Y., WU, H., DAI, Y., ZHAO, M. & LU, Q. 2016. Characters, functions and clinical perspectives of long non-coding RNAs. *Mol Genet Genomics,* 291**,** 1013-33.

WU, S. G., KUO, Y. W., CHANG, Y. L., SHIH, J. Y., CHEN, Y. H., TSAI, M. F., YU, C. J., YANG, C. H. & YANG, P. C. 2012. EML4-ALK translocation predicts better outcome in lung adenocarcinoma patients with wild-type EGFR. *J Thorac Oncol,* 7**,** 98-104.

XAVIER, C. P., PESIC, M. & VASCONCELOS, M. H. 2016. Understanding Cancer Drug Resistance by Developing and Studying Resistant Cell Line Models. *Curr Cancer Drug Targets,* 16**,** 226-37.

XIA, H., NHO, R. S., KAHM, J., KLEIDON, J. & HENKE, C. A. 2004. Focal adhesion kinase is upstream of phosphatidylinositol 3-kinase/Akt in regulating fibroblast survival in response to contraction of type I collagen matrices via a beta 1 integrin viability signaling pathway. *J Biol Chem,* 279**,** 33024-34.

XIE, S., CHEN, M., YAN, B., HE, X., CHEN, X. & LI, D. 2014. Identification of a role for the PI3K/AKT/mTOR signaling pathway in innate immune cells. *PLoS One,* 9**,** e94496.

XIE, Y., ZHANG, Y., DU, L., JIANG, X., YAN, S., DUAN, W., LI, J., ZHAN, Y., WANG, L., ZHANG, S., LI, S., XU, S. & WANG, C. 2018. Circulating long noncoding RNA act as potential novel biomarkers for diagnosis and prognosis of non-small cell lung cancer. *Mol Oncol,* 12**,** 648-658.

XU, Y., JIN, J., XU, J., SHAO, Y. W. & FAN, Y. 2017. JAK2 variations and functions in lung adenocarcinoma. *Tumour Biol,* 39**,** 1010428317711140.

YADAV, U. C., RANI, V., DEEP, G., SINGH, R. K. & PALLE, K. 2016. Oxidative Stress in Metabolic Disorders: Pathogenesis, Prevention, and Therapeutics. *Oxid Med Cell Longev,* 2016**,** 9137629.

YAMAMOTO, H., SHIGEMATSU, H., NOMURA, M., LOCKWOOD, W. W., SATO, M., OKUMURA, N., SOH, J., SUZUKI, M., WISTUBA, I. I., FONG, K. M., LEE, H., TOYOOKA, S., DATE, H., LAM, W. L., MINNA, J. D. & GAZDAR, A. F. 2008. PIK3CA mutations and copy number gains in human lung cancers. *Cancer Res,* 68**,** 6913-21.

YANG, J., NIE, J., MA, X., WEI, Y., PENG, Y. & WEI, X. 2019a. Targeting PI3K in cancer: mechanisms and advances in clinical trials. *Mol Cancer,* 18**,** 26.

YANG, L., CHEN, Y., CUI, T., KNÖSEL, T., ZHANG, Q., ALBRING, K. F., HUBER, O. & PETERSEN, I. 2012. Desmoplakin acts as a tumour suppressor by inhibition of the Wnt/β-catenin signaling pathway in human lung cancer. *Carcinogenesis,* 33**,** 1863-70.

YANG, L. & LIU, G. 2019. lncRNA BANCR suppresses cell viability and invasion and promotes apoptosis in non-small-cell lung cancer cells in vitro and in vivo. *Cancer Manag Res,* 11**,** 3565-3574.

YANG, X., TANG, Z., ZHANG, P. & ZHANG, L. 2019b. (Research Advances of JAK/STAT Signaling Pathway in Lung Cancer). *Zhongguo Fei Ai Za Zhi,* 22**,** 45-51.

YANO, S., KONDO, K., YAMAGUCHI, M., RICHMOND, G., HUTCHISON, M., WAKELING, A., AVERBUCH, S. & WADSWORTH, P. 2003. Distribution and function

of EGFR in human tissue and the effect of EGFR tyrosine kinase inhibition. *Anticancer Res,* 23**,** 3639-50.

YAO, Y., LI, J. & WANG, L. 2014. Large intervening non-coding RNA HOTAIR is an indicator of poor prognosis and a therapeutic target in human cancers. *Int J Mol Sci,* 15**,** 18985-99.

YE, B., CAPPEL, J., FINDEIS-HOSEY, J., MCMAHON, L., YANG, Q., XIAO, G. Q., XU, H. & LI, F. 2016. hASH1 is a specific immunohistochemical marker for lung neuroendocrine tumours. *Hum Pathol,* 48**,** 142-7.

YIP, P. Y. 2015. Phosphatidylinositol 3-kinase-AKT-mammalian target of rapamycin (PI3K-Akt-mTOR) signaling pathway in non-small cell lung cancer. *Transl Lung Cancer Res,* 4**,** 165-76.

YOO, J., KIM, C. H., SONG, S. H., SHIM, B. Y., JEONG, Y. J., AHN, M. I., KIM, S., CHO, D. G., JO, M. S., CHO, K. D., CHO, H. J., KANG, S. J. & KIM, H. K. 2004. Expression of caspase-3 and c-myc in non-small cell lung cancer. *Cancer Res Treat,* 36**,** 303-7.

YOSHIDA, T., AKATSUKA, T. & IMANAKA-YOSHIDA, K. 2015. Tenascin-C and integrins in cancer. *Cell Adh Migr,* 9**,** 96-104.

YOULDEN, D. R., CRAMB, S. M. & BAADE, P. D. 2008. The International Epidemiology of Lung Cancer: geographical distribution and secular trends. *J Thorac Oncol,* 3**,** 819-31.

YOUNG, L. C., CAMPLING, B. G., COLE, S. P., DEELEY, R. G. & GERLACH, J. H. 2001. Multidrug resistance proteins MRP3, MRP1, and MRP2 in lung cancer: correlation of protein levels with drug response and messenger RNA levels. *Clin Cancer Res,* 7**,** 1798-804.

YU, G., YAO, W., GUMIREDDY, K., LI, A., WANG, J., XIAO, W., CHEN, K., XIAO, H., LI, H., TANG, K., YE, Z., HUANG, Q. & XU, H. 2014. Pseudogene PTENP1 functions as a competing endogenous RNA to suppress clear-cell renal cell carcinoma progression. *Mol Cancer Ther,* 13**,** 3086-97.

YU, T., ZHAO, Y., HU, Z., LI, J., CHU, D., ZHANG, J., LI, Z., CHEN, B., ZHANG, X., PAN, H., LI, S., LIN, H., LIU, L., YAN, M., HE, X. & YAO, M. 2017a. MetaLnc9 Facilitates Lung Cancer Metastasis via a PGK1-Activated AKT/mTOR Pathway. *Cancer Res,* 77**,** 5782-5794.

YU, W., LU, W., CHEN, G., CHENG, F., SU, H., CHEN, Y., LIU, M. & PANG, X. 2017b. Inhibition of histone deacetylases sensitizes EGF receptor-TK inhibitor-resistant non-small-cell lung cancer cells to erlotinib in vitro and in vivo. *Br J Pharmacol,* 174**,** 3608-3622.

YUN, C. H., MENGWASSER, K. E., TOMS, A. V., WOO, M. S., GREULICH, H., WONG, K. K., MEYERSON, M. & ECK, M. J. 2008. The T790M mutation in EGFR kinase causes drug resistance by increasing the affinity for ATP. *Proc Natl Acad Sci U S A,* 105**,** 2070-5.

ZAHREDDINE, H. & BORDEN, K. L. 2013. Mechanisms and insights into drug resistance in cancer. *Front Pharmacol,* 4**,** 28.

ZHANG, C. G., YIN, D. D., SUN, S. Y. & HAN, L. 2017a. The use of lncRNA analysis for stratification management of prognostic risk in patients with NSCLC. *Eur Rev Med Pharmacol Sci,* 21**,** 115-119.

ZHANG, E., LI, W., YIN, D., DE, W., ZHU, L., SUN, S. & HAN, L. 2016a. Erratum to: c-Myc-regulated long non-coding RNA H19 indicates a poor prognosis and affects cell proliferation in non-small-cell lung cancer. *Tumour Biol,* 37**,** 5653.

ZHANG, L., ZHOU, X. F., PAN, G. F. & ZHAO, J. P. 2014. Enhanced expression of long non-coding RNA ZXF1 promoted the invasion and metastasis in lung adenocarcinoma. *Biomed Pharmacother,* 68**,** 401-7.

ZHANG, Q., ZHANG, B., SUN, L., YAN, Q., ZHANG, Y., ZHANG, Z., SU, Y. & WANG, C. 2018. Cisplatin resistance in lung cancer is mediated by MACC1 expression through PI3K/AKT signaling pathway activation. *Acta Biochim Biophys Sin (Shanghai),* 50**,** 748-756.

ZHANG, R., SHI, H., REN, F., LI, X., ZHANG, M., FENG, W. & JIA, Y. 2016b. Knockdown of MACC1 expression increases cisplatin sensitivity in cisplatin-resistant epithelial ovarian cancer cells. *Oncol Rep,* 35**,** 2466-72.

ZHANG, R., XIA, Y., WANG, Z., ZHENG, J., CHEN, Y., LI, X., WANG, Y. & MING, H. 2017b. Serum long non coding RNA MALAT-1 protected by exosomes is up-regulated and promotes cell proliferation and migration in non-small cell lung cancer. *Biochem Biophys Res Commun,* 490**,** 406-414.

ZHANG, X., YASHIRO, M., QIU, H., NISHII, T., MATSUZAKI, T. & HIRAKAWA, K. 2010. Establishment and characterization of multidrug-resistant gastric cancer cell lines. *Anticancer Res,* 30**,** 915-21.

ZHANG, Y., KWOK-SHING NG, P., KUCHERLAPATI, M., CHEN, F., LIU, Y., TSANG, Y. H., DE VELASCO, G., JEONG, K. J., AKBANI, R., HADJIPANAYIS, A., PANTAZI, A., BRISTOW, C. A., LEE, E., MAHADESHWAR, H. S., TANG, J., ZHANG, J., YANG, L., SETH, S., LEE, S., REN, X., SONG, X., SUN, H., SEIDMAN, J., LUQUETTE, L. J., XI, R., CHIN, L., PROTOPOPOV, A., WESTBROOK, T. F., SHELLEY, C. S., CHOUEIRI, T. K., ITTMANN, M., VAN WAES, C., WEINSTEIN, J. N., LIANG, H., HENSKE, E. P., GODWIN, A. K., PARK, P. J., KUCHERLAPATI, R., SCOTT, K. L., MILLS, G. B., KWIATKOWSKI, D. J. & CREIGHTON, C. J. 2017c. A Pan-Cancer Proteogenomic Atlas of PI3K/AKT/mTOR Pathway Alterations. *Cancer Cell,* 31**,** 820-832.e3.

ZHANG, Y., LI, T., ZHANG, L., SHANGGUAN, F., SHI, G., WU, X., CUI, Y., WANG, X., LIU, Y., LU, B., WEI, T., WANG, C. C. & WANG, L. 2019. Targeting the functional interplay between endoplasmic reticulum oxidoreductin-1α and protein disulfide isomerase suppresses the progression of cervical cancer. *EBioMedicine,* 41**,** 408-419.

ZHANG, Z., LIU, T., WANG, K., QU, X., PANG, Z., LIU, S., LIU, Q. & DU, J. 2017d. Down-regulation of long non-coding RNA MEG3 indicates an unfavorable prognosis in non-small cell lung cancer: Evidence from the GEO database. *Gene,* 630**,** 49-58.

ZHAO, G., LI, W. Y., CHEN, D., HENRY, J. R., LI, H. Y., CHEN, Z., ZIA-EBRAHIMI, M., BLOEM, L., ZHAI, Y., HUSS, K., PENG, S. B. & MCCANN, D. J. 2011. A novel, selective inhibitor of fibroblast growth factor receptors that shows a potent broad spectrum of antitumour activity in several tumour xenograft models. *Mol Cancer Ther,* 10**,** 2200-10.

ZHAO, W., LUO, J. & JIAO, S. 2014. Comprehensive characterization of cancer subtype associated long non-coding RNAs and their clinical implications. *Sci Rep,* 4**,** 6591.

ZHONG, L., COE, S. P., STROMBERG, A. J., KHATTAR, N. H., JETT, J. R. & HIRSCHOWITZ, E. A. 2006. Profiling tumour-associated antibodies for early detection of non-small cell lung cancer. *J Thorac Oncol,* 1**,** 513-9.

ZHOU, G., LIU, Z. & MYERS, J. N. 2016a. TP53 Mutations in Head and Neck Squamous Cell Carcinoma and Their Impact on Disease Progression and Treatment Response. *J Cell Biochem,* 117**,** 2682-2692.

ZHOU, G., YANG, L., GRAY, A., SRIVASTAVA, A. K., LI, C., ZHANG, G. & CUI, T. 2017. The role of desmosomes in carcinogenesis. *Onco Targets Ther,* 10**,** 4059-4063.

ZHOU, H., LUO, Y. & HUANG, S. 2010. Updates of mTOR inhibitors. *Anticancer Agents Med Chem,* 10**,** 571-81.

ZHOU, L., YU, L., ZHU, B., WU, S., SONG, W., GONG, X. & WANG, D. 2016b. Metastasis-associated in colon cancer-1 and aldehyde dehydrogenase 1 are metastatic and prognostic biomarker for non-small cell lung cancer. *BMC Cancer,* 16**,** 876.

ZHU, G., ZHAO, M., HAN, Q., TAN, Y., SUN, Y. U., BOUVET, M., SINGH, S. R., YE, J. & HOFFMAN, R. M. 2020. Pazopanib Inhibits Tumour Growth, Lymph-node Metastasis and Lymphangiogenesis of an Orthotopic Mouse of Colorectal Cancer. *Cancer Genomics Proteomics,* 17**,** 131-139.

ZIMNA, A. & KURPISZ, M. 2015. Hypoxia-Inducible Factor-1 in Physiological and Pathophysiological Angiogenesis: Applications and Therapies. *Biomed Res Int,* 2015**,** 549412.

ZIPPO, A., DE ROBERTIS, A., SERAFINI, R. & OLIVIERO, S. 2007. PIM1-dependent phosphorylation of histone H3 at serine 10 is required for MYC-dependent transcriptional activation and oncogenic transformation. *Nat Cell Biol,* 9**,** 932-44.

ZITO MARINO, F., BIANCO, R., ACCARDO, M., RONCHI, A., COZZOLINO, I., MORGILLO, F., ROSSI, G. & FRANCO, R. 2019. Molecular heterogeneity in lung cancer: from mechanisms of origin to clinical implications. *Int J Med Sci,* 16**,** 981-989.

ŠVAJDLER, M., MEZENCEV, R., ŠAŠKOVÁ, B., ONDIČ, O., MUKENŠNÁBL, P. & MICHAL, M. 2019. Triple marker composed of p16, CD56, and TTF1 shows higher sensitivity than INSM1 for diagnosis of pulmonary small cell carcinoma: proposal for a rational immunohistochemical algorithm for diagnosis of small cell carcinoma in small biopsy and cytology specimens. *Hum Pathol,* 85**,** 58-64.